Investigating disease associated immune signatures in Diffuse Large B-cell Lymphoma

Edward Truelove

Supervisor: Professor J G Gribben

A thesis submitted for the degree of

Doctor of Philosophy at the University of London

April 2021

Centre for Haemato-Oncology

Barts Cancer Institute

Queen Mary University of London

Statement of Originality

I, Edward Truelove, confirm that the research included within this thesis is my own work or that where it has been carried out in collaboration with, or supported by others, that this is duly acknowledged below, and my contribution indicated. Previously published material is also acknowledged below.

I attest that I have exercised reasonable care to ensure that the work is original and does not to the best of my knowledge break any UK law, infringe any third party's copyright or other Intellectual Property Right, or contain any confidential material.

I accept that the College has the right to use plagiarism detection software to check the electronic version of this thesis.

I confirm that this thesis has not been previously submitted for the award of a degree by this or any other university.

Signature: Edward Truelove
12/04/2021

Abstract

Diffuse large B-cell lymphoma (DLBCL) not otherwise specified (NOS) is the most frequent subtype of lymphoma with approximately 4,800 new cases per year in the UK. Although it is a curable disease with standard immunochemotherapy, up to one third of patients are primary refractory or relapse after a period of remission. Until recently the prognosis for these patients was extremely poor. The recent approval of chimeric antigen receptor T (CAR-T) cell therapy has significantly improved the outlook for this group, however over half of the patients treated will progress and many others will not be suitable due to rapid disease progression. There are currently a multitude of new agents in development which hold much promise and will likely improve the outlook further for the highest risk patients. However, there remain several unmet needs including improved translation of biological insights to directly benefit patient care.

Recent studies have focused on the genomic landscape in DLBCL, with new subgroups proposed based on the presence of recurrent and potentially actionable mutations, including many which facilitate escape from immune detection. In addition to molecular signals from the malignant lymphoma cells, there are reproducible signals from the non-malignant compartment in both the tissue and peripheral blood microenvironment, with relevance to disease biology. Considerable variation is seen in immune cell composition and function between individuals in both health and disease, but this has not been well characterised in DLBCL.

We focused predominantly on the peripheral blood immune compartment in this work, confirming the presence of a relative monocytosis and lymphopenia in DLBCL and their relevance to survival. We present a detailed description of the immune landscape in DLBCL, and document disease and outcome associated immune signatures. We identify mechanisms to account for these variations, widespread cytokine dysregulation and multiple bases of immune dysfunction. We also establish monocytes as the main peripheral blood source of cytokine production in DLBCL. Finally, we establish a pipeline for detailed characterisation of the tissue immune microenvironment using imaging mass cytometry.

Dedication

Mum, Dad, George, Mina, Jena and Johar.

My friends.

My colleagues.

My patients.

Erland Cooper for the Orkney Triptych.

Acknowledgements

Supervisors

Professor John Gribben - with thanks for his belief, support and mentorship both in the lab and clinically. I will always be grateful for the opportunity.

Professor Maria Calaminici – for her support and advice.

Colleagues and Co-workers

Dr Jeff Davies – for his helpful advice and thoughts.

Dr Joseph Taylor – for his enthusiasm for science, always being willing to discuss ideas and collaboration with developing an analysis pipeline for the imaging mass cytometry work.

Dr Frances Seymour – for her help getting started with mass cytometry.

Dr Jenny Ball – for her help with cell culture.

Dr James Aries – for his enthusiasm for all things mass cytometry.

Dr Arantxa Romero Toledo – for her support in the lab.

Dr Thomas Erblich – for his enthusiasm.

Dr Julfa Begum, Mr Stephen Rodgers, Mr Hira Ale, Dr Shreya Sharma and Mr Joseph Hartlebury – for their support with mass cytometry and imaging mass cytometry.

With thanks also to Dr Rebecca Gresham, Dr Sabari Vallath, Elen McCabe, Sara Muradi and Helena Church.

Funding

This work was supported by Barts Charity and London clinic grants to Professor John Gribben.

Table of Contents

List of Figures

List of Tables

Abbreviations

A	Adenine
ADC	Antibody drug conjugate
ADCC	Antibody dependent cellular cytotoxicity
ALC	Absolute lymphocyte count
AMC	Absolute monocyte count
B-NHL	B-cell non-Hodgkin's lymphoma
B2M	Beta-2-microglobulin
BCL-2	B-cell lymphoma 2 protein
BCL-6	B-cell lymphoma 6 protein
BCOR	BCL6 corepressor
BCR	B cell receptor
BiTE	Bispecific T cell engager
BM	Bone marrow
BMAT	Bone marrow aspirate and trephine
BTLA	B and T lymphocyte attenuator
C	Cytosine
CAR-T	Chimeric antigen receptor T cells
CARD11	Caspase recruitment domain family member 11
CCL3	C-C chemokine ligand 3
CCR2	C-C chemokine receptor 2
CD	Cluster of differentiation
cDC	Conventional dendritic cells
CDKN1A	Cyclin dependent kinase inhibitor 1A
CDKN2A	Cyclin dependent kinase inhibitor 2A
CIITA	Class II major histocompatibility complex transactivator
CM	Central memory
CMV	Cytomegalovirus
CNS	Central nervous system
CR	Complete remission

CREBBP	CREB binding protein
CRS	Cytokine release syndrome
CSB	Cell staining buffer
CSF-1	Colony stimulating factor 1
CSF-1R	Colony stimulating factor 1 receptor
CSR	Class switch recombination
ctDNA	Circulating tumour DNA
CTLA-4	Cytotoxic T lymphocyte associated protein 4
CyTOF	Cytometry by time of flight
DA	Differential abundance
DC	Dendritic cells
DE	Differential expression
DEL	Double expressor lymphoma
DLBCL, NOS	Diffuse large B-cell lymphoma, not otherwise specified
DMSO	Dimethyl sulfoxide
DNA	Deoxyribonucleic acid
DNMT	DNA methyltransferase
ECM	Extracellular matrix
ECOG PS	Eastern Cooperative Oncology Group performance status
EDTA	Ethylenediaminetetraacetic acid
EM	Effector memory
ETV6	ETS variant transcription factor 6
EZH2	Enhancer of Zeste homolog 2
FAS	Fas cell surface death receptor
FBS	Foetal bovine serum
FC	Fold change
FDC	Follicular dendritic cells
FDR	False discovery rate
FL	Follicular lymphoma
FMO	Fluorescence minus one
G	Guanine

GC	Germinal centre
Gd	Gadolinium
GNA13	Guanine nucleotide binding protein subunit alpha 13
HBV	Hepatitis B virus
HCV	Hepatitis C virus
HDAC	Histone deacetylase
HGBL-DH/TH	High grade B-cell lymphoma with MYC and BCL2 and / or BCL6 rearrangements (double-hit / triple-hit)
HIV	Human immunodeficiency virus
HLA	Human leucocyte antigen
HVEM	Herpes virus entry mediator
ICAM-1	Intracellular adhesion molecule 1
ID3	Inhibitor of DNA binding 3
Ig	Immunoglobulin
IgH	Immunoglobulin heavy chain
IgL	Immunoglobulin light chain
IKBKB	Inhibitor of nuclear factory kappa B kinase subunit beta
IL	Interleukin
IL-1RA	Interleukin 1 receptor antagonist
IMC	Imaging mass cytometry
IPI	International prognostic index
Ir	Iridium
IRF4	Interferon regulatory factor 4
IRF8	Interferon regulatory factor 8
Kappa	Kappa light chains
KMT2B	Lysine methyltransferase 2B
KMT2D	Lysine methyltransferase 2D
La	Lanthanum
LAG-3	Lymphocyte activation gene 3 protein
LAM	Lymphoma associated macrophages
Lambda	Lambda light chains

LDH	Lactate dehydrogenase
LLMPP	Leukaemia/Lymphoma Molecular Profiling Project
LN	Lymph node
LP	Lumbar puncture
M	Metal
M-CSF	Macrophage colony stimulating factor receptor
M-CSF R	Macrophage colony stimulating factor
MC	Mass cytometry
MDSC	Myeloid derived suppressor cells
MEF2B	Myocyte enhancer binding factor 2B
MHC	Major histocompatibility complex
Miz1	MYC interacting zinc finger protein 1
MMO	Metal minus one
MMR	Mismatch repair pathway
MRI	Magnetic resonance imaging
MZL	Marginal zone lymphoma
NCCN	National Comprehensive Cancer Network
ncMMR	Non-canonical mismatch repair
Nd	Neodymium
NFKBIA	NF kappa B inhibitor alpha
NFKBIE	NF kappa B inhibitor epsilon
NLRC5	Nod like receptor family CARD domain containing 5
ns	Not significant
OS	Overall survival
PB	Peripheral blood
PBMC	Peripheral blood mononuclear cells
PC	Plasma cells
PCNSL	Primary central nervous system lymphoma
PD-1	Programmed death 1
PD-L1	Programmed death ligand 1
PD-L2	Programmed death ligand 2

pDC	Plasmacytoid dendritic cells
PIM1	Pro-viral integration for Moloney murine leukaemia virus1
PLO	Primary lymphoid organ
PMBL	Primary mediastinal B-cell lymphoma
PolaBR	Polatuzumab, Bendamustine, Rituximab
PRDM1	PR domain zinc finger protein 1
PS	Performance status
PTEN	Phosphatase and tensin homolg
R-IPI	Revised international prognostic index
R/R	Relapse / refractory
RAG	Recombination activating gene
rcf	Relative centrifugal force
RCHOP	Rituximab, cyclophosphamide, doxorubicin, vincristine, prednisolone
RDHAP	Rituximab, dexamethasone, cytarabine, cisplatin
RGDP	Rituximab, gemcitabine, dexamethasone, cisplatin
RGEMP	Rituximab, gemcitabine, methylprednisolone, cisplatin
RHOA	Ras homolg family member A
RLNT	Reactive lymph node / tonsil
RNA	Ribonucleic acid
rpm	Revolutions per minute
RPMI	Roswell Park Memorial Institute medium
Rt	Room temperature
RT	Radiotherapy
S	Switch region
SCS	Single cell suspension
SGK1	Serine/Threonine protein Kinase 1
SHM	Somatic hypermutation
SIRPα	Signal regulatory protein alpha
SLO	Secondary lymphoid organ
Sm	Samarium
SPEN	Spen family transcriptional repressor

SPIB	Spi-B transcription factor
T	Thymine
T_C	Cytotoxic T cell
TCF4	Transcription factor 4
TCRDLBCL	T cell rich diffuse large B cell lymphoma
TEMRA	T effector memory RA
TET2	Tet methylcytosine dioxygenase 2
T_{FH}	Follicular helper T cell
T_H	Helper T cell
TIL	Tumour infiltrating lymphocytes
TLS	Translesion synthesis
TMA	Tissue microarray
TMEM30A	Transmembrane protein 30A
TNF	Tumour necrosis factor
TNFAIP3	TNF alpha induced protein 3
TNFRSF14	Tumour necrosis factor superfamily member 14
U	Uracil
VDJ	Variable, diversity and joining genes
WM	Waldenstrom's macroglobulinaemia
Y	Yttrium
Yb	Ytterbium

1. Introduction

The B-cell Non-Hodgkin's Lymphomas (B-NHL) are a heterogeneous group of disorders, consisting of many distinct clinical and biological entities. They share the common feature of accumulating malignant B-cells, predominantly in lymphoid tissue but also at extra-nodal sites (1). They are broadly divided into aggressive and indolent types based on clinical behaviour, which is a consequence of the stage of differentiation of the clonal B-cell at maturation arrest, as well as the genetic aberrations they harbour (2, 3). It is also increasingly recognised that malignant cells coevolve with varying numbers of genetically stable immune and stromal cells, forming dynamic and bidirectional interactions in a complex tissue environment (4). This work will focus on the non-malignant compartment in Diffuse Large B-cell Lymphoma (DLBCL), not otherwise specified (NOS), referred to as DLBCL in this thesis. In order to begin to understand the pathogenesis of DLBCL, we must first consider normal B cell development with particular reference to the germinal centre (GC) reaction.

1.1 B cell development

Mature B cells are a subtype of lymphocyte defined by expression of a B cell receptor (BCR). BCRs consist of clonally diverse surface membrane immunoglobulin (Ig) for antigen recognition, in association with CD79a (Igα) and CD79b (Igβ), the transmembrane signalling components (5). B cells have two main functions in adaptive immune responses which are achieved through BCR activation, antibody production (humoral immunity) and antigen presentation to T cells (cellular immunity). B cell development and differentiation are also controlled through the BCR, beginning in primary lymphoid tissue (foetal liver / adult bone marrow) from a common lymphoid progenitor cell and progressing through maturation in secondary lymphoid organs (SLO) (lymph nodes / spleen) (6).

1.1.1 VDJ recombination

B cells are dependent on BCR diversity for their role in immune responses. This diversity arises as a consequence of recombination events during development in the bone marrow (BM). Igs, also known as antibodies, are large glycoproteins produced by B cells with specialised immune functions. They exist in 2 forms, either attached to the cell surface as a component of the BCR or a soluble secreted form (7). All Ig, including that of the BCR is composed of four polypeptides, two identical pairs of heavy (IgH) and light (IgL) chains, held together by disulphide bridges. The antigen binding sites of the surface Ig are distal to the membrane and are known as the variable regions, whose gene sequences are randomly rearranged during B cell development to generate the unique BCR in a process called V(DJ) recombination (7, 8). The IgH genes are located on chromosome 14 and IgL on chromosomes 2 (kappa, κ) and 22 (lambda, λ), with the 5' end of each encoding the antigen binding domain (variable region) and consisting of numerous variable (V), diversity (D, IgH only) and joining (J) gene segments (9). The IgH locus can produce 5 major subtypes (isotype) of heavy chain (IgM, IgA, IgG, IgD and IgE) whereas the IgL loci produce a single light chain isotype each (10). These genes, together with those for the T cell receptors (TCR), exist in the germline in a non-functional state, requiring assembly through these recombination events to generate antigen receptor diversity (11). Each developing B cell undergoes multiple such recombination events, each requiring the introduction of breaks in chromosomal DNA. The risk of occasional errors during this process represents an important mechanism of genome instability with the potential to contribute to lymphomagenesis (12). The double strand DNA breaks essential to the somatic recombination of the V(D)J segments are initiated by the RAG recombinase complex encoded by recombination activating gene 1 (*RAG1*) and recombination activating gene 2 (*RAG2*), which binds and cleaves DNA at specific sequences adjacent to each V, D and J gene segment (11, 13).

V(D)J recombination during B cell development occurs in distinct steps beginning with D_H to J_H rearrangement at the IgH locus (pro-B cell), followed by V_H rearrangement with D_HJ_H, resulting in the random joining of one gene segment from each, and subsequent generation of a new heavy chain variable region (14-16). This 'pre-BCR' Ig is assessed for functional capacity and if competent, VDJ recombination of the other allele is suppressed (allelic

exclusion) and the developing lymphocyte reaches the pre-B stage (17, 18). Light chain V_L to J_L recombination now takes place at the κ loci on chromosome 2, and in case of non-functional rearrangements, the λ loci on chromosome 22 are rearranged. As a result, B cells express either κ or λ light chains (isotype exclusion) (19). V(D)J recombination has been estimated to generate an Ig repertoire of > 5 x 10^{13} antigen specificities (20) but at this stage the heavy chain is exclusively of the IgM isotype and coupled with the signalling subunits CD79a and CD79b mediates BCR activity. Lymphocytes with self-reactive BCRs are negatively selected and removed from the B cell pool, while those naïve B cells with a functional BCR progress to co-express IgM and IgD via differential splicing of the heavy chain variable region exon to the constant region exons of the IgM and IgD isotypes. Co-expression of both IgM and IgD indicates the mature naïve B cell is ready for antigen encounter. VDJ recombination essentially results in the generation of a primary repertoire of relatively low affinity Ig prior to antigen encounter and further B cell development takes place subsequent to this in SLOs.

1.1.2 Antigen encounter

Following successful V(D)J recombination and expression of a functional BCR in the BM, naïve B cells circulate in the peripheral blood (PB) and SLO until they are activated by encounter with their cognate antigen. A fraction of such activated B cells proliferate and differentiate to form short lived plasma cells (PC), mainly in the extra-follicular areas of SLOs and express low affinity IgM antibodies (21). The remainder, migrate to the T cell rich areas of the SLO where interaction with CD4+ T helper cells (T_H) results in further stimulation, proliferation and development of primary follicles to form GCs (22). B cell maturation in the GC involves clonal expansion and Ig affinity maturation, processes which require rapid proliferation in the context of physiologic genetic remodelling processes, involving DNA strand-breaks, recombination and mutation, posing a high risk to B cells for lymphomagenesis (23-25).

1.1.3 Class switch recombination

After interaction and priming with cognate T_H, activated B cells alter the isotype and hence function of the Ig they produce via the process of class-switch recombination (CSR) (26). CSR involves rearrangement of intrachromosomal DNA at the Ig heavy chain locus whereby the IgH constant region is changed from IgM to another isotype (IgG, IgA or IgE) (26, 27). The resulting isotype switched B cell produces Ig that retains antigen specificity but can trigger immune responses via different effector pathways. CSR was widely believed to take place in the GC for many years, however recently published data point to its occurrence prior to the establishment of the GC (27).

The genetic remodelling events of CSR are primarily driven by an enzyme called activation-induced cytidine deaminase (AID), which is a member of the APOBEC family of cytidine deaminases and catalyses targeted deamination of deoxycytidine on single-strand DNA of rearranged Ig genes to deoxyuridine (28). The consequence of AID activity is the conversion of C:G pairs to U:G mis-pairs. Uracil is not a usual DNA nucleotide base and the outcome following deamination depends on how the U:G lesion is recognised and processed by DNA repair mechanisms. During CSR, the result is removal of segments of the Ig heavy chain gene locus, which are deleted followed by re-joining of the of the adjacent segments to form a functional gene. More specifically, enzymatic targeting of switch (S) regions located upstream of the heavy chain constant regions for all isotype genes, except IgD, introduce DNA double strand breaks (DSB) allowing recombination of the variable heavy-chain (VDJ) segment with the heavy chain constant gene segment for an alternative isotype (26).

Following initiation by AID, subsequent error prone repair mechanisms such as the base excision repair (BER) pathway create single-strand breaks (SSB) and if sufficiently close to an SSB on the opposite strand a DSB occurs, otherwise the mismatch repair (MMR) pathway facilitates a DSB (26). In the BER pathway, the enzyme Uracil DNA glycosylase (UNG) can excise the mismatched U resulting in an abasic site – deoxyribose-phosphate backbone with no nucleotide base – which can be recognised and cleaved by apurinic/apyrimidinic endonuclease 1/2 (APE1/2) (10). In the MMR pathway, the U can be recognised by an MSH2-MSH6 heterodimer, which in turn recruits MLH1-PMS2 and exonuclease 1 (Exo 1),

facilitating the DSB (29). The 'switched' IgM or IgD heavy chain constant gene segments between two S regions are removed, allowing substitution of an IgG, IgA or IgE constant region gene segment. CSR is completed by non-homologous end joining (NHEJ) between blunt ends of donor and acceptor S regions, linking a variable domain gene segment with a new constant region (10, 26). In the presence of staggered DNA breaks the segments are linked by alternative NHEJ (30).

1.1.4 The germinal centre reaction

Activated B and T_H cells in the T cell zones of SLO migrate into B cell follicles and initiate the GC reaction (31). GCs are transient histological structures with a distinct architecture specialised for the generation of high-affinity antibody producing B cells, an orchestrated process controlled by dynamic transcriptional networks (25). Morphologically, the GC consists of a dark zone, populated by highly proliferating B cells known as centroblasts, and a light zone, populated by resting B cells known as centrocytes. The centrocytes of the light zone are present together with follicular T helper (T_{FH}) cells, macrophages and follicular dendritic cells (FDC). Dark zone centroblasts undergo Ig gene remodelling in a process called somatic hypermutation (SHM), whereas in light zone centrocytes are selected for further maturation or apoptosis based on the antigen affinity of their BCR (25, 32). Although the GC is functionally polarised into 2 zones, B cell development following antigen encounter is not a unidirectional process from dark to light zone but instead involves 'cyclic re-entry' in which GC B cells return to the dark zone for further SHM and proliferation after selection in the light zone (33). Ultimately, the GC reaction results in terminal differentiation of antigen experienced B lymphocytes into either memory B cells or PCs.

1.1.5 Somatic Hypermutation

SHM takes place in rapidly proliferating dark zone centroblasts, shares similarities with CSR and is responsible for improving the affinity of the BCR for its cognate antigen (34). SHM is dependent on transcriptional activity and introduces non-random iterative single nucleotide substitutions, resulting in point mutations, deletion and duplications, in the Ig variable

region genes (29, 35). As with CSR, SHM is initiated by AID and the resulting uracil can be subsequently processed in a number of ways to create the nucleotide substitutions characteristic of the process (36). AID preferentially targets certain hotspot motifs downstream of the IgV promoter together with a few other loci, including genes involved in regulating the GC reaction (37). Physiologic SHM increases the mutational rate in target genes by approximately one million-fold to an estimated frequency of every 1000 base pairs per cell division, with all four nucleotide bases targeted (29).

SHM typically results in both transversions, pyrimidine nucleotide (C/T) to purine (A/G) or vice versa, and transitions, where the targeted nucleotide is replaced by the other in its class (38). Following initiation by AID, five different mechanisms of uracil processing have been implicated in generating the mutational spectrum of SHM. First, replication across the template uracil, due to its similarity to thymine, results in pairing with an adenine creating a C/G to T/A transition (39). Second, UNG2 mediated excision of the uracil results in a non-informative abasic site that can be bypassed by the trans-lesion synthesis (TLS) polymerase REV1, playing a key role in C/G to G/C transversions (40, 41). Third, C/G transversions can also result from cooperation between UNG2 and the non-canonical mismatch repair pathway (ncMMR), however the details of this interaction remain unclear (29, 38). Fourth, A/T mutations can be generated by the ncMMR with MSH2/MSH6 recognition of the uracil mismatch followed by EXO1 generation of single-strand DNA and activity of the error prone TLS polymerase eta (*POLH*) key steps (42). Finally, a subset of A/T mutations are thought to occur independently of ncMMR, with sites downstream of UNG2 generated abasic sites being subject to the BER pathway involving the activity of polymerase eta (38).

Thus, multiple complex mechanisms which introduce B cell genomic instability are at play during Ig affinity maturation and errors here can contribute to the multistep process of B-NHL development. AID has been shown to mutate recognised oncogenes outside of its physiological targets and DNA strand breaks, required for CSR, have been implicated in pathogenic chromosomal translocations (28, 43).

1.1.6 Control of the germinal centre reaction

Initiation of the GC reaction requires the coordinated induction of a number of related transcriptional networks. MYC is a transcription factor oncogene whose target genes influence cellular proliferation and metabolism. Its expression is tightly regulated but is an early requirement for GC formation (44). MYC is then silenced by the transcriptional repressor B cell lymphoma 6 (BCL6), which can silence >1000 target genes via recruitment of co-repressors (45). BCL6 is critical for the initiation and maintenance of GC reactions and considered the master regulator - it is first detected in developing B cells of the interfollicular zone that have encountered antigen and engaged T_H cells (25). Its expression involves the transcription factors interferon regulatory factor 8 (IRF8), IRF4 (also known as multiple myeloma 1, MUM1) and monocyte-specific enhancer factor 2B (MEF2B) (25). Although precise details of this control are not known, gain of function mutations in MEF2B lead to increased BCL6 expression (46). BCL6 has key roles in the formation and maintenance of the GC that require fine control of its expression such that following induction, it exerts a negative feedback mechanism in which it binds its own promotor to repress transcription with failure of this regulatory mechanism identified in a subset of lymphomas (47).

The function of BCL6 as a transcriptional repressor requires binding at specific DNA motifs and recruitment of histone deacetylase complexes either directly or via co-repressors, however it can also promote gene expression indirectly via repression of repressors, including microRNAs (25). Targets relevant to GC reaction control include repression of DNA damage response genes such as tumour protein 53 (*TP53*), cell cycle checkpoints including cyclin-dependent kinase inhibitor 1A (*CDKN1A*), the anti-apoptotic protein BCL2 and repression of negative regulating miRNAs to promote AID expression, facilitating an environment permissive to dark zone B cell SHM and cell cycle progression (48-50). Pathways involved in B cell differentiation are also repressed to prevent premature exit from the GC. The critical role of BCL6 in GC biology was confirmed by the absence of GC formation in BCL6 deficient mice and the promotion of lymphomagenesis by its constitutive expression (51, 52).

Enhancer of zeste homologue 2 (EZH2), the catalytic component of the Polycomb repressive complex 2, is a lysine methyltransferase enzyme that tri-methylates the lysine 27 residue of histone 3 (H3K27 to H3K27me3), resulting in transcriptional repression (53, 54). EZH2 expression is required for GC development and in mature B cells is restricted to the GC stage, where it directs epigenetic silencing in the dark zone to promote proliferation and block terminal differentiation (55, 56). EZH2 and BCL6 share target promoters and cooperate in transcriptional silencing, with the key role of EZH2 confirmed by reduced GC development in murine models with deletion / inhibition of its activity and GC hyperplasia and lymphomagenesis seen with gain of function (55).

Dark zone B cells also preferentially express the transcription factor E2A, encoded by *TCF3*, which induces gene expression to promote proliferation and regulation of BCR expression / signalling, and is required for GC formation (25). IRF4 has a bimodal expression pattern, being transiently expressed at initiation to promote BCL6 expression, followed by repression in dark zone proliferating centroblasts and is then re-expressed in the light zone centrocytes destined for PC differentiation (57). Nuclear factor-κB (NF-κB) is also expressed in a bimodal distribution, being active during GC initiation, absent in most dark zone B cells and re-expressed in light zone B cells following antigen re-encounter (22, 33, 58).

Dark zone B cells, having undergone cycles of proliferation and SHM transit to the light zone where they are selected based on high antigen affinity and subsequently either move back to the dark zone 'cyclic re-entry' or terminally differentiate into memory B cells or PCs. Those B cells without sufficient antigen affinity do not receive survival signals via their BCR from immune interactions with T_H and FDC and are programmed for apoptosis (22). As with initiation of the GC reaction, the GC B cell fate is governed by dynamic epigenetic and gene expression profiles which in turn are controlled by various transcription factors based on their recruitment of co-activator / co-repressor complexes (59). Having been silenced in the majority of dark zone centroblasts by BCL6, MYC expression is reinduced in those light zone B cells with high affinity BCRs selected for 'cyclic re-entry' back into the dark zone to experience further proliferation (45). Once a GC reaction has been established, deletion of MYC results in disruption and collapse of GCs, establishing it and hence 'cyclic re-entry' as critical elements in maintaining the GC reaction (44, 45).

Exit from the GC is controlled via differentiation signals received by B cells through their BCR, toll-like receptors (TLR) and CD40 (25). CD40 signalling converges on NF-κB activation which in turn induces IRF4 re-expression, which having cooperated in BCL6 expression at initiation, now plays a role in BCL6 downregulation, which is accompanied by release of CREB binding protein (CREBBP) and E1A binding protein 300 (EP300) from BCL6 repression (60, 61). CREBBP and EP300 are both histone acetyltransferases involved in epigenetic regulation of genes driving GC exit terminal differentiation. The opposing actions of IRF4 on BCL6 regulation during the GC reaction likely involve differential recruitment of co-activators and co-repressors. IRF4 also plays a key role in PC differentiation through *PRDM1*, which encodes B lymphocyte-induced maturation protein 1 (BLIMP1), the master regulator of PC differentiation, directly via up-regulation and indirectly by release from BCL6 mediated repression (62). Multiple other pathways are also involved in BCL6 inhibition, including mitogen activated protein kinase (MAPK) mediated phosphorylation and degradation, F-box only protein 11 (FBXO11) mediated ubiquitylation and degradation and acetylation by CREBBP and EP300, disrupting its ability to recruit co-repressors and rapidly attenuating BCL6 function (59).

Although the control mechanism for memory B cell differentiation remains unclear, evidence supports differential affinity selection whereby precursors are selected based on broadly reactive lower affinity and precursors of PCs on high affinity, such that T_{FH} interactions in the light zone are key to this process (63). PC development requires a change in transcriptional programme from that driven by transcription factors such as paired box 5 (PAX5) and BCL6, to a PC expression profile driven by IRF4, BLIMP1 and X-box binding protein (XBP1) (21, 25). BLIMP1 is a transcriptional repressor which maintains BCL6 down-regulation, inhibits proliferation and activates a PC specific gene expression profile together with an antibody secreting phenotype via XBP1 (64).

1.2 Diffuse large B-cell lymphoma, not otherwise specified

DLBCL, NOS is the most frequent lymphoma subtype with an annual incidence of 7.5 per 100,000 and an estimated 4880 new cases each year diagnosed in the UK (Haematological Malignancy Research Network, www.hmrn.org). It is slightly more common in males than females and is increasingly common with age, with a median age at diagnosis of 70 (figure 1.1). The cause remains largely unknown with epidemiological studies suggesting a likely complex interplay between genetic and environmental factors, including immune dysregulation, viruses and environmental and / or occupational exposures playing a role (65). It is not considered a heritable disease, but first-degree relatives of affected patients have a modestly increased risk and multiple genetic susceptibility loci have been identified through genome-wide association studies (66, 67).

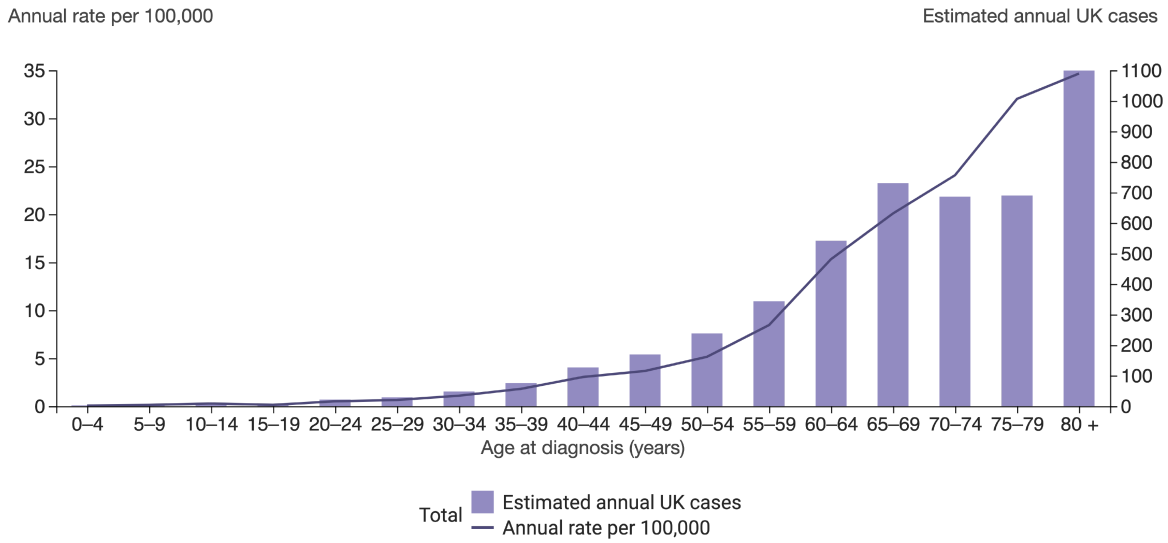

Figure 1.1 Age-specific incidence of Diffuse large B-cell lymphoma. DLBCL is increasingly common with age. Figure from www.hmrn.org.

The vast majority of patients present de novo, but DLBCL can arise following transformation of a previously diagnosed or occult low-grade NHL, most commonly follicular lymphoma (FL). It is an aggressive disease which would be universally fatal if left untreated, with a median survival of < 12 months without treatment, but shows marked clinical heterogeneity and response to therapy, representing one of only a few malignancies that remain curable even when widely disseminated. Current standard first line immuno-chemotherapy with Rituximab, a monoclonal antibody targeting CD20, and anthracycline based chemotherapy (RCHOP, Rituximab, Cyclophosphamide, Doxorubicin, Vincristine and Prednisolone) cures up to two thirds of patients (68). Despite this success, approximately 10-15% will be primary refractory and a further 20-30% relapse after initial remission (69). A minority of these relapse / refractory (R/R) patients can achieve long-term disease-free survival with conventional therapy but the outlook for this group is generally poor. These differential outcomes are a reflection of the marked biological heterogeneity within a histologically uniform disease, which was first appreciated following landmark gene expression profiling (GEP) studies identifying molecular subtypes based on cell of origin (COO) (70, 71).

DLBCLs have somatically mutated *Ig* genes in their genomes and are considered to have arisen from the GC stage of development, perhaps as a consequence of the high risk nature of this process (72). Lymphomagenesis is stepwise, whereby characteristic oncogenic chromosomal translocations may occur prior to the GC stage but differentiation arrest and hence malignant transformation, occur during the GC reaction, with the precise stage reflected in the COO (figure 1.2). The latest World Health Organisation (WHO) classification revision incorporates GEP and chromosomal rearrangements alongside morphology, immunohistochemistry (IHC) and clinical features, however it is now recognised that there is significant molecular granularity beyond the COO subgroups such that DLBCL should no longer be considered a single disease entity, with a novel taxonomy to facilitate personalised therapeutic approaches the likely direction of travel (73, 74). However numerous barriers remain before this can be achieved in the routine clinical setting. We will next review the current state of knowledge across various aspects of the disease and set out the rationale for this work.

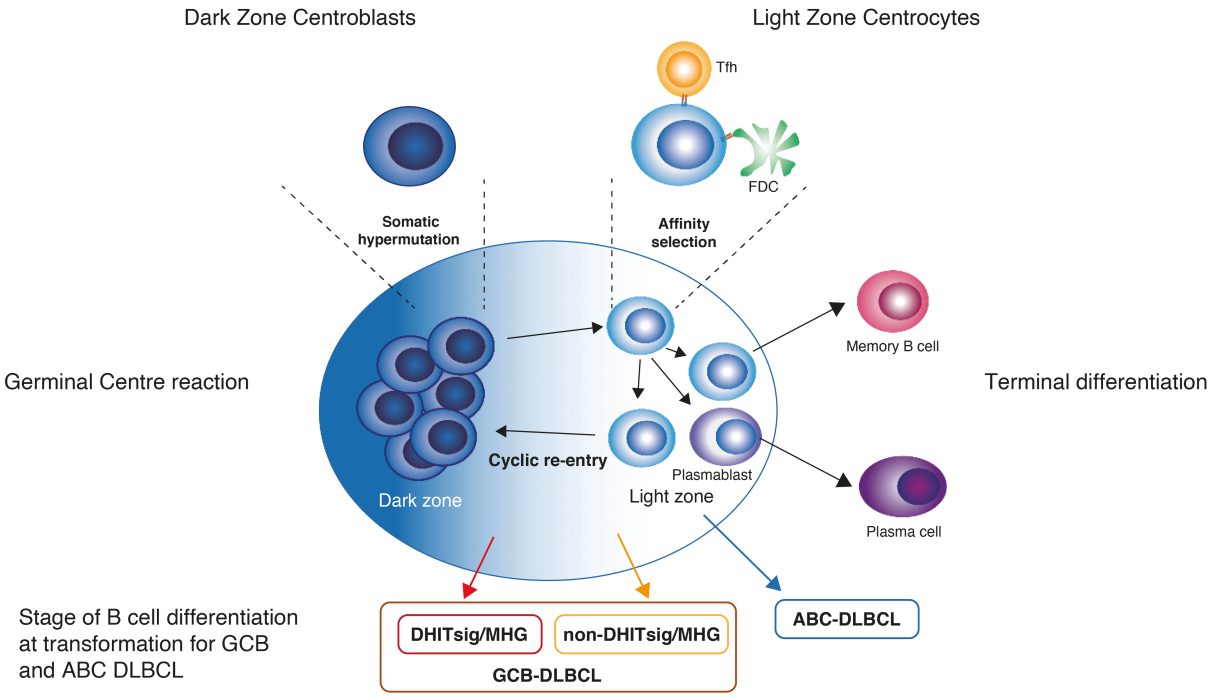

Figure 1.2 The germinal centre reaction with the relevant stage of differentiation indicated for each cell of origin (COO) subtype of DLBCL. Somatic hypermutation (SMH) occurs in the dark zone and affinity selection in the light zone. For the germinal centre B (GCB) subtype, double hit signature / molecular high grade (DHITsig/MHG) arise from cells resembling dark zone centroblasts and non-DHITsig/MHG resemble light zone centrocytes. Activated B cell (ABC) cases more closely resemble the plasmablast stage of differentiation. Tfh, T follicular helper cell; FDC, follicular dendritic cell. Figure adapted from Ennishi et al (73).

1.2.1 Clinical features and diagnostic workup

Clinical presentation can vary from an otherwise asymptomatic single lymph node swelling to a rapidly enlarging mass with widespread organ involvement with extra-nodal disease identified in up to one third and systemic 'B symptoms' (fever, weight loss, drenching night sweats) in a similar number (75, 76). The diagnosis is based on tumour tissue morphology and immunophenotype which is dependent on an adequate histological specimen, with an excisional biopsy preferred to fully assess tissue architecture but increasingly replaced by

radiological core needle biopsy (69). The diagnostic tissue examination requires expert haemato-pathologist review within the context of a specialist integrated haematological malignancy diagnostic service and clinical / radiological correlation in the multidisciplinary team (MDT) setting (www.nice.org). Typical lymph node morphology is effacement of the normal architecture by sheets of large atypical lymphoid cells most commonly resembling centroblasts, or occasionally immunoblasts or a mix of both. The immunophenotype is confirmed by IHC, which demonstrates positivity for pan B cell markers (CD19, CD20, CD22, CD79a) and the leucocyte common antigen CD45. A variable number also express BCL2, BCL6, CD10 and IRF4/MUM1 with the proliferation fraction determined by ki67 staining usually > 40% (77-80). Confirmation of a pathological diagnosis essentially involves elimination of other B-cell lymphoproliferations in the context of morphology, immunophenotype and clinical features.

1.2.2 Cell of origin assignment

The subtypes identified by GEP based on COO include one expressing genes characteristic of germinal centre B cells (GCB) and another expressing genes induced during activation of peripheral blood B cells, activated B-like DLBCL (ABC) (70). Subsequent work confirmed a third 'unclassified' group representing 10-15% of cases, defined primary mediastinal B-cell lymphoma (PMBL) as a separate disease entity and demonstrated that the COO subtypes differed in biology and outcome following RCHOP (71, 81-83). The COO is prognostic, with the GCB group having improved survival and the current WHO classification requires COO assessment at diagnosis (1). Although COO assignment was originally based on GEP, this is not widely available in routine clinical practice and surrogate IHC algorithms are considered acceptable. The Hans algorithm - based on staining with CD10, BCL6 and IRF4/MUM1 - is most widely adopted in the UK but several others have been developed (84, 85).These IHC algorithms generally correlate with GEP but fail to identify the 'unclassified' group, giving a binary result of GCB or non-GCB, have reproducibility issues and do not have the same prognostic value as COO based on GEP (86). The COO is documented at diagnosis as per the WHO recommendation, along with the algorithm used, but does not guide clinical decision making except in the setting of clinical trials.

1.2.3 Molecular and cytogenetic characteristics

Aberrations of the *MYC* gene are also associated with prognosis in the Rituximab era (87). Expression of MYC protein is increased in up to half of DLBCL and is associated with BCL2 overexpression in approximately one third when measured by IHC (1). The majority of these cases do not harbour chromosomal rearrangements of these genes and are known as 'double expressor lymphomas' (DEL), which mostly occur in the ABC subgroup and are associated with inferior outcome (88-90). DEL are not considered as a separate classification given that increased protein expression may result from distinct molecular mechanisms, but DEL are considered a prognostic group and expression of both proteins should be documented at diagnosis.

MYC chromosomal rearrangements occur in 5-15% of DLBCL, with additional translocations involving *BCL2* and / or *BCL6* frequently co-identified resulting in 5-10% of newly diagnosed patients with 'double-hit' or 'triple-hit' genetics (90). These cases usually have a GCB phenotype but poor outcomes following RCHOP and are now considered as a separate entity – high grade B-cell lymphoma with *MYC* and *BCL2* and / or *BCL6* rearrangements (HGBL-DH/TH) (1). It is appreciated that many of these tumours lack distinctive morphological features and therefore all newly diagnosed DLBCL require fluorescence in situ hybridisation (FISH) testing for MYC rearrangements to be incorporated into the workup. Nice guidelines recommend screening all patients with high grade B-cell lymphoma for *MYC* rearrangements and if present, screening for the Ig partner and for the presence of *BCL2* and *BCL6* rearrangements, although in practice most patients will be screened for all 3 routinely. The importance of the *MYC* translocation gene partner in HGBL-DH/TH has recently been highlighted in a study by the Lunenburg Lymphoma Biomarker Consortium (LLBC) which suggests the historical negative impact is largely due to cases with an Ig gene partner (91). It is also recognised that rare cases with high grade or blastoid morphology lack chromosomal rearrangements and these cases are now grouped as HGBL, NOS.

1.2.4 Clinical assessment and staging

The presence of B symptoms, physical examination and performance status (PS) assessment should be documented. A full blood count (FBC), biochemistry including lactate dehydrogenase (LDH) and uric acid together with serological screening for human immunodeficiency virus (HIV), hepatitis B (HBV) and hepatitis C (HCV) are recommended (75). Fluorodeoxyglucose positron emission tomography (FDG-PET)/computed tomography (CT) imaging is the gold standard for radiological staging of DLBCL (92). FDG-PET/CT is more sensitive than bone marrow aspirate and trephine (BMAT) for bone marrow involvement and is highly specific, however may miss low level involvement and discordant low-grade lymphoma (93). BMAT is not required when there is bone or marrow FDG positivity but still recommended for patients without these, especially where limited stage disease exists, and an abbreviated course of therapy considered (75). Magnetic resonance imaging (MRI) and lumbar puncture (LP) should be considered where central nervous system (CNS) involvement is suspected. Cardiac function should be assessed with electrocardiogram (ECG) and echocardiography considered where appropriate in view of anthracycline (doxorubicin) based therapy. Risks to fertility and fertility preservation strategies should be discussed and local guidelines followed. Final staging according to the Ann Arbor classification should be documented.

1.2.5 Clinical prognostic tools

A number of prognostic scoring systems have been employed to guide risk assessment based on routinely available clinical and radiological parameters but do not routinely alter therapy outside of clinical trials. The international prognostic index (IPI) and an age adjusted version (aa-IPI) for younger patients were first developed over quarter of a century ago and remain in clinical use today (94). The IPI pre-dates the incorporation of Rituximab into treatment and identified 4 risk groups with overall survival (OS) at 5 years following chemotherapy of 73%, 51%, 43% and 26% based on 5 factors (table 1.1). The significant improvements seen across all outcome metrics with the addition of Rituximab to CHOP resulted in the revised IPI (R-IPI) based on the same 5 factors but defining 3 risk groups with

4-year OS from 94% to 55% (table 1.2) (95). The limited effectiveness of the R-IPI in identifying those patients with aggressive disease at high risk of progression following RCHOP resulted in the development of the National Comprehensive Cancer Network IPI (NCCN-IPI) which was again based on the same clinical parameters but redistributed the scoring resulting in 4 risk groups with 5-year OS rates ranging from 96% to 33% (table 1.3) (96). Ruppert and colleagues evaluated all 3 risk scoring systems in a large cohort of patients treated in multi-site clinical trials during the Rituximab era and found that the NCCN-IPI had the greatest absolute difference between highest and lowest risk groups but that none of the scores clearly identified a poor risk group with less than 50% long-term survival (97). The prognostic tools were also compared in a cohort of patients treated in a large UK trial with their utility acknowledged but with the conclusion that novel prognostic tools are required to identify the highest risk patients (98).

Table 1.1 International prognostic index (IPI) factors. One point is scored for the presence of each IPI factor. The standard IPI consists of four groups, low risk with 0 or 1 factor, low-intermediate risk with 2 factors, high-intermediate risk with 3 factors and high risk with 4 or 5 factors. The revised-IPI (R-IPI) consists of three groups, very good risk with 0 factors, good risk with 1 or 2 factors and poor risk with 3, 4 or 5. ECOG PS, Eastern Cooperative Oncology Group performance status; LDH, lactate dehydrogenase; EN, extra-nodal.

IPI factors	IPI	R-IPI
Age > 60	Low (0,1)	Very Good (0)
ECOG PS ≥ 2	Low-int (2)	Good (1,2)
LDH elevated	High-int (3)	
EN sites >1	High (4,5)	Poor (3,4,5)
Stage III/IV		

Table 1.2 Outcome according to the international prognostic index (IPI) and revised-IPI (R-IPI). Data for 365 patients treated with RCHOP in British Columbia. Table from Sehn et al (95).

Risk group	No. of IPI factors	% Patients	4-year PFS, %	4-year OS, %
Standard IPI				
Low	0, 1	28	85	82
Low-intermediate	2	27	80	81
High-intermediate	3	21	57	49
High	4, 5	24	51	59
Revised IPI				
Very good	0	10	94	94
Good	1, 2	45	80	79
Poor	3, 4, 5	45	53	55

Table 1.3 National Comprehensive Cancer Network IPI (NCCN-IPI). The risk factors are the same as for the IPI and R-IPI except the age and lactate dehydrogenase (LDH) are redistributed as indicated. Extra-nodal (EN) disease is only a risk factor if the indicated sites are involved. BM, bone marrow; CNS, central nervous system; GI, gastrointestinal; ECOG PS, Eastern cooperative Oncology Group performance status. Four risk groups are defined, low with 0 or 1 points, low-intermediate with 2 or 3 points, intermediate with 4 or 5 points and high 6 or more points.

NCCN IPI factors		Score
Age, y		
	>40 to ≤60	1
	>60 to ≤75	2
	>75	3
LDH, normalised		
	>1 to ≤3	1
	>3	2
Ann Arbor Stage	III/IV	1
EN disease	BM, CNS, liver/GI tract or lung	1
ECOG PS	≥2	1

Several recent studies have focused on quantifying circulating tumour DNA (ctDNA) as a prognostic factor at diagnosis as well as for early relapse detection (99-102). Both pre-treatment levels of ctDNA and those after the first and second cycles of chemotherapy could stratify patients with distinct outcome, but again this method did not clearly select the highest risk patients, and the techniques employed remain outside routine clinical practice at this time.

1.3 Genetics and pathogenesis of DLBCL

The development of clinically apparent DLBCL represents the culmination of a multistep process of accumulating genetic aberrations that influence the expression and / or function of proto-oncogenes and tumour suppressor genes involved in normal B-cell development. Similar to many other cancers, multiple mechanisms of genetic disruption can drive the malignant process such as non-silent somatic mutations and gene copy number alterations. However, the DLBCL genome is also susceptible to alteration by chromosomal translocations, as a consequence of errors during VDJ recombination / CSR / SHM, and aberrant SHM (ASHM) mediated by AID (43, 103). Following the initial discovery of molecular subtypes of DLBCL there have been numerous attempts to further characterise this heterogeneity and distil it into biologically meaningful entities in order to improve patient outcomes. This was initially through the lens of the COO classification with the discovery of their distinct transcriptional, genetic and epigenetic alterations and more recently moving beyond the COO, through recurrent genetic subgroups and their pathway dependencies, together with the associated role of the microenvironment.

1.3.1 Cell of origin assignment

Tumour profiling studies approximately 20 years ago resulted in the COO classification, with the 2 major subtypes having transcriptional programmes representative of different GC stages and distinct clinical outcomes. Both closely relate to GC light zone B-cells, but GCB DLBCL shares features of both dark zone centroblasts and light zone centrocytes, and lacks expression of early post-GC differentiation markers, whereas the ABC transcriptional phenotype is that of GC experienced B cells committed to PC differentiation (70, 104).

GCB is the most frequent COO subtype comprising 50% of DLBCL cases with a 5-year OS of 78% in the Rituximab era (105, 106). The pathogenesis of GCB is complex and only partially understood, sharing a number of features with FL including chromosomal translocations of *BCL2*, resulting in ectopic expression of the anti-apoptotic protein BCL2, which are found in up to 40% of GCB as well as all HGBL-DH/TH, which also display a GCB transcriptome (107-

109). Recurrent genetic alterations in the epigenetic chromatin / histone modifying genes *EZH2*, *CREBBP* and *KMT2D* (MLL2), as well as *TNFRS14*, similar to those observed in FL have all been reported (37, 110-112). Other biologically relevant pathway disruptions include inactivation of *PTEN* with resultant PI3K (phosphatidylinositol 3-kinase) pathway activation and mutations of *GNA13* associated with B-cell survival and dissemination from the GC (73, 112, 113).

ABC DLBCL is associated with worse outcome, with 5-year OS rates of 56% in the Rituximab era and accounts for approximately 30% of cases (105, 106). This subtype is characterised by constitutive activation of the NFκB pathway and inhibition of PC differentiation, both of which result from distinct genetic events (37, 114). NFκB represents a family of inducible transcription factors involved in the regulation of a vast number of genes essential for B-cell development, with its activation conferring a survival advantage to ABC DLBCL (25). Constitutive NFκB activation occurs due to a variety of genetic lesions involving multiple signalling molecules downstream of the BCR and Toll-like receptor (TLR), often complemented by lesions blocking terminal differentiation (37). BCR signalling can occur via antigen independent, 'tonic' and antigen dependent 'chronic active' mechanisms, the latter dependent on a signalling cascade initiated by CD79A and CD79B involving SYK (spleen tyrosine kinase), BTK (Bruton's tyrosine kinase), PKCβ (protein kinase C) resulting in the formation of the CARD11/BCL10/MALT1 (CBM, caspase recruitment domain family member 11, B-cell lymphoma 10, mucosa-associated lymphoid tissue lymphoma translocation gene 1) complex and subsequent NFκB activation (figure 1.3) (3, 25). TLR signalling, which involves the recruitment of adapter proteins including MYD88 (myeloid differentiation primary response 88), can also activate NFκB as well as the JAK/STAT pathway (51). Recurrent mutations in a number of components of these pathways are described in ABC DLBCL. They frequently occur in association with terminal differentiation blockade, which is usually a consequence of genetic lesions converging on inactivation of BLIMP1, either directly or via BCL6 upregulation (37). Data from mouse models support the concept of constitutive NFκB signalling cooperating with BLIMP1 disruption in the development of ABC DLBCL (115). Details of the lesions identified in these pathways are discussed in the section on mutational profiling.

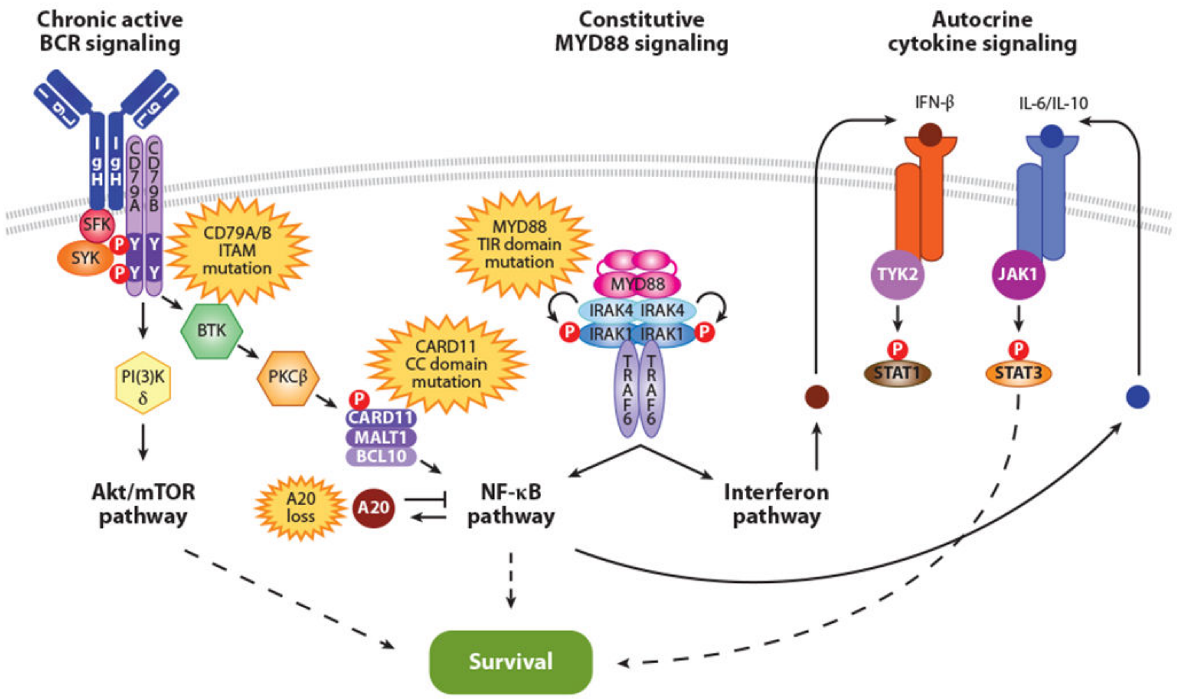

Figure 1.3 Disrupted signalling pathways in activated B cell (ABC) DLBCL. ABC DLBCL is defined by a variety of mutations, including gain of function mutation in *CD79A*, *MYD88*, and *CARD11* and loss of *A20* (*TNFAIP3*), that converge on constitutive NFκB activation. Adapted from Shaffer et al (3).

Given the differential pathway disruptions between subtypes and reports of COO specific activity of novel agents, there exists a rationale for COO to guide management strategy in DLBCL. However, any prospective application of COO in guiding treatment decisions is dependent on highly accurate classification, which is currently beyond the reach of available IHC algorithms (85, 86). The microarray technology using fresh frozen tissue samples in the initial COO studies prevented the adoption of GEP into clinical practice, however the intervening years have seen a number of methodologies for GEP applied to the formalin fixed paraffin embedded (FFPE) tissue widely available in clinical practice. One such method, the Lymph2Cx assay (Nanostring), measures the expression of 20 genes and is reported to have high concordance with GEP methods using fresh frozen tissue and between independent laboratories (116). Another, known as the DASL assay (cDNA-mediated annealing selection, extension and ligation) generates transcriptomic data with COO determined by a machine learning tool and has been employed 'real-time' in a prospective

phase 3 clinical study in DLBCL (117, 118). At the current time these methods remain outside widespread clinical use but with the likelihood of one or a similar method being increasingly incorporated into future practice.

1.3.2 Molecular high-grade signatures

Two independent groups have recently identified a poor risk GCB subgroup based on gene expression signatures associated with HGBL-DH/TH but lacking characteristic chromosomal translocations, termed 'DHITsig' and molecular high grade (MHG) (119, 120). Both groups found that almost all HGBL-DH/TH expressed this signature together with an equal number of non-HGBL-DH/TH GCB cases, which had a similarly poor outcome following RCHOP. Those HGBL-DH/TH without this expression signature did not have a worse outcome than other GCB cases. Defining HGBL by GEP would result in approximately double the number of cases as currently identified on the basis of FISH testing. The cases with high grade expression profiles were enriched for mutations in epigenetic modifiers, had proliferation signatures that closely resembled dark zone centroblasts or intermediate zone GC B-cells, and were immunologically 'cold', with reduced tumour infiltrating lymphocytes (TIL) and frequent loss of MHC-I and/or MHC-II expression (major histocompatibility complex I / II) (73). These studies, together with reports of *MYC* and *BCL2* rearrangements not detected by FISH, suggest that reclassification of such tumours together with the majority of HGBL-DH/TH based on GEP will likely follow once the technology to identify them is routinely available (121).

1.3.3 Genetic subtypes of DLBCL

In recent years, the advances in high throughput sequencing technologies have resulted in a number of independent studies providing insight into the mutational landscape of the DLBCL genome across > 2000 cases (112, 122-124). There have now been over 150 putative driver genes identified, with many featuring recurrent alterations which are now beginning to form the basis of novel classification systems centred on shared genomic abnormalities with potentially actionable lesions and therapeutic implications (73, 74). However, these

studies have also highlighted the extensive mutational heterogeneity of DLBCL, with one of the larger studies identifying a median of 17 genetic alterations per case with a range of 0-48, with no mutations identified in approximately 5% of patients (122). The findings that although a number of mutations characteristically enrich according to the COO, many more do not, with a sizeable fraction detected in < 10% of patients, results in another layer of genetic complexity and a typical long tail of mutational frequencies (figure 1.4) (112, 122). It is worth noting that genetic heterogeneity may also exist within individual cases of DLBCL, in both space (biopsy location) and time (relapse v diagnosis) and that the non-coding genome remains understudied, with some studies suggesting lesions at regulatory sites may play a role in pathogenesis (125-127). Despite these potential barriers there has been a clear trend towards viewing DLBCL in the context of genetic subtypes with 3 major studies identifying broadly consistent molecular groups across independent cohorts and with distinct approaches supporting the validity of their findings, which are discussed below (122-124).

The integration of mutational data together with information on chromosomal translocations and copy number alterations in these studies has accelerated progress towards a more meaningful classification. The work by Schmitz et al, the NCI (National Cancer Institute) cohort, reported 4 prominent genetic groups (MCD, BN2, N1 and EZB), with aberrations affecting multiple genes that distinguished each subtype from other DLBCL but only classified 45% of cases (123). Chapuy and colleagues identified 5 genetic clusters (C1-C5) with a sixth (C0) lacking genetic drivers, classifying all samples studied (122). The HMRN cohort was resolved into 5 molecular groups (MYD88, BCL2, SOCS1/SGK1, TET2/SGK1 and NOTCH2), together with 27% of cases ‘not elsewhere classified’ (NEC) (124). A recent revision of the NCI classification proposed 7 genetic subtypes (figure 1.5) together with a small genetically composite group with characteristics of >1 subtype and 37% classified as ‘other’, largely aligning the findings of these 3 studies (74).

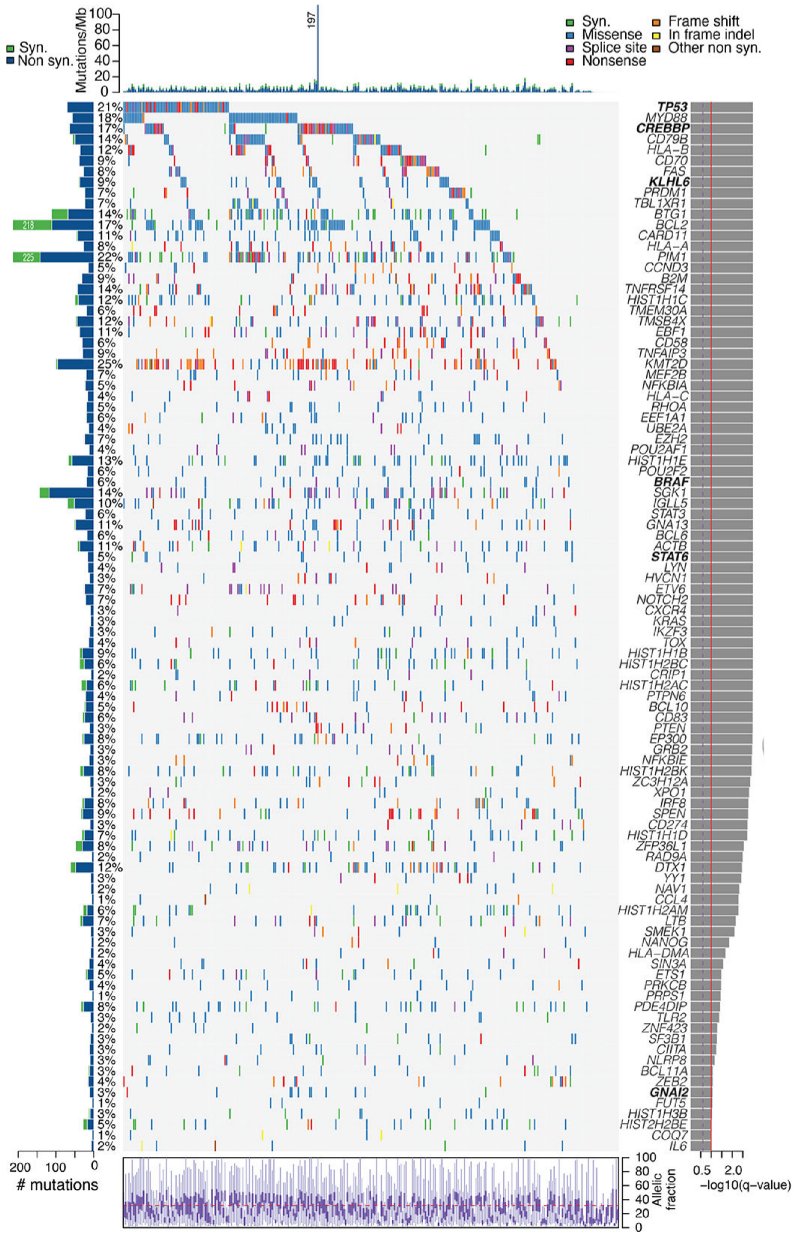

Figure 1.4 Genomic landscape in DLBCL. Recurrently mutated genes in 304 DLBCL cases demonstrating the genetic heterogeneity, both in terms of number of mutations per patient and frequency of each mutation in the cohort. Adapted from Chapuy et al (122).

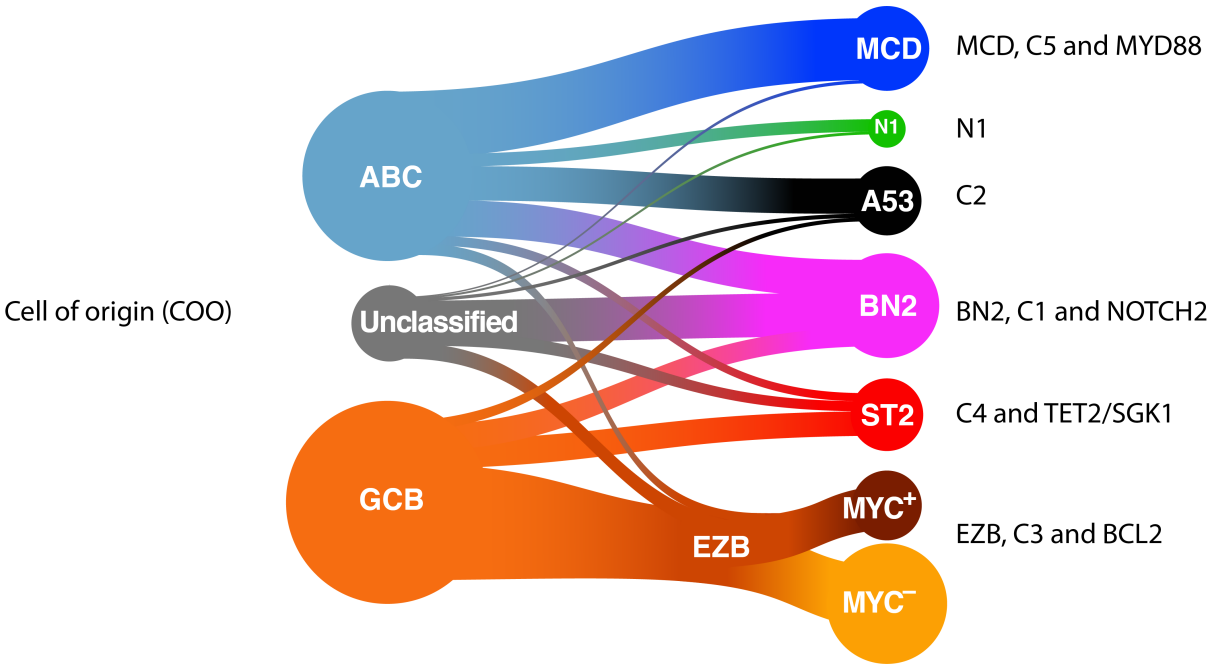

Figure 1.5 Genetic subtypes of DLBCL. The seven genetic subtypes of DLBCL proposed by Wright et al to align the recent genomic landscape studies. Each subtype was named differently (right) in the original publications (see text). The not elsewhere classified (NEC) or cluster (C0) group is not shown. Figure adapted from Wright et al (74).

MCD, C5 and MYD88

The cases in this group have an ABC expression profile and are enriched for $MYD88^{L265P}$ mutations and mutations / amplifications of CD79B, resulting in constitutive NFκB activation via the bypassing of TLR signalling or chronic active BCR signalling (37, 128, 129). $MYD88^{L265P}$ mutations result in a gain-of-function that drives lymphoma development through regulation of kinases and transcription factors, which can be demonstrated in mouse models where B-cell specific expression results in lymphoproliferation (130). Gain-of-function mutations in CD79B drive activation of NFκB through attenuation of a negative feedback loop resulting in unchecked BCR signalling (128). Although CD79B mutations disrupt the regulation of BCR signalling they do not directly activate the pathway and a role for autoantigen BCR stimulation in ABC DLBCL has been demonstrated (131). The dependence of some cases of ABC DLBCL on BCR signalling has been demonstrated by the

clinical responses seen with BTK inhibition, including in some with the absence of CD79B mutations (132). Importantly, patients with MYD88 mutations did not respond, with the exception of those cases carrying both MYD88 and CD79B mutations, suggesting functional coupling of these pathways.

This subtype also features very frequent gain / amplifications of 18q, one of the most common alterations in ABC DLBCL, with resultant BCL2 overexpression and associated poor outcome (122). The gene for transcription factor 4 (*TCF4*) is also located at this site (18q21), with gains resulting in upregulated MYC expression consequent on increased binding of TCF4 to the *MYC* enhancer (133). Other dominant aberrations in this group include mutations of *PIM1* and *ETV6* and frequent loss of *CDKN2A* (124). Inactivating mutations of *PRDM1* (BLIMP1) as well as gain / amplification of *SPIB* also occur, which contribute to the characteristic phenotype of ABC DLBCL by blocking formation of PCs while promoting plasmacytoid differentiation (115, 123).

Immune editing was another prominent feature in this subgroup with many acquiring inactivating lesions of HLA -A, HLA-B or HLA-C (human leucocyte antigen) and CD58 (123, 134). Chapuy et al noted that their C5 cluster signature resembled the lesions their group had previously described in testicular and primary central nervous system lymphoma (PCNSL), suggesting an extra-nodal tropism for DLBCL within this group, which was recapitulated in the HMRN study, which also found cases with breast involvement clustered here (122, 124, 135). The genetic lesions identified in this group were typical of AID activity and ASHM, consistent with B-cells that have transited through the GC.

BN2, C1 and NOTCH2

This group consisted of cases with all 3 gene expression profiles, with ABC and unclassified most frequent, and associated with favourable outcomes. The cases assigned here enriched for BCL6 structural variants and activating NOTCH2 mutations, resulting in increased transcriptional abundance of their target genes and suggestive of a marginal zone B-cell origin with biological similarity to marginal zone lymphoma (MZL) (73, 124). *BCL6* translocations occur in up to one-third of DLBCL preventing BCL6 downregulation by a

mechanism known as ‘promotor substitution’ whereby the *BCL6* gene is positioned under the control of another promotor, most commonly those of Ig genes (37). NOTCH pathway aberrations other than NOTCH2 mutations were also found, including truncating mutations of its negative regulator *SPEN* (122). *BCL6* fusions were more frequent in cases with NOTCH activation suggesting cooperation between these pathways within this group.

Lesions activating the NFκB pathway were also prominent including deletion of its negative regulator *TNFAIP3*, which encodes A20, and direct activation through gains / amplifications of *BCL10* a component of the CBM (122, 123). In addition, mutations resulting in loss of TMEM30A are clustered here which are associated with increased BCR signalling and a favourable prognosis (124, 136). It is also notable that these cases featured multiple genetic lesions to facilitate immune escape including inactivation of *B2M* (beta-2-microglobulin), *CD70* and *FAS* (CD95) and structural variants of *PD-L1* and *PD-L2* (122).

EZB, C3, and BCL2

The majority of cases assigned here were of the GCB phenotype and characteristically had mutations of *BCL2* with concordant translocations (t(14:18)), bringing its expression under the control of the *IgH* enhancer, as well as mutations of chromatin modifiers, frequently *EZH2* but also *CREBBP* and *KMT2D* (122-124). Gene expression profiling revealed a predominance of the MHG signature, the presence of which subdivides this group into 2, each with distinct phenotype and outcome (73). Transformed FL cases, which were included in the HMRN study, also mapped to this subgroup (124). BCL2 is an antiapoptotic protein usually negatively controlled by BCL6, but their inverse relationship is frequently disrupted in DLBCL. Ectopic BCL2 expression driven by chromosomal translocation, as well as ASHM induced promoter mutations with resultant increased sensitivity to Miz1 activation, promotes GCB cell survival in the presence of death signals (Fas) or absence of survival signals (BCR) in DLBCL (137).

Epigenetic dysregulation was also a prominent feature of this grouping. *EZH2* gain-of-function mutations are common in GCB-DLBCL and promote lymphoma via repression of genes controlling proliferation checkpoints (*CDKN1A*) and terminal differentiation (IRF4 and

PRDM1) (59). Mutations of *EZH2* are heterozygous and target the catalytic domain resulting in synergy with the wild-type protein and increased methyltransferase activity (138). As well as cooperating with BCL6 via shared target genes, EZH2 has also been shown to cooperate with BCL2 overexpression to drive lymphomagenesis in murine models (55). *EZH2* mutations have recently been shown to epigenetically reprogramme the GC microenvironment. This occurs via repression of genes involved in immune synapse formation, attenuating B-cell need for T cell help and by promoting downregulation of MHC-I and -II expression, with accompanying impairment of T cell infiltration (139, 140).

Inactivating mutations of *KMT2D* are the single most frequent somatic mutation in DLBCL and result in loss of methyltransferase activity and gene repression, epigenetically deregulating BCL6 target genes and cooperating with BCL2 overexpression to contribute to lymphoma development (59, 141). KMT2D is required for recruitment of the histone acetyltransferases CREBBP and EP300, whose genes are also inactivated in a mutually exclusive, haplo-insufficient manner in this subtype (73, 110). CREBBP usually opposes BCL6 activity via direct acetylation of the BCL6 protein as well as acetylation of histones at regulatory sequences of its target genes (142, 143). CREBBP mediated acetylation also plays a critical role in activation of the tumour suppressor p53 as well as expression of key antigen presentation and processing machinery, with its loss facilitating oncogenesis and immune escape (37).

Other alterations included those of the B-cell transcription factors genes *MEF2B* and *IRF8,* and inactivation of *TNFRSF14* (*HVEM*) and *PTEN*. MEF2B promotes GC formation and modulates genes involved in proliferation, DNA repair, apoptosis and confinement of B-cells to the GC, with mutant forms gaining function through resistance to co-repressor binding to contribute to lymphomagenesis (144). Loss-of-function mutations of *TNFRSF14* facilitate cell-autonomous B-cell proliferation while inducing a supportive microenvironment due to disruption of TNFRSF14 interaction with BTLA (145). PTEN loss occurs via focal loss at 10q23.31 as well as by truncating mutations, activating signalling downstream of the BCR via the PI3K pathway (146).

C4 and SOCS1/SGK1 and TET2/SGK1

The C4 cluster was described by the Shipp group (122) and included predominantly cases with a GCB expression profile and favourable outcome compared with the GCB cases found in the C3, EZB and BCL2 group described above. The more recently published work by the HMRN group described 2 separate groups which seem to mostly align here, and the recent revised classification of the original NCI cohort labelled most of these cases ST2 (74, 123, 124). The C4 cluster was characterised by genetic alterations of H1 linker histones and core histones including *HIST1H1/2*, together with multiple immune evasion bases (CD83, CD58 and CD70), BCR/PI3K signalling intermediates (*RHOA*, *GNA13* and *SGK1*), NFκB modifiers (*CARD11*, *NFKBIE* and *NFKBIA*) and RAS/JAK/STAT pathway molecules (*BRAF* and *STAT3*) (122). The SOCS1/SGK1 group contained mutations in many known targets ASHM, including SOCS1 and had significant overlap with the C4 cluster. SOCS1 and SGK1 inactivation are associated with promotion of JAK/STAT and PI3K signalling respectively (74). The authors also noted that *SOCS1* mutation is frequently found in PMBL and cases in this subgroup with no clinical features of PMBL enriched for gene expression signatures associated with PMBL, suggestive of biological similarity and consistent with the observation that some cases with a PMBL expression profile lacked mediastinal masses (124, 147). The other subgroup of C4 identified by the HMRN group was labelled TET2/SGK1 and enriched for mutations of both *TET2* and *SGK1*, along with mutations in multiple components of the ERK pathway (124). Inactivation of *TET2* has been shown to trigger GC hyperplasia, disrupt terminal differentiation and block GC exit, confirming its role in lymphoma development (148). Some of the cases not originally grouped in the NCI cohort were found to have recurrent truncating mutations of SGK1, these DLBCL were associated with TET2 mutations and significantly overlap with C4 and TET2/SGK1 and are now classified as ST2 by the NCI group (74).

C2

The hallmark of this cluster was the presence of *TP53* inactivation (122). C2 has recently been aligned with some of the DLBCL not classified in the NCI cohort, with *TP53* being the most frequently mutated gene (25%) not significantly present elsewhere within these cases

(74). Inactivation of *TP53* is associated with aneuploidy in DLBCL, a finding confirmed within the NCI cohort by the presence of gains and losses of chromosomal segments in cases with homozygous deletion or heterozygous deletion and mutation of *TP53* (74), which have now been classified as A53 (aneuploid with TP53 inactivation) (74). Biallelic inactivation of *TP53BP1*, which codes for the DNA damage sensor 53BP1 also occurs in this group with consequent increased risk of chromosomal arm gains / losses (149). The C2 cluster was also found to feature loss of 9p21.13 (*CDKN2A*) and 13q14.2 (*RB1*), with associated chromosomal instability and cell cycle disruption (122). Other abnormalities included the prognostically significant gain of 13q31.31 (*miR-17-92*) as well as the ABC associated deletion of 6q (*TNFAIP3* and *PRDM1*) and *BCL2* amplification (122, 150). The microRNA miR-17-92 regulates the expression of many genes, is intimately involved in regulation of MYC activity and overexpression in murine models drives lymphoproliferation (151, 152). These cases also frequently evolved immune escape mechanisms, commonly via inactivation of *B2M* (134). DLBCL with both ABC and GCB expression profiles were included here and generally had less favourable outcomes.

N1

This small subgroup consisting of <2% of DLBCL was described in the NCI cohort and characterised by activating NOTCH1 mutations similar to those seen in other B-NHL (74). Other lesions identified targeted regulators of B-cell differentiation such as *IRF4*, *ID3* and *BCOR* and regulators of NFκB including *IKBKB* (IκB kinase β, IKK-β) and *TNFAIP3* (A20), consistent with the highly expressed plasma cell signature that was observed (123). This group also expressed signatures of multiple immune cell types and had less favourable outcomes with RCHOP.

C0 and NEC

Genetic driver aberrations were not identified in a small cluster labelled C0, which included cases of the rare entity T-cell/histiocyte rich large B-cell lymphoma (TCRDLBCL) (122). The HMRM group report included 27% that were 'not elsewhere classified' which included many cases classified by the NCI group as N1 and some from A53, as well as 5% with no

abnormalities detected by their targeted panel (124). The NCI group originally classified 47% of their cases which increased to 63% following development of their revised classifier (74).

There was a consistent feature throughout these independent studies that some cases had few or no genetic lesions, or lesions characteristic of >1 subgroup, or novel aberrations not recurrently reported in DLBCL. Although a small number of these may have been due to sample quality or technical considerations, each study found a significant proportion of patients that did not fit into a specific genetic subtype. This means that any new classification system is still likely to have a group of patients with unclassified DLBCL. These studies have clearly moved the field forwards and identified genetically distinct entities with potential for personalised therapy, but requirements for further validation together with widely available reproducible assays are currently limiting adoption into a clinically useful taxonomy.

1.4 Microenvironment biology in DLBCL

Malignant tissues consist not only of cancerous cells but also a complex and continuously evolving tumour microenvironment (ME), comprised of immune populations, fibroblasts, stroma and endothelial cells, together with signalling molecules, and their interactions with the malignant cells (153, 154). Interactions within the tumour ME are dynamic and are generally considered to be pro-tumoral, through various mechanisms including stimulation of tumour proliferation and survival as well as facilitating treatment resistance and immune escape (153). DLBCL generally efface the normal structures of involved lymph nodes and as such have been considered less dependent on their surrounding ME for growth and survival signals than other cancers including low-grade B-NHLs (155). This is supported experimentally by the relative ease of establishment of many DLBCL cell lines in culture compared with other lymphoma subtypes (156). Each DLBCL subtype exerts different patterns of influence over their ME and this variability exists both between and within lymphoma entities, relating to the genetic lesions they harbour and the composition of infiltrating non-malignant cells, together with their arrangement in the supporting structures of the extracellular matrix (ECM), blood and lymphatic vessels. The influence of the host immune system on cancer development and progression may paradoxically be either supportive or inhibitory, a relationship described in the process of 'immunoediting' which is recognised to consist of 3 stages, elimination, equilibrium and escape (157). During development, DLBCL cells must initially survive immune elimination, with potentially lymphoma-genic events thought to be common in health but most do not progress beyond the elimination stage (158). Ultimately, to form a clinically relevant lymphoma, transformed cells must escape host immune surveillance, with increasing evidence that the ME and disrupted crosstalk with various immune cells facilitates this process as well as subsequently contributing to therapeutic resistance (153).

The potential importance of the microenvironment in DLBCL was first highlighted by the Leukaemia/Lymphoma Molecular Profiling Project (LLMPP) which defined 2 groups based on 'stromal' signatures from the non-malignant cells, occurring independently of COO, with

distinct outcomes (106). The stromal-1 signature was associated with a favourable outcome and included genes associated with ECM deposition (collagens and laminins) and remodelling (matrix metalloproteinases) as well as those associated with mononuclear phagocytes. The stromal-2 signature predicted a less favourable outcome and included genes associated with endothelial cells (von Willebrand factor and CD31) and angiogenesis.

The relevance of the immune system is also highlighted by genome-wide association studies, which have identified several susceptibility loci at pathways involved in critical immune functions (66, 67). Exposure to certain viruses which are known to negatively impact the immune system are also associated with an increased risk of DLBCL, as well as other types of lymphoma, including Epstein-Barr virus (EBV), human immunodeficiency virus (HIV) and hepatitis viruses B and C (HBV, HCV) (65). Other associations relevant to immune function are autoimmune and connective tissue disorders, which involve B-cell activation, immune suppressing drugs such as methotrexate, as well as post-transplant immunosuppression, for both solid-organ and stem cell (159). Lymphoma arising in the context of a transplant is frequently of DLBCL histology, again highlighting the critical role of immune suppression but is considered a separate entity, Post-Transplant Lymphoproliferative disorder (PTLD) (1).

Recently, a large transcriptomic analysis of multiple independent DLBCL cohorts described four ME subtypes, each with distinct cellular and pathways associations (160). In addition to the differential microenvironment composition within these four categories, each was associated with specific biological aberrations and outcome following therapy. The four MEs were termed ‘germinal centre-like’, with a similar composition to the GC, ‘mesenchymal’, with an abundance of stromal cell and ECM pathway signals, ‘inflammatory’, associated with inflammatory cells and pathways and ‘depleted’, which in contrast to the other groups had a lower presence of ME cells and signals and a high incidence of MHC class I and II negativity, and increased lymphoma proliferation. The ‘germinal centre-like’ group was associated with the best response to therapy and the ‘depleted’ with the worst, followed by ‘inflammatory’.

ME biology clearly plays a critical role in DLBCL development and response to therapy with multiple lines of evidence supporting this, however inconsistent and contradictory findings

have limited its incorporation into classification systems, with the recent successes in genomic landscape studies resulting in a shift of attention. As we shall see in this and the next section on management, the ME has importance for disease biology, prognosis and therapeutic targeting in DLBCL.

1.4.1 Immune escape

DLBCL cells have developed a number of mechanisms to escape from the host immune system and there is evidence to suggest that the efficacy of chemotherapy may in part depend on reinstating immune recognition, emphasizing the importance of this mechanism in aggressive lymphoma (161). An anti-lymphoma immune response requires presentation of a tumour antigen in the context of major histocompatibility complex (MHC) molecules expressed on the surface of professional antigen presenting cells (APC) or the malignant cells followed by T-cell activation. All nucleated cells express MHC-I and can present endogenous antigen to cytotoxic CD8 T cells (T_C) whereas APC, which include malignant B-cells as well as monocytes, macrophages and dendritic cells (DC), can present exogenous antigens to both CD4 T-cells via MHC-II and CD8 T-cells via MHC-I (162). T cell activation is a process that requires two distinct signals, the first occurs via T-cell receptor (TCR) recognition of antigen presented in the context of MHC and the second is a costimulatory signal via CD28 on the T-cell surface, usually provided by engagement of a B7 molecule (B7-1, CD80 or B7-2, CD86) on the surface of the APC (figure 1.6) (163). Following activation, T-cells undergo differentiation and expansion, however if antigen is presented without a costimulatory signal the T-cell becomes anergic and undergoes apoptosis. Immune activation in this way is tightly regulated to prevent threats from infected or malignant cells but also autoimmunity and unnecessary tissue destruction, a process involving immune regulatory cells, expression of coinhibitory receptors and checkpoints together with soluble mediators (164). T-cell activation in health and disease therefore involves complex interplay between a number of immunomodulatory signals with key activating signals also received via CD137 (4-1BB), CD134 (OX40) and CD27 and inhibitory signals through CTLA-4 (cytotoxic T-lymphocyte antigen 4), PD-1 (programmed death 1), BTLA (B and T lymphocyte attenuator, CD272), LAG-3 (lymphocyte activation gene 3, CD223) and TIM-3 (T-cell

immunoglobulin mucin-3, CD366) (165). Over 70% of DLBCL have genetic bases of immune escape, which occurs through 2 broad mechanisms - lymphoma cells can either 'hide' by evading immune detection or 'defend' themselves against immune destruction (166).

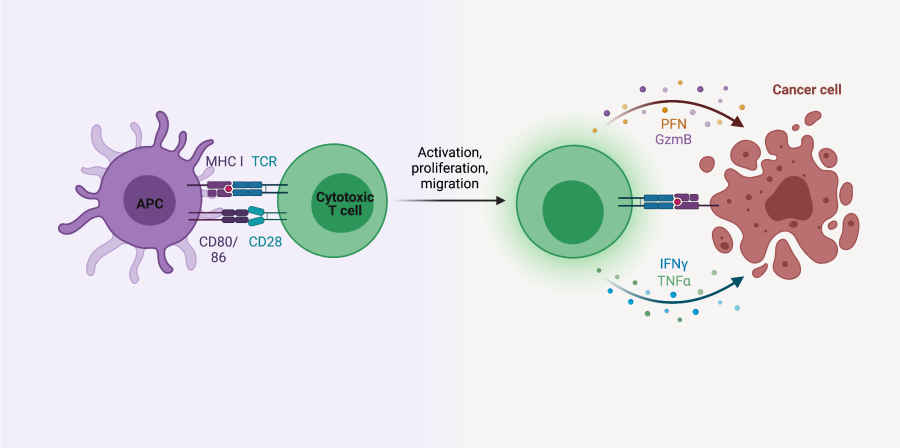

Figure 1.6 T cell activation requires two distinct signals. The first signal is mediated by antigen presented to the T cell receptor (TCR) in the context of major histocompatibility complex (MHC) molecules. The second signal is mediated via the interaction of CD28 on the T cell surface with costimulatory molecules (CD80/86). APC, antigen presenting cell; PFN, perforin; GzmB, granzyme B; IFN, interferon; TNF, tumour necrosis factor. Figure made with Biorender.

1.4.1.1 Mechanisms to hide from the immune system

A common mechanism by which DLBCL can become 'invisible' to the immune system is through attenuation of antigen presentation machinery expression, with loss of MHC-I occurring in 40-60%, in both GCB and ABC, and loss of MHC-II in 20-40%, more frequently in ABC (134, 167-169). Mutation of *B2M* is the most common cause of MHC-I disruption in DLBCL (134). Challa-Malladi et al reported that inactivating mutations/deletions in *B2M*, which is required for MHC-I assembly, frequently co-occurred with similar lesions in *CD58*, impairing the cytolytic capacity of natural killer (NK) cells, resulting in evasion from T_C and NK mediated destruction. Alterations directly affecting *HLA* genes, which in humans code for MHC molecules, also frequently accounts for MHC-I loss in DLBCL including loss of HLA-I loci at 6p21 (140). Mutations of *EZH2*, *GNA13* and *MEFD2B*, and *PTEN* deletions were significantly associated with MHC-I loss whereas deletions of *CD70* and *TP53* were

associated with MHC-I expression (140). Antigen presentation by MHC-II can be perturbed by several mechanisms, including aberrant cytoplasmic localisation, deletion of *HLA-II* loci and inactivation of MHC-II trans activator CTIIA, resulting in downregulation of MHC-II surface expression and reduced tumour immunogenicity (170, 171). MHC-II expression is epigenetically regulated by CREBBP, which upregulates *CTIIA* expression via acetylation at its regulatory sequences, with *CREBBP* mutations in DLBCL preventing CTIIA, and hence MHC-II expression (142, 143). Histone deacetylase inhibitors have been demonstrated to restore MHC-II expression in *CREBBP* mutated cell lines (172). Genetic lesions associated with ABC DLBCL including PRDM1 and *TNFAIP3* were frequently seen with MHC-II loss, consistent with MHC-II loss being more common in ABC (140, 173). MHC-II loss is also seen in GCB, with GEP data suggesting that GCB tumours with MHC-II loss were more closely related to DZ centroblasts, while those expressing MHC-II resembled LZ centrocytes (140). Within GCB cases, MHC loss was associated with a reduction in both CD4 and CD8 T cells, whereas no difference in T-cell infiltration was observed in ABC cases based on MHC expression, indicative of COO dependent effects of MHC on the ME (140). *EZH2* mutations were enriched in DLBCL with MHC-II loss, as in cases with MHC-I loss, with the likely mechanistic link repression of their respective trans-activators, *NLRC5* and *CIITA*. EZH2 mutations were shown to induce MHC deficiency and immunologically cold tumours in vivo, with EZH2 inhibition in *EZH2* mutated DLBCL cell lines restoring MHC expression (140). Consistent with the report of 39% of the EZB molecular subtype having lesions in MHC-II pathway genes (123). It is also worth noting that even when expressed, MHC-II may drive immune inhibition via interaction with LAG-3 and other immune checkpoints, which are frequently expressed on TILs, with increased expression of immune checkpoint genes observed in MHC-II positive cases (140, 166).

The B7 family molecules CD80 and CD86 can have either co-stimulatory activity via CD28, or co-inhibitory activity via CTLA-4 effects on T-cells, with a greater affinity for the inhibitory pathway (174). The B7 molecules can be expressed both by the lymphoma cells and in the ME in DLBCL with loss of CD86 associated with reduced TILs and representing a further strategy to avoid immune recognition (175). Intracellular adhesion molecule 1 (ICAM-1, CD54) is involved in cell interactions and has a key role in immune synapse formation, with

its loss reported in 7% of DLBCL and associated with decreased TILs and immune evasion (175).

1.4.1.2 Mechanisms to defend from the immune system

Lymphoma cells can defend from immune attack via resistance to apoptosis, with upregulation of BCL2 a frequent event in DLBCL that can occur via a number of mechanisms. The BCL2 family regulate the cell intrinsic pathway of mitochondrial apoptosis with both pro- and anti-apoptotic members, with BCL2 a key anti-apoptotic protein (176). Its overexpression by DLBCL cells confers a survival advantage over immune killing which was associated with inferior outcomes pre-Rituximab, and still is when found in association with MYC upregulation (88, 89). The extrinsic pathway of apoptosis activated through interactions with T and NK cells via death receptors can also be co-opted to support lymphoma survival in DLBCL. FAS (CD95) is a TNF receptor family member with the capacity to induce apoptosis in malignant cells following ligation with FAS ligand (FASL, CD95L) expressed on T_C and NK cells, via a caspase dependent mechanism (177). This process is of physiological importance during affinity selection in the light zone of the GC for those B-cells not selected (178). Inactivating mutations of FAS occur in 20% of DLBCL, with increased frequency in cases with extra-nodal involvement and association with the BN2, C1 and NOTCH2 clusters, facilitating escape from immune induced apoptosis (166). It is also reported that DLBCL can express FASL, by which they can trigger apoptosis in FAS expressing cytotoxic immune cells and is an adverse prognostic marker (179).

DLBCL may also utilise the expression of inhibitory ligands to control immune responses in their favour, with MYC expression known to induce inhibitory checkpoints (180). The PD-1/PD-L1 axis is an immune checkpoint which functions to regulate the balance between T-cell activation, self-tolerance and autoimmunity, which delivers an inhibitory signal resulting in T-cell anergy/exhaustion (181). Corruption of this pathway can facilitate immune escape. PD-L1 is known to be expressed in DLBCL by both the lymphoma cells and immune cells in the ME, whereas PD-1 expression is generally restricted to the non-malignant, T-cell compartment (182). Genetic aberrations involving the PD-L1 locus have been described in 10-27% of DLBCL, with the Ig locus and CIITA common partners resulting in overexpression, but the overall contribution of this pathway to disease biology remains unclear and the

efficacy of checkpoint inhibitors in early phase clinical trials have been modest (183-186). The C1 cluster was noted to have 20% of cases with gains, amplifications and translocations of the *PD-L1/2* locus associated with upregulation, consistent with the association of PD-L1 expression with non-GCB DLBCL (122, 182). Cases with PD-L1 aberrations have also been reported to associate with downregulated MHC but increased presence of TILs, NFκB activation and higher relapse rates (186).

CD47 is a ubiquitous transmembrane protein known to interact with monocytes, macrophages and DC via signal regulatory protein α (SIRPα) to form an innate immune checkpoint, delivering an inhibitory, anti-phagocytic signal (187). Expression of CD47 is reported in DLBCL and associates with worse outcome, constituting an interaction with the myeloid ME that could contribute to Rituximab resistance by suppressing phagocytic activity (188). Currently there are a number of promising innate checkpoint inhibitors in development to target this mechanism in DLBCL and other cancers, which may act synergistically with Rituximab and other monoclonal antibodies (mAb) (187-189). In addition to induction of phagocytosis, blocking of this innate checkpoint pathway can also facilitate antitumour T-cell responses through presentation of lymphoma antigens following phagocytosis (190).

1.4.2 Microenvironment composition

DLBCL typically arise in lymphoid tissues and hence the composition of the ME is usually representative of the remaining underlying lymph node structure and despite the frequent presence of immune populations, they do not eradicate the lymphoma cells but rather exert a regulatory or suppressive effect over the immune response (155). During lymphoma development an immunosuppressive ME is induced to promote lymphoma growth and further facilitate immune escape mechanisms intrinsic to the malignant cell. This process occurs via a number of strategies including suppressive cell populations, ME expression of inhibitory checkpoints and excretion of soluble signalling proteins known as cytokines.

1.4.2.1 Peripheral blood monocytes and lymphocytes

A number of retrospective studies have shown that pre-treatment absolute monocyte and absolute lymphocyte counts (AMC and ALC) provide independent prognostic information at both diagnosis and relapse (191-193). These studies have employed the full blood count (FBC) to assess the AMC and ALC as surrogate markers of the ME and immunity with higher AMC and lower ALC at diagnosis associated with worse outcome after therapy, in both the pre- and post-Rituximab era. Although a detailed understanding of the underlying mechanism is lacking, myeloid cells play a critical role for innate immunity and regulation of T-cell responses by bridging innate and adaptive response. Expansion of circulating myeloid-derived suppressor cells (MDSC) of monocytic origin have been identified in DLBCL and linked to T-cell suppression and outcome (194, 195). These suppressive myeloid cells have reduced HLA-DR (MHC-II) expression with consequent effects on antigen presentation and are thought to develop in response to IL-10 of malignant B-cell origin (196). MDSC mediated suppression has been linked to IL-10 release, PD-L1 expression and modulation of amino-acid metabolism, as well as correlating with circulating regulatory T cells (T_{regs}) (194). In-vitro work has also demonstrated that co-culture of monocytes with DLBCL cells results in proliferation, enabling prolonged B-cell survival (197), with evidence to suggest direct cell contact was important, and that the addition of B-cell activating factor of the TNF family (BAFF) and IL-2 (interleukin-2) enhanced this proliferative effect. Monocytes from NHL patients have also been demonstrated to have impaired innate and adaptive immune stimulatory functions (195). Taken together these studies support impaired innate immunity in DLBCL and highlight a level of dependency on signals from the myeloid ME, however this aspect of ME biology remains understudied (198). Although low ALC has been consistently associated with worse outcomes there are only limited data attempting to explore this aspect of ME biology. A reduced percentage of CD3 T-cells compared with healthy donors has been reported and low CD4 T cell counts have been associated with poor prognosis (199, 200). There have been contradictory reports on the levels of circulating immunosuppressive T_{regs} in DLBCL and their relevance to prognosis (200-203).

1.4.2.2 Tissue macrophages

Monti et al performed GEP on a large cohort of newly diagnosed DLBCL, reporting variable expression of macrophage genes between different disease subsets, and while this did not predict survival it reinforced the expression profile heterogeneity in DLBCL and relevance of the ME (204). Several groups have employed immunohistochemistry using CD68 as a target for macrophage identification in diagnostic biopsy specimens. Work from our own laboratory did not find any relation between CD68 staining and outcome (205) and results from other groups have been inconsistent (206), perhaps reflecting differences in methods and patient populations. Other groups have employed additional markers - including HLA-DR, CD163 and SPARC - to define subsets of tumour-associated macrophages (TAM) with variable results (207-209). Recently the German high grade NHL study group published a lymphoma-associated macrophage interaction score based on GEP applicable to FFPE biopsies which had a prognostic impact in their cohort (210). An interesting observation by Riihijarvi et al was that an increase in TAM in diagnostic samples, as measured by CD68, predicted poor outcome in patients treated with chemotherapy alone, but that the opposite was seen in patients with the addition of Rituximab to chemotherapy (211). Although the precise in-vivo mechanism of action for Rituximab in not known, experimental data supports a prominent role for antibody-dependant cellular cytotoxicity (ADCC) of innate immune cells, including monocytes and macrophages, via engagement of their FcγR with opsonised B-cells, resulting in phagocytosis (212-214). It has also been reported that lymphoma patients harbouring a polymorphism in FcγRIIIa (CD16a) - an Fc receptor expressed on NK cells, monocytes and macrophages which is important for ADCC – which results in a higher affinity receptor, have improved responses to Rituximab (215, 216). Negative regulators of phagocytosis such as the CD47-SIRPα axis and adenosine, are known to impair ADCC and hence Rituximab activity (217). Induction of an adaptive T-cell response against tumour antigens following presentation by APC including macrophages may play a critical role in long term disease control following anti-CD20 therapy. These observations would support the hypothesis that Rituximab can influence the prognostic impact of TAM in DLBCL.

Interestingly, unpublished data from our laboratory has also identified highly differential transcriptomes between macrophages isolated from DLBCL specimens and reactive tissues,

and that macrophage depletion in a murine model of aggressive B-cell lymphoma reduced tumour volume, further supporting the rationale to explore the myeloid ME in DLBCL.

1.4.2.3 Tumour infiltrating lymphocytes

A recently published study interrogating the DLBCL tissue ME with GEP and IHC reported that the proportion of T-cell infiltration did not associate with survival and as with previous studies, lymphoma expression of HLA-I and -II associated with an increased T-cell infiltrate (154). They also observed significant heterogeneity within T-cell phenotypes, with a higher proportion of immune checkpoint positive T-cells associating with poor outcome, especially with a high proportion of TIM-3, LAG-3 and PD-1 positive T-cells, with TIM-3 positivity an independent predictor of survival (154). Infiltration by Tregs was frequent in a subset of cases but their impact on outcome could not be validated. A previous study assessing TILs by flow cytometry on fresh lymphoma tissue identified an increased CD4 T infiltrate as a good prognostic factor, with a subsequent study by this group employing ratios of immune effector cells as prognostic factors (218, 219). A further study also confirmed the importance of immune checkpoint expression in the T-cell compartment finding that LAG-3 high TILs were a negative prognostic factor and enriched for PD-1 and TIM-3 expression. IHC data from our lab found that increased density of CD3 and FOXP3 (forkhead box P3, T_{reg} marker) staining were both markers of improved outcome in RCHOP treated patients (205). Overall, published studies to date have consistently highlighted the importance of TIL signatures but have found inconsistent results with the identification of specific phenotypes and / or functional subsets, such as exhausted T-cells expressing multiple inhibitory checkpoints, likely key to improved understanding.

1.4.2.4 Cytokines

Cytokines are small signalling proteins secreted by immune cells to communicate, mediating many of the bidirectional interactions between lymphoma cells and the ME, with levels of various cytokines found to be upregulated and associated with outcome in DLBCL (220-223). Common polymorphisms in *TNF* and *IL-10* have been identified as susceptibility loci for risk of DLBCL, suggesting a key role for immune signalling in lymphoma development (224, 225).

Cytokines may be secreted by DLBCL cells directly or from the ME cells both within the tumour site and at distant sites, with potent immunomodulatory effects on both the lymphoma and immune function. IL-10 is a multifunctional immunosuppressive cytokine which has been associated with MDSC development and function in DLBCL, induction of T_{regs} to support immune tolerance and stimulates B-cell growth and differentiation, all with the potential to enhance lymphoma survival (196, 223). High levels of IL-10 at diagnosis are linked to higher AMC and worse outcomes (196, 223). Increased TNFα levels are also found in DLBCL and associated with outcome (221). It is an immunostimulatory cytokine which plays a role in a number of inflammatory disorders and tumour promotion. IL-6 is a potent growth factor for B-cells and has been shown to promote MYC driven lymphomagenesis in murine models with increased serum levels associating with poor outcomes (221, 226). Finally, TGFβ is a T-cell suppressive cytokine expressed by lymphoma cells that induces an exhausted T-cell phenotype with high inhibitory checkpoint molecule expression, T_{reg} differentiation and impairment of monocyte antigen presentation (163, 227). TGFβ is a key suppressive molecule secreted by T_{regs} but can also inhibit lymphoma growth through effects on proliferation and apoptosis, with some lymphomas known to acquire resistance to its effects (228). TGFβ therefore has both the potential to restrict and promote lymphoma growth with no clear prognostic impact identified (166).

1.5 Management of patients with DLBCL

DLBCL is a curable disease. The addition of Rituximab to the anthracycline containing CHOP backbone has improved outcome across all measures, with the benefit maintained over extended follow-up such that approximately 60-65% of patients with be cured with frontline therapy (68, 229-231). Real world data from our own experience and that reported by the HMRN is consistent with this picture. As we have seen with the clinical prognostic scores, there is great heterogeneity in outcome in DLBCL but there is currently no reliable method to select the highest risk patients not destined to gain benefit from RCHOP. Several attempts have been made to improve outcomes by increasing dose and time intensity of chemotherapy delivery without clear benefit (232-235). Several retrospective studies from the Nordic groups have reported improved outcomes in younger patients with the addition of etoposide to standard therapy (RCHOEP), but randomised data are lacking (236-238). The GELA (Groupe d'Etudes des Lymphomas de l'Adulte) reported a randomised phase 3 trial comparing the intensified regimen RACVBP (Rituximab, Doxorubicin, Cyclophosphamide, Vindesine, Bleomycin, Prednisolone) with RCHOP in younger patients with 1 IPI factor, which demonstrated superiority over RCHOP at the cost of increased toxicity and their reported outcomes with RCHOP were in the lower range of those expected (239). Both RCHOEP and RACVBP are included as options for younger patients in the most recent ESMO (European Society for Medical Oncology) guidelines but have not been adopted in UK practice (75). A phase 3 trial of the infusion-based regimen dose-adjusted REPOCH, containing the same agents as RCHOEP, demonstrated no benefit over RCHOP (240). The recently reported UK phase 2 trial of the dose and time intensive regimen R-CODOX-M / R-IVAC (Rituximab, Cyclophosphamide, Vincristine, Doxorubcin, Methotrexate / Rituximab, Ifosfamide, Etoposide, Cytarabine) in patients with IPI scores 3-5 demonstrated a 2 year progression free survival of 68% comparing favourably with historical RCHOP data in this group however toxicity, especially in patients >50, and requirement for prolonged hospital admission will likely limit its use outside selected patients (241). Taken together these studies suggest that there is little to be gained from increasing dose and time intensity of conventional chemotherapy in DLBCL.

A number of attempts have also been made to incorporate novel agents into frontline therapy based on biologically actionable insights and efficacy in the relapse setting, but again without demonstrating superiority over standard therapy (118, 242-244). Addition of an alternative anti-CD20 mAb, Obinutuzumab, to CHOP demonstrated almost the same outcomes as with Rituximab, with increased adverse events reported with novel antibody (242, 245). The addition of Bortezomib, a proteosome inhibitor targeting the NκFB pathway, to RCHOP in the REMoDL-B study also failed to demonstrate benefit over RCHOP, including in the ABC subtype as defined by GEP, who were confirmed to have activation of the NκFB pathway (118). Targeting of the BCR with the BTK inhibitor Ibrutinib in combination with RCHOP in ABC DLBCL also failed to demonstrate benefit over RCHOP in the frontline setting, with a subgroup analysis suggesting benefit in younger patients (244). The immunomodulatory drug Lenalidomide (Revlimid) is known to have multiple effects on both the cellular and cytokine ME, activating NK and T-cell antitumour responses, down regulating pro-tumour cytokines and enhancing Rituximab activity, as well as direct anti-tumour activity, with single agent efficacy in relapsed DLBCL (246, 247). It has also been reported to have preferential activity in the ABC subtype with a small phase 2 study reporting feasibility of combination with RCHOP (R2CHOP) and abrogation of the negative impact of the non-GCB phenotype, as assessed by IHC, compared with database controls (248). However, a subsequent phase 3 trial comparing R2CHOP with RCHOP in untreated ABC subtype patients, as defined by GEP using a Nanostring platform, failed to meet its primary end point with equivalence in PFS (243). Lenalidomide has also been studied in the maintenance setting for older patients responding to RCHOP, where 24 months of Lenalidomide was compared to placebo, with a PFS but no OS benefit demonstrated, at the cost of increased toxicity (249).

Therefore, despite considerable efforts and incorporation of novel agents with efficacy in the relapse setting, there has been no improvement on first-line treatment of DLBCL with RCHOP, which remains standard of care in the UK. In certain situations, additional therapy is recommended for CNS prophylaxis and radiotherapy (RT) to specific sites (e.g., bulk) as well as combined modality abbreviated RCHOP and involved field RT (IFRT) for early-stage non-bulky disease (69, 250). For patients not considered fit enough for RCHOP, dose modified immunochemotherapy or substituting the anthracycline for Gemcitabine are options (251,

252). It seems likely that either incorporation of biological insights beyond the COO into patient stratification, or new combinations based on the RCHOP-X strategy, will be required to improve frontline results. However, if robust methods to identify the highest risk patients can be developed, moving away from RCHOP in a subset of patients, to entirely novel combinations based around immunotherapy may be appropriate.

1.5.1 Management of patients with relapsed / refractory DLBCL

Approximately 10-15% of patients will progress either during or very shortly following initial therapy with up to a further 20-30% relapsing after a period of remission (69). Progressive disease occurs early in DLBCL, with time to relapse prognostic and event free survival at 24 months (EFS24) clinically relevant, with those achieving EFS24 having comparable survival to age and sex matched controls (253, 254). Late relapses do occur but are infrequent and a significant subset of these patients present with low-grade histology highlighting the need for repeat biopsy at relapse (255). For patients fit enough, the current standard of care at relapse remains re-induction with intensive non-cross resistant chemotherapy followed by high-dose chemotherapy and autologous stem cell transplant (ASCT) in chemo-sensitive patients (253, 256). Consistent with the requirement to demonstrate chemo-sensitivity prior to ASCT, the pre-transplant PET/CT is highly predictive of outcome (257, 258). The randomised CORAL study found no difference between 2 commonly employed re-induction regimens, with a subgroup analysis indicating that RDHAP (Rituximab, Cisplatin, Cytarabine, Dexamethasone) may be more effective in GCB DLBCL (253, 259). The LY12 study showed non-inferior results with RGDP (Rituximab, Gemcitabine, Dexamethasone, Cisplatin) compared with RDHAP, with less toxicity (260). Although responses to re-induction chemotherapy are lower in the Rituximab era, patients who relapse >12 months after RCHOP and those with chemo-sensitive disease still gain similar benefit from ASCT as Rituximab naïve patients (253, 261). Attempts to improve re-induction strategies including addition of Ofatumumab to chemotherapy and maintenance Rituximab post ASCT have failed to improve outcomes (253, 262). Currently, only in the region of 10% of patients relapsing post RCHOP will gain long-term disease free survival following conventional approaches with re-induction followed by ASCT, with many patients not considered fit

enough, not demonstrating chemo-sensitivity or progressing post-transplant (figure 1.8) (263).

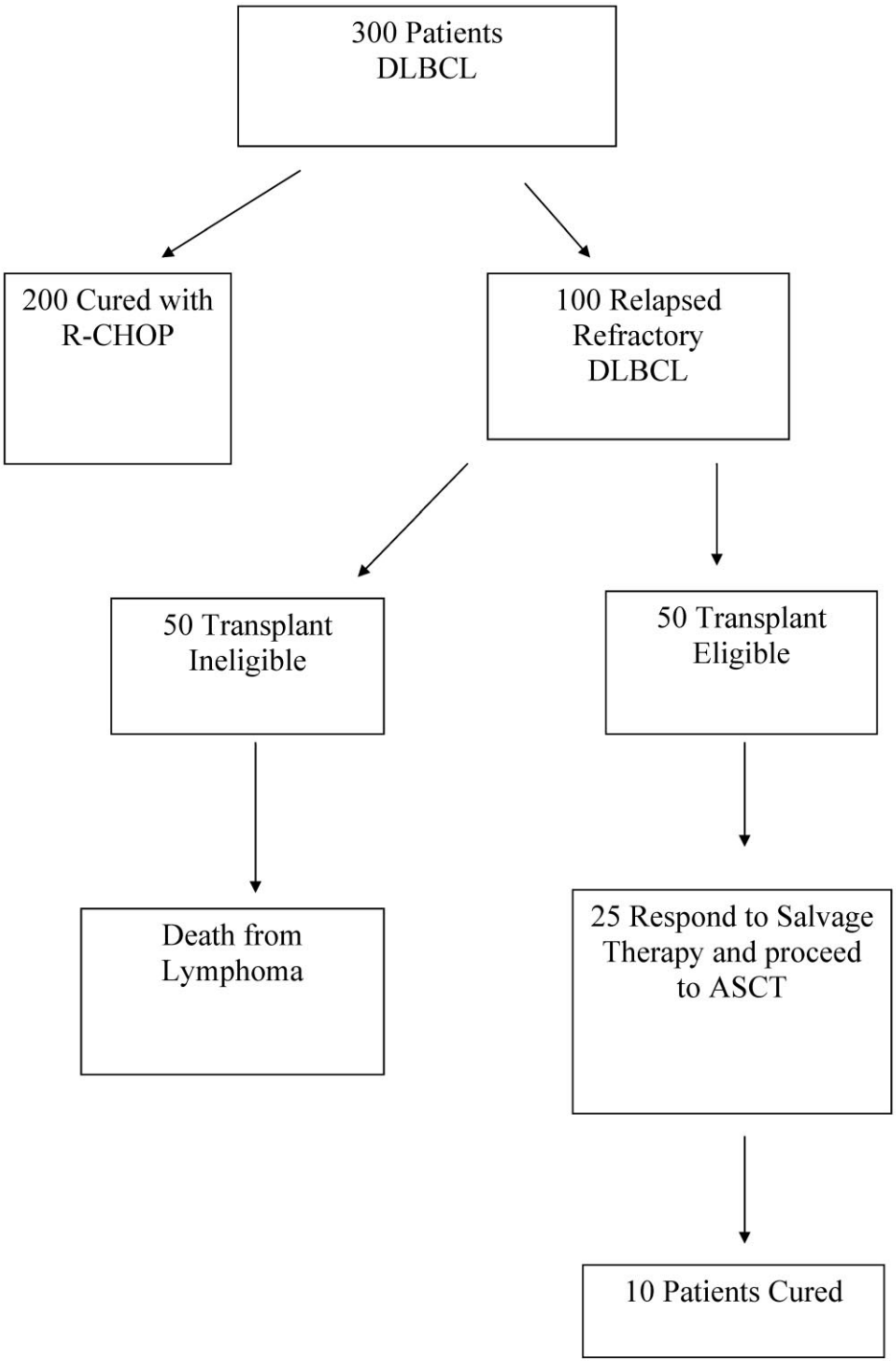

Figure 1.8 Limited role of autologous stem cell transplant (ASCT) in the rituximab era. Only in the region of 10% of relapse patients will be cured with conventional approaches. Figure from Friedberg 2011 (263).

1.5.1.1 Chimeric antigen receptor T-cells (CAR-T)

For patients not responding to re-induction chemotherapy, outcomes are poor with conventional approaches (264, 265). A pooled analysis of several studies in relapse / refractory NHL, the SCHOLAR-1 study, reported that median OS for patients with chemo-resistant disease at relapse was 6 months and only 20% were alive at 2 years (266). In the past selected patients with a matched donor, refractory to re-induction or relapsing post-ASCT, were considered for allogeneic stem cell transplant, with some gaining long-term benefit (267-269). However, in early 2019 NICE (www.nice.org.uk) approved the use of chimeric antigen receptor T-cells (CAR-T) for patients with DLBCL progressing after 2 or more lines of therapy and those relapsing after stem cell transplant, and this is now the standard approach for this situation. CAR-T cells are adoptive cellular therapy produced from apheresis collected autologous T-cells, which are genetically engineered to express CAR constructs. The construct consists of an extracellular tumour antigen binding receptor (anti-CD19) to facilitate non-MHC restricted target recognition, a hinge region, a transmembrane domain and an intracellular costimulatory / TCR signalling domain to activate cell signalling (figure 1.9) (270). Data from 2 pivotal studies of CAR-T therapy in refractory DLBCL led to its approval, with remarkable response rates in patients with expected poor outcomes with conventional approaches (271, 272). The ZUMA-1 study included PMBL and transformed FL as well as DLBCL patients and reported an ORR of 82% in 101 patients with complete responses (CR) in 54% and OS at 18 months of 52% with axicabtagene ciloleucel (271). The updated results show that median OS was not reached, and 2-year survival was >50% suggestive of long-term disease control (273). The JULIET study reported similarly impressive results with 40% CR and high rates of durable responses with tisagenlecleucel (272). It is worth noting that although applicable to some patients not considered fit enough for intensive chemotherapy, CAR-T cell therapy is associated with a unique set of complications including cytokine release syndrome (CRS) and immune effector cell associated neurotoxicity syndrome (ICANS) which require in-patient hospital management.

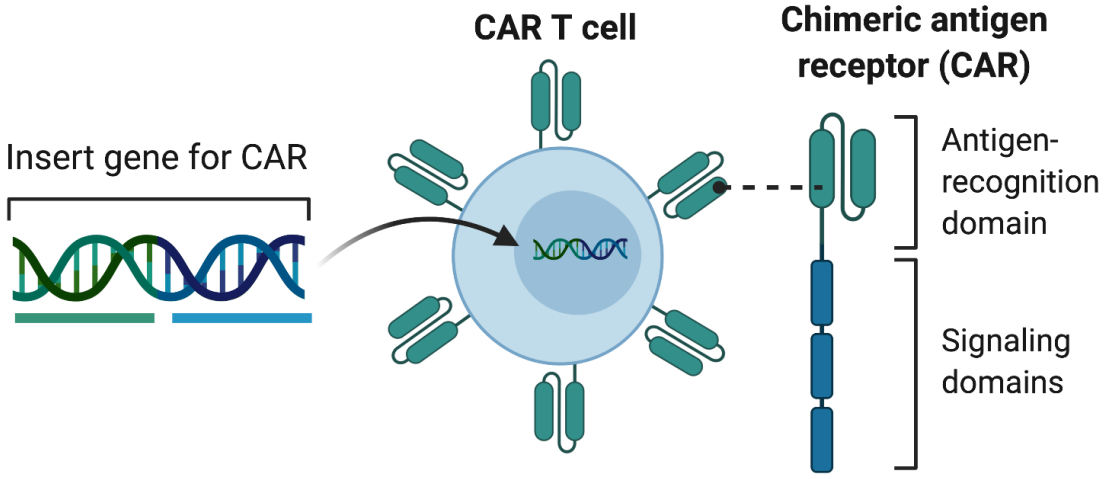

Figure 1.9 Schematic representation of a chimeric antigen receptor (CAR) T cell. Figure made with Biorender.

1.5.1.2 Relapse in unfit patients

For those patients with relapsed disease not considered fit for ASCT options were fairly limited until recently. One strategy involved use of a reinduction regimen delivered predominantly as an out-patient and associated with less toxicity, but without consolidation ASCT. This would include regimens such as RGDP or RGEMP, which incorporates methylprednisolone over the dexamethasone in RGDP (260, 274). Other options include Gemcitabine and Oxaliplatin combinations, single agent Pixantrone or purely palliative approaches but whatever the approach expected outcomes were very poor (275, 276). The recent approval, however, of the antibody-drug conjugate (ADC) Polatuzumab, which targets the BCR component CD79b, in combination with the alkylating agent Bendamustine and Rituximab (PolaBR) has improved the outlook for ASCT ineligible patients, with reported CR rates of 40% and median OS >12 months (277). Polatuzumab consists of an antibody with specificity for CD79b covalently linked to a cytotoxic microtubule disrupting drug called MMAE (monomethyl auristatin) which is released following internalisation into the target

cell. Patients receiving PolaBR would then be potentially eligible for CAR-T cell therapy at progression, if deemed appropriate.

1.5.2 Novel approaches in development

There are several novel agents in development for DLBCL therapy which have shown great promise, many of which target or modulate the immune system shifting the paradigm from cytotoxic chemotherapy. It is likely that some of these agents will gain approval in the relapse setting in the near future and may be incorporated into novel combinations for frontline trials.

Targeting CD19

CD19 is a highly expressed target on DLBCL as well as normal B-cells and continues to be expressed post anti-CD20 mAb therapy in the relapse setting, as demonstrated by the success of CAR-T cells against CD19. Tafasitamab is a humanised CD19 directed mAb with an Fc domain engineered to reduce affinity for the inhibitory FcγRIIa (CD32) and increase affinity for the stimulatory FcγRIIIa (CD16) on immune effectors, resulting in more potent ADCC (278). A recent phase 2 study of Tafasitamab in combination with Lenalidomide in patients with relapsed DLBCL not eligible for ASCT reported a 43% CR rate with median PFS of just over 12 months and a number of durable responses (279). This agent is currently being explored in the relapse setting with BR and frontline in combination with RCHOP +/- Lenalidomide (280). Loncastuximab is an ADC consisting of a humanised anti-CD19 mAb with a cytotoxic pyrrolobenzodiazepine dimer attached (281). A phase 2 study reported response rates of 45% and it is currently being investigated in combination with other agents in the relapse setting (280). A number of CAR-T cell strategies targeting CD19 are also in development with the aims of reducing toxicity and increasing activity (282-284).

Targeting CD20

Bispecific antibodies link 2 antibody fragments, resulting in dual specificity for targets on both lymphoma and T-cells in the ME, bringing immune effectors into proximity with the malignant cell and stimulating cytotoxicity and cytokine release. Mosunetuzumab is one such bispecific T cell engager (BITE) which binds both CD20 (lymphoma) and CD3 (T-cell) and has demonstrated efficacy in the relapse setting including relapse post CAR-T cell therapy with response rates of 37% and CR rates approaching 20% (280, 285). It is currently being trialled in newly diagnosed elderly patients unfit for chemotherapy and updated results are awaited. Another BITE currently in development is Glofitamab, which also targets CD20 and CD3, but in a '2:1' ratio so that it has two CD20 binding moieties and one for CD3 as well as a modified structure to extend its half-life (285). It has been safely combined with anti-CD20 mAbs to mitigate toxicity and has shown promising results in heavily pre-treated patients. Odronextamab, previously known as REGN1979, is a third BITE being studied which also targets CD20 and CD3, and has shown efficacy and tolerability in relapsed DLBCL, including those patients previously treated with CAR-T cell therapy (280). Finally, Epcoritamab is a subcutaneous BITE targeting CD20 and CD3 which can induce potent T-cell mediated cytotoxicity in DLBCL with a favourable safety profile also in development (286). Bispecific CAR-T cells targeting CD20 as well as CD19, to overcome antigen loss as a mechanism of resistance are under investigation (280).

Targeting CD79b

As discussed above, the ADC Polatuzumab is currently licensed for relapsed patients not suitable for reinduction chemotherapy and has also been used in the UK as a bridging therapy for patients proceeding CART-T cells. It is now being studied in the relapse setting in combination with anti-CD20 mAbs and Lenalidomide as well as frontline in a phase 3 trial with RCHOP versus standard RCHOP, which has now completed accrual with results awaited (285).

Targeting CD47

The innate immune checkpoint pathway mediated by the interaction of CD47, expressed on DLBCL as well as many other tumours, and SIRPα expressed on monocytes and macrophages, is the dominant 'don't eat me' signal employed by normal cells to avoid phagocytosis but co-opted in malignancy. Magrolimab is a humanised anti-CD47 mAb that induces macrophage phagocytosis by releasing the block on this pathway and has demonstrated clinical activity in DLBCL in combination with Rituximab, which provides a positive 'eat me' signal, with updated results reporting response rates of 36% with durable responses seen (189, 280). It was safely combined with other agents and well tolerated with anaemia as the main side effect, which was expected given red cells express CD47.

Targeting the BCR pathway

Although inhibiting the BCR with Ibrutinib did not show a clear benefit in frontline therapy in combination with RCHOP, some patients with DLBCL do gain benefit and alternative combinations may prove more fruitful (244). As well as inhibiting the BTK, Ibrutinib also has activity against ITK (IL-2 inducible kinase) which can promote T helper type 1 (TH1) expansion and an antitumour immune response (287). It is currently being investigated with Rituximab and Lenalidomide (IR2), which has shown impressive activity in relapsed non-GCB DLBCL with response rates in the region of 65%, some of which were durable (288). IR2 has also show activity in untreated DLBCL where initial chemo-free treatment with IR2 followed by chemotherapy has resulted in impressive responses in high-risk patients (280).

Targeting BCL2

As we have seen, the BCL2 antiapoptotic protein is overexpressed in up to 30% of DLBCL, where in association with concomitant MYC expression (DEL) it confers worse outcome (89). Venetoclax is a highly selective inhibitor of BCL2 which is currently licensed in chronic lymphocytic leukaemia (CLL) and acute myeloid leukaemia (AML). It has efficacy in patients with relapsed disease and has shown high response rates in combination with RCHOP, with most DEL cases achieving CR, with further investigation ongoing (289).

Targeting epigenetic pathways

DLBCL patients harbour frequent mutations across many epigenetic controls and disruption of these pathways have been implicated in therapeutic resistance as well as immune evasion (290). For example, DNA methylation constitutes one of the main epigenetic pathways and abnormal patterns of methylation, particularly targeting key genes such as *BCL6*, *EZH2* and *MYC*, occur in DLBCL and are associated with worse survival (291). Abnormal methylation patterns influence chemoresistance through dysregulated control of genes involved in cell cycle, DNA repair and apoptosis, and restoring normal methylation patterns can restore chemosensitivity (290). The DNA methyltransferase (DNMT) inhibitor 5-Azacytidine can reverse aberrant methylation induced chemoresistance and has been investigated in combination with RCHOP in DLBCL with high CR rates (292). We have already seen that activating EZH2 mutations occur recurrently in DLBCL, being a seed for one of the genetic subtypes, cooperate with BCL6 activity and are linked to loss of MHC expression (123, 140, 293). EZH2 mutations have therefore been considered to uncouple GCB cells from the normal selection process facilitating growth and survival independent of antigen affinity (294). EZH2 inhibitors have demonstrated activity in restoring MHC expression in experimental work and combinations with other agents are in clinic development, and while responses are more frequent in mutated cases, they also occur in unmutated disease (140, 294). Inactivating mutations in the histone acetyltransferase CREBBP also occur recurrently, with reduced acetylation and resultant gene silencing facilitating immune escape and promoting lymphoma development in cooperation with BCL2 overexpression (142). This has led to trials of epigenetic modulation with histone deacetylase (HDAC) inhibitors, to restore expression of CREBBP regulated genes and hence immune responses, with pre-clinical data to suggest combination with checkpoint blockade (e.g., PD-1/PD-L1) may be successful (294). HDAC inhibitors are also currently under investigation in combination with chemotherapy across various trials in an attempt to circumvent chemoresistance (290). Epigenetic modifiers are therefore rational partners for both chemotherapy and immunotherapy in DLBCL therapy.

Allogeneic CAR-T cells

In order to reduce the manufacturing time currently required to produce CAR-T cells and improve T-cell fitness compared with current autologous T-cells, which may have been exposed to cytotoxic agents, and provide economic advantages, premanufactured allogeneic CAR-T cells are under study. There is evidence from patients previously in receipt of an allogeneic stem cell transplant with subsequent relapse, then treated with CAR-T cells, that donor-derived T-cells are effective with minimal graft versus host disease (GVHD) (295). Potential complications of an allogeneic product would be rejection due to HLA mismatching and GVHD. Genetic engineering techniques have used to produce allogeneic T cells expressing a CAR but with HLA expression knocked out (296).

Concluding remarks on novel approaches

A number of therapies have shown remarkable activity in patients with advanced disease, but as with CAR-T cell therapy potentially face a number of challenges to maximise success and improve outcomes. CAR-T cell efficacy is currently negated by T-cell exhaustion and immune evasion, antigen loss and lack of persistence, with at least half of patients treated not gaining long term benefit. Although manageable in most patients, toxicities of CAR-T cells can also limit their use together with excessive costs. Many of these limitations will apply to other immunomodulatory strategies being developed. It is likely that combination with other novel agents to overcome some of these issues or with chemotherapy earlier during the disease course will be result in improved efficacy. Sequencing of therapies will also be a challenge, as efficacy of certain agents may be impaired after failure of another with the same target. Other potential issues include understanding and abrogating the unique side-effects, which are very different from conventional cytotoxic drugs, determining appropriate combinations based on biology and mechanisms of resistance, as well as the development of predictive biomarkers and health economic restraints. The future outlook has significantly improved over recent years for patients with DLBCL not cured by RCHOP, which may soon come under threat as the standard of care, with trials incorporating additional agents such as Polatuzumab yet to report, but there remains much work still to be done.

1.6 Mass cytometry and imaging mass cytometry

Mass cytometry (MC) and imaging mass cytometry (IMC) are relatively recently developed techniques using CyTOF (cytometry by time of flight) technology to study cell suspensions and solid tissue architecture respectively. MC shares many features with traditional fluorescence-based cytometry (FC) in single cell analysis, however instead of fluorophores MC utilises stable isotopes of rare earth metals coupled with antibodies as reporters of protein expression, which are detected and quantified by the CyTOF mass cytometer (297). The CyTOF is an adaptation of an inductively coupled plasma mass spectrometry (ICP-MS) detection system. Samples are vaporised one cell at a time in a high temperature plasma, creating an elemental ion cloud which is detected and analysed to reveal the relative abundance of each isotopic reporter. Heavy metal isotopes give discrete atomic mass readouts allowing many more parameters to be measured simultaneously without the concern of spectral overlap seen with FC (298). Since the isotopes used as reporters rarely occur in biological tissues and laboratory environments there is little background signal analogous to auto fluorescence (299).

Until recently MC technology had only been applied to cell suspension samples. IMC was developed to couple immunohistochemistry (IHC) methods with MC based high-resolution laser ablation to facilitate highly multiplexed tissue imaging with spatial information (300). Tissues are stained using an adapted IHC workflow with antibodies tagged with metal isotope reporters. A region of interest (ROI) on the stained slide is then laser ablated in a Hyperion imaging system (Fluidigm) and the resulting ion cloud, corresponding to a single laser shot, is detected and analysed. IMC allows interrogation of multiple protein markers in tissue sections at cellular and subcellular resolution (approximately $1\mu m^2$) while preserving tissue architecture and cell morphology. Nuclear stains and membrane counter stains facilitate cell boundary definition and segmentation. A data matrix is produced which can be used to generate false-colour images in which several markers can be viewed simultaneously in different colours. A number of analysis tools are available or in development to facilitate single cell and spatial analysis from tissues analysed with IMC (301, 302). Both MC and IMC will be used in this work.

1.7 Summary and hypothesis

A number of lines of evidence including disease associations, susceptibility loci, GEP studies, recurrent genetic lesions, the prognostic nature of PB immune cell counts and the success of many immune targeting / modulating approaches, all suggest that the non-malignant immune ME is critical to DLBCL development and outcome following therapy. Currently the major unmet needs include improved patient stratification at diagnosis, a clinically actionable sub-classification, predictive biomarkers, improved outcome following frontline therapy, novel options for those patients not fit enough for RCHOP and better outcomes for those with relapsed disease, all while minimising toxicity. Although great progress has been made across many of these needs, improved understanding of disease biology will be key to further advancement.

It is known that PB immune cell populations vary enormously between individuals but are remarkably stable within healthy individuals (303). Despite this, the simple metrics of AMC and ALC have repeatedly been shown to be prognostic in DLBCL, yet interpretation of individual features can be difficult, with variation across immune populations and signalling proteins often coordinated. Therefore, understanding the system in a more complete way is likely key to identifying relevant patterns associated with disease and response to therapy. This work will focus primarily on the PB immune compartment in DLBCL to perform comprehensive immune monitoring at diagnosis. We will also develop novel methods to facilitate the interrogation of diagnostic tissue biopsies with relevance to the ME based on our immune monitoring work.

We hypothesise that detailed study of the ME immune populations in DLBCL will reveal key insights into the immune system at the population, single-cell and signalling protein levels, and provide key insights into the mechanism of the prognostic significance of the AMC and ALC as well as the influence of the ME on disease biology and response to therapy. Ultimately, we aim to develop immune signatures associated with both disease and outcome with translational relevance to patient stratification and targeted therapy.

2. Materials and Methods

2.1 Human samples and clinical data

2.1.1 Ethics statement

All human blood and tissue samples used in this work were collected from patients prior to receiving any treatment are detailed in the relevant chapter. Samples were accessed under approval from the London Research Ethics Committee (LREC) of east London and the city health authority for the study 'the impact of the tissue microenvironment and immune system on haematological malignancies' (05/Q0605/140). All patients gave written informed consent according to the Declaration of Helsinki and blood and tissue suspension samples were collected and stored by the Barts Cancer Institute (BCI) tissue bank team.

2.1.2 Healthy donor peripheral blood mononuclear cells (PBMCs)

Human leucocyte cones produced during apheresis platelet donation by anonymous healthy blood donors were obtained from the National Health Service blood and transplant (NHSBT). All donors gave informed consent and cones were received by the transfusion laboratory at St Bartholomew's hospital (Barts). PBMCs were isolated by density gradient centrifugation using Lymphoprep (Stemcell technologies) as per manufacturer's instructions. Briefly, cones were cut open at both ends and inserted into a 50ml falcon tube, the blood product was pushed through the cone by injection of air followed by rinsing with phosphate buffered saline (PBS). The blood product was made up to 50ml in PBS and mixed thoroughly. Lymphoprep was then added in 5ml aliquots to 5 x 15ml falcon tubes, followed by 10mls of the blood product PBS mix such that it layered on top of the Lymphoprep with minimal mixing. The 5 x 15ml falcons were then centrifuged at 1500 revolutions per minute (rpm) for 30 minutes at room temperature (rt) with slow acceleration / deceleration. Following centrifugation, the buffy coat, the middle layer consisting of the leucocytes, was aspirated with a Pasteur pipette from each tube into a single 50ml falcon and made up to

50ml in PBS and centrifuged at 1500 rpm for 5 minutes at rt. The wash step was repeated, and the supernatant discarded, followed by a 5-minute incubation with Red Cell Lysis Buffer (Biolegend) at rt. Cells were washed x 2 in PBS followed by cell counting with the LUNA-II automated cell counter and cryopreserved or rested overnight at 37 °C in a 5% CO2 humidified incubator for immediate applications.

2.1.3 PBMC cryopreservation

Following the final PBS wash the supernatant was discarded and the cell pellet resuspend in complete medium of Roswell Park Memorial Institute 1640 medium (RPMI) with 10% FBS and 1% Penicillin-Streptomycin at 2 x the required cell concentration per ml. A cryoprotectant mix of 20% dimethyl sulfoxide (DMSO) in foetal bovine serum (FBS) was prepared. A mix of 0.5ml cells and 0.5ml cryoprotectant was added to each cryovial for a final concentration of 10% DMSO. Cryovials were then place in a Mr. Frosty (Nalgene) filled with 100% isopropyl alcohol and placed at -80 °C for 24 hours prior to storage in liquid nitrogen. PBMCs were stored at 10, 30, 50 or 100 x 10^6/ml.

2.1.4 DLBCL patient PBMCs

Cryopreserved (liquid nitrogen) PBMCs isolated from patients with newly diagnosed DLBCL prior to any therapy, including steroids, were obtained from the BCI tissue bank. Patients were identified from the Barts clinical database as those treated in the Rituximab era who received treatment and subsequent follow up at our institution. Patients subsequently identified to have transformed from another type of lymphoma and those diagnosed in the context of immune suppression (HIV, PTLD, methotrexate treatment) were excluded, as were patients with PMBL and TCRDLBCL.

2.1.5 DLBCL patient and healthy donor serum

Frozen serum samples stored at -80 °C which had been collected from patients with newly diagnosed DLBCL prior to therapy were obtained from the BCI tissue bank. Samples were chosen based on availability and to overlap where possible with the DLBCL PBMC samples. Exclusions as previously. Healthy donor serum was collected by the BCI tissue bank from anonymised healthy donors working at BCI.

2.1.6 Tissue Single cell suspensions (SCS)

Cryopreserved (liquid nitrogen) tissue SCSs from both non-lymphoma patients, reactive lymph nodes and tonsils (RNLT) and DLBCL patients, lymph node (LN), were obtained from the BCI tissue bank based on availability. Surplus material from diagnostic biopsies was collected under sterile conditions by tissue bank technicians. Briefly, samples were dissected on a pre-cooled tray and passaged through a 70μm filter under gravity followed by x2 washes (1500 rpm, 5 minutes, rt) in sterile complete media. Following viability assessment, SCSs were the cryopreserved as described above for healthy donor PBMCs.

2.1.7 Formalin-fixed paraffin-embedded (FFPE) tissues

Patients were identified by searches of the Barts lymphoma database and the Barts clinical pathology reporting system. Diagnostic histology reports were then assessed to identify cases with sufficient tissue that would be appropriate for tissue microarray (TMA) preparation. Samples with potential suitability were retrieved from the pathology archive or BCI histology storage. Clinical databases were used to confirm pre-treatment status. Exclusions as previously. Reactive tissues and Hodgkin's lymphoma samples that had been well characterised in other work were used for validation work and control groups.

2.1.8 Clinical and follow-up data

The Barts clinical information systems and lymphoma database were used to confirm diagnosis and pre-treatment status in all patients included in this study. Patient characteristics, including IPI factors and diagnostic FBC were documented. All patients were confirmed to have been treated with RCHOP. Follow-up and outcome data were collected for all patients.

2.2 Mass cytometry (MC)

2.2.1 Antibody panels

Initial feasibility experiments were carried out with the Maxpar human monocyte / macrophage phenotyping panel kit (Fluidigm) using healthy donor PBMCs and RNLT SCSs. Subsequently, four broad antibody panels were designed to identify the main immune populations and subsets, and to interrogate the expected phenotypic and functional heterogeneity within the DLBCL PB and tissue MEs. Target antigens were selected based on their ability to identify specific populations ('lineage markers'), subsets within populations and activation / functional status. The four panels were termed 'Myeloid', 'T-cell', 'Cytokine' and 'Lymph node' with certain essential markers represented in each panel (Table 2.1).

2.2.2 Choice of metal reporter

Although panel design for MC is less problematic than for flow cytometry due to the use of metal reporter molecules, overlap or signal interference may still occur, and a number of factors need to be considered when pairing antibodies with metal tags in panel design (304).

Commercially available pre-conjugated antibody-metal pairs: Validated, published antibody-metal tag pairs that were available from Fluidigm were selected where available. Where an

antibody was available with multiple tags, the tag with the least signal interference according to the Maxpar panel designer was chosen.

Metal Sensitivity: mass cytometers are set up for maximum ion detection in the mass range of 153 - 176 – up to 3 x higher than at either end of the spectrum. Therefore, it is considered standard practice to use 'bright markers' which are highly expressed on positive cells (e.g., CD45) conjugated to metals detected in the least sensitive mass window (e.g., 89 Y, Yttrium). This also reduces signal interference from abundant targets. Conversely, markers with lower abundance per positive cell or with a continuum of expression are paired with metals detected in higher sensitivity channels, allowing for maximum signal detection.

Table 2.1 MC antibody panels used in this study. See appendix for vendor, clone and staining concentration. Grey – common lineage markers used across panels. CD, cluster of differentiation; HLA, human leucocyte antigen; PECAM1, platelet endothelial adhesion molecule 1; IL, interleukin, IL-1RA; LAG-3, lymphocyte activation gene 3 protein; CCR2, C-C chemokine receptor 2; TIM-3, T cell immunoglobulin and mucin domain-containing protein 3; CCL3, CC chemokine ligand 3; TGF, transforming growth factor; IFN, interferon; NKG2D, natural killer group 2D; MMR, macrophage mannose receptor; CTLA-4, cytotoxic T lymphocyte associated protein 4; CX3CR1, CX3C chemokine receptor 1; PD-1, programmed cell death protein 1; PD-L1, programmed death-ligand 1; CXCR4, C-X-C chemokine receptor 4 (Table on next page).

Metal Tag	Myeloid	T-Cell	Cytokine	Lymph node
89 Y	CD45	CD45	CD45	CD45
141 Pr		CD47	IL-10	CD47
142 Nd	CD19	CD19	CD19	CD19
143 Nd	HLA-DR	CD197	HLA-DR	CD197
144 Nd	CD38	CD38	CD38	CD38
145 Nd	PECAM-1 (CD31)			
146 Nd	CD64			
147 Sm	CD11c	CD20	CD20	CD20
148 Nd	CD14	CD14	CD14	CD14
149 Sm	CD56	CD56	CD56	CD56
150 Nd		CD223 (LAG-3)	IL-1RA	CD223 (LAG-3)
151 Eu	CD123		CD123	CD107a
153 Eu	CCR2 (CD192)			GATA-3
154 Sm	CD3	CD3	CD3	CD3
155 Gd	CD172a	T-Bet	T-Bet	T-Bet
156 Gd		CD366 (TIM-3)	CCL3	CD366 (TIM-3)
158 Gd	CD33	CD134 (OX40)	IL-2	CD134 (OX40)
159 Tb	CD274			CD274
160 Gd		CD28	CD28	CD28
161 Dy		CD25	IL-6	CD25
162 Dy	CD8	CD8	CD8	CD8
163 Dy	CD272		TGFβ	
164 Dy	CD86			
165 Ho	CD163		IFNɣ	NKG2D
166 Er	CD13	FoxP3	FoxP3	FoxP3
167 Er	CD11b	CD27	CD27	CD27
168 Er	MMR (CD206)			
169 Tm	CD32	CD45RA	CD45RA	CD45RA
170 Er	CD40	CD152 (CTLA-4)	IFNα	CD152 (CTLA-4)
171 Yb		CD226 (DNAM-1)	Ki67	CD226 (DNAM-1)
172 Yb	CX3CR1	CD279 (PD-1)	CD279 (PD-1)	CD279 (PD-1)
173 Yb	CD91	Granzyme B	Granzyme	Granzyme
174 Yb		CD127		CD127
175 Lu	CXCR4 (CD184)	Perforin	Perforin	Perforin
176 Yb	CD4	CD4	CD4	CD4
191/193 Ir	Iridium	Iridium	Iridium	Iridium
195 Pt	Cisplatin	Cisplatin	Cisplatin	Cisplatin
209 Bi	CD16	CD16	CD16	CD16

Table 2.1 MC antibody panels used in this study. Legend on previous page.

Signal Interference: there are 3 sources of 'overlap' in MC experiments, termed isotopic impurity, metal oxidation and abundance sensitivity (figure 2.1) (304). The metal tags available from Fluidigm, either pre-conjugated to an antibody or for custom conjugation, are of high purity (97-99%), with any impurity originating from trace presence of other isotopes of the same metal. Isotopic impurity is usually the most prominent source of signal overlap. All custom conjugations were performed with metal isotopes acquired from Fluidigm. Prior to acquisition of a sample, the CyTOF instrument is tuned to ensure that oxidation is less than 3% for Lanthanum (La), the most readily oxidised metal. The two metals used as reporters with the potential to form significant oxides are Nd (Neodymium) and Sm (Samarium), and where possible these metals were paired with less abundant targets or those where the antibody paired with the channel at risk of signal interference was a mutually exclusive target. Signal from oxidation is detected in the metal (M) +16 channel, for example oxidation from 146 Nd would be detected in the 162-mass channel. Abundance sensitivity, where a highly detected signal spills into the adjacent channel, either immediately above or below (M +/-1), was generally negligible except where the adjacent channel was also a target for isotopic impurity. All antibodies were titrated to minimise signal interference.

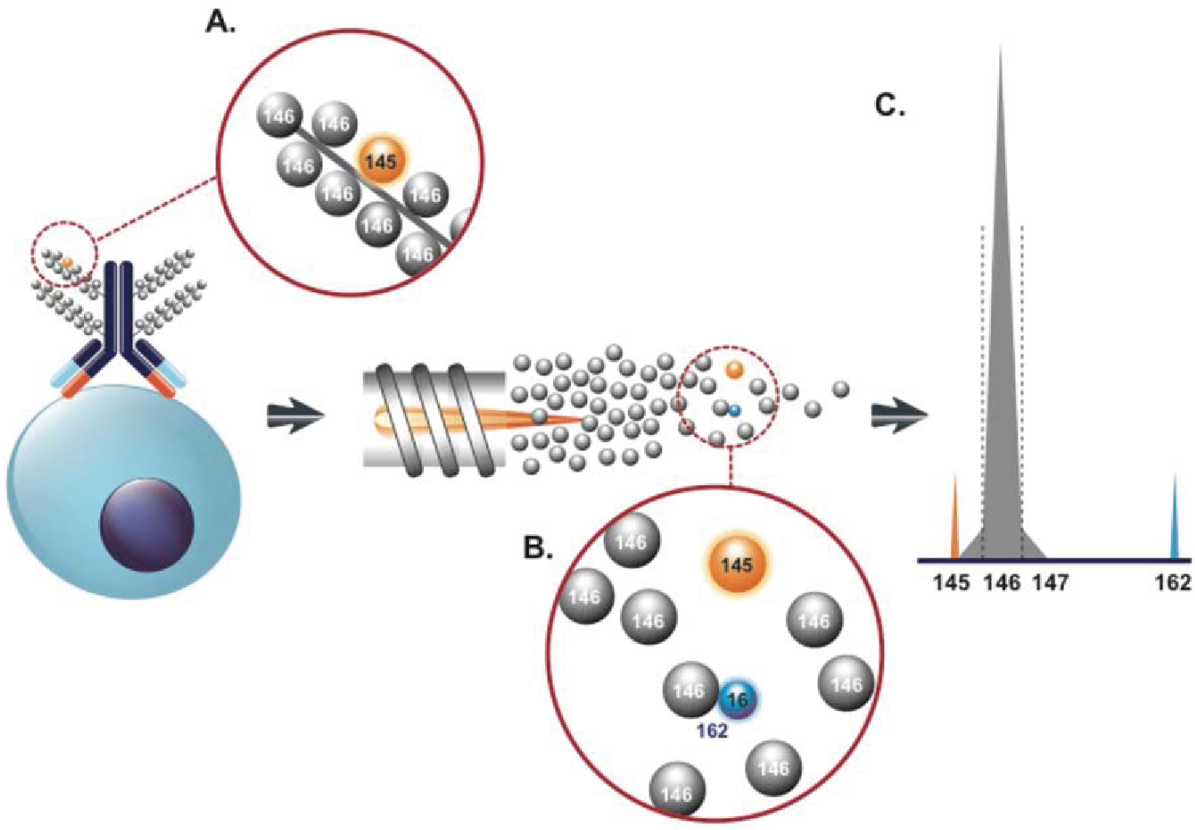

Figure 2.1 Mass cytometry sources of signal interference. There are 3 potential sources of signal interference or overlap in MC experiments a. Isotopic impurity occurs due to the presence of traces of other isotopes of the specific metal tag for a particular antibody (e.g., naturally occurring neodymium Nd has 5 stable isotopes 142, 143, 145, 146 and 148). b. Oxidation occurs during plasma ionisation of isotopes (cells are re-suspended in water prior to acquisition). Oxide formation gives a predictable signal at M+16 (oxygen has an atomic mass of 16). c. Abundance sensitivity results in signal detection in the M+/- 1 channel. Figure from Takahashi et al, 2016 (304).

2.2.3 Heavy-metal conjugation of antibodies

The majority of antibodies used in this study were purchased from Fluidigm already pre-conjugated with the appropriate heavy-metal isotope. Where required, custom conjugations were performed using Maxpar X8 antibody labelling kits according to the manufacturer's protocol. Purified antibodies in PBS for the required target were purchased prior to conjugation. The conjugation process involves 3 steps, preloading or chelating the polymer with the appropriate heavy-metal isotope, partially reducing the antibody, to break the disulphide bonds in the Fc portion, exposing sulfhydryl groups, and conjugation of the antibody with the metal-loaded polymer. Briefly, antibody concentration was determined using a spectrophotometer (Nanodrop) at 280nm, followed by buffer exchange by washing 100ug of antibody with R buffer (Fluidigm) using a 50 kDa Amicon Ultra centrifugal unit, 0.5ml (Millipore). The polymer was then preloaded by incubation with L buffer (Fluidigm) and the appropriate heavy-metal isotope at 37 °C for 40 minutes. The metal-loaded polymer was washed x 2 with L buffer using a 3 kDa Amicon Ultra centrifugal unit. The antibody was partially reduced by incubation with 4mM TCEP (Tris (2-carboxyethyl) phosphine hydrochloride, Thermo Fisher) solution at 37 °C for 30 minutes. The partially reduced antibody was conjugated with the washed metal-loaded polymer by incubation at 37 °C for 90 minutes. Conjugated antibodies were washed x 5 with W buffer (Fluidigm) and collected by adding W buffer to the filter and inverting into a new collection tube and centrifuging x 2. Protein content was measured with the Nanodrop and the conjugated antibody was stored in antibody stabilisation buffer (Candor Bioscience) supplemented with 0.05% (w/v) sodium azide at 4 °C. To ensure that the recovered antibody had been tagged with the metal reporter following conjugation, capture beads (BD biosciences) were stained and acquired prior to titration.

2.2.4 Antibody titration and validation of cryopreserved samples

For MC experiments, antibodies are titrated not to saturating levels, but to the minimum concentration that would allow robust identification of positive and negative populations while minimising signal interference. This was most relevant to highly abundant target

antigens where potential for spill over was greatest. Metal minus one (MMO) staining was also performed, analogous to fluorescence minus one (FMO) in FC, to assess potentially significant signal interference (figure 2.2). Titration and validation experiments were carried out using healthy donor PBMCs. Given that all patient samples available for this work were cryopreserved and stored in liquid nitrogen, an assessment was made of staining consistency on a single healthy donor (JF) both pre- and post-cryopreservation whereby PBMCs were stained following isolation from a leucocyte cone and again following resuscitation after a short period of time in liquid nitrogen. The same donor was used throughout the study as a quality control sample and staining consistency was monitored throughout the study. This allowed assessment of technical variation induced by the cryopreservation process. The cryopreservation process resulted in some cell loss as well as some minor loss in signal intensity from a number of markers, which was most prominent for CD16 on NK cells (figure 2.3). However, both manual gating and unsupervised clustering of cell populations was highly consistent as were staining patterns for all markers tested. Following these initial validation experiments the original CD16 antibody, conjugated to 148 Nd was substituted for CD16 – 209 Bi (Bismuth) and CD14, previously tagged with 160 Gd (Gadolinium) was moved to 148 Nd, which resulted in consistent staining patterns with improved CD16 signal on cryopreserved samples.

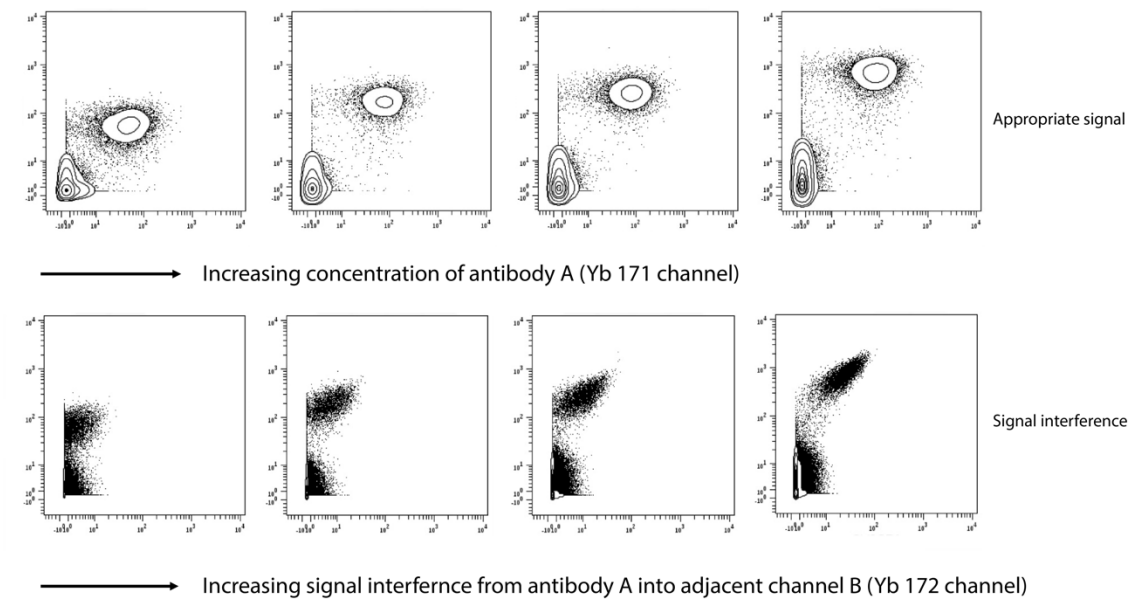

Figure 2.2 Metal minus one (MMO) experiment to assess signal interference. Healthy donor PBMCs were stained with antibody A (171Yb) but not antibody B (172Yb). Increasing concentration of antibody, A (left to right) results in increasing signal detected in the 171Yb channel (upper panel, x-axis) but also increasing signal 'spill' into the 172Yb channel (lower panel, x-axis). Signal interference occurs here due to both isotopic impurity (171Yb tag contains traces of 172Yb) and abundance sensitivity (adjacent channel). Titrating down the staining concentration of antibody A reduces spill while still allowing separation of A+ and A- cells (far left upper and lower panels).

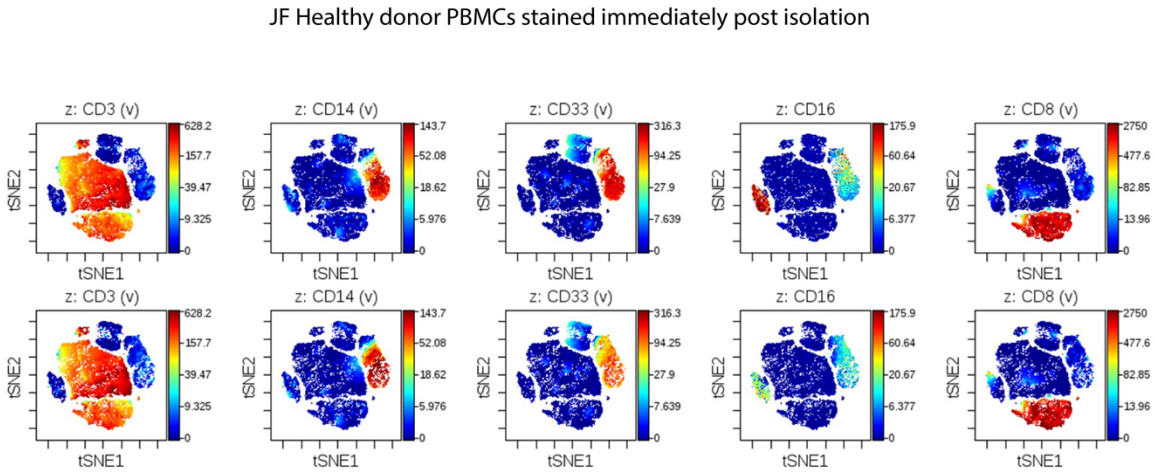

Figure 2.3 Healthy donor JF PBMCs stained post isolation from the leucocyte cone (top row) and following cryopreservation and thaw (bottom row). These viSNE plots show expression of selected antigen markers to highlight T cells, myeloid cell and NK cells. Each point on the map represents a single cell, with cells of a similar phenotype being placed close to each other, such that each population can be recognised as a distinct 'island' on the map. The cryopreservation resulted in some minor signal loss but with consistency of staining for all markers except CD16, particularly on NK cells. An alternative CD16 antibody with a more consistent pattern of staining on cryopreserved samples was used for patient samples.

2.2.5 Cell resuscitation following cryopreservation

Cryovials were transferred from liquid nitrogen storage to the laboratory on dry ice. Aliquots of 1mg/ml DNase 1 (Sigma) were thawed at rt. Complete media was warmed to 37 °C. Cryovials were thawed rapidly at 37 °C. A volume of 1ml DNase 1 diluted to 0.05mg/ml in complete media was added dropwise with a Pasteur pipette directly into the cryovial and the cells and media were transferred to 15ml falcons containing 8mls of complete media with 0.05% DNase 1. Cells were washed at 1500 rpm for 8 minutes at rt. The supernatant was discarded, and the cell pellet resuspend in 0.5ml of 1mg/ml DNase 1. A volume of 1ml

of warm media was added and the cells and media were filtered through a 70μm sterile CellTrics cell strainer (Sysmex) into a new 15ml falcon. The cells were topped up to 10ml with media and washed as previously. The supernatant was discarded, 1ml of media added and cell-counts and viability assessed with the LUNAR-II. Cells were adjusted to required concentration for staining or rested in a humidified incubator prior to functional experiments. This protocol was applied to both PBMC and SCS samples.

2.2.6 Cell stimulation for functional assays

Cell stimulation was performed in a 250μl volume in a 96 well plate for PBMCs and in a 500μl volume for SCSs. For monocyte stimulation in PBMC samples, LPS (lipopolysaccharide) solution 500x was added at 0.5μl per well together with 0.5μl of protein transport inhibitor cocktail 500x for 6 hours in a humidified incubator. The protein transport inhibitor cocktail is a mixture of brefeldin A and monensin. For T-cell stimulation, cell stimulation cocktail plus protein transport inhibitors 500x was added at 0.5μl per well for PBMCs and at 1μl in SCSs for 6 hours in a humidified incubator. The cell stimulation cocktail is a mixture of phorbol 12-myristate 13-acetate (PMA), ionomycin, brefeldin A and monensin. For unstimulated samples only the protein transport inhibitor cocktail was added at 0.5μl for PBMCs and 1μl for SCSs. All cell stimulation reagents were purchased from eBiosciences (Thermo Fisher).

2.2.7 Cell surface staining protocol

PBMCs were stained in 96 well v-bottom plates (Grenier-Bio) and SCSs were stained in 5ml falcons. A cell-surface antibody staining master-mix (x2) was prepared with appropriate volumes of each antibody diluted in cell staining buffer (CSB, Fluidigm) to a total volume of 50μl per sample to be stained. The master-mix was made up in a 0.1μm spin-filter (Millipore) and centrifuged at 12000 rcf (relative centrifugal force) at rt for 1 minute to remove antibody aggregates. See relevant chapter for antibody staining concentrations. Aliquots of up to 3 x 10^6 cells were washed in CSB at 300 rcf at rt for 5 minutes and resuspended in 35ul CSB, then 15μl of human TruStain FcX Fc receptor blocking solution

(BioLegend) was added at rt for 15 minutes. After Fc block, 50ul of the cell-surface antibody staining master-mix (x2) was added to each sample and incubated at 4 °C for 45-60 minutes followed by x 2 CSB washes. Cells were then stained with cisplatin (Fluidigm), a viability reagent able to permeate the membranes of dead cells and bind covalently to cellular proteins, by spiking the cell pellet with 100ul of 5μm cisplatin in PBS at rt for 3 minutes. A final concentration of 2.5μm was used for SCSs. The cisplatin reagent contains a mixture of naturally occurring platinum (Pt) isotopes and was best detected in the 196 Pt channel. The cisplatin reaction was quenched with CSB, and cells were washed x 3 in CSB. Cells were then fixed in 2% formaldehyde freshly diluted from the stock supply of Pierce 16% Formaldehyde (w/v), (Thermo Fisher), in PBS and stored overnight at 4 °C prior to intracellular staining. For surface staining only, the fix step and cell-ID iridium intercalator step were combined, see below.

2.2.8 Intracellular staining protocol

Intracellular staining for both transcription factors and cytokines was with the eBiosciences FoxP3 / transcription factor staining buffer set (Thermo Fisher), according to the manufacturer's protocol. Fixed samples were retrieved from 4 °C storage and washed x 2 with CSB at 800 rcf at rt for 5 minutes. The cell pellet was resuspended in 200μl of FoxP3 Fix/Perm working solution at rt for 60 minutes, followed by 2 x Perm buffer washes at 600 rcf at rt for 5 minutes. Intracellular staining antibody master-mix (x2) as per surface staining. See relevant chapter for antibody staining concentrations. The cell pellet was resuspended in 50μl of Perm buffer and 50μl of the intracellular staining antibody master-mix (x2) was added to each sample and incubated at rt for 30-45 minutes followed by x 2 Perm buffer washes.

2.2.9 Cell-ID iridium intercalator staining protocol

Cell-ID iridium (Fluidigm) is a cationic nucleic acid intercalator which contains natural abundance iridium (Ir), 191 Ir and 193 Ir. It is live cell membrane impermeable but following fixation it can freely diffuse inside stained cells and form non-covalent interactions with

DNA in the cell nucleus. It is used to mark nucleated cells and for doublet exclusion. A working intercalator solution was prepared by adding Cell-ID iridium to freshly prepared 1.6% formaldehyde to a final concentration of 125nM. For surface staining only, this step was combined with fixation such that the intercalator solution was prepared in 2% formaldehyde to the same concentration. Cell pellets were resuspended in 100μl of intercalator solution and incubated at 4 °C overnight.

2.2.10 Data acquisition

Prior to acquisition, samples were washed x 2 in CSB at 800 rcf at rt for 5 minutes followed by 2 x washes in Maxpar water (Fluidigm). Cells were resuspended at 0.5 - 0.75 x 10^6 cells/ml (PBMCs) or 0.25 – 0.3 x 10^6 cells/ml (SCSs) in Maxpar water supplemented with 1 x EQ four element calibration beads (Fluidigm) and acquired on a CyTOF2 mass cytometer (Fluidigm) via a super-sampler fluidics system at an event rate of < 500/second.

2.2.11 Cryopreservation of samples post staining

On occasion, due to technical issues with the CyTOF instrument it was not possible to acquire samples immediately after staining as planned. In this situation if the delay was a short duration samples were kept stored in the intercalator solution for up to 48 hours prior to acquisition. However, for longer periods, samples were cryopreserved as per Sumatoh et al (305). Briefly, following cell-ID iridium staining samples were washed x 2 in CSB and resuspended in 150μl of FBS with 10% DMSO and snap frozen at -80 until acquisition. This was only required for some PBMC samples and not for SCSs. Plates were thawed at rt on the day of acquisition and final washes were as per data acquisition section.

2.2.12 Number of events to acquire on the CyTOF2

In order to ensure acquisition of an appropriate number of events it is helpful to know the estimated frequency of the rarest population of interest in the relevant sample. However, when high-dimensional single-cell techniques are used to analyse complex biological samples there is potential to discover uncharacterised populations where frequency data is unknown. In the process of MC, stained cells (events) are presented for ablation and hence analysis at random and their distribution will be described by Poisson statistics. Any subset of (rare) cells (of interest) will also be distributed at random with the parent population. The essential feature of Poisson distributions is that if N target events are collected, the standard deviation (SD) of that number of target events is the square root of N. The coefficient of variation (CV) is given by 100 x SD/N (306). This has important consequences in determining how many events to collect, for example if a cell subset of interest is smaller by a factor of S than another population of interest then the total number of events processed must be increased S x to maintain precision. Table 2.2 demonstrates how this information can be used to determine the total number of events to be acquired for a given precision.

Desired CV (%)		**1**	**2.5**	**5**	**10**	**20**
Events of interest		10,000	1,600	400	100	25
Occurring at a frequency of		**Total number of events required for a given precision**				
%	**1 in**					
10	**10**	100,000	16,000	4,000	1000	250
1	**100**	1,000,000	160,000	40,000	10,000	2,500
0.1	**1000**	10,000,000	1,600,000	400,000	100,000	25,000
0.01	**10,000**	100,000,000	16,000,000	4,000,000	1,000,000	250,000

Table 2.2 Determination of the total number of events to be acquired for a given coefficient of variation (CV). For single cell techniques, including mass cytometry, simple calculations based on Poisson statistics can be used to determine the total number of events to be acquired for a given precision, for populations of interest occurring at varying frequencies. Table adapted from Hedley and Keeney, 2013.

Therefore, for a CV of 5% and a population of interest occurring at 10% frequency of PBMCs a total of 4,000 events would need to be collected, whereas if the frequency was 1% of PBMCs, a total of 40,000 events would need to be acquired to maintain the same CV. The majority of sample acquisitions for this work have been > 50,000 events which gives a practical balance between efficient use of machine time and likely frequency of immune populations of interest in the peripheral blood. Some patient samples contained fewer events than this, with 5,000 live CD45+ events considered the minimum acceptable for population frequency analysis. However, all events were combined for initial data exploration with approximately four million events analysed, facilitating rare population discovery.

2.2.13 Data normalisation and gating

Following acquisition, data were transformed into fcs file format by the CyTOF2 software and normalised. Normalised fcs files were then uploaded to either Cytobank (www.cytobank.org) or OMIQ (www.omiq.ai) and manually gated to remove beads, debris, doublets and dead cells. Live singlets were gated for CD45+ events. Plots of CD19 v CD3 and CD14 v CD3 were viewed to estimate remaining doublets from the dual positive populations and gating refined where necessary to ensure this was <0.5%. Manual gating of immune cell subsets and further analysis using a combination of high-dimensional data analysis tools was performed in OMIQ.

2.2.14 High-dimensional data analysis methods

Visual inspection of 2-dimensional marker plots to identify known cell populations positive for lineage and/or functional markers traditionally used in FC data analysis has a number of limitations, which are magnified with the increasing number of parameters used in MC data generation (307). These limitations include problems with operator bias, reproducibility and identification of unknown or unexpected populations. To address these issues a number of clustering and dimensionality reduction algorithms have been developed to facilitate data analysis. Clustering algorithms essentially define populations of cells with similar expression patterns of the markers used for clustering in an automated way. These automated analysis techniques are generally grouped into unsupervised and supervised methods (308). Unsupervised approaches use clustering methods to detect cell populations, which can be from a single sample or from multiple samples, allowing the potential for unknown populations to be identified in an unbiased manner. Such algorithms are useful for exploratory analyses, assessing the diversity of populations within and between samples and have been used to compare population frequencies between groups of samples (309). Supervised approaches rely on inputs of a biological and / or clinical variables, for example disease status or outcome, describing each sample to train a model, which can then be used for differential abundance analysis or to predict the status of a new sample (307). These methods are useful for biomarker discovery, where a cell population abundance or

expression of a specific marker can be used to predict future occurrence of the input variable e.g., disease status. Unsupervised analysis techniques used during this work for dimensionality reduction were viSNE, Opt-SNE and UMAP and for clustering Phenograph and FlowSOM (310-313). The edgeR framework and SAM (statistical analysis of microarrays) were used for statistical differential abundance and feature analysis described by disease and outcome status (314-316).

2.2.15 Quality control (QC)

Daily calibration: sensitivity drift for signal detection in individual mass channels of the CyTOF2 are accounted for by daily acquisition of a high purity standard tuning solution, containing known quantities of elements, prior to running samples. Only when the signal interference from oxidation of 139 La in the tuning solution is <3% is the instrument considered ready for sample acquisition, thus minimising undesired signal.

EQ calibration beads: errors can also result from signal sensitivity drift across all channels over time during acquisitions due to variations in instrument performance (317). This can be accounted for by mixing samples with polystyrene beads embedded with metal isotopes, EQ calibration beads, prior to acquisition, followed by data normalisation to correct for signal fluctuations. The EQ beads contain a mixture of natural abundance cerium (Ce), europium (Eu), holmium (Ho) and lutetium (Lu), metals which cover the mass range of the CyTOF2. The beads can be used to assess the sensitivity of the CyTOF2 and sample transmission efficiency prior to running samples, as well as normalisation post acquisition. Any variation in the bead signal following normalisation may be used to determine data quality, following which the beads are gated out prior to further analysis.

Control PBMCs: A standard healthy donor control PBMC sample (JF) was stained and run with each batch of patient PBMC samples for QC purposes. These samples were assessed to ensure signal intensities and frequency of immune populations were consistent with each batched run. See figures 2.4 -2.6 demonstrating manually gated events for each JF control sample from 10 batches acquired with the myeloid panel (parent CD45+ live events) and

from 7 batches acquired with the T-cell panel. The samples acquired with the cytokine and lymph node panels were run in 2 batches with control samples.

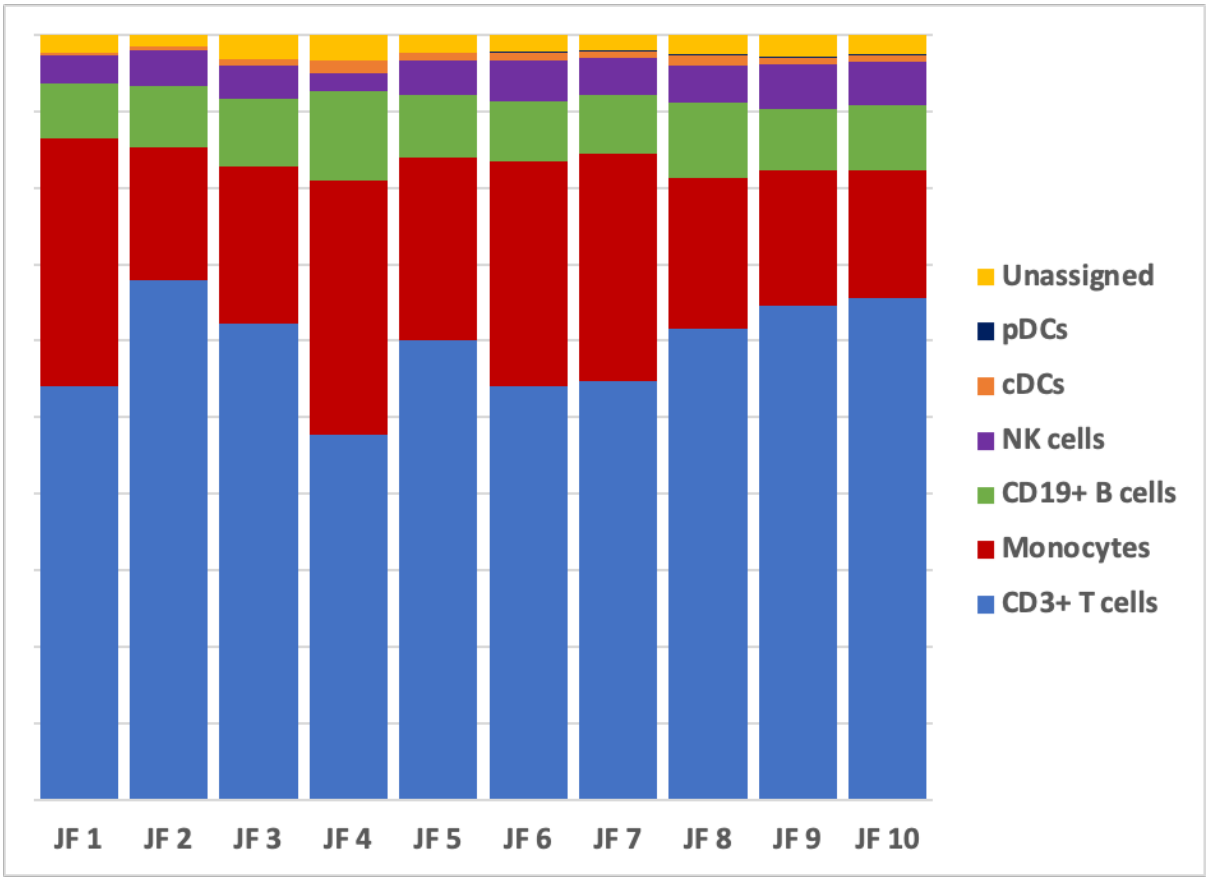

Figure 2.4 Frequencies of gated immune populations for healthy donor JF across each of 10 MC PBMC Myeloid panel staining batches. Parent population CD45+ live events. Populations as per key. NK, natural killer, cDC, conventional dendritic cells, pDC, plasmacytoid dendritic cells.

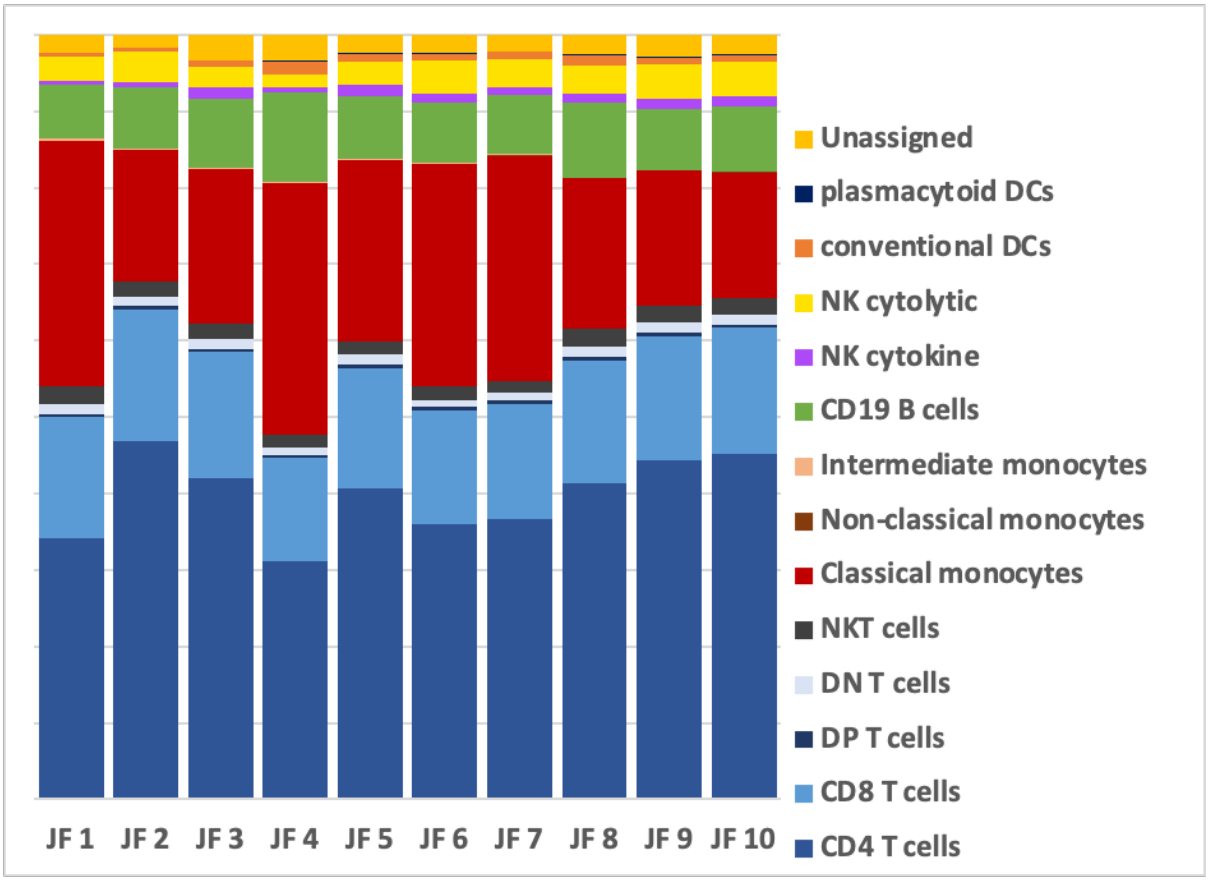

Figure 2.5 Frequencies of gated immune populations for health donor JF across each of 10 MC PBMC Myeloid panel staining batches. Parent population CD45+ live events. Populations as per key. DP, double positive, DN, double negative, NK, natural killer, cDC, conventional dendritic cells, pDC, plasmacytoid dendritic cells.

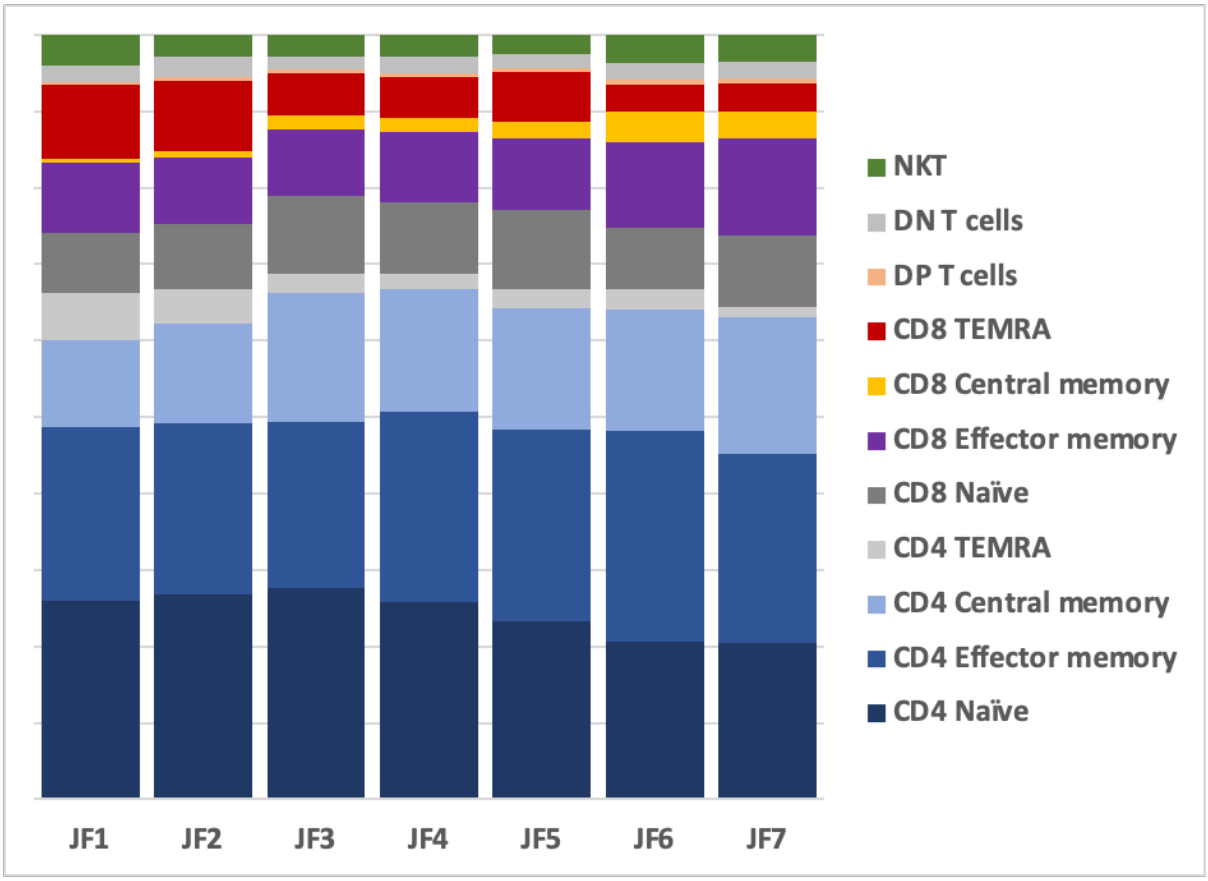

Figure 2.6 Frequencies of gated immune populations for health donor JF across each of 7 MC PBMC T-cell panel staining batches. Parent population CD3+ live events. Populations as per key. TEMRA, CD45RA positive effector memory, DP, double positive, DN, double negative, NKT, natural killer T cells.

2.3 Mesoscale discovery (MSD) electrochemiluminescence cytokine detection

2.3.1 Principles of assay

The MSD electrochemiluminescence platform was used to assay cytokine and chemokine levels in the serum of healthy donors and pre-treatment DLBCL patients. MSD multi-array technology enables multiplex detection of soluble proteins using electrochemiluminescence technology. Specifically, SULFO-TAG labels are used which emit light upon electrochemical stimulation initiated at the electrode surfaces of multi-spot microwell plates. This system offers the ability to simultaneously measure 10 analytes in the same well with minimal background and high signal to background ratios since the electrical stimulation mechanism is uncoupled from the light signal detection mechanism. The U-plex system was used, which facilitated design of a multiplex assay with a custom combination of analytes. The principle of the assay is that biotinylated capture antibodies are coupled to U-plex linkers which assemble onto unique spots in each well of the U-plex plate. Analytes of interest in the sample then bind to the capture antibody. A detection antibody conjugated to a SULFO-TAG, which acts as the electro-chemiluminescent label, binds the analyte to complete the sandwich immunoassay (figure 2.7). Once the assay is complete, the U-plex plate is loaded into the MSD instrument (MESO QuickPlex) where a voltage is applied to the plate electrodes causing any bound detection antibody SULFO-TAG to emit a light signal. The instrument measures the intensity of the emitted light signal, which is proportional to the amount of analyte, giving a quantitative measure of each analyte of interest detected in the sample. Each assay is supplied with a set of calibrators containing known concentrations of all the analytes of interest, which are assayed in duplicate along with the samples. The calibrators are used to generate a standard curve from the maximum calibrator standard (point 1, top of curve), across 6 serial dilutions (4-fold dilutions, points 2-7) and zero (point 8, bottom of curve) to generate an 8 point standard calibration curve, from which the signal assayed samples are quantified.

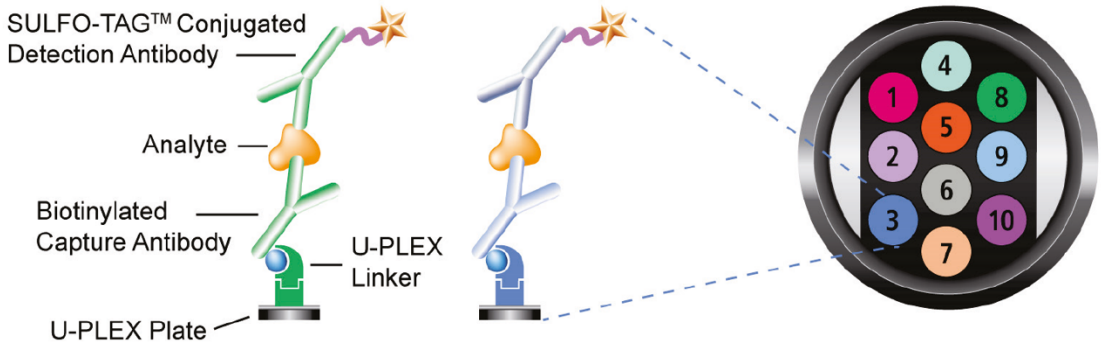

Figure 2.7 MSD U-Plex immunoassay on a 10-assay plate. Biotinylated capture antibodies are coupled to U-plex linkers, which bind to specific spots on the assay plate (numbered). Analytes of interest in the sample bind to the capture antibody. The sandwich assay is completed by binding of the detection antibody, which has an electrochemiluminescent label (Sulfo-tag) which is detected by the plate reader (figure adapted from www.mesoscale.com).

2.3.2 Assay workflow

All cytokines and chemokines were assayed in duplicate with serum samples according to the manufacturer's instruction. All assays were done in 96-well plates with 10 analytes assayed per plate, all reagents were from MSD. Briefly, all reagents and samples were brought to room temperature (rt) and each antibody was assigned to a unique linker, corresponding with the numbered spot in the well as per figure 2.8. Each biotinylated antibody was coupled with its selected unique linker by combining and incubating at rt for 30 minutes. Each of the 10 linker-coupled antibodies per plate were combined and coated to each well. The plate was sealed and incubated with shaking at rt for 1 hour. The plate was washed x 3 with PBS-T (PBS with 0.05% Tween-20, Thermo Fisher). The calibrator standards were prepared in serial 4-fold dilutions. Calibrator standards and samples were added to each well and the plate was sealed and incubated at rt for 1 hour, followed by x 3 washes with PBS-T. Detection antibody was then added to each well and the plate incubated with shaking at rt for 1 hour, followed by x 3 washes with PBS-T and addition of MSD gold read buffer. The plate was immediately read using the MSD instrument. Initial data generation

was done in the MSD discovery workbench software and raw data was exported for further analysis. See figure 2.8 for schematic workflow overview.

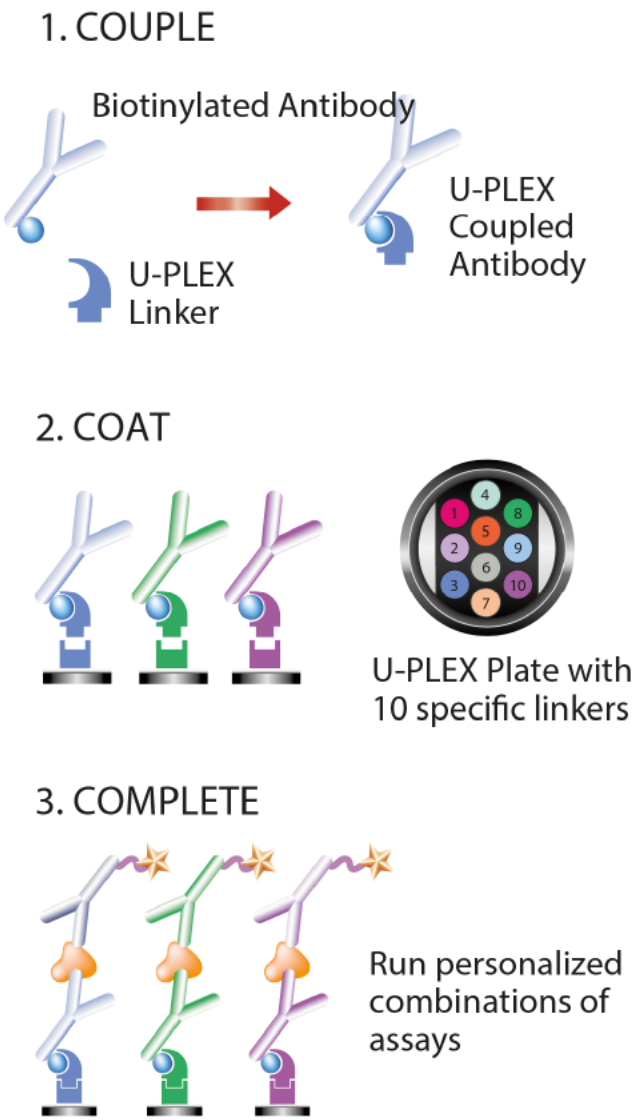

Figure 2.8 MSD U-plex workflow overview. The workflow involves three steps, coupling the capture antibodies to the corresponding U-plex linkers, coating the plate with the coupled antibodies, followed by addition of the sample and detection of the analytes of interest (figure adapted from www.mesoscale.com).

2.4 Immunohistochemistry (IHC) and imaging mass cytometry (IMC)

2.4.1 FFPE tissues for IHC and IMC

All tissues used were FFPE, either individual tissue blocks or TMAs. All sections were cut by, and TMAs constructed by Andrew Clear. All tissues were reviewed by an expert Haemato-pathologist, Professor M Calaminici, to confirm diagnosis and select arears of tissue appropriate to array. Patients were selected to array based on availability of quality tissue and where possible to overlap with availability of other diagnostic samples. Validation work was done with individual tissue sections from both reactive tissues (tonsil) and Hodgkin lymphoma tissue (lymph node) that had been extensively characterised by my colleague Dr Joseph Taylor with IHC as part of another project. The TMA construction process involved expert pathology review of a Haematoxylin & Eosin (H&E) stained section, followed by marking of areas of interest on the slide and also corresponding areas on the original tissue block. Marked donor blocks were then arrayed by taking a core of tissue from the block and inserting it into a recipient block in either duplicate or triplicate. In this way many patient cases can be analysed on the same slide at the same time. Also, due to the time constraints of ablating large areas of tissues across many slides, IMC is ideally suited to analysing TMAs.

2.4.2 IHC staining

IHC was used primarily to validate antibodies to be conjugated to heavy-metal isotope reporters for development of an IMC panel of antibodies and to confirm consistency of tissue staining between the 2 modalities. Tissue sections were cut to 3μm thickness and dried overnight at 60 °C in an oven. Sections were then de-waxed and dehydrated through 2 x 10-minute changes of xylene and 1 x 10-minute change of industrial methylated spirits (IMS). This was followed by blocking of endogenous peroxidase activity in 2% H_2O_2 in IMS solution for 2 x 5-minute incubations and 1 x 5-minute incubation in IMS. Slides were then transferred to distilled water. Heat induced epitope retrieval was performed using a pressure cooker with slides incubated in citric acid based unmasking solution (Vector) at full pressure for 10 minutes. Slides were cooled in running tap water followed by x 1 wash in

distilled water for 10 minutes. Slides were marked with a hydrophobic barrier pen and rinsed x 2 in wash buffer (tris-buffered saline with tween, Dako), followed by x 2 PBS washes and then blocked with SuperBlock blocking buffer (Thermo Fisher) for 45 minutes at rt. Slides were then incubated with the appropriate dilution of primary antibody in Signal stain antibody diluent (Cell Signalling Technologies, CST) in a hydration chamber at 4 °C overnight. Detection was performed with the Vectastain ABC HRP kit (Vector) as per manufacturer's instructions. Slides were rinsed x 2 in wash buffer and incubated with the appropriate Vector biotinylated secondary antibody, diluted in antibody diluent, to recognise the primary antibody of interest at rt for 30 minutes. Slides were rinsed x 2 in wash buffer and incubated with the ABC reagent at rt for 20 minutes. Finally, slides were rinsed x 2 in wash buffer and DAB applied at rt for 10 minutes. Slides were then rinsed in distilled water and dried prior to Haematoxylin counterstaining.

2.4.3 Haematoxylin counterstaining

Following antibody staining and detection slides were counter stained by immersion in Gill's Haematoxylin for 5 minutes, running tap water wash, 3 x rapid dips in acid alcohol, running tap water wash, immersion in Scott's solution for 3 minutes and running tap water wash. The sections were then dehydrated through 3 x 2 minutes in IMS followed by 3 x 5 minutes in xylene to clear. Slides were then cover slipped by Andrew Clear. Once dried slides were scanned using a digital slide scanner (Pannoramic 250 Flash, 3DHISTECH or NanoZoomer, Hamamatsu).

2.4.4 IMC staining

An extensive panel of antibodies was developed and validated to characterise the tissue microenvironments of both DLBCL and Hodgkin lymphoma, working with another project by Joe Taylor. I focused mainly on the antibody validation and staining, while Joe Taylor worked on image analysis, specifically cell segmentation pipelines for downstream analysis. Antibodies were purchased pre-conjugated to heavy-metal isotope reporters (Fluidigm) or purified in PBS for custom conjugation. Maxpar X8 antibody labelling kits were purchased

from Fluidigm, and the conjugation protocol was as described above. The staining protocol was optimised based on our pre-optimised IHC protocol. Briefly, antigen retrieval steps were performed as per IHC staining, following the pressure cooker step, slides were washed for 10 minutes in distilled water, encircled with a hydrophobic barrier pen, rinsed x 2 in wash buffer, washed x 2 in PBS and blocked with SuperBlock at rt for 45 minutes. During the blocking step, the required antibody master-mix (x1) was prepared by diluting appropriate volumes of each antibody in antibody diluent in a 0.1μm spin-filter, followed by centrifugation at 12000 rcf at rt for 1 minute, to remove antibody aggregates. Slides were then incubated with 100 - 200μl of antibody master-mix depending on tissue area and incubated in a hydration chamber at 4 °C overnight. The following morning, slides were washed x 2 with wash buffer and x 2 with PBS followed by nuclear staining with iridium intercalator diluted in PBS to 125nM in a hydration chamber at rt for 30 minutes. Slides were washed x in distilled water and air died overnight. Prior to acquisition, the Hyperion imaging mass cytometry system was tuned with a 3-element tuning slide (Fluidigm) for daily QC as per manufacturer's protocol. Regions of interest were selected based H&E slides or whole cores for TMAs. Tissue was ablated at 200Hz. Data was exported as MCD files and assessed for staining quality visually using MCD viewer (Fluidigm, figure 2.9). TIFF image stacks were exported from MCD viewer and uploaded to Visiopharm for cell segmentation.

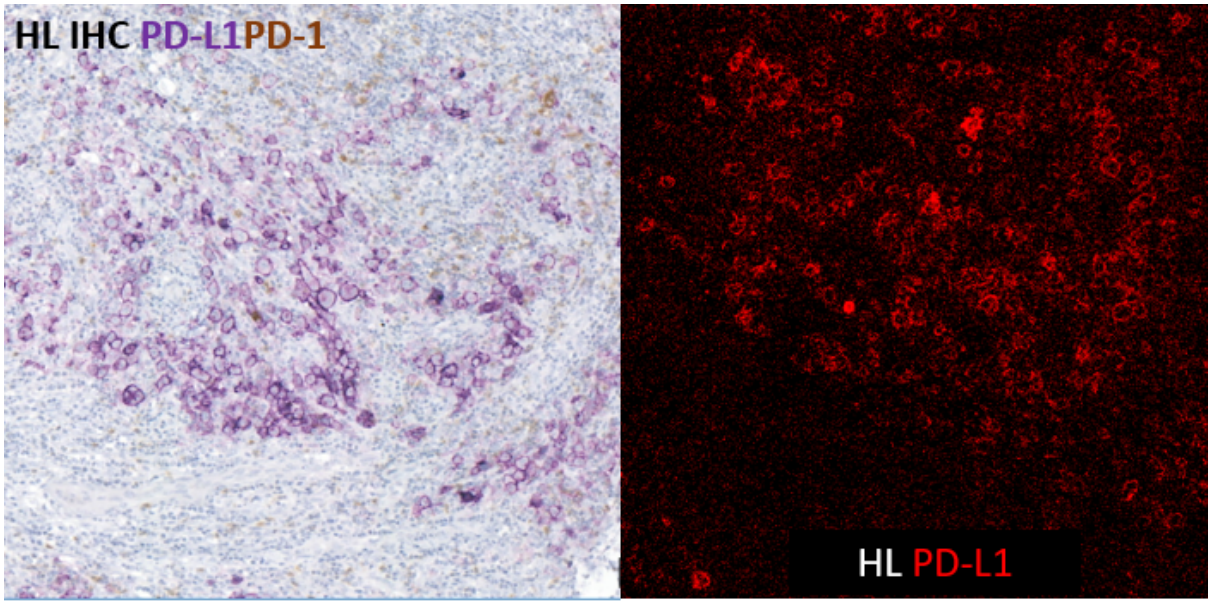

Figure 2.9 Hodgkin lymphoma lymph node for IMC validation. Sections stained with both PD-L1 and PD-1 by IHC (left, staining by Dr Joseph Taylor) and with PD-L1 by IMC (right, stained by Dr Ed Truelove).

2.5 Statistical analysis

Raw data were uploaded to Cytobank and OMIQ for MC experiments. MSD data were generated used workbench discovery. Data were exported and processed in Microsoft Excel and R (version 4.0.3). Statistical comparisons were performed in OMIQ, GraphPad Prism 9 and R. For frequency correlations between different batches of CyTOF runs linear regression was used to compare gated populations from the health donor JF. Data was assessed for normal distribution visually and by both D'Agostino-Pearson and Shapiro-Wilk normality tests. For normally distributed data, the paired t-test was performed, where not normally distributed, the Mann-Whitney test was used for paired analysis. For correlation of non-normally distributed data, Spearman's rank correlation was used. Overall survival was estimated using the Kaplan-Meier method and compared with the log-rank test. EdgeR was used for differential abundance analysis performed in OMIQ with a false discovery rate (FDR) of 0.05 (318).

3. Clinical prognostic tools and diagnostic full blood counts in DLBCL

3.1 Introduction

DLBCL is a curable disease but there is heterogeneity in outcome among individual patients. One strategy with potential to improve outcomes would be development of reproducible tools to identify the highest risk patients at diagnosis, facilitating upfront treatment with an alternative strategy, such as entry into a clinical trial of RCHOP X, with a novel agent added to standard care or cellular therapies currently reserved for relapsed disease. As we have seen, there are a number of clinical prognostic tools available and routinely used including the IPI, R-IPI and NCCN-IPI, but while these scoring systems give useful prognostic information, they fail to identify sufficiently those patients who do not benefit from RCHOP (94-96). The improved outcomes seen in the rituximab era, together with the intrinsic biological heterogeneity of DLBCL hinder the ability of the clinical parameters incorporated into these tools to act as surrogates for the genetic and molecular features of the tumour. However, although recent genetic studies have identified reproducible subtypes, a significant proportion of cases were not classified, and the molecular techniques required for classification are not available to most patients (122-124). The prognostic tools include factors specific to the patient, such as age and performance status, and to the lymphoma such as stage, involved sites of disease and LDH but do not incorporate parameters reflecting immune system variation. A number of retrospective studies have utilised peripheral blood counts as surrogates for the lymphoma ME and host immune response, which have been shown to provide prognostic information at both diagnosis and relapse (191-193, 319). These studies demonstrate that a higher absolute monocyte count (AMC) and lower absolute lymphocyte count (ALC) at diagnosis consistently associate with worse outcome. A detailed understanding of the underlying mechanism is lacking but monocyte populations have been linked to immune suppression and tumour supportive functions in DLBCL (194-197). A further layer of supportive evidence for the importance of immune cells in DLBCL is provided by the mechanism of action of a number of novel therapies, including bispecific T cell engager (BiTE) antibodies, innate immune checkpoint inhibitors and cellular therapies, which harness the power of immune effector cells (189, 271, 280, 285, 320).

3.2 Aims

We sought to assess the prognostic nature of the clinical prognostic tools (IPI, R-IPI and NCCN-IPI) and diagnostic AMC and ALC in patients treated with RCHOP or RCHOP-like therapy at our centre.

3.3 Methods

3.3.1 Patient selection

Patients were identified through the Barts lymphoma data base and pathology reporting system and confirmed to have a diagnosis of DLBCL or as healthy stem cell donors, used for a comparator group. Patients with clinical samples available for analysis, detailed in relevant chapters, were prioritised for inclusion together with patients with available IPI parameters and pre-treatment FBC. All available data were confirmed using clinical information systems with reference to pathology reports, radiology reports, MDT forms and clinical letters. Date of diagnosis was confirmed by diagnostic histopathology report and date of last clinic follow-up or date of death recorded. All patients received RCHOP, RCHOP plus bortezomib or RCODOXM/RIVAC as first line therapy. Patents with PMBL, TCRDLBCL, underlying low grade lymphoma and lymphoma diagnosed in the context of immune suppression (HIV, PTLD, methotrexate) were excluded. The IPI, R-IPI and NCCN-IPI were calculated as previously described (94-96).

3.3.2 Statistical analysis

Overall survival was calculated from the date of diagnosis to date of last follow-up or death and estimates were obtained by the Kaplan-Meier method and compared between groups using the two-tailed log-rank test (321). The AMC and ALC were analysed as dichotomised variables either split as determined by X-tile (http://www.yalepath.org/edu//PathCamp/x-tile/) or as previously published (191, 322, 323). The Cox proportional hazards model was used to evaluate the AMC, ALC and IPI factors as prognostic variables.

3.4 Results

3.4.1 Patient characteristics

A total of 195 patients with histologically confirmed DLBCL, treated at our centre with frontline rituximab and anthracycline based therapy with available follow-up data were identified. Of these patients, full IPI data were available for 179, NCCN-IPI data for 169 and pre-treatment FBC for 146. Patient characteristics and prognostic groups are summarised in table 3.1. The median age was 62 years (range, 17-90) and 56% were age over 60 years. Most patients had Ann Arbor stage III/IV disease (57%), ECOG performance status of 0 or 1 (76%) and a raised LDH (70%). Extra-nodal involvement at 2 or more sites was identified in 21% of patients. The median follow-up was 4 years (range, 0.1-13.7) and median overall survival (OS) was 10.9 years, with an estimated 5-year OS of 72% (95% confidence interval, 62-74) and 68 deaths recorded (figure 3.1).

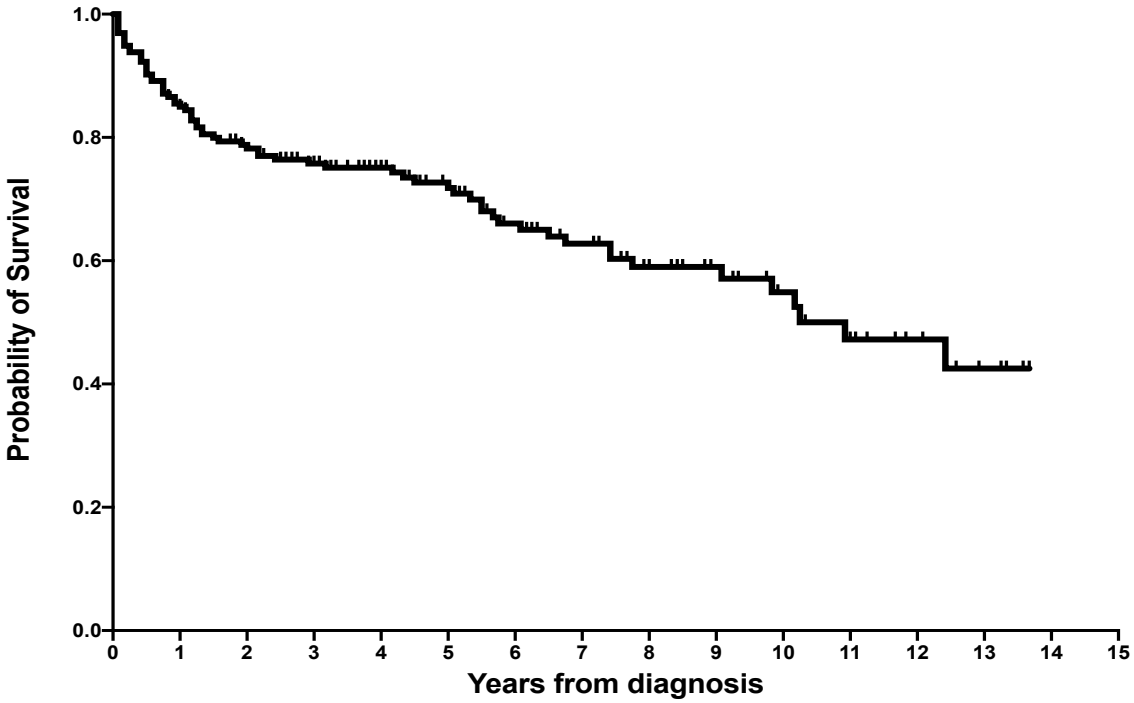

Figure 3.1 Probability of overall survival for all patients with diffuse large B-cell lymphoma (n=195). Vertical lines at censored events.

Table 3.1 Patients characteristics (n=179 for IPI and R-IPI, n=169 for NCCN-IPI). Data are n (%) except age, median (range). NCCN organ involvement = bone marrow, central nervous system, liver/gastrointestinal tract or lung

Characteristic	Data
Age, years	
Median (range)	62 (17-90)
Age groups, years	
≤40	26 (15)
41-61	52 (29)
61-75	63 (35)
>75	38 (21)
Ann Arbor stage	
I/II	77 (43)
III/IV	102 (57)
ECOG performance status	
0/1	136 (76)
≥2	43 (24)
LDH	
Normal range	53 (30)
1-3 x ULN	94 (52)
>3 x ULN	32 (18)
Extranodal sites	
0/1	141 (79)
≥2	38 (21)
NCCN organ involvement	
No	122 (72)
Yes	47 (28)
IPI risk group	
Low (0/1)	60 (34)
Low-intermediate (2)	38 (21)
High-intermediate (3)	42 (23)
High (4/5)	39 (22)
R-IPI risk group	
Very good (0)	18 (10)
Good (1/2)	80 (45)
Poor (3/4/5)	81 (45)
NCCN-IPI risk group	
Low (0/1)	23 (14)
Low-intermediate (2/3)	64 (38)
High-intermediate (4/5)	53 (31)
High (6/7/8)	29 (17)

3.4.2 Performance of the clinical prognostic tools

Patients were allocated into groups according to each of the 3 prognostic tools (table 3.1). The IPI identified 34% as low risk, 21% as low-intermediate risk, 23% as high-intermediate risk and 22% as high risk. The R-IPI categorised 10% as very good risk, 45% as good risk and 45% as poor risk. The NCCN-IPI, which applies a weighted score to age and LDH and recognises only specific extra-nodal sites as prognostic indicators, identified 14% as low risk, 38% as low-intermediate risk, 31% as high-intermediate risk and 17% as high risk.

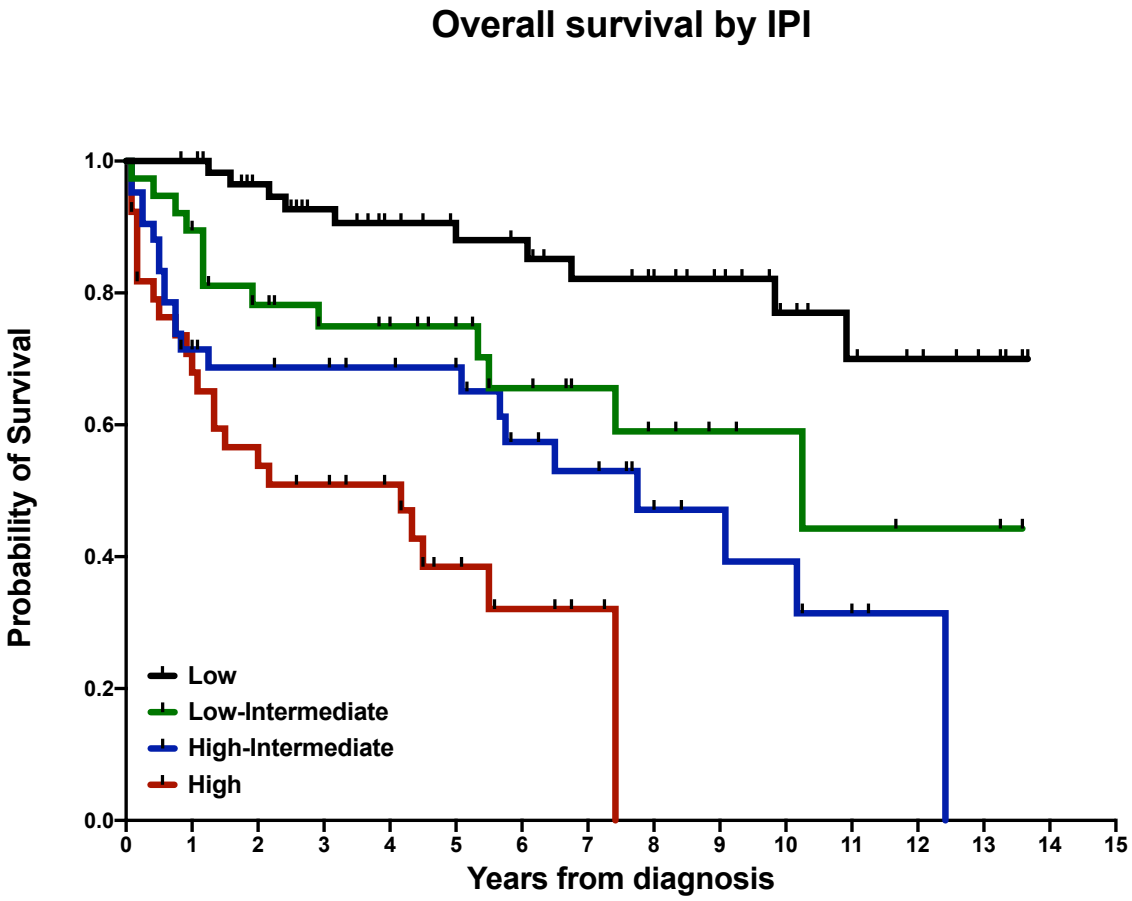

Figure 3.2 Probability of overall survival by the international prognostic index (IPI), n=179. Vertical lines at censored events, Log-rank p-value<0.0001.

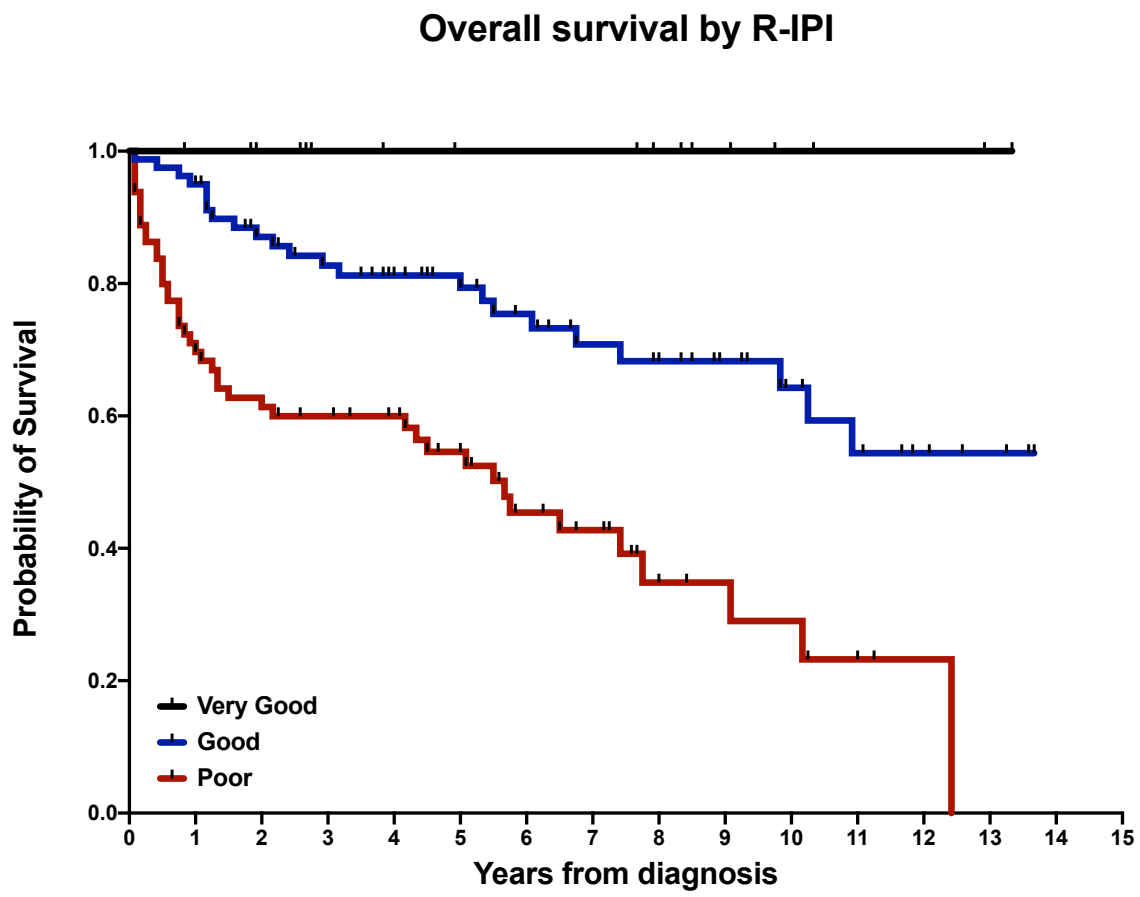

Figure 3.3 Probability of overall survival by the revised international prognostic index (R-IPI), n=179. Vertical lines at censored events, Log-rank p-value<0.0001.

The IPI, R-IPI and NCCN-IPI all defined risk groups with significantly different OS (p<0.0001). The 5-year OS estimates for the four IPI groups were 88%, 75%, 69% and 39% (figure 3.2), for the three R-IPI groups were 100%, 81% and 55% (figure 3.3), and for the four NCCN-IPI groups were 100%, 82%, 64% and 33% (figure 3.4). The NCCN-IPI had the greatest absolute difference between 5-years OS for the highest and lowest risk groups defined. The R-IPI and NCCN-IPI both identified a subgroup of patients with very favourable long-term outcomes with no deaths recorded during the follow-up period. However, the R-IPI in particular allocated a poor risk group with heterogeneous outcome, with 5-year OS estimates > 50%. The IPI and NCCN-IPI identified high risk groups with 5-year OS estimates of 39% and 33% respectively.

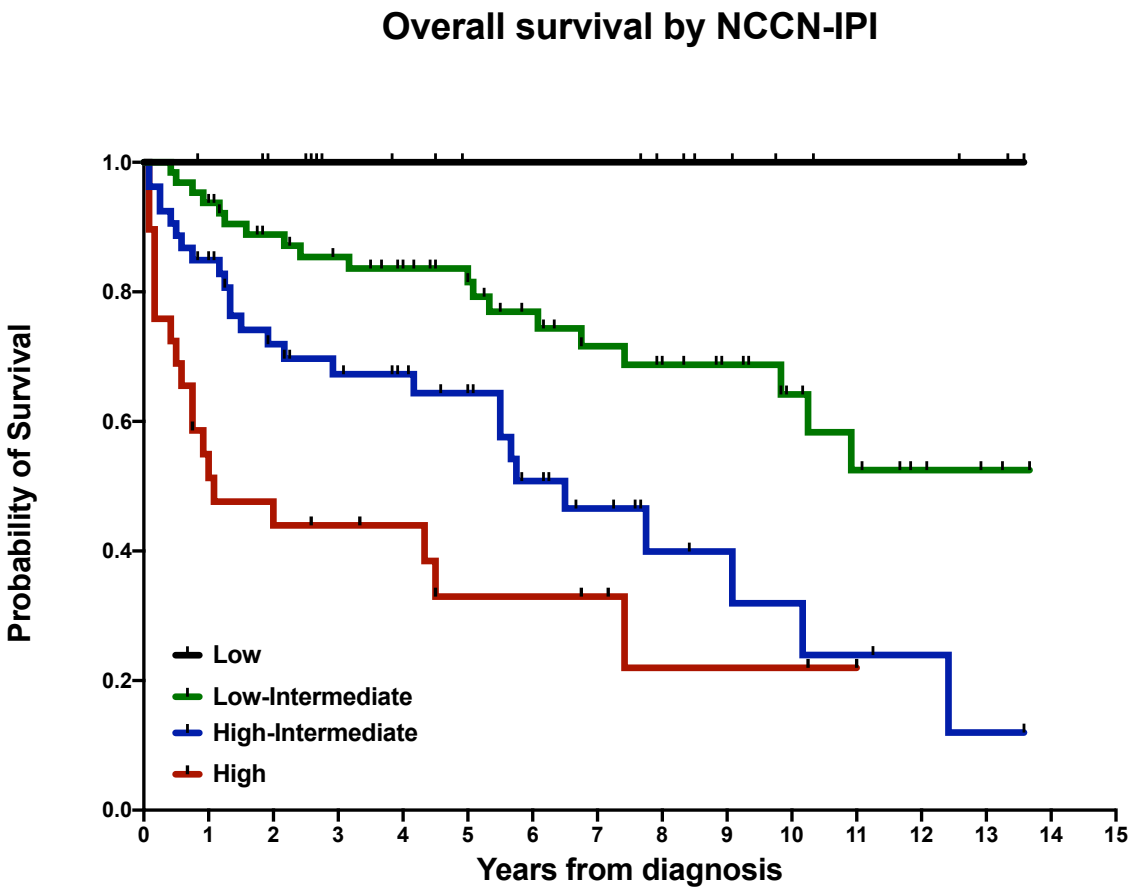

Figure 3.4 Probability of overall survival by national comprehensive cancer network international prognostic index (NCCN-IPI), n=169. Vertical lines at censored events, Log-rank p-value<0.0001.

3.4.3 Absolute monocyte and lymphocyte count in DLBCL and healthy donors

For the 146 DLBCL patients with FBC data available prior to commencing therapy, the AMC and ALC were compared to a healthy donor group consisting of 116 stem cell donors (figure 3.5). The median AMC was higher in DLBCL patients (0.6 x 10^9/L range, 0.1-2.3 x 10^9/L) than in healthy donors (0.4 x 10^9/L range, 0.2-0.9 x10^9/L). The median ALC was lower in DLBCL patients (1.5 x 10^9/L range, 0.2-6.8 x 10^9/L) than in healthy donors (1.68 x 10^9/L range, 0.79-3.76 x10^9/L). The normal ranges for AMC and ALC at our centre are 0.2-1.0 x 10^9/L and 1.0-3.0 x 10^9/L respectively. The median age of the healthy donors was 47 years (range, 18-62).

Although the age of the healthy donor group was lower than the DLBCL patients, there were no correlations between either AMC or ALC and age within either group (figure 3.6).

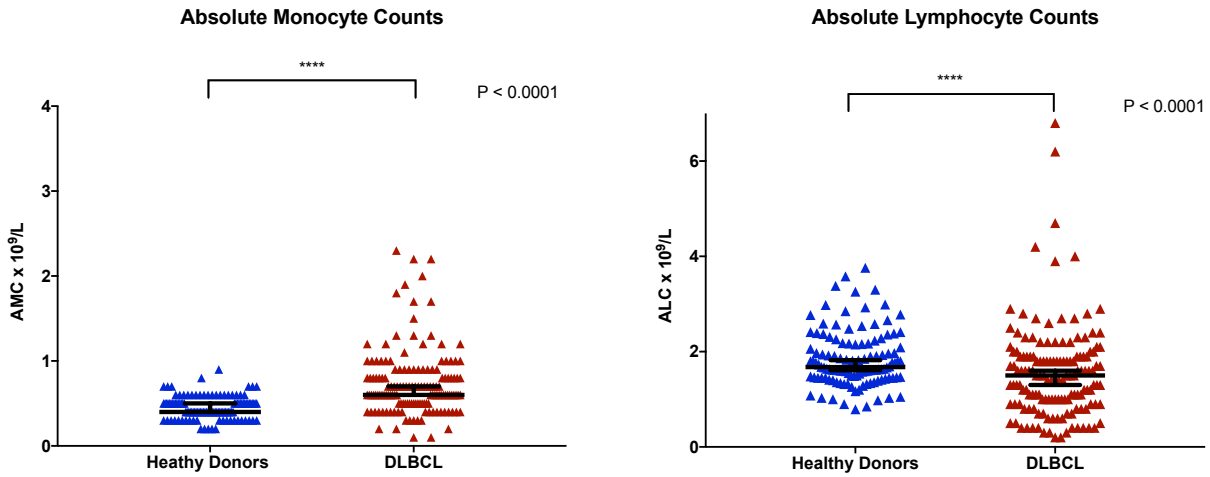

Figure 3.5 Absolute monocyte and lymphocyte count data from healthy stem cell donors (n=116) and DLBCL patients (n=146). Median AMC is higher and ALC lower in DLBCL (p<0.0001). Comparisons by Mann-Whitney U-test.

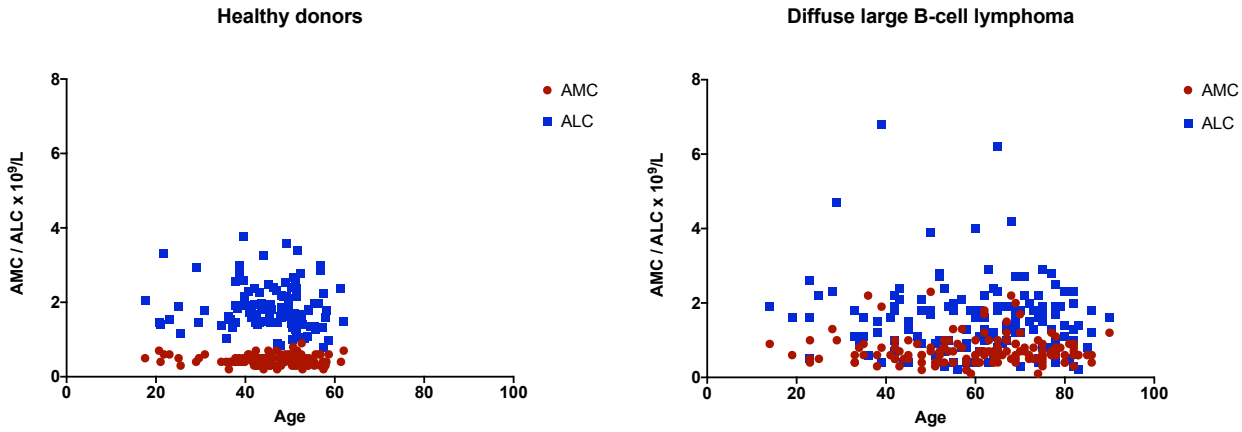

Figure 3.6 No correlation of age with absolute monocyte and lymphocyte counts from healthy stem cell donors (n=116) and DLBCL patients (n=146). All correlations not significant (ns) by Spearman rank. Age v AMC (red), r=-0.04 (healthy donors), r= 0.03 (DLBCL). Age v ALC (blue), r=-0.1 (healthy donors), r= -0.06 (DLBCL).

3.4.4 Absolute monocyte and lymphocyte count as prognostic factors in DLBCL

To evaluate the prognostic significance of the pre-treatment AMC and ALC, they were assessed as dichotomised variables, using cut-points defined by X-tile as well as those previously reported (191, 322, 323). The optimal cut-points identified by X-tile were 1.1 x 10^9/L for AMC and 0.9 x 10^9/L for ALC, which both separated our cohort into groups with different outcome ($p<0.05$, figure 3.7). In the published literature, 0.6 x 10^9/L and 1.1 x 10^9/L have been used as cut-points for AMC and ALC, respectively. These cut-points were also able to separate our cohort into groups with distinct outcome ($p<0.05$, figure 3.8). Although the cut-points identified in our cohort by X-tile performed slightly better in separating outcome groups, the previously published cut-points were taken forward for further analysis as they demonstrated significance in our patients as well as in independent cohorts. On univariate analysis, both AMC high (≥ 0.6 x 10^9/L) and ALC low (< 1.1 x 10^9/L) were associated with inferior outcome with hazard ratios of 2.6 (95% CI, 1.1-5.8, p=0.023) and 3.0 (95% CI, 1.6-5.5, $p<0.01$), respectively. For comparison, each of the IPI factors were also assessed on univariate analysis with all except >1 extra-nodal site of disease being associated with inferior outcome ($p<0.05$). Including the IPI factors with significance on univariate analysis with AMC high and ALC low on multivariate analysis demonstrated that ALC low, age, performance status and stage all retained significance as adverse prognostic factors (figure 3.9). The AMC and ALC were not different in DLBCL based on the cell of origin (COO) subtype defined by immunohistochemistry (IHC) (p ns by Mann-Whitney U-test).

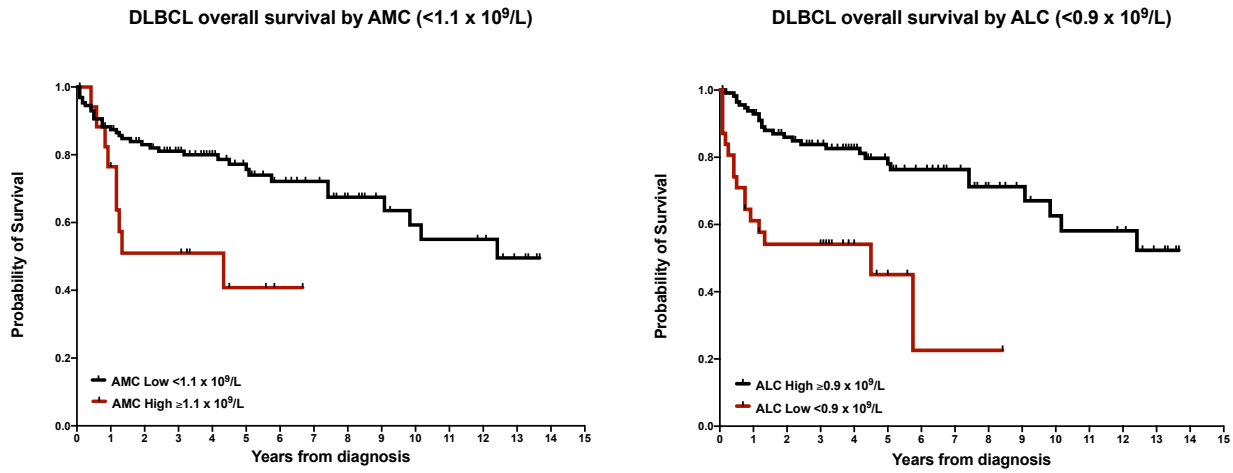

Figure 3.7 Probability of overall survival for DLBCL patients separated by AMC and ALC. DLBCL patients with AMC < 1.1 x10^9/L had superior outcomes that those with AMC ≥ 1.1 x 10^9/L, while patients with ALC < 0.9 x 10^9/L had inferior outcomes to those with ALC ≥ 0.9 x 10^9/L ($p<0.05$). Cut-points defined by X-tile.

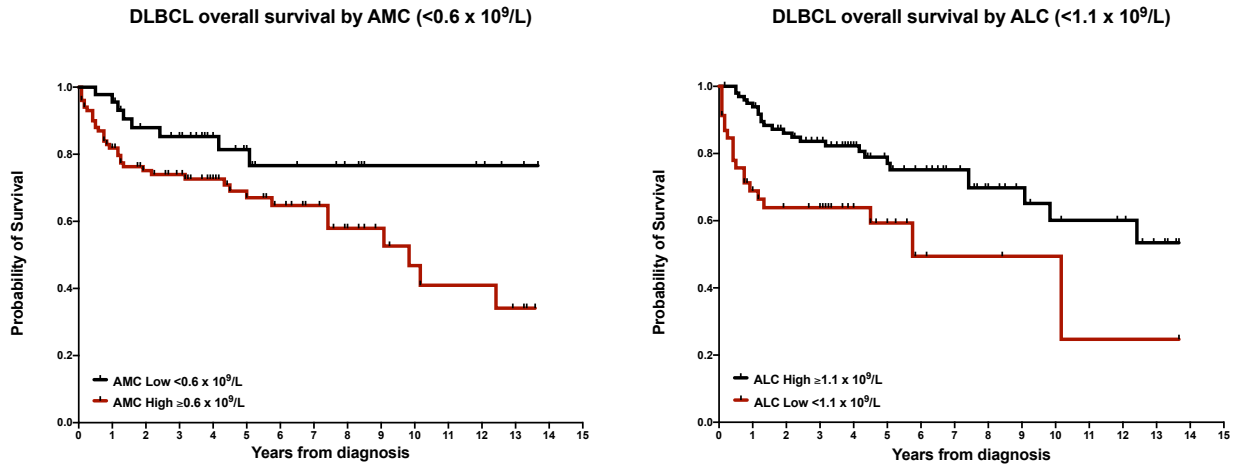

Figure 3.8 Probability of overall survival for DLBCL patients separated by AMC and ALC. DLBCL patients with AMC < 0.6 x10^9/L had superior outcomes that those with AMC ≥ 0.6 x 10^9/L, while patients with ALC < 1.1 x 10^9/L had inferior outcomes to those with ALC ≥ 1.1 x 10^9/L ($p<0.05$). Cut points defined by previously published studies (191).

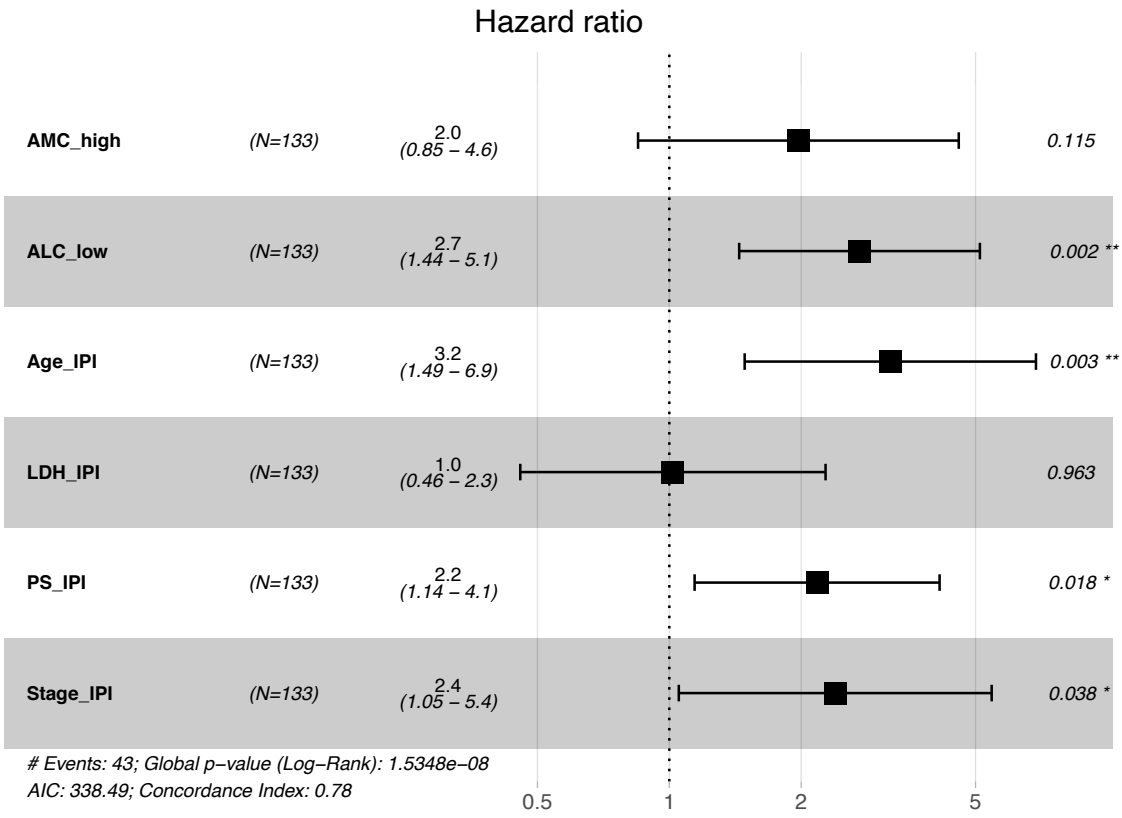

Figure 3.9 Multivariate analysis for overall survival in DLBCL. Hazard ratio > 1 indicates an increased risk of death in the presence the specific factor. AMC high, absolute monocyte count ≥ 0.6 x10^9/L; ALC low, absolute lymphocyte count < 1.1 x10^9/L; IPI, international prognostic index; LDH, lactate dehydrogenase; PS, performance status.

3.4.5 Absolute monocyte and lymphocyte count prognostic score

The AMC / ALC prognostic score has also been developed as a tool to stratify patients based on the pre-treatment FBC (191). This groups patients into 3 categories based on the presence of AMC high and ALC low as adverse factors, such that low risk patients have neither, intermediate risk have one and high risk both. Applying this score to our cohort separated 3 groups with distinct outcome, but as with the IPI scores failed to clearly identify the highest risk patients (p<0.0001, figure 3.10).

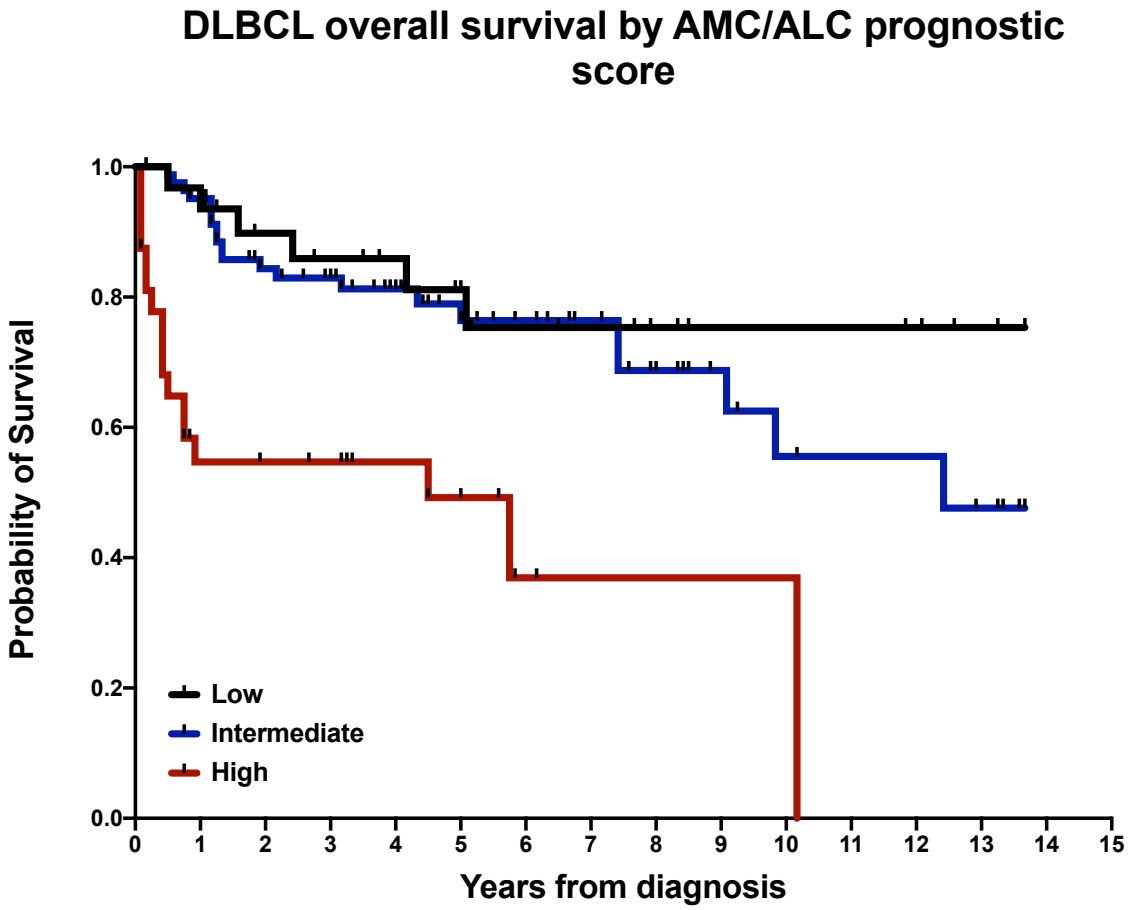

Figure 3.10 Probability of overall survival for DLBCL patients separated by AMC / ALC prognostic score. The prognostic score is based on presence of AMC high (≥ 0.6 x 10^9/L) and ALC low (< 1.1 x 10^9/L) as adverse factors. Low risk patients have neither adverse factor, intermediate risk 1 and high risk both. Log-rank p-value<0.0001.

Applying the AMC / ALC prognostic score to the highest risk patients identified by each of the prognostic tools was able to further stratify these groups. Patients with a high AMC / ALC prognostic score in each of the highest risk groups according to the IPI, R-IPI and NCCN-IPI had 1-year OS estimates of 32%, 38% and 24% with 5-year OS estimates of 16%, 32% and 0%, respectively (all p<0.05), with the NCCN-IPI and prognostic score combining to identify the highest risk group in our cohort (table 3.2).

OS estimates for high risk prognostic tool groups with AMC / ALC prognostic score high					
	1-year OS	(95% CI)	5-year OS	(95% CI)	p value
IPI high	32%	(9-59%)	16%	(1-47%)	0.020
R-IPI poor	38%	(18-57%)	32%	(12-52%)	0.002
NCCN-IPI high	24%	(4-52%)	0%	NA	0.020

Table 3.2 Overall survival estimates at 1-year and 5-years for patients in the high-risk prognostic tool groups with a high AMC / ALC prognostic score.

3.5 Discussion

Each of the clinical prognostic tools developed for DLBCL could identify distinct groups of patients based on outcome in our cohort of patients. The NCCN-IPI performed best in terms of identifying a group with the poorest outcome as well those with a very favourable long-term survival. The R-IPI also identified a group with very favourable outcome but failed to discriminate a group with < 50% 5-year OS. All 3 risk scores were unable to clearly identify patients with the most aggressive disease for whom RCHOP could be considered inadequate, consistent with their performance in other independent cohorts (97, 98).

Data from both preclinical studies and trials of novel agents have highlighted the importance of the immune system in DLBCL, and a number of groups have demonstrated the ability of parameters from the pre-treatment FBC to define prognostic groups (106, 163, 189, 191, 192, 194, 195, 197, 201, 203, 218, 280, 284, 285, 324, 325). We have shown in our cohort that DLBCL patients have a higher AMC and lower ALC than healthy donor controls and confirmed that within DLBCL patients, both AMC high and ALC low are adverse prognostic factors. The presence of both factors predicts poor outcome and further stratifies the poor risk patients identified by each of the IPI, R-IPI and NCCN-IPI. This

suggests that incorporation of features relevant to the immune ME into conventional prognostic scores may improve discrimination of the poorest risk patients.

Cells of the myeloid lineage have the potential to impact disease progression both negatively, by suppressing anti-tumour T-cell mediated immunity and through lymphoma supportive functions, but also positively via their innate phagocytic capacity, critical to the mechanism of action of monoclonal antibodies (mAb) and disruption of the CD47-SIRPα pathway (189, 194, 326). The observed relative monocytosis has prognostic significance in DLBCL, which may be explained by the presence of suppressive populations, acting via inhibitory ligand or suppressive cytokine expression, and / or by secretion of factors supporting lymphoma growth and proliferation (194, 195, 327, 328). The recent success seen in relapsed DLBCL with CAR-T cells suggest that T-cell suppression likely plays a key biological role in lymphoma immune evasion, which can be overcome in some patients treated with immune effector cells, whereas in others continued ME suppression is critical to their failure (284). This is likely facilitated, at least in part by cells of the myeloid ME.

The relative lymphopenia we have observed in DLBCL, again with prognostic significance, may also feasibly represent a biomarker of impaired immunity. The examples of PTLD and HIV associated lymphoma allude to a key role of immune suppression in development and progression of lymphoma. The ALC also represents a key marker of immune reconstitution and outcome predictor following both autologous and allogeneic stem cell transplantation (323, 329-331). As we have seen, genetic mechanisms of evasion from T and NK cell recognition, lineages represented in the ALC, frequently co-occur in DLBCL, suggesting that the relative lymphopenia may represent a quantitative mechanism of immune escape in DLBCL (134). Taken together these data imply that the relative lymphopenia seen in DLBCL reflects underlying immune dysfunction.

The evidence linking both AMC high and ALC low with adverse outcomes in DLBCL raises the possibility that improved biological understanding of these immune cell populations might facilitate development of novel prognostic models and therapeutic strategies. To address this question and understand the biological basis of these changes in immune cell populations, we performed a detailed phenotypic single-cell analysis of the peripheral blood

immune ME and explored cytokine signatures together with the cytokine producing capacity of immune cell populations in DLBCL. These data will be presented in the next two chapters.

Limitations of the study

Whilst the findings in this study have confirmed the utility of the clinical prognostic scores and the AMC / ALC in separating patients in our cohort into groups with distinct outcome, there are limitations which must be acknowledged. Firstly, there were several patients with missing data, with 10 excluded from NCCN-IPI assessment and 33 from AMC / ALC assessment. The blood count data proved particularly challenging due to a change in pathology results technology at St. Barts hospital during the late 2000's. This resulted in a 'black hole' period in which retrospective pathology reporting data was not easily available. During the data collection phase, patient sex was not documented since it does not feature in the prognostic scoring systems. However, some studies have suggested male sex to be an adverse factor, especially in those treated with Rituximab containing therapy (332). Finally, we did not capture cytomegalovirus (CMV) status during data collection for our patient cohort. As with sex, CMV status does not feature in the clinical assessment tools but, however is known to influence immune responses and this data would have been interesting considering our subsequent work detailed in the remainder of the thesis.

4. Comprehensive immunophenotyping of peripheral blood immune populations in DLBCL

4.1 Introduction

The human immune system consists of a complex network of many cell populations and signalling molecules with specialised functions and shows considerable inter-individual variation but with relative stability within an individual over time, at least in healthy subjects (303). Immune cell populations can vary according to a broad range of host specific and environmental factors including genetics, aging, sex, the microbiome, viral exposure and vaccination, as well as various disease states (333). A given individual's immune system will encounter a unique combination of myriad exposures, but despite this, patterns emerge within groups of patients which can facilitate our understanding of immunological response to disease. In recent years the emergence of immune monitoring with mass cytometry (MC) has facilitated the simultaneous analysis of multiple immune populations in high dimension within a single sample across many patients (334). Single-cell technologies such as MC lend themselves to the study of complex and variable immune cell populations found in human samples. Such approaches can define the cellular landscape at both a global and population level, as well as cellular behaviours down to a single cell, with the potential for discovery of immune signatures associated with disease and response to treatment. Once such pattern is the relative increase in monocytes and decrease in lymphocytes seen in DLBCL which consistently associate with outcome following therapy. Although a number of studies point to potential mechanisms for this observation, a detailed characterisation of these populations in DLBCL patients is lacking, with study of the heterogeneous myeloid compartment particularly neglected (198, 335). Further, given the shift in focus towards harnessing the power of the immune system for therapeutic benefit in lymphoma there exists a clear rationale to improve our biological understanding of the immune landscape in DLBCL. We hypothesised that a detailed phenotypic analysis by MC of the monocyte and lymphoid populations in DLBCL would help us to understand the pathophysiology of the immune environment in this disease.

4.2 Aim

To comprehensively phenotype the peripheral blood immune cell populations in DLBCL with a focus on delineating myeloid heterogeneity and lymphocyte subsets with known phenotypic and functional characteristics.

4.3 Methods

4.3.1 Patient selection

Peripheral blood mononuclear cells (PBMCs) were accessed via the Barts tissue bank for 43 different DLBCL patients collected at the time of diagnosis prior to commencing any therapy based on availability of samples. All samples were cryopreserved and stored in liquid nitrogen. Diagnostic biopsy reports were reviewed to confirm the diagnosis. All patients were treated with RCHOP except for two, who were both randomized and received bortezomib plus RCHOP in the ReMoDL-B study (118). Several patients received additional methotrexate, either intravenously or intrathecally for central nervous system (CNS) prophylaxis as per established local guidelines. PBMCs from eight healthy blood donors isolated from leucocyte cones were included as a control group with an aliquot from one of these, healthy donor 'JF', included with each experiment for quality control.

4.3.2 Immunophenotyping antibody panels

The major immune cell lineages that make up the AMC and ALC are found in PBMC samples and consist of myeloid populations together with lymphocytes of the T, B and NK cell subtypes. We therefore designed and optimised two antibody panels targeting predominantly surface proteins, but also several intranuclear transcription factors, to identify the relevant cell lineages, together with their known phenotypic and functional subsets. These panels were termed 'Myeloid' and 'T-cell' (see table 2.1). For T-cells, multiple cell subpopulations, together with maturation and antigen-experience states can be

identified robustly based on expression of surface markers and transcription factors (336-338). In addition to subset discrimination, the capacity to identify expression of various immune checkpoint molecules, with relevance to T-cell activation states and therapeutic targeting, was also key to our panel development. For the myeloid compartment, subsets of monocytes and dendritic cells can be delineated based on expression of surface markers, but great diversity is known to exist in these populations in both health and disease, and therefore a number of targets with relevance to myeloid biology, function and activation states were included (339-344). Figure 4.1 details the protein targets selected for this study with their relevance to cell identification and functional / activation states.

Leucocytes	
CD45	Leucocyte common antigen
CD47	Provides 'don't eat' signal to phagocytes
T cells	
CD3	T cells
CD4	CD4+ T cells
CD8a	CD8+ T cells
CD25	Regulatory T cells (Treg), activation
CD27	Maturation
CD28	Co-stimulation signals
CD38	Maturation
CD45RA	Naïve cells
CD56	NKT cells
CD127	T cell subsets, low expression on Treg
CD134 (OX40)	Co-stimulation signals
CD152 (CTLA-4)	Immune checkpoint
CD197 (CCR7)	Naïve / memory cells
CD223 (LAG-3)	Immune checkpoint
CD279 (PD-1)	Immune checkpoint
CD366 (TIM-3)	Immune checkpoint
FoxP3	Treg transcription factor
Granzyme B	Cytotoxicity
Perforin	Cytotoxicity
T-bet	T helper (TH1) transcription factor
B cells	
CD19	B cells
CD20	B cells, target for rituximab
CD25	Activation
CD27	Memory
CD38	Naïve
HLA-DR	Antigen presentation (MHC-II)
NK cells	
CD8a	NK subsets
CD16	NK subsets
CD56	NK cells
CD226 (DNAM-1	Activation
Granzyme B	Cytotoxicity
Perforin	Cytotoxicity
T-bet	Maturation
Myeloid cells	
CD11b	Complement receptor, Myeloid cells
CD11c	Complement receptor, Monocytes, DCs
CD13	Aminopeptidase
CD14	LPS receptor, Monocyte subsets
CD16	Fcγ Receptor III, Monocyte subsets
CD31 (PECAM-1	Angiogenesis
CD32	Fcγ Receptor II
CD33	Myeloid cells
CD38	Activation
CD40	Co-stimulation signals
CD64	Fcγ Receptor I (high affinity)
CD86	Co-stimulation signals
CD91	Phagocytosis
CD123	pDCs
CD172a	SIPRα, 'don't eat' signal, binds CD47
CD163	Scavenger receptor
CD184 (CXCR4)	Receptor for SDF-1, chemotaxis
CD192 (CCR2)	Monocyte migration
CD206 (MMR)	Macrophage mannose receptor
CD272 (BTLA)	Inhibitory signals
CD274 (PD-L1)	Inhibitory signals
CX3CR1	Chemotaxis, myeloid subsets
HLA-DR	Antigen presentation (MHC-II)

Figure 4.1 Antigen targets for comprehensive immunophenotyping of peripheral blood immune cells in DLBCL. Proteins were selected based on their relevance to subpopulation identification and to define maturation, activation and functional states.

4.3.3 Mass cytometry staining

PBMC samples were resuscitated from liquid nitrogen storage and stained as described in chapter 2. Samples were stained in 96-well plates in batches of 20 patient or healthy donor control samples, with an aliquot from the same healthy donor control 'JF' also stained with each plate. Patient samples were selected at random for staining and where enough cells were available or multiple vials existed, were split evenly between 2 plates, one stained with the 'myeloid' and one with the 'T-cell' panel, although as detailed below, not all samples had sufficient cells to allow staining with both panels. Due to the majority of the healthy donor control samples being stored in a lower number of large aliquots, all healthy donor samples were stained on the same plate for each antibody panel, together with the 'JF' control and a batch of patient samples. This allowed optimal usage of the available cells from the healthy donors, which once resuscitated were divided and stained with both phenotyping panels and also used for functional experiments as detailed in chapter 5. Antibody master-mixes were made up for each plate for n=21 samples (20 patient / healthy donors and 1 reference 'JF' sample) with 10% excess for every staining run to ensure consistency of pipetting volume across experiments. Samples were acquired on the CyTOF2 in batches of 6-8 depending on the cell numbers post staining. Staining consistency was checked for each batch with reference to the EQ beads and the 'JF' control sample.

4.4 Results

4.4.1 Patient characteristics

The characteristics of all the patients included in this study are summarised in table 4.1. Of the 43 DLBCL patient PBMC samples used in this study, 42 were analysed with the 'Myeloid' panel and 32 with the 'T-cell' panel, with 31 patients having data acquired with both panels. The median age at diagnosis of these was 63 (range, 30-84) and 26 patients were over 60 years of age. Twenty-seven patients were in maintained complete remission at > 24 months from completion of frontline therapy and 15 had documented relapse / refractory disease, 12 of whom progressed within 12 months of initial treatment. For one patient, no follow up

data was available and therefore this patient was included in the initial analysis but excluded from the outcome analysis. The cell of origin (COO) based on immunohisto-chemistry (IHC) was available for 30 patients. IPI data was available for all patients and pre-treatment AMC and ALC for 27. All but 7 patients had a serum sample also available for cytokine / chemokine analysis (see chapter 5).

Table 4.1 Patient characteristics for the peripheral blood immunophenotyping study. Table on the next page. Patient ID, anonymised identification code; Vial ID, vial identification code; Myeloid panel, stained with this panel (Yes) or not (x); T-cell panel, stained with this panel (yes) or not (x); Diagnosis, Diffuse large B-cell lymphoma (DLBCL); Outcome, unknown for one patient, COO, cell of origin based on the Han's algorithm, GCB, germinal centre B cell or not (Non_GCB); Age, at diagnosis; IPI factors, number of international prognostic index factors; Serum, sample available for cytokine analysis; Treatment, RCHOP, rituximab, cyclophosphamide, doxorubicin, vincristine, prednisolone, with addition of bortezomib (B) in 2 patients; AMC, absolute monocyte count; ALC, absolute lymphocyte count.

Patient ID	Vial ID	Myeloid panel	T cell panel	Diagnosis	Outcome	COO	Age	IPI factors	Serum	Treatment	AMC (x 10^9/L)	ALC (x 10^9/L)
6518	R2225	Yes	Yes	DLBCL	Remission	GCB	72	1	Yes	RCHOP	0.5	2.0
6541	R2157	Yes	x	DLBCL	Relapse	Non_GCB	65	3	Yes	RCHOP	0.6	0.8
6561	R2102	Yes	Yes	DLBCL	Relapse	GCB	47	3	Yes	RCHOP	0.9	1.1
6623	R2928	Yes	Yes	DLBCL	Remission	Non_GCB	71	1	Yes	RCHOP	0.7	2.7
6649	R3448	Yes	x	DLBCL	Relapse	GCB	61	4	Yes	RCHOP	0.7	0.7
6651	R3056	Yes	Yes	DLBCL	Remission	GCB	35	0	Yes	RCHOP	0.6	1.6
6657	R2795	Yes	Yes	DLBCL	Remission	GCB	58	3	Yes	RCHOP	0.2	0.4
6719	R3134	Yes	x	DLBCL	Remission	GCB	52	1	Yes	RCHOP	0.4	2.7
6722	R3615	Yes	x	DLBCL	Remission	Unknown	66	3	Yes	RCHOP	0.6	0.9
6797	R3101	Yes	Yes	DLBCL	Remission	GCB	58	1	Yes	RCHOP	0.4	0.9
7065	R1959	Yes	Yes	DLBCL	Unknown	Unknown	65	4	x	RCHOP	x	x
7140	R5448	Yes	Yes	DLBCL	Relapse	Unknown	67	3	Yes	RCHOP	x	x
7189	R5749	Yes	x	DLBCL	Remission	Unknown	30	0	x	RCHOP	x	x
7238	R5935	Yes	Yes	DLBCL	Remission	Unknown	69	1	Yes	RCHOP	x	x
7306	R6229	Yes	x	DLBCL	Remission	Non_GCB	72	3	Yes	RCHOP	x	x
7318	R6517	Yes	x	DLBCL	Remission	Non_GCB	57	3	Yes	RCHOP	x	x
7351	R6907	Yes	Yes	DLBCL	Remission	Unknown	84	1	Yes	RCHOP	x	x
7354	R6732	Yes	Yes	DLBCL	Remission	GCB	61	1	Yes	RCHOP	x	x
7368	R6408	Yes	Yes	DLBCL	Remission	Unknown	57	1	Yes	RCHOP	x	x
7373	R7214	Yes	x	DLBCL	Remission	GCB	59	1	Yes	RCHOP	x	x
7374	R7219	Yes	x	DLBCL	Relapse	Unknown	32	2	Yes	RCHOP	x	x
7407	R6852	Yes	Yes	DLBCL	Remission	Non_GCB	67	3	Yes	RCHOP	x	x
7638	R8792	Yes	Yes	DLBCL	Relapse	Unknown	68	3	Yes	RCHOP	x	x
7723	R8950	Yes	Yes	DLBCL	Relapse	Non_GCB	63	5	x	RCHOP	x	x
7889	R9481	Yes	Yes	DLBCL	Relapse	Non_GCB	79	4	Yes	RCHOP	x	x
7951	R9903	Yes	Yes	DLBCL	Remission	Non_GCB	34	0	x	RCHOP	x	x
8107	T0833	Yes	x	DLBCL	Remission	Non_GCB	79	5	Yes	RCHOP	0.8	1.9
8479	T1962	Yes	Yes	DLBCL	Remission	Non_GCB	43	0	Yes	RCHOP	0.3	2.1
8686	T3714	Yes	Yes	DLBCL	Remission	Non_GCB	78	3	Yes	RCHOP	0.6	1.7
8792	T4358	Yes	Yes	DLBCL	Remission	Non_GCB	77	2	Yes	RCHOP	1.2	1.3
9115	T5632	Yes	Yes	DLBCL	Remission	GCB	62	3	Yes	RCHOP	1.2	1.3
9231	T6117	Yes	Yes	DLBCL	Relapse	Non_GCB	65	3	x	RCHOP	0.4	1.9
9311	T6450	Yes	Yes	DLBCL	Relapse	Unknown	69	3	Yes	RCHOP	2.0	2.7
9371	T6696	Yes	Yes	DLBCL	Remission	Non_GCB	80	4	Yes	RCHOP	0.4	1.4
9394	T6808	Yes	Yes	DLBCL	Relapse	Unknown	42	3	x	RCHOP	1.0	1.0
9440	T7002	Yes	Yes	DLBCL	Remission	Non_GCB	48	2	Yes	RCHOP	0.2	0.9
9618	T7615	Yes	Yes	DLBCL	Relapse	Non_GCB	75	1	Yes	RCHOP	0.7	1.6
9974	T8690	Yes	Yes	DLBCL	Relapse	Non_GCB	39	2	Yes	RCHOP	1.9	6.8
10115	T9536	Yes	Yes	DLBCL	Remission	Non_GCB	50	1	x	B + RCHOP	0.8	1.8
10146	T9596	Yes	Yes	DLBCL	Remission	Unknown	62	3	x	B + RCHOP	1.8	1.6
10403	C0685	Yes	Yes	DLBCL	Remission	Non_GCB	65	1	Yes	RCHOP	0.3	1.7
10416	C0339	Yes	x	DLBCL	Relapse	Unknown	53	4	Yes	RCHOP	0.8	0.3
10900	C1872	x	Yes	DLBCL	Relapse	Non_GCB	82	4	Yes	RCHOP	0.7	1.0

4.4.2 Healthy donors

PBMCs from 8 healthy donors were included in this study. All were isolated from leucocyte cones from health blood donors from which no further demographic data was available. All healthy donor samples were analysed with both immunophenotyping panels and 'JF' was analysed on every plate and every batch acquisition.

Table 4.2 Healthy donor samples for the peripheral blood immunophenotyping study.

Donor ID	Myeloid panel	T cell panel	Diagnosis
CB	Yes	Yes	Healthy Donor
CK	Yes	Yes	Healthy Donor
CP	Yes	Yes	Healthy Donor
JA	Yes	Yes	Healthy Donor
JB	Yes	Yes	Healthy Donor
JE	Yes	Yes	Healthy Donor
JF	Yes	Yes	Healthy Donor
NC	Yes	Yes	Healthy Donor

4.4.3 Peripheral blood immune cell subsets

Following staining and acquisition, data were normalised using the EQ beads and cleaned to remove the beads, debris, doublets and dead cells with DNA+, live CD45+ single events taken forward for further analysis. A sequential gating strategy based on that used by Hartmann et al (334) was employed to identify the major peripheral blood immune cell populations present in the PBMC samples (figures 4.2-4.5). All expected immune populations could be identified using canonical lineage markers with further subsets identified based on relevant marker expression, with all population frequencies for healthy donors consistent with those previously reported (333). A small percentage of cells were left unassigned due to the cut-offs imposed by manual gating but were included in the analysis using dimensionality reduction and clustering approaches discussed below. The experimental approach was demonstrated to yield largely consistent results over time with

an aliquot of PBMCs from the healthy donor ‘JF’ being acquired with every run and gated cell percentages compared between runs (see chapter 2).

A number of dimensionality reduction algorithms have been developed to facilitate exploratory analysis of large datasets of single cell cytometry data (309, 310, 313, 345). This is a useful approach to assess the overall structure of data, especially that containing multiple diverse cell populations, while conserving the single cell nature and high dimensional structure. In essence, all cells within the analysis are projected onto a 2-dimensional map, which can then be coloured by expression of markers, gates or clusters. The location of each cell on the map is determined by its position in high dimensional space, such that cells that are similar to each other with respect to the analysed parameters are located in proximity and those that are dissimilar are far apart. Immune cell subsets can thus be differentiated in an automated way without the reliance on manual gating, which can potentially miss unexpected or unknown populations, and is subject to operator bias / reproducibility issues. Therefore, together with the gating strategy outlined above, data were also assessed by dimensionality reduction. Figure 4.6 demonstrates examples of opt-SNE and UMAP projections, which include data from all 8 healthy donors in his study.

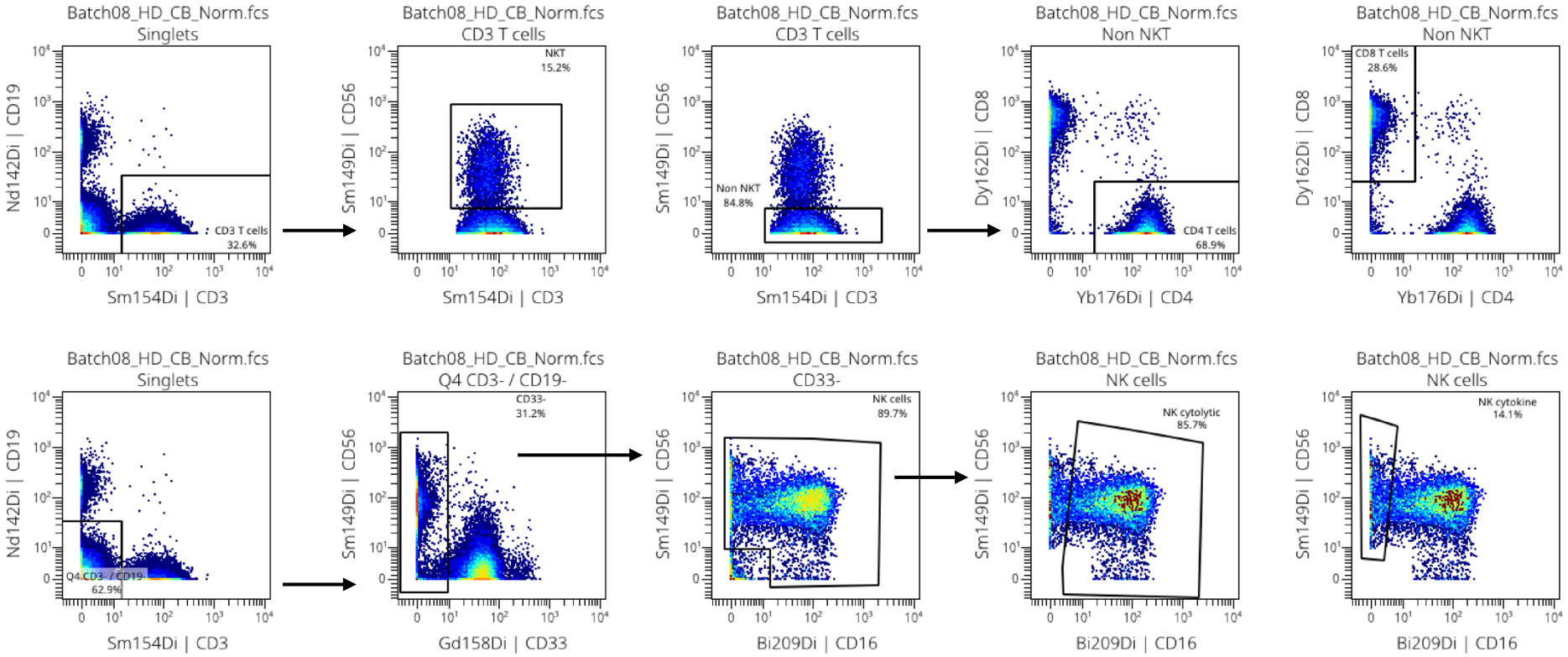

Figure 4.2 Gating strategy for T cell and NK cells with the 'Myeloid' panel. Cells were pre-gated to DNA+, live CD45+ events. An initial CD19 v CD3 gate facilitated assessment of doublets (dual positive events) and separation of B, T and non-B/T cells for further gating as indicated. HD_CB, healthy donor CB; CD, cluster of differentiation; NK, natural killer.

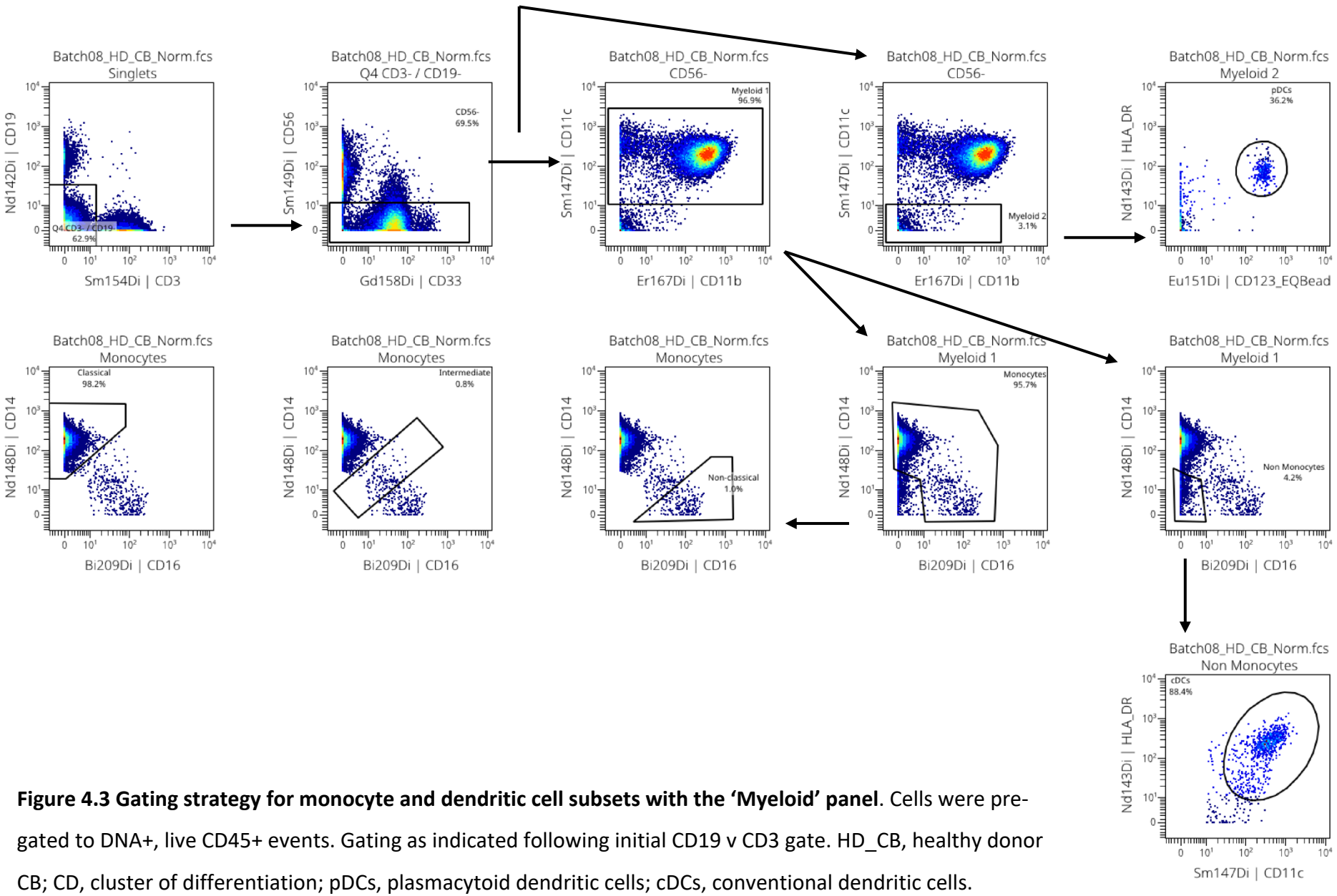

Figure 4.3 Gating strategy for monocyte and dendritic cell subsets with the 'Myeloid' panel. Cells were pre-gated to DNA+, live CD45+ events. Gating as indicated following initial CD19 v CD3 gate. HD_CB, healthy donor CB; CD, cluster of differentiation; pDCs, plasmacytoid dendritic cells; cDCs, conventional dendritic cells.

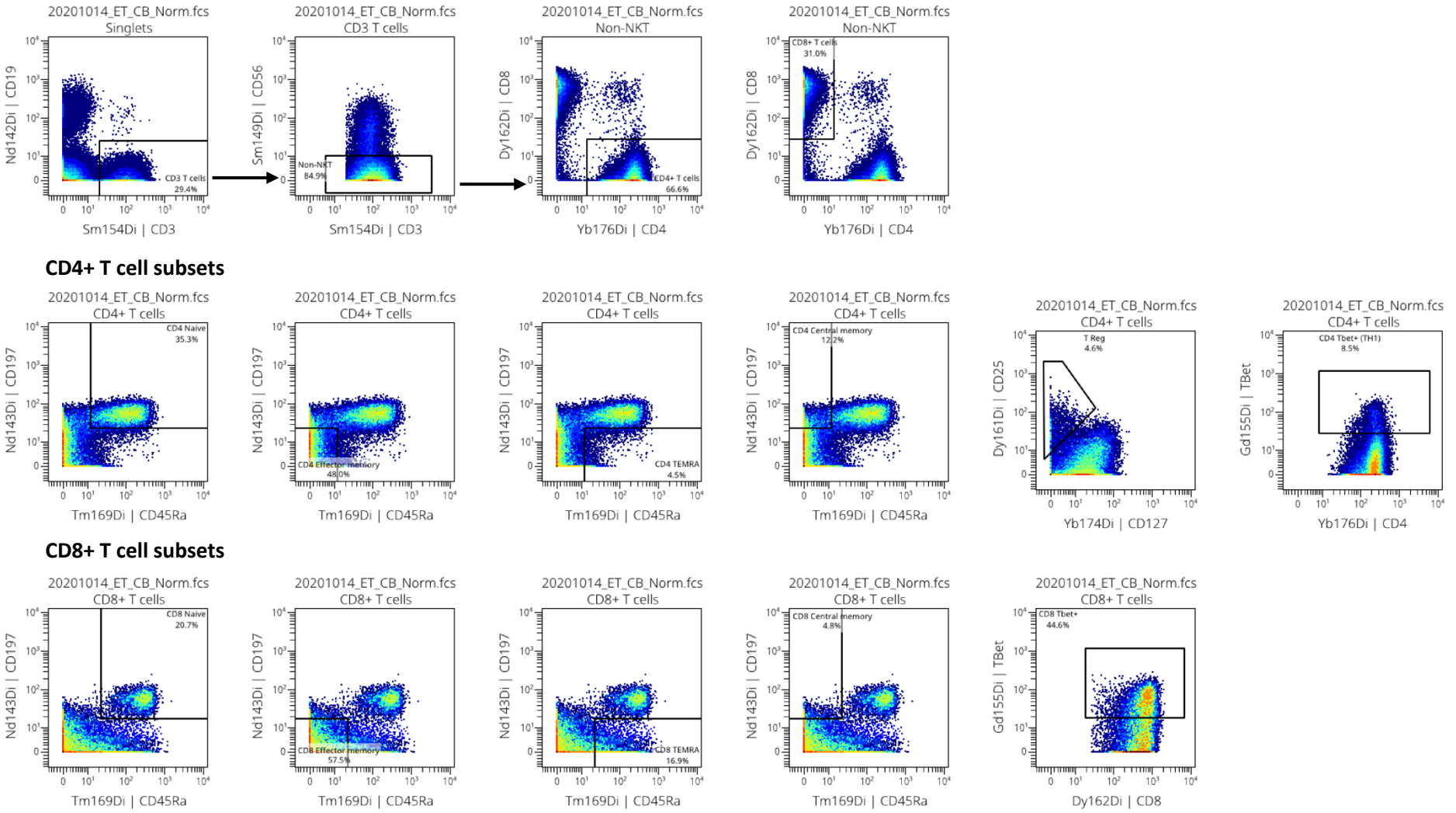

Figure 4.4 Gating strategy for T cell subsets with the 'T-cell' panel. Cells were pre-gated to DNA+, live CD45+ events. Gating as indicated following initial CD19 v CD3 gate. NKT, natural killer T; TEMRA, T effector memory RA; T reg, regulatory T cell; TH1, T helper 1.

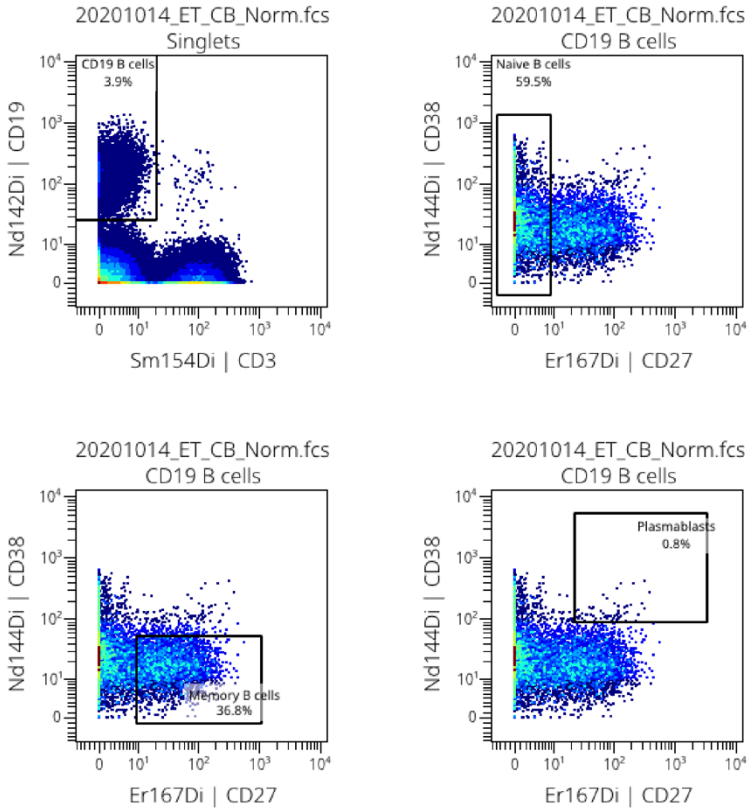

Figure 4.5 Gating strategy for B cell subsets with the 'T-cell' panel. Cells were pre-gated to DNA+, live CD45+ events. Gating as indicated following initial CD19 v CD3 gate. HD_CB, healthy donor CB; CD, cluster of differentiation; NK, natural killer.

In the left plot, cells are coloured according to assignment from manual gating and in the right, by expression of CD4, highlighting CD4+ T cells and CD4 expressing myeloid cells. The manual and automated approaches demonstrated high concordance based on canonical lineage markers, with some further separation into subpopulations evident on the opt-SNE map. In addition, clustering algorithms are also useful in high-dimensional data analysis, in which cells with similar patterns of marker expression are clustered together in an automated way (307, 311, 312, 346). This enables the discovery of unknown or unexpected subpopulations which may otherwise be missed. The FlowSOM algorithm, which uses self-organising maps followed by hierarchical consensus meta-clustering to merge clusters was used in this study. It is able to perform rapidly with large datasets giving an overview of how all markers are expressed on all cells in the analysis and has been shown to effectively identify multiple subpopulations within complex samples (307, 308, 312).

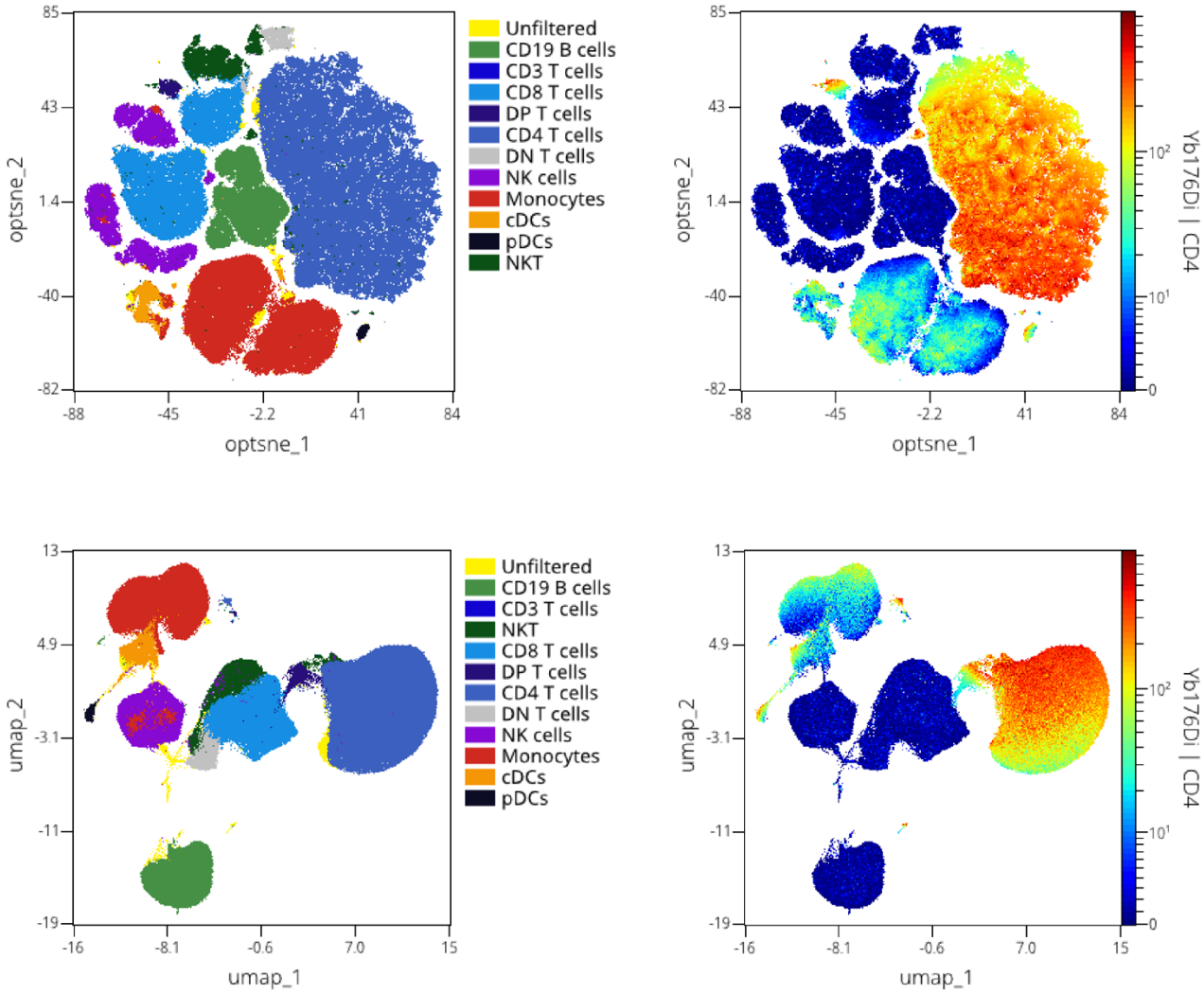

Figure 4.6 Dimensionality reduction with opt-SNE and UMAP. Data from all healthy donors (n=8) was randomly subsampled to 50,000 CD45+ events and subject to dimensionality reduction with the opt-SNE (top) and UMAP (bottom) algorithms using the lineage markers CD3, CD4, CD8a, CD11b, CD11c, CD14, CD16, CD19, CD33, CD56, CD123 and HLA-DR. Cells are coloured according to their lineage assignment by manual gating (left plot). The yellow unfiltered cells were unassigned by gating. Cells coloured by expression of CD4 (right plot). DP, double positive; DN, double negative; NK, natural killer; cDCs, conventional dendritic cells; pDCs, plasmacytoid dendritic cells; NKT, natural killer T cells.

4.4.4 Disease associated immune signatures in DLBCL

Data from all DLBCL patient and healthy donor samples were initially explored by manual gating as described above, with the results summarised in figures 4.7 for the myeloid panel and 4.8 for the lymphoid panel. The effector memory populations could be further gated to EM1 – EM4 based on expression of CD27 and CD28 (347). There were no differences in the frequency of B-/T-/NK-cells and monocytes as a percentage of CD45+ events between DLBCL and healthy donors. We did, however find significant differences in the frequency of intermediate monocytes, non-classical monocytes, T-bet+ CD4 T cells, T-bet+ CD8 T cells and CD8 TEMRA, which were all increased in DLBCL, and pDCs, CD4 effector memory 1 (EM1) and CD8 central memory (CM) which were decreased, compared to healthy donors ($p<0.05$, Mann-Whitney U-test).

To investigate for the presence of a peripheral blood immune signature in DLBCL we performed a differential abundance (DA) analysis with EdgeR to calculate fold change (FC), p values and false discovery rates (FDR), corrected for multiple-hypothesis testing, for each cell type identified by manual gating. This confirmed significant differences in intermediate and non-classical monocytes, pDCs, T-bet+ CD4, CD8 TEMRA, CD4 EM1 and CD8 CM between DLBCL and healthy donors (FDR<0.05, figures 4.9 and 4.10). Plasma-blasts / plasma cells were also increased in DLBCL, but these cells were present in the peripheral blood in extremely low frequencies overall. The increase in T-bet+ CD8 T cells in DLBCL failed to reach significance in the DA analysis.

Overall, the manual gating strategy identified a relative increase in the frequency of intermediate and non-classical monocytes and a decrease in plasmacytoid DCs in DLBCL, consistent with the increased AMC observed. While there was no abundance difference in classical monocytes, we observed marked heterogeneity in marker expression within this population, with distinct subpopulations apparent on dimensionality reduction. We further interrogated this monocyte heterogeneity within the DLBCL patients with unsupervised FlowSOM clustering, as discussed below.

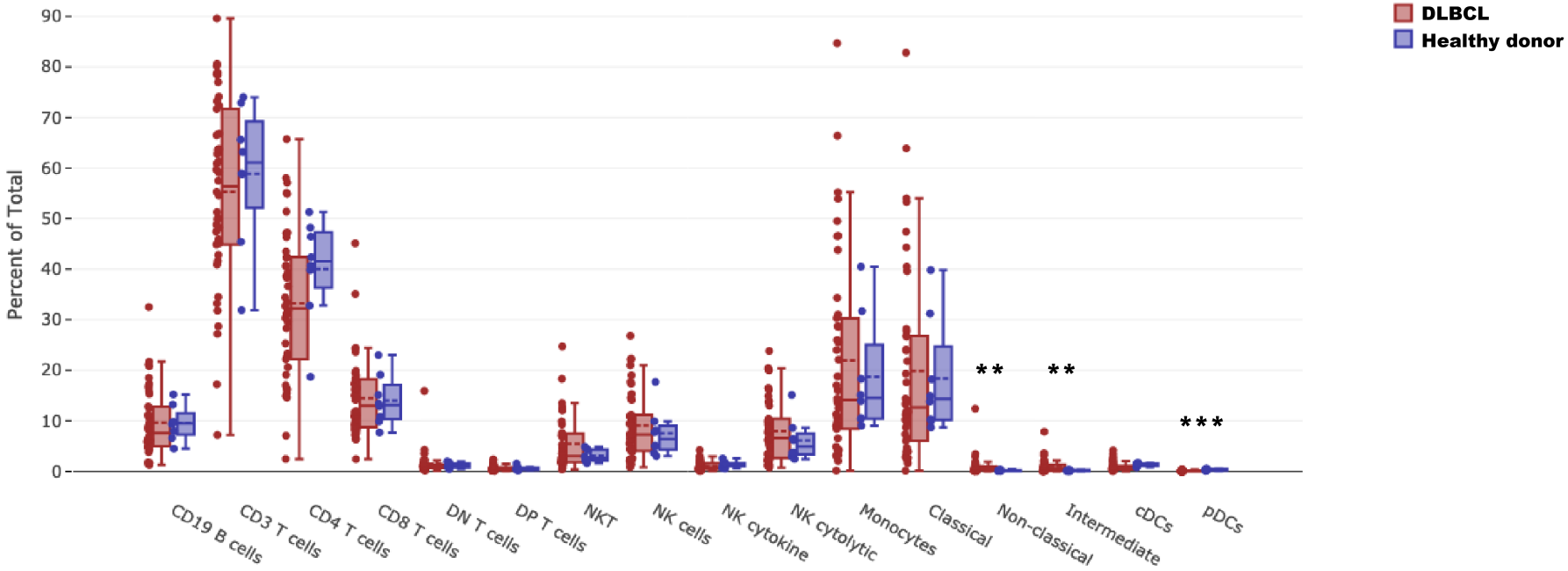

Figure 4.7 Gating derived frequencies of immune populations for all DLBCL patients (n=42, red) and healthy donors (n=8, blue) analysed with the 'myeloid' panel. Data from all patients analysed with the 'myeloid' panel. DN, double negative; DP, double positive; NKT, natural killer T cells; NK, natural killer; cDCs, conventional dendritic cells; pDCs, plasmacytoid dendritic cells. (Mann-Whitney U-test ** $p<0.01$, *** $p<0.001$).

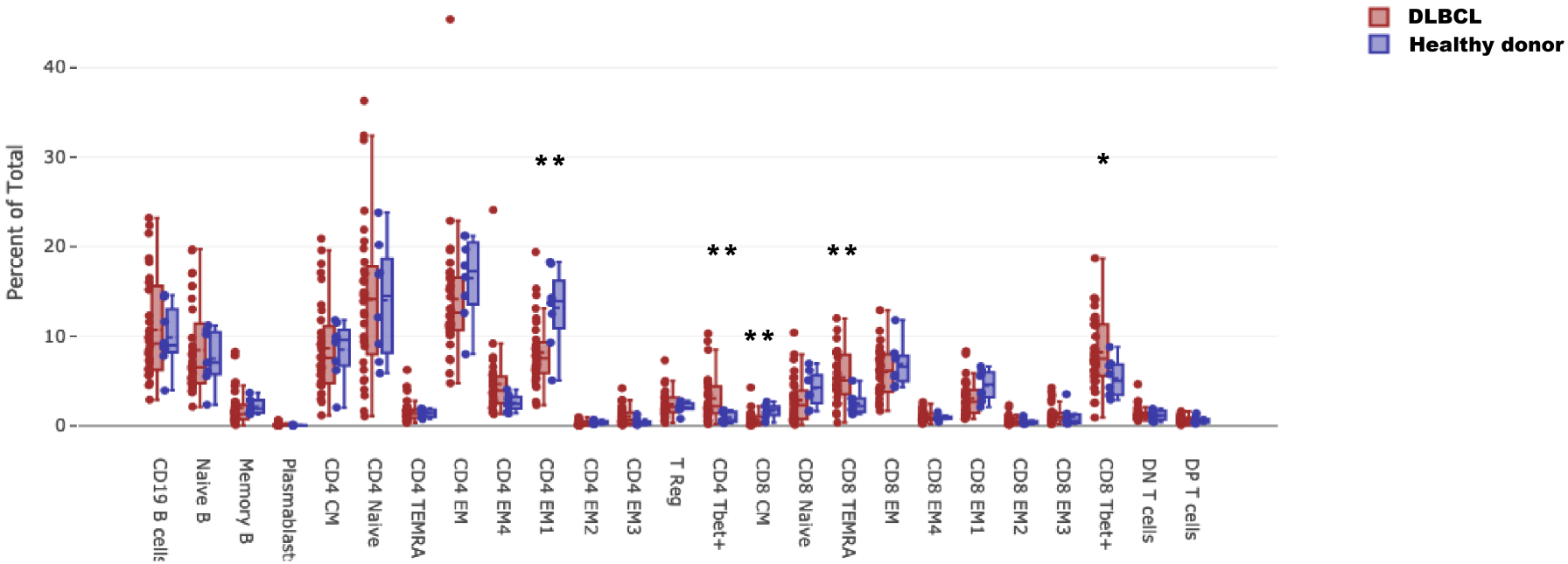

Figure 4.8 Gating derived frequencies of immune populations for all DLBCL patients (n=32, red) and healthy donors (n=8, blue) analysed with the 'T-cell' panel. Data from all patients analysed with the 'T-cell' panel. CM, central memory; EM, effector memory; TEMRA, T effector memory RA; T Reg, regulatory T cell; DN, double negative; DP, double positive. (Mann-Whitney U-test * $p<0.05$, ** $p<0.01$).

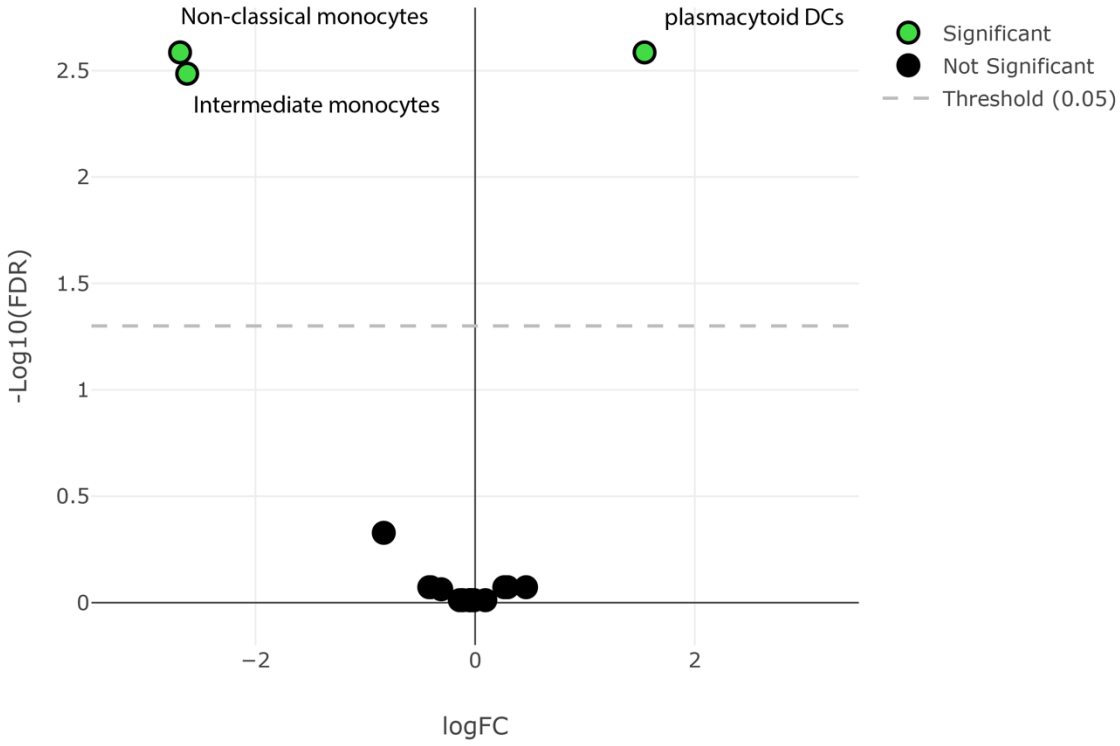

Figure 4.9 Differential abundance analysis between DLBCL patients (n=42) and healthy donors (n=8). Volcano plot showing false discovery rate (FDR) against fold change (FC) of immune cell populations between healthy donors and DLBCL. Left of centre indicates population is increased in DLBCL, right increased in healthy donors, green indicates statistical significance (FDR<0.05). Analysis from data acquired with the 'Myeloid' panel.

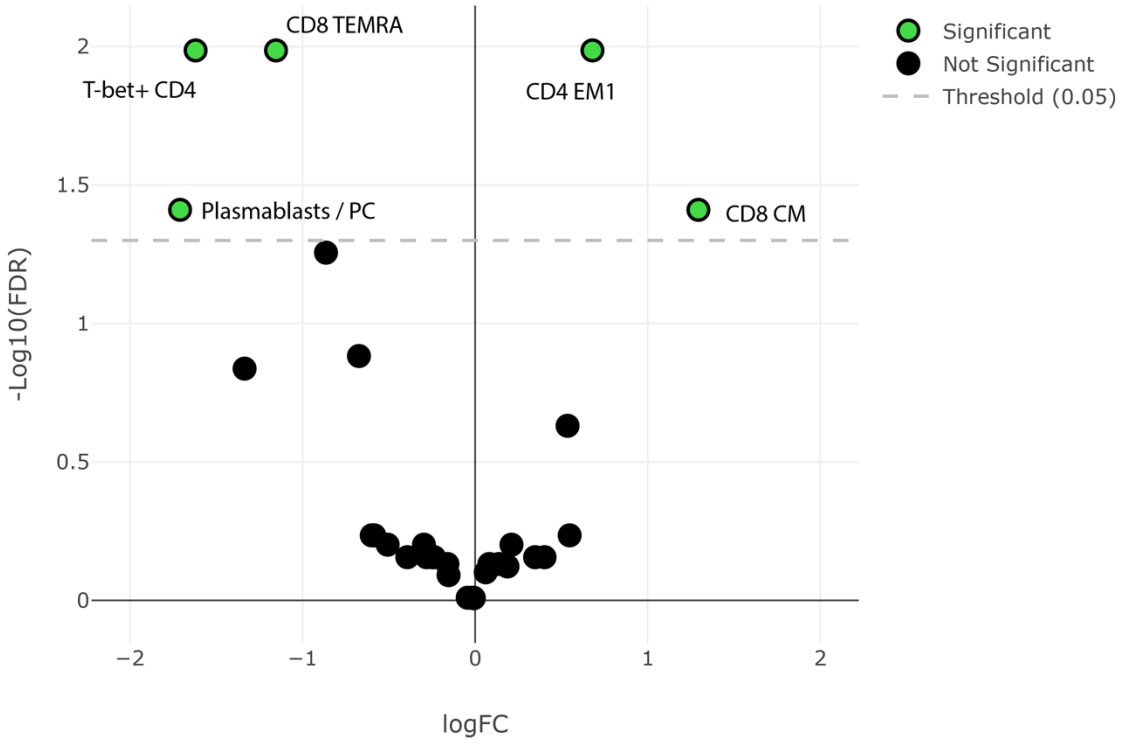

Figure 4.10 Differential abundance analysis between DLBCL patients (n=32) and healthy donors (n=8). Volcano plot showing false discovery rate (FDR) against fold change (FC) of immune cell populations between healthy donors and DLBCL. Left of centre indicates population is increased in DLBCL, right increased in healthy donors, green indicates statistical significance (FDR<0.05). CM, central memory; EM, effector memory; PC, plasma cell; TEMRA, T effector memory RA. Analysis from data acquired with the 'T-cell' panel.

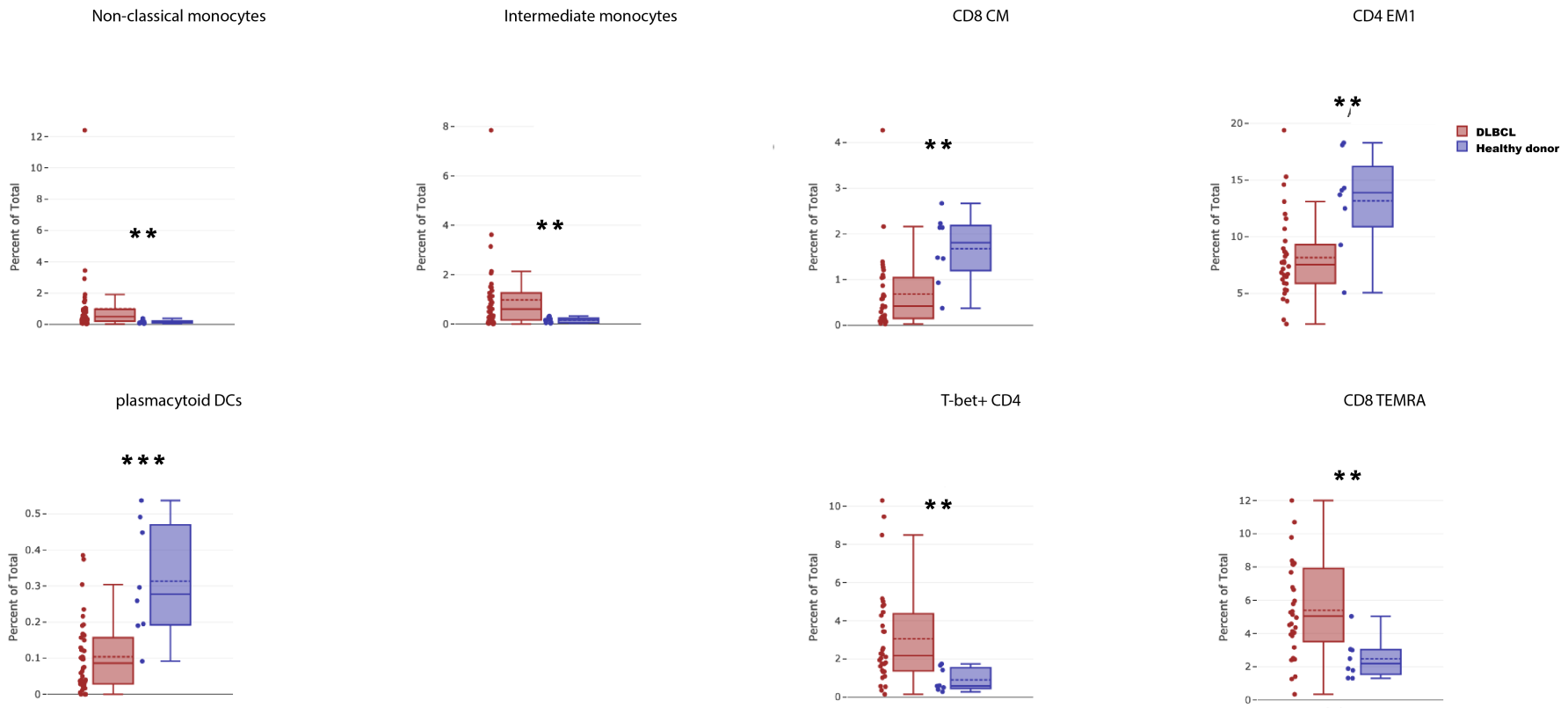

Figure 4.11 Differentially abundant immune populations in DLBCL. Non-classical and intermediate monocytes, T-bet+ CD4 and CD8 effector memory RA (TEMRA) are all increased in DLBCL. Plasmacytoid dendritic cells (DC), CD8 central memory (CM) and CD4 effector memory (EM1) are all decreased in DLBCL. Box plots show the interquartile range with lines at the median (solid) and mean (dash). All false discovery rate (FDR) <0.05, n=42 DLBCL for left 3 plots ('Myeloid' panel) and n=32 for right 4 plots ('T-cell' panel), n=32 healthy donors. (Mann-Whitney U-test ** p<0.01, *** p<0.001).

There was no overall difference in the frequency of the major lymphocyte populations, but there was a trend to reduced T cells and CD4 T cells in DLBCL. We identified differences in T cell subsets, with a relative increase in DLBCL in CD4 T cells with a T_H1 phenotype (T-bet), and reduced frequencies of CD8 CM and CD4 EM1 effector memory subset, which express both of the co-stimulatory molecules CD27 and CD28 (347, 348). Frequencies from the differentially abundant immune populations defined by gating are shown in boxplots in figure 4.11.

4.4.5 Outcome associated immune signatures in DLBCL

Given the association of AMC and ALC with outcome in DLBCL, we next sought to further dissect these populations within the patient samples with reference to outcome. Those who remained in complete remission 24 months after frontline therapy were termed 'CR' and those whose disease was refractory or subsequently relapsed, 'R/R'. One patient did not have outcome data available and was excluded from this analysis. The data for all samples in this study is summarised in figure 4.12, which demonstrates the pattern of increased monocyte and decrease T cell frequencies at diagnosis in patients with subsequent R/R disease. The frequency of CD3 T cells was increased at diagnosis in cases with maintained CR whereas the frequency monocytes and the non-classical subset were increased in cases with subsequent R/R ($p<0.05$, Mann-Whitney U-test). Within the T cell population, there was a global trend to reduced frequency of most subsets at diagnosis in patients with R/R disease but with only the reduced frequency of CD8 TEMRA reaching significance ($p<0.05$, Mann-Whitney U-test). The data for immune population frequencies at diagnosis, with comparison between CR and R/R patients is summarised in figures 4.13 and 4.14. Next, we performed DA analysis with EdgeR, which identified non-classical monocytes and CD8 effector memory 3 (EM3) cells as being significantly more abundant at diagnosis in patients who went on to relapse (FDR<0.05, figures 4.15 and 4.16). Although there were no significantly increased lymphocyte subsets in the CR group discovered by DA analysis, there was an overall increase in CD3 T cell frequency and a trend for increased frequency within many T cell subsets, including CD4 CM, CD4 naïve, T-bet+ CD4, CD4 TEMRA and T-bet+ CD8, as well as CD8 TEMRA, which was significant by Mann-Whitney.

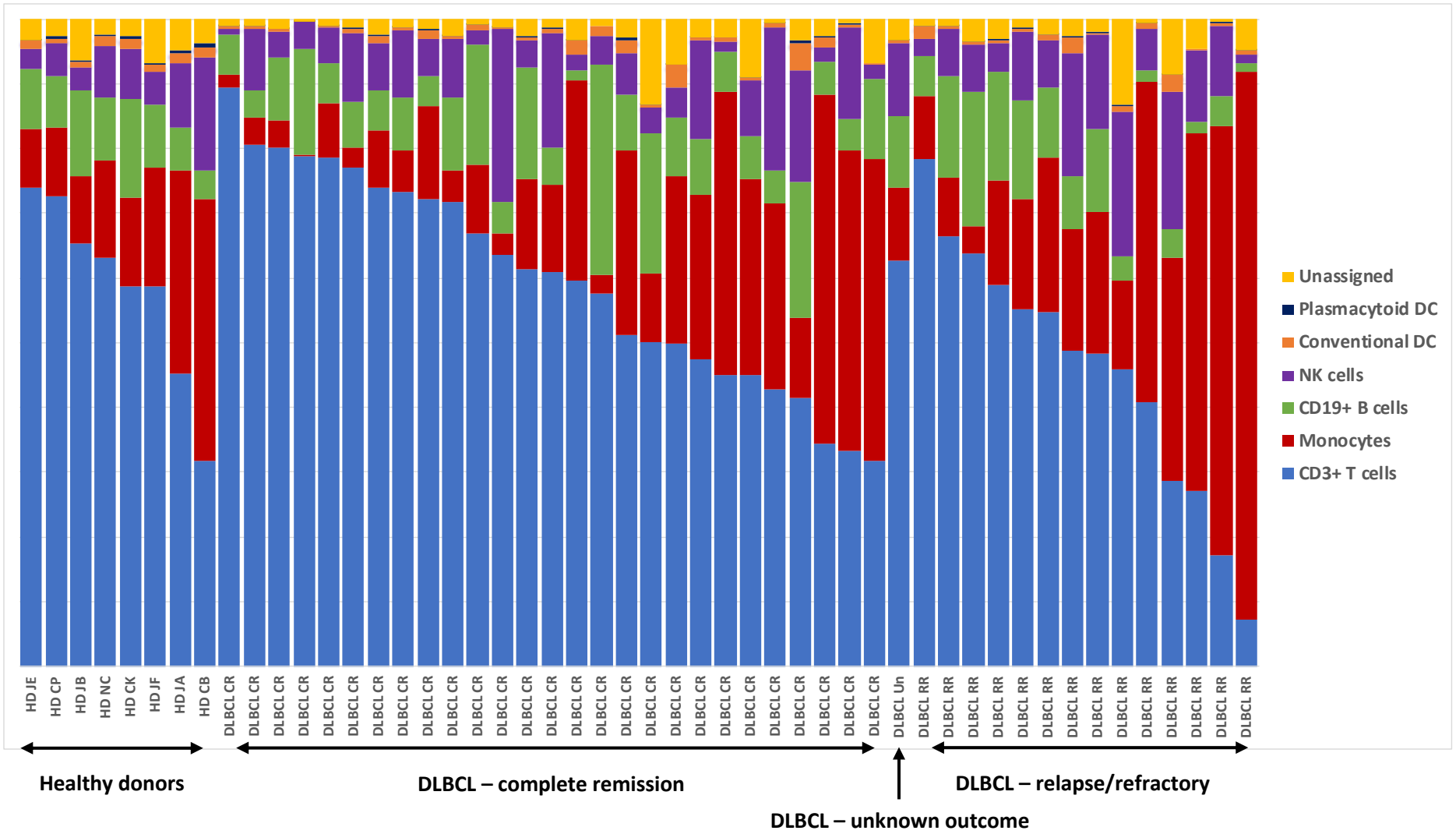

Figure 4.12 Overview of immune composition of all healthy donor and patients PBMC samples (n=50). Frequencies % of CD45+ events. CR, complete remission; Un, unknown; RR, relapse/refractory; DC, dendritic cells; NK, natural killer.

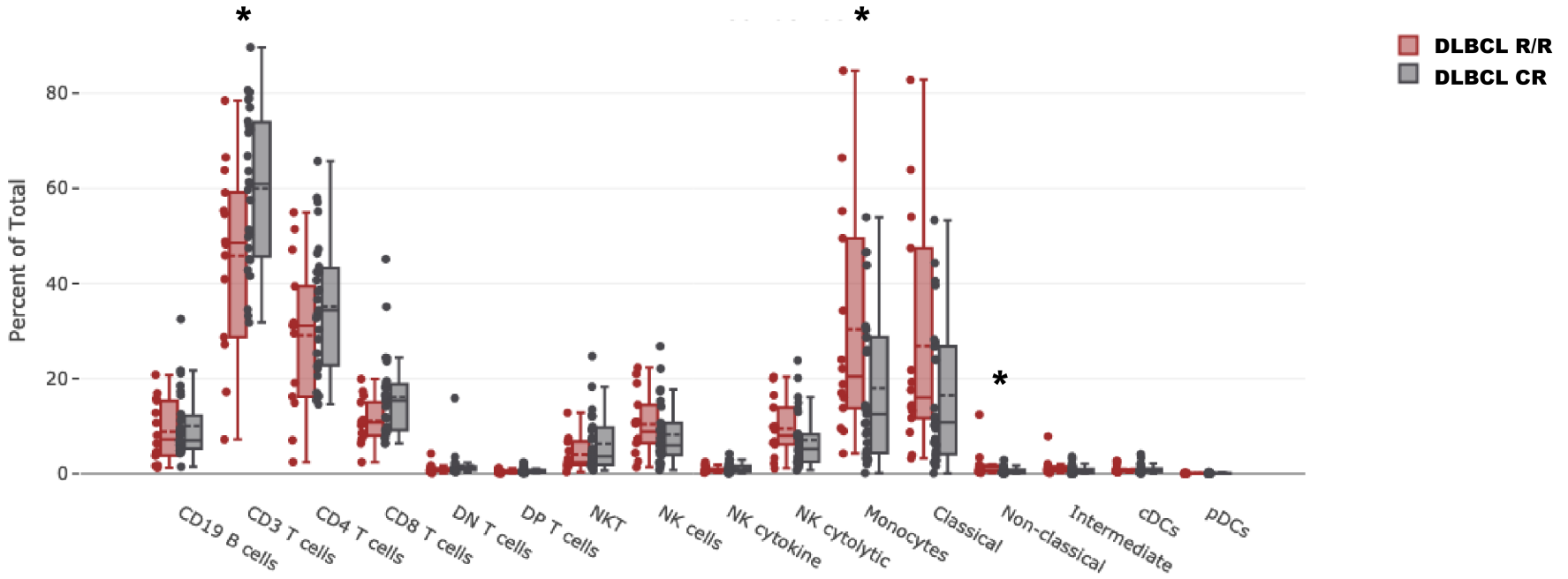

Figure 4.13 Gating derived frequencies of immune populations for all DLBCL patients (n=41) separated by outcome. R/R, relapse / refractory (n=14); CR, complete remission (n=27). Data from all DLBCL patients analysed with the 'myeloid' panel and outcome data available. DN, double negative; DP, double positive; NKT, natural killer T cells; NK, natural killer; cDCs, conventional dendritic cells; pDCs, plasmacytoid dendritic cells. (Mann-Whitney U-test * $p<0.05$).

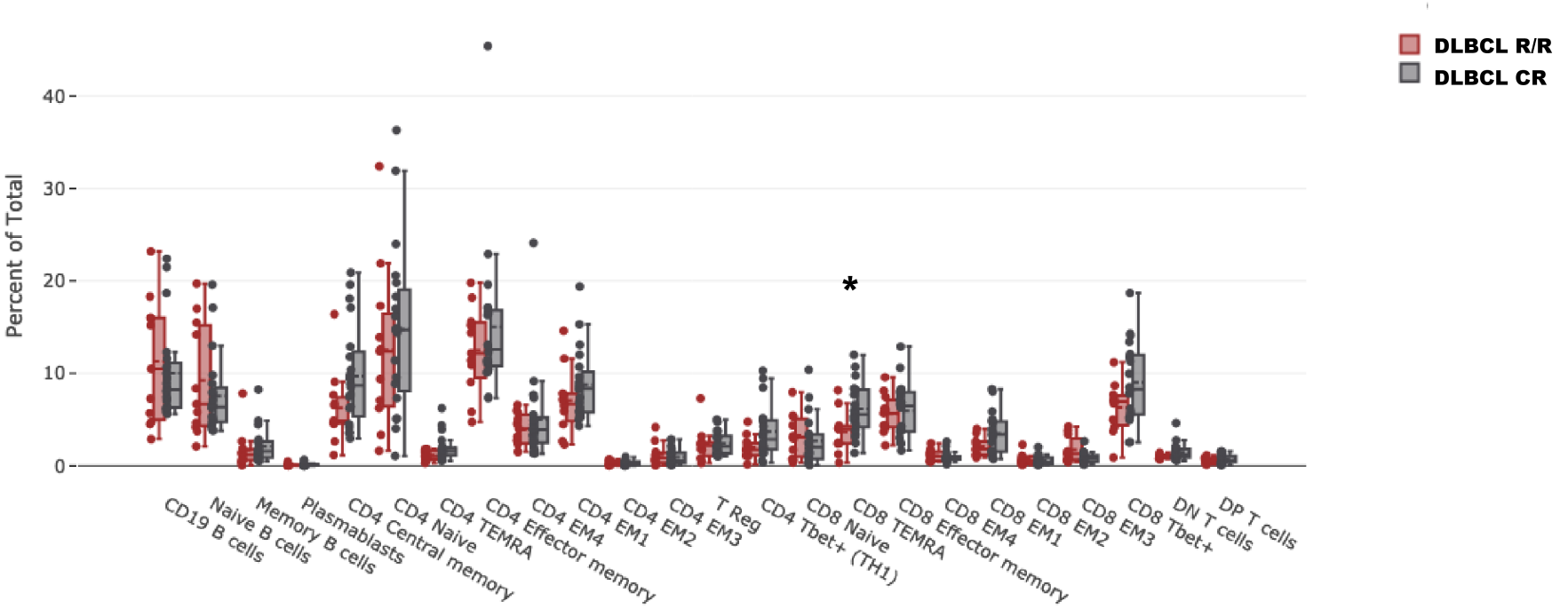

Figure 4.14 Gating derived frequencies of immune populations for all DLBCL patients (n=31) separated by outcome. R/R, relapse / refractory (n=11); CR, complete remission (n=20). Data from all DLBCL patients analysed with the 'T-cell' panel and outcome data available. CM, central memory; EM, effector memory; TEMRA, T effector memory RA; T Reg, regulatory T cell; DN, double negative; DP, double positive. (Mann-Whitney U-test * $p<0.05$).

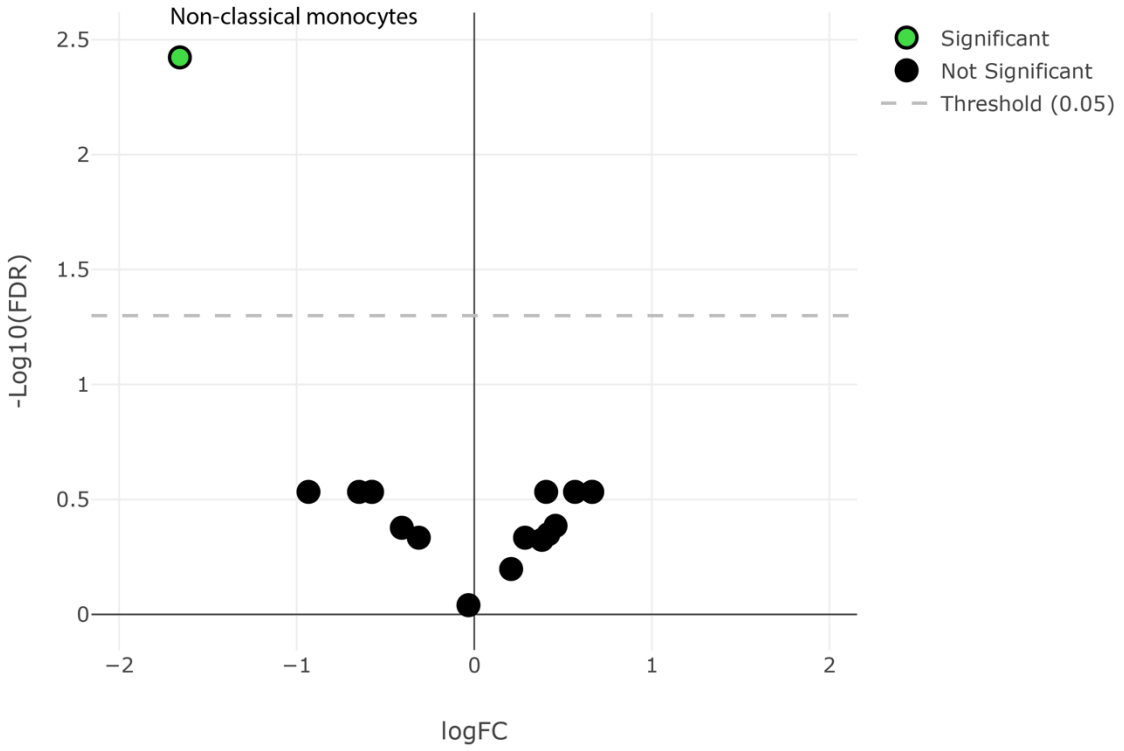

Figure 4.15 Differential abundance analysis at diagnosis between DLBCL patients with R/R (n=14) and CR (n=27). Volcano plot showing false discovery rate (FDR) against fold change (FC) of immune cell populations between DLBCL. Left of centre indicates population is increased at diagnosis in relapse/refractory (R/R) disease; right increased in complete remission (CR); green indicates statistical significance (FDR<0.05). Analysis from data acquired with the 'Myeloid' panel.

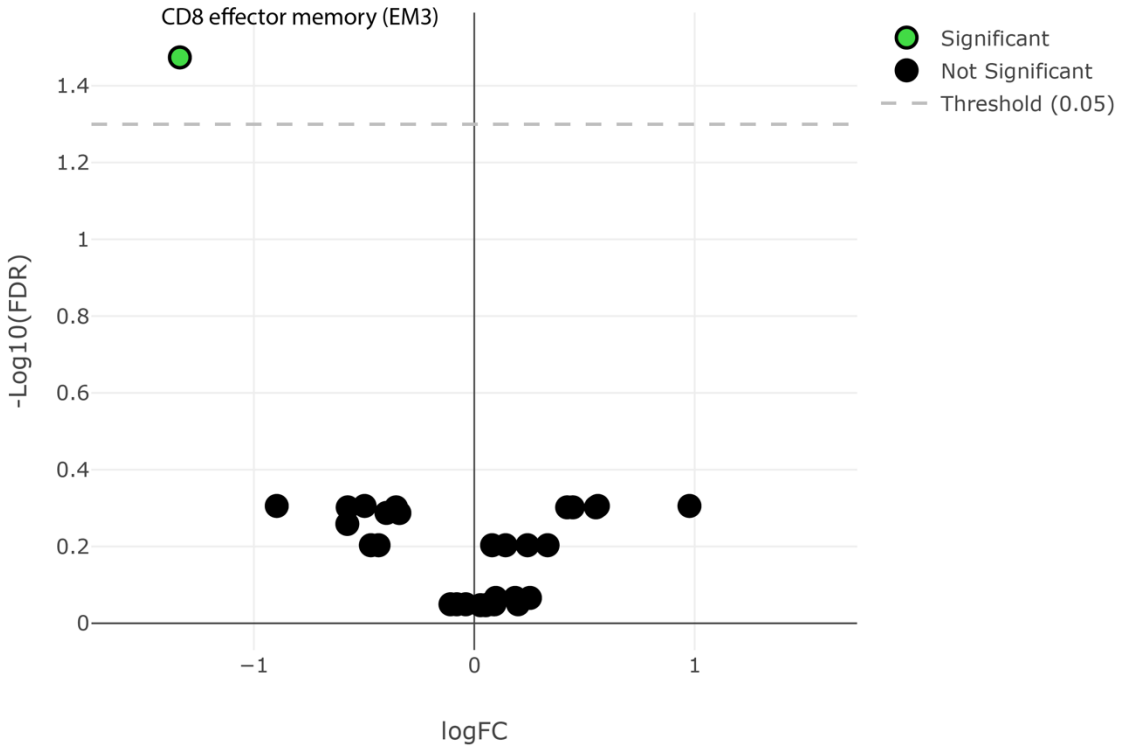

Figure 4.16 Differential abundance analysis at diagnosis between DLBCL patients with R/R (n=11) and CR (n=20). Volcano plot showing false discovery rate (FDR) against fold change (FC) of immune cell populations between DLBCL. Left of centre indicates population is increased at diagnosis in relapse/refractory (R/R) disease; right increased in complete remission (CR); green indicates statistical significance (FDR<0.05). EM, effector memory. Analysis from data acquired with the 'T-cell' panel.

To further explore monocyte heterogeneity, we performed unsupervised clustering with FlowSOM. We clustered all of the monocytes from the DLBCL patient samples acquired with the 'Myeloid' panel. The clustering used all markers except for CD3, CD4, CD8, CD19 and CD56, given the lymphoid and NK cell populations were excluded from this part of the analysis. This approach identified 20 clusters of cells within the monocyte population based on differential patterns of expression of the analysed markers. This is represented in figure 4.17, with each cluster represented by a different colour and overlaid on to an opt-SNE map, the overlay of gated monocyte subsets is shown for comparison. The complementary techniques of dimensionality reduction and clustering both demonstrate much heterogeneity beyond the subsets defined by CD14 and CD16 expression. To define a monocyte immune signature at diagnosis associated with outcome, we performed DA analysis of the monocyte clusters between R/R and CR patients (figure 4.18). This identified 2 classical and 1 intermediate monocyte clusters present at diagnosis associated with treatment failure following RCHOP-like therapy. These clusters all expressed the myeloid markers CD11b, CD11c, CD13, CD14, CD31, CD33 and CD172a (SIRPα) as well as the Fcγ receptors CD32 and CD62, and the activation marker CD38. The most differentiating cluster 09, with the greatest fold change (FC) difference had a suppressor phenotype with low HLA-DR (MHC-II) and high expression of CD163, CD184 (CXCR4) and CD192 (CCR2). Both of the other differentiating clusters expressed HLA-DR. Cluster 07 was positive for CD192, the co-stimulatory molecules CD40 and CD86, and highly expressed CD206. Consistent with an intermediate phenotype, cluster 10 had strong expression of CD16 and low CD192, together with strong expression of both CD40 and CD86. The non-classical monocytes were clustered largely into 2 subclusters, cluster 15 and cluster 20, which individually did not reach significance in the DA analysis. The median expression levels of all antigens for each of the monocyte clusters are demonstrated in the heatmap, figure 4.19.

Differences in T cell subsets were also assessed by FlowSOM clustering. The CD3 T cells from all patient samples acquired with the "T-cell" panel were clustered with all markers except CD14 and CD19, given the monocytes and B cells were excluded from this part of the analysis. This identified 40 T cell clusters representing different subpopulations based on patterns of antigen expression, shown by colour overlay on to an opt-SNE map (figure 4.20).

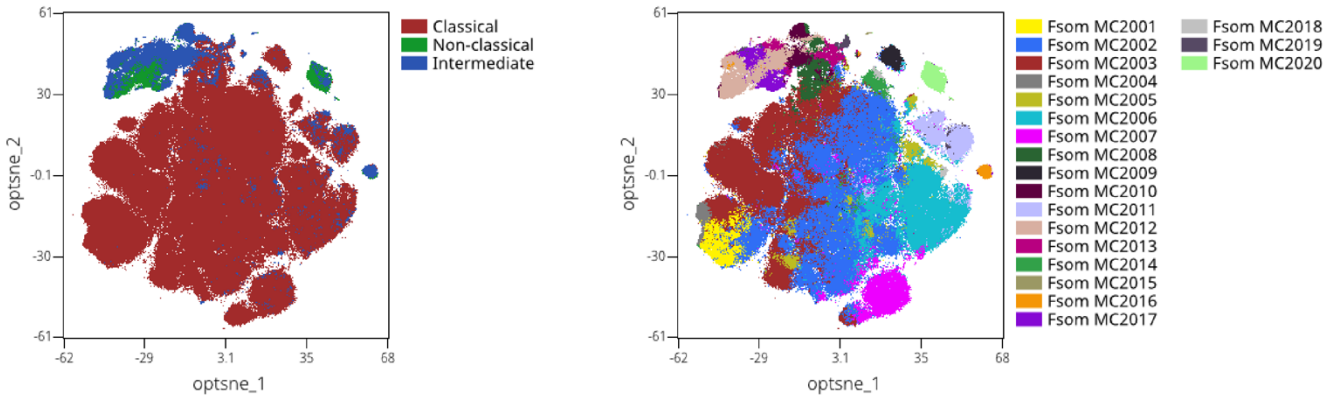

Figure 4.17 Dimensionality reduction with opt-SNE for all DLBCL patient monocytes analysed with the 'Myeloid' panel (n=41). Maps are coloured by gated monocyte populations (left) and FlowSOM clusters (right).

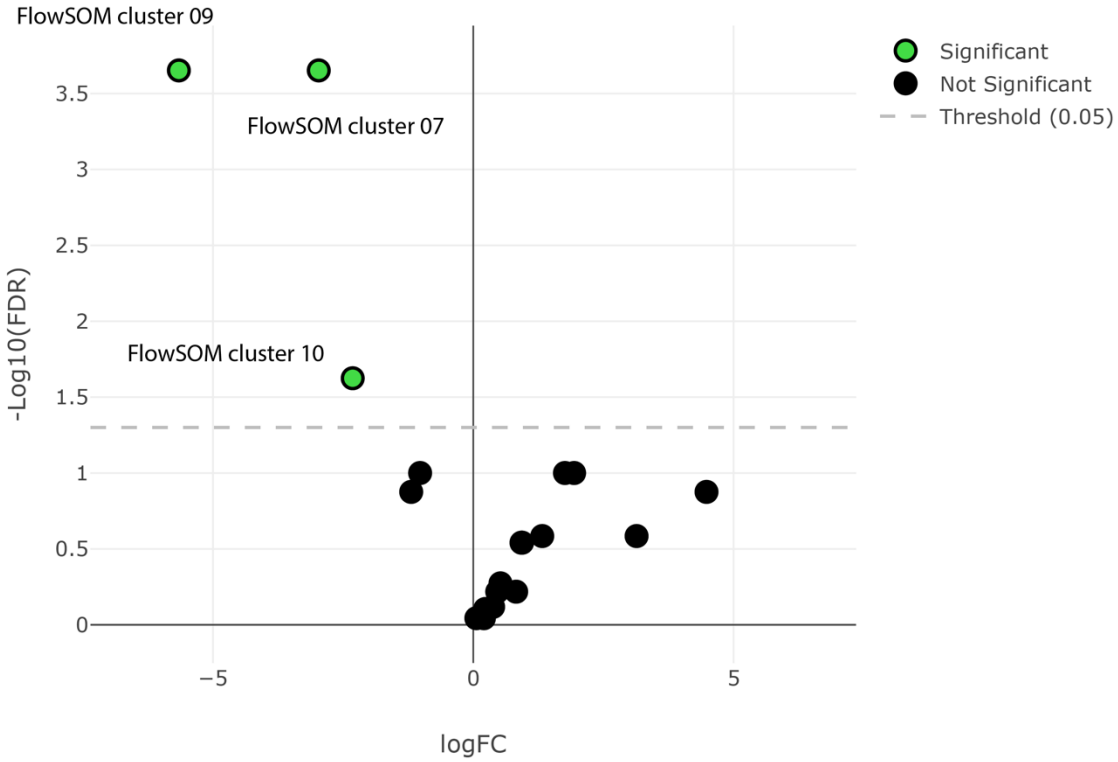

Figure 4.18 Differential abundance analysis of monocyte FlowSOM clusters at diagnosis between DLBCL patients with R/R (n=14) and CR (n=27). Left of centre indicates cluster is increased at diagnosis in R/R, right increased in CR. Green indicates significance (FDR<0.05).

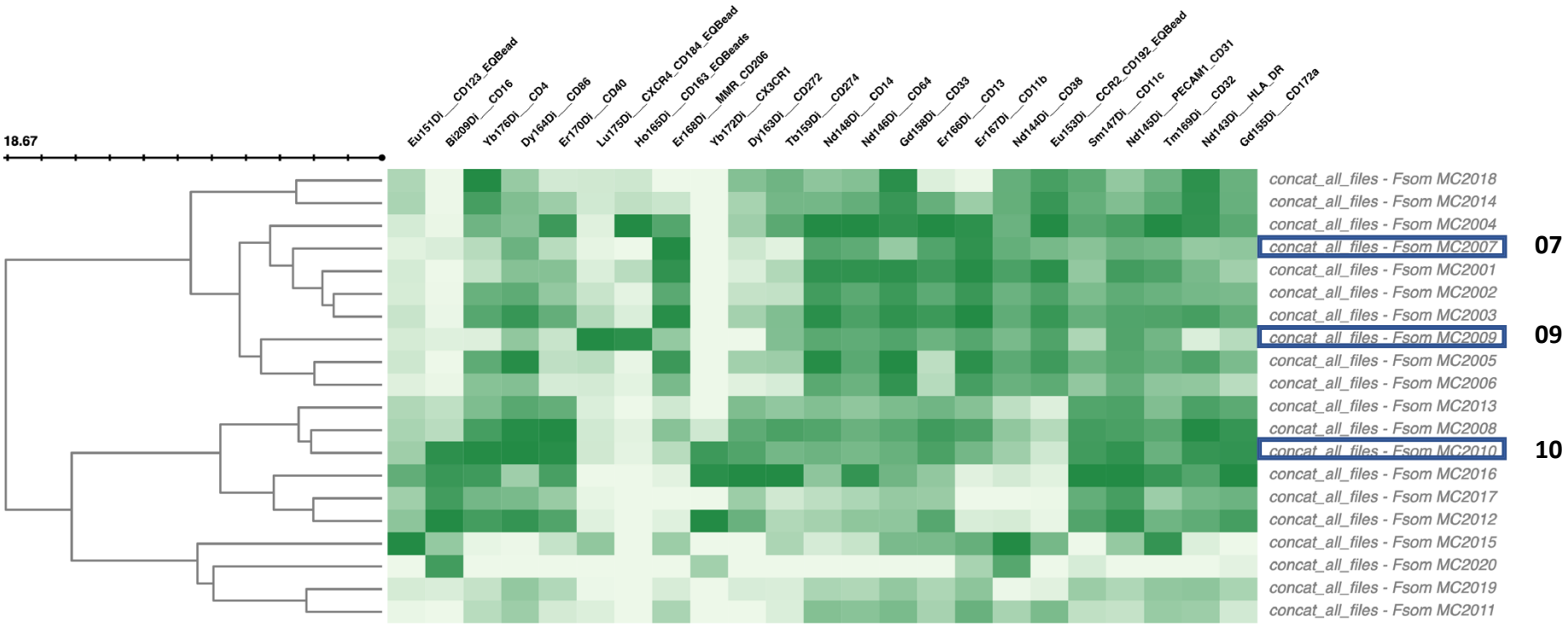

Figure 4.19 Heatmap of antigen expression for FlowSOM monocyte clusters. Median expression of all analysed antigen markers (columns) for each FlowSOM identified cluster (rows). Clusters 07, 09 and 10 were present in increased abundance at diagnosis in patients with subsequent R/R disease (boxed).

In order to establish a T cell immune signature at diagnosis with relevance to outcome, DA analysis was next performed on the T cell clusters identified by FlowSOM. This discovered 3 CD8 T cell clusters with increased abundance at diagnosis in patients with subsequent R/R disease (figure 4.21). As with the gating analysis, no T cell clusters were identified as being significantly more abundant in the CR cases at diagnosis, with a trend for increased abundance across many of the bigger clusters, suggestive of a global reduction in T cell frequency across many subsets explaining the adverse nature of a low ALC at diagnosis. The heatmap in figure 4.22 displays the median expression of the 'T-cell' panel antigens for each of the FlowSOM defined clusters. The most differentiating population, cluster 13, was negative for CD45RA, CD197 (CCR7), CD27 and CD28, consistent with the CD8 effector memory 3 (EM3) population identified by gating and DA analysis. Cluster 13 was positive for T-bet, consistent with a T_C1 phenotype, the cytotoxic markers, granzyme B and perforin, as well as PD-1. Cluster 17 had an EM1 phenotype, expressing both the co-stimulatory receptors CD27 and CD28, together with T-bet and PD-1. CD38, the activation marker, was highly expressed but the cytotoxic markers were low. Cluster 14 had a similar phenotype to cluster 17 but with stronger expression of T-bet and positivity for both granzyme B and perforin.

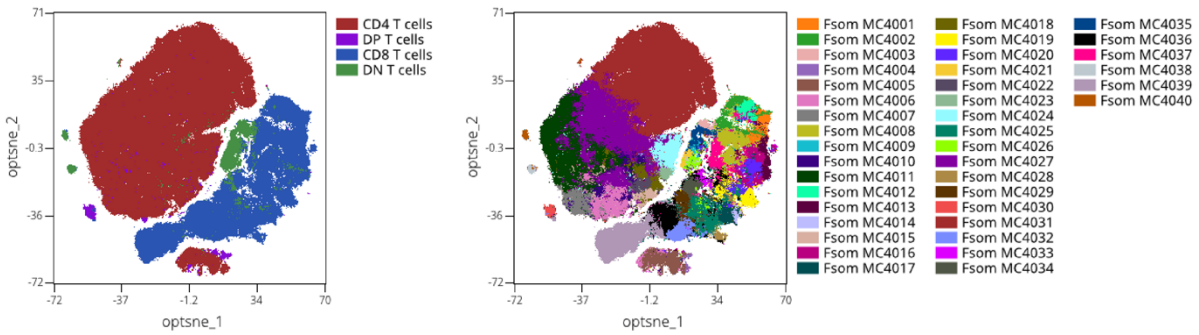

Figure 4.20 Dimensionality reduction with opt-SNE for all DLBCL patient T cells analysed with the 'T-cell' panel (n=31). Maps are coloured by gated T cell populations (left) and FlowSOM clusters (right). DN, double negative; DP, double positive.

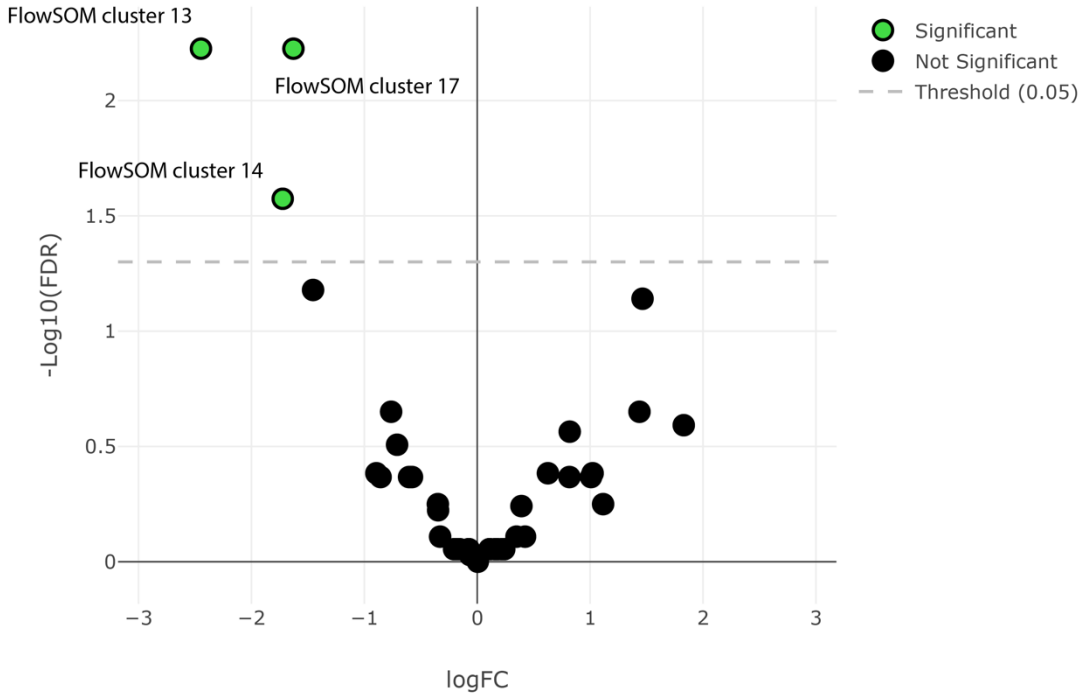

Figure 4.21 Differential abundance analysis of T cell FlowSOM clusters at diagnosis between DLBCL patients with R/R (n=11) and CR (n=20). Left of centre indicates cluster is increased at diagnosis in R/R, right increased in CR. Green indicates significance (FDR<0.05).

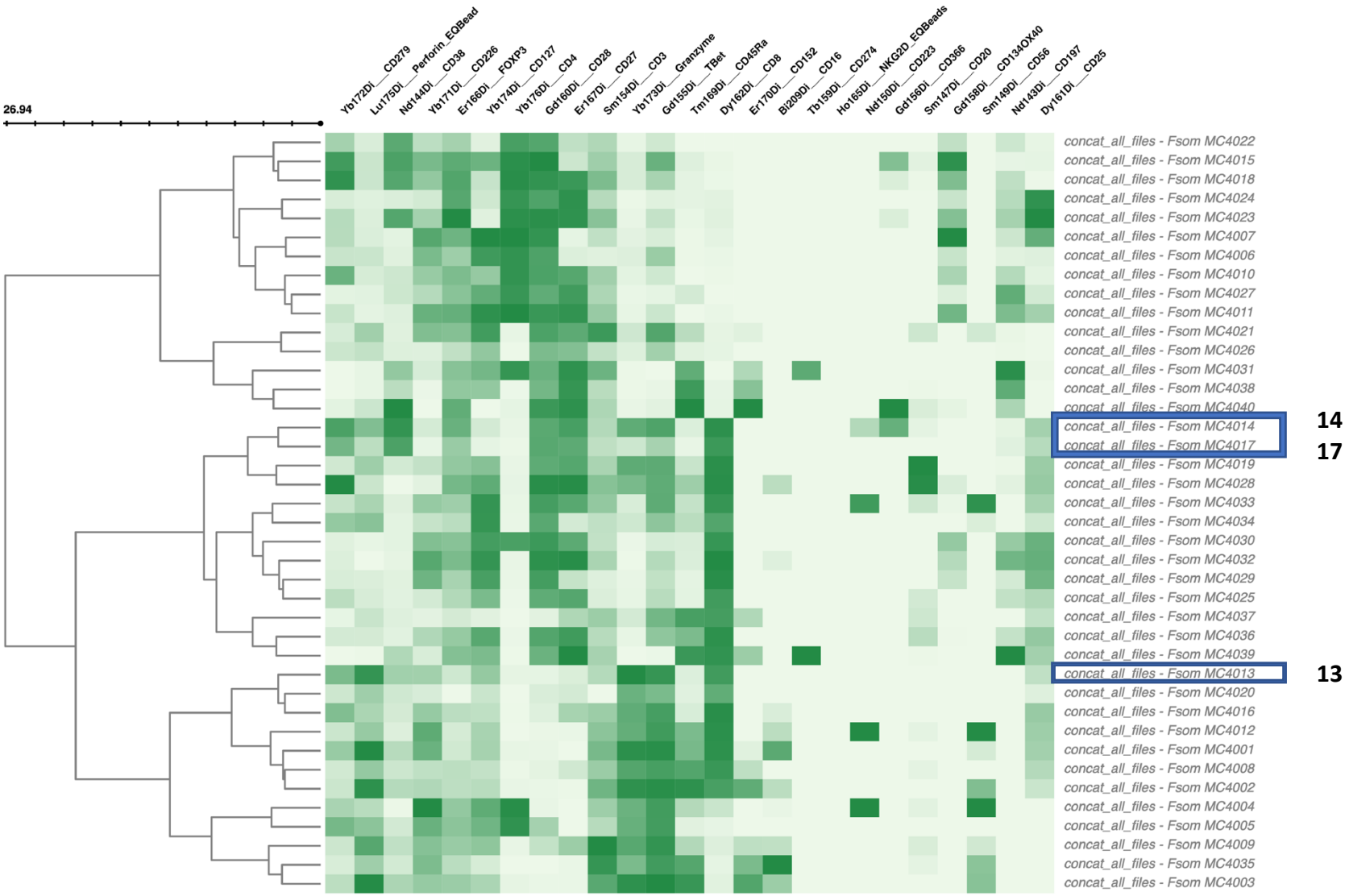
26.94
Yb172Di___CD279
Lu175Di___Perforin_EQBead
Nd144Di___CD38
Yb171Di___CD226
Er166Di___FOXP3
Yb174Di___CD127
Yb176Di___CD4
Gd160Di___CD28
Er167Di___CD27
Sm154Di___CD3
Yb173Di___Granzyme
Gd155Di___TBet
Tm169Di___CD45Ra
Dy162Di___CD8
Er170Di___CD152
Bi209Di___CD16
Tb159Di___CD274
Ho165Di___NKG2D_EQBeads
Nd150Di___CD223
Gd156Di___CD366
Sm147Di___CD20
Gd158Di___CD134OX40
Sm149Di___CD56
Nd143Di___CD197
Dy161Di___CD25
concat_all_files - Fsom MC4022
concat_all_files - Fsom MC4015
concat_all_files - Fsom MC4018
concat_all_files - Fsom MC4024
concat_all_files - Fsom MC4023
concat_all_files - Fsom MC4007
concat_all_files - Fsom MC4006
concat_all_files - Fsom MC4010
concat_all_files - Fsom MC4027
concat_all_files - Fsom MC4011
concat_all_files - Fsom MC4021
concat_all_files - Fsom MC4026
concat_all_files - Fsom MC4031
concat_all_files - Fsom MC4038
concat_all_files - Fsom MC4040
concat_all_files - Fsom MC4014
concat_all_files - Fsom MC4017
concat_all_files - Fsom MC4019
concat_all_files - Fsom MC4028
concat_all_files - Fsom MC4033
concat_all_files - Fsom MC4034
concat_all_files - Fsom MC4030
concat_all_files - Fsom MC4032
concat_all_files - Fsom MC4029
concat_all_files - Fsom MC4025
concat_all_files - Fsom MC4037
concat_all_files - Fsom MC4036
concat_all_files - Fsom MC4039
concat_all_files - Fsom MC4013
concat_all_files - Fsom MC4020
concat_all_files - Fsom MC4016
concat_all_files - Fsom MC4012
concat_all_files - Fsom MC4001
concat_all_files - Fsom MC4008
concat_all_files - Fsom MC4002
concat_all_files - Fsom MC4004
concat_all_files - Fsom MC4005
concat_all_files - Fsom MC4009
concat_all_files - Fsom MC4035
concat_all_files - Fsom MC4003
14
17
13

Figure 4.22 Heatmap of antigen expression for FlowSOM T cell clusters. Median expression of all analysed antigen markers (columns) for each FlowSOM identified cluster (rows). Clusters 14, 17 and 13 were present in increased abundance at diagnosis in patients with subsequent R/R disease (boxed). Figure on previous page.

4.4.6 Differential expression analysis

In order to compare immune cell states between health and disease, as well as outcome in DLBCL, we also performed differential expression (DE) analysis using SAM (significance analysis of microarrays) on the gated monocyte and lymphocyte populations (315). SAM is a statistical method used to find significant feature differences between populations based on median expression of specified markers. The gated populations were used for this analysis rather than the FlowSOM clusters, since the gated populations were defined based on lineage markers only, whereas clustering with FlowSOM incorporated all of the markers. The lineage markers were therefore excluded from the DE analysis, with all cell state, co-stimulatory and checkpoint molecules included. The DE analysis between healthy donors and DLBCL using the 'Myeloid' panel data defined CD184 (CXCR4) as being expressed at reduced intensities in DLBCL patients across all of the myeloid subsets identified in the gating strategy (figure 4.23). Expression of CD38 was reduced on non-classical monocytes and conventional DCs, and CD86 reduced on classical and intermediate monocytes in DLBCL. Non-classical monocytes in DLBCL had significantly higher expression of CD32 and CD40 compared to healthy donors. Within the DLBCL patients, the myeloid populations in those who went on to relapse demonstrated increased expression of co-stimulatory molecules and activation markers at diagnosis. Intermediate monocytes had increased CD86 expression, whereas CD40 was increased on all monocyte subsets and on conventional DCs, and CD38 was increased on classical and intermediate monocytes.

DE analysis with the 'T-cell' panel data demonstrated that expression of CD38 and the co-stimulatory molecules CD27 and CD28 was lower across a range of T cell subsets, B cells and NK cells in DLBCL compared to healthy donors, again consistent with a global immune defect in DLBCL. The TH1, TC1 and NKT populations in DLBCL all expressed higher levels of the

cytotoxic markers granzyme B and perforin. There was also increased expression of the checkpoint molecule PD-1 on CD4 subsets in DLBCL. Within the DLBCL patients, median expression of both CD27 and CD28 was higher on CD4 and CD8 subsets at diagnosis in those patients who achieved prolonged CR after therapy (figure 4.24). This suggests a pattern of decreased expression of these co-stimulatory molecules across various T cell subsets in DLBCL, which is more pronounced in those patients who subsequently fail RCHOP.

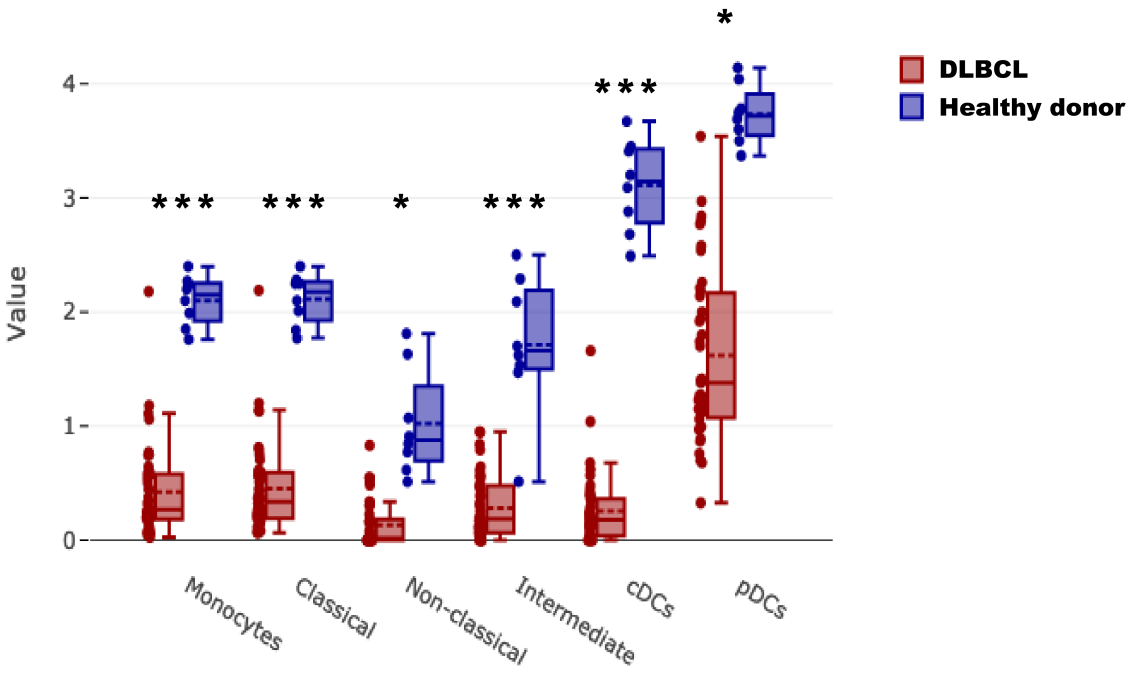

Figure 4.23 Differential expression of CD184 (CXCR4) between DLBCL (n=42) and healthy donors (n=8). Median expression of CD184 was decreased in DLBCL compared to healthy donors across all myeloid subsets. cDCs, conventional dendritic cells; pDCs, plasmacytoid dendritic cells. (Unpaired t-test * FDR<0.05, ** FDR<0.01 *** FDR<0.001).

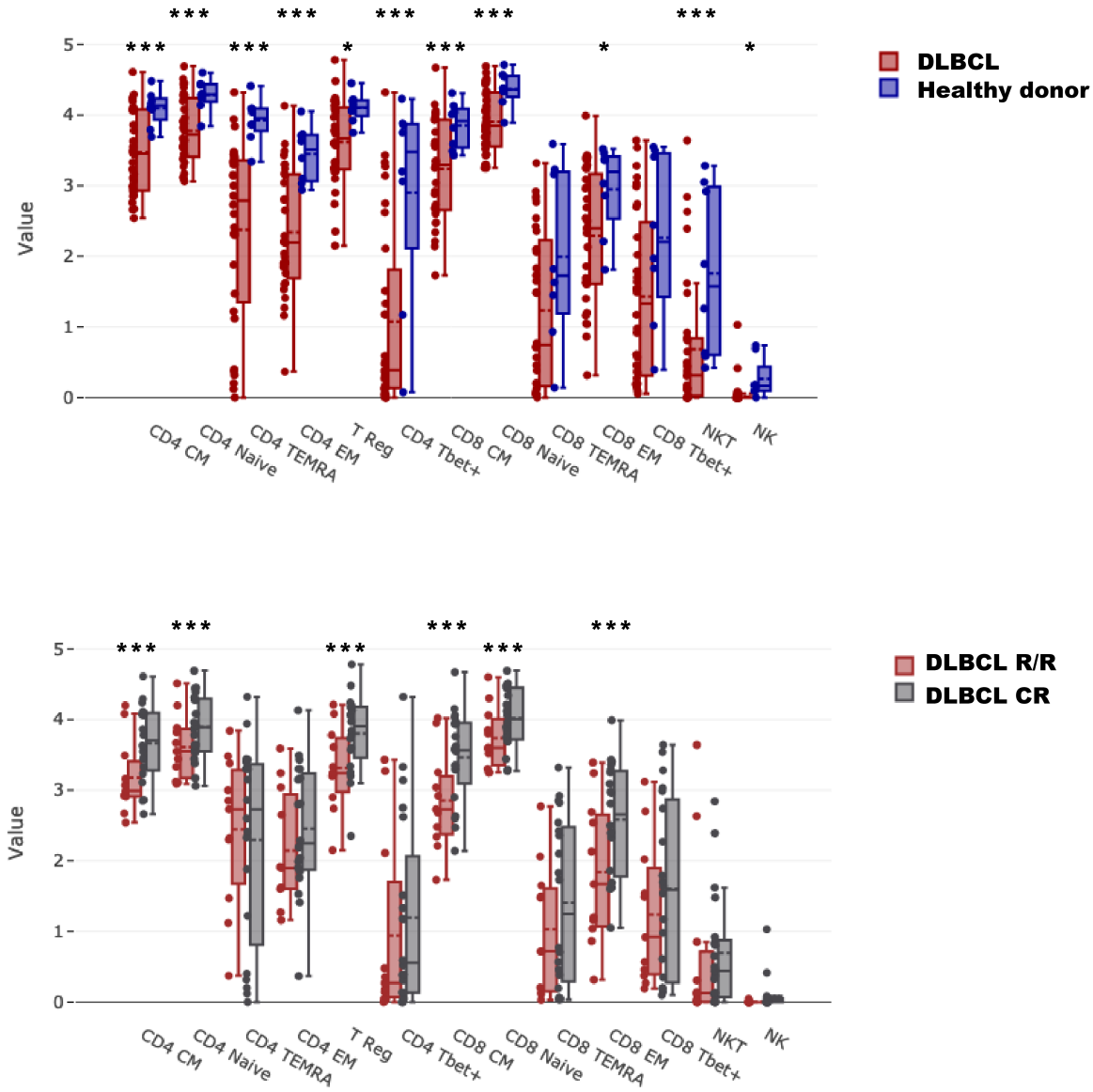

Figure 4.24 Differential expression of CD27 between DLBCL (n=32) and healthy donors (n=8), top and DLBCL R/R (n=11) and CR (n=20), bottom. Median expression of CD27 was globally decreased across a number of T and NK cell subsets in DLBCL, and within DLBCL this was more pronounced at diagnosis in patients who went on to relapse. CM, central memory; TEMRA, T effector memory RA; EM, effector memory; T reg, regulatory T cell; NKT, natural killer T; NK, natural killer. (Unpaired t-test * FDR<0.05, ** FDR<0.01 *** FDR<0.001).

4.5 Discussion

The peripheral blood immune compartment is of interest in DLBCL given the association of absolute monocyte and lymphocyte counts with outcome (191, 193). Immune monitoring approaches with mass cytometry (MC) have been applied to blood samples to study the phenotype and behaviour of immune populations in both health and disease (303, 334, 349-351). However, the peripheral immune cells and their subsets have not been studied in detail in DLBCL. We therefore comprehensively explored this compartment with MC, targeting both the myeloid and lymphocyte populations. We analysed the resulting data with both traditional biaxial gating and automated high dimensional data analysis approaches to define disease and outcome associated immune signatures in DLBCL. We validated our method with healthy donor PBMCs and ensured data quality and reproducibility through acquisition of the same standard health donor control with each experimental run.

We found an increased frequency of intermediate and non-classical monocytes at diagnosis in DLBCL consistent with the increased AMC. The frequency of classical monocytes was not elevated but did reveal great heterogeneity in marker expression. In particular, there was a striking reduction in CD184 expression on all myeloid subsets in DLBCL which differentiated these patients from healthy donors. CD184 plays key roles in chemotaxis and haematopoiesis, with expression on monocytes linked to their return to the bone marrow (BM) niche (352). Thus, loss of CD184 may promote the increase in circulating monocytes in DLBCL by blocking return to the BM. The differential expression analysis also revealed reduced CD86 expression on monocytes in DLBCL, predominantly on the classical and intermediate subsets, which is known to play a key role in T cell activation. Within the DLBCL samples, the patients who subsequently relapsed had increased frequencies of monocytes and non-classical monocytes consistent with the prognostic nature of AMC high, with the non-classical subset remaining significant on DA analysis. Clustering further dissected the monocyte heterogeneity in DLBCL to identify 2 classical and 1 intermediate monocyte clusters with increased abundance at diagnosis in patients who went on to relapse. The most differentiating cluster was consistent with a suppressor phenotype with low HLA-DR and expressed both CD163 and CD184. Expression of CD163 in the myeloid ME has been

linked to IL-6 driven pro-tumoral functions in human malignancy (353). The other classical monocyte cluster was distinguished by CD206 positivity. CD206 expression by myeloid cells has also been linked to tumour support, both via T cell suppression and directly inducing proliferation (354, 355). Both classical monocyte clusters expressed CD192 (CCR2) highly which is the primary mediator of monocyte recruitment in malignancy (356).

In the T cell compartment, consistent with the lower ALC seen in DLBCL, we found a trend to decreased frequency of total CD3 and CD4 T cells compared to healthy donors, but with only subset reductions in CD4 EM1 and CD8 CM reaching significance. CD4 T cells with a T_H1 (T-bet+) phenotype and CD8 TEMRA were present at increased frequency in DLBCL. The reduced frequency of CD8 CM and increase in CD8 TEMRA are suggestive of increased T cell differentiation and reduced expansion potential (348, 357). CD8 TEMRA are known to increase with chronic antigen stimulation and have been linked to senescence and aging (348, 358, 359). They have also been reported to have potent effector functions and to play a role in pathogenic processes, including transplant rejection (360, 361). Decreased CD4 EM1 frequency is also reported with aging (348), while the increase in T_H1 in DLBCL is consistent with an inflammatory response (362, 363). Consistent with the adverse nature of ALC low, patients with subsequent relapse had a lower CD3 T cell frequency at diagnosis than those with CR. There was a trend to reduced frequency in a number of T cell subsets in the R/R patients at diagnosis, with CD8 TEMRA reaching significance on the DA analysis. Although increased CD8 TEMRA are associated with DLBCL in our cohort, within DLBCL patients, increased CD8 TEMRA are associated with prolonged remission following therapy. We also identified a CD8 effector memory 3 (EM3) population by both manual gating and FlowSOM clustering that was enriched in patients who went on to relapse. In the clustering analysis this population had a T_C1 (T-bet+) phenotype, expressed markers of cytotoxicity as well as the activation / exhaustion marker PD-1. CD8 EM3 T cells have been shown to represent a more differentiated effector subset, which have experienced a high number of cell divisions and have marked cytolytic activity (347). Interestingly, we identified a global reduction in CD27 expression across multiple T cell subsets as well as NK cells at diagnosis in DLBCL, with the reduction more marked in patients who went on to relapse. This was also seen with CD28 but was less pronounced. CD27 and CD28 are co-stimulatory molecules which regulate T cell activation with CD27 critical to the generation and maintenance of T

cell immunity (364, 365). Progressive loss of CD27 and CD28 is associated with differentiation and upregulation of markers of cytotoxicity (347). Thus, the differential expression pattern of CD27 is consistent with increased T cell differentiation in DLBCL, with reduced capacity for co-stimulation and activation. Of note, CD27 agonist antibodies have been demonstrated to enhance the anti-tumour activity of anti-CD20 therapy in murine models of B-cell lymphoma (366). This would support our finding that CD27 loss is associated with relapse following rituximab-based therapy.

Overall, we find distinct immune signatures associated with DLBCL and outcome following therapy. We identify marked myeloid heterogeneity with consistent downregulation of CD184 in DLBCL across all subsets, distinguishing them from healthy donor myeloid populations. Increased abundance of 2 classical and 1 intermediate monocyte clusters at diagnosis differentiated patients who went on to relapse. These clusters expressed markers associated with pro-tumoral function and likely contribute to the adverse nature of AMC in DLBCL. A trend for reduced frequency of T cells was observed across multiple subsets in DLBCL, together with an associated increase in differentiation. Features associated with the aging process were also seen in the DLBCL cohort, consistent with the demographics of this population. Strikingly, we report a marked reduction in CD27 expression across many T cell and NK populations at diagnosis in DLBCL. This was more pronounced in the patients who subsequently relapsed. Taken together these findings are suggestive of immune dysfunction in DLBCL with immunosuppressive / pro-tumoral myeloid populations and increase T cell differentiation with global impairment in T cell immunity.

Limitations of the study

Although our cohort of patients represents the largest described in any mass cytometry (MC) based peripheral blood immune monitoring study in DLBCL, given the clinical and biological heterogeneity of the disease, very large cohorts of patients are required for the most meaningful conclusions to be drawn. It would have also been of interest to analyse samples post therapy to identify immune variation at different time points in the disease course, as well as at relapse. A small number of samples at relapse were potentially available for this study, however these were not pair with diagnostic samples and therefore

the focus of the study remained immune monitoring at diagnosis, in view of the signal from the pre-treatment AMC and ALC.

All samples available for this work were cryopreserved, with the peripheral blood processed as peripheral blood mononuclear cells (PBMCs) with the potential to introduce technical variation. With regard to cryopreservation, we clearly demonstrated that beyond cell loss and some negligible loss in signal intensity, immune populations in healthy donor PBMCs were not significantly affected by storage. In addition, our study would not have been feasible to run with fresh samples as this would have resulted in many more staining batches, with the risk of increased batch effect. Although processing the samples to PBMCs could have resulted in technical variation, this is the predominant tissue used for both flow cytometry (FC) and MC research, and the immune composition of both our patient and control samples were consistent with those previously reported in studies using whole blood (303). One feature unique to MC is that during acquisition, samples are nebulised and hence destroyed and unavailable for further downstream applications in contrast to FC, which resulted in some samples not having enough cells available for functional analysis. However, this was recognised during the study design, with the trade-off between higher parameter phenotyping with MC versus FC and sample loss following MC analysis accepted.

In addition to the factors discussed above, any phenotyping study is potentially limited by the choice of parameters to analyse. Most markers for T cell subset identification are accepted with reproducibility demonstrated in the published literature, however monocytes represent a highly plastic immune population with dynamic phenotypes and less supporting data available. Therefore, the markers incorporated into the phenotyping panel where selected based on the published literature from both FC and MC based studies of PBMCs in both health, lymphoma and other malignant disorders to facilitate subset identification, activation states, checkpoint marker expression and functional state. During the optimisation phase of the work several cytokine receptors were assessed for inclusion in the 'myeloid' panel, including interleukin 4 (IL-4) receptor alpha (CD124) and colony stimulating factor receptor 1 (CSFR1). However, we were unable to optimise and demonstrate consistent staining with either of these antibodies on cryopreserved samples and therefore they were excluded from the experimental design.

5. Cytokine dysregulation in DLBCL

5.1 Introduction

Cytokines are key signalling molecules secreted by immune cell populations to coordinate the regulation of immune responses and drive haematopoiesis and cellular differentiation. Many cytokines exhibit polyfunctionality, affecting survival, differentiation, maturation and functional status of target cells (367). Cytokines act via specific receptors on target cells, the binding of which triggers signalling cascades and ultimately results in altered gene expression to effect a change in cell state or function. Cytokines often act in concert and can exert their effects in an autocrine (act on cell of production), paracrine (act on neighbouring cell) or endocrine (act on distant cell) fashion (368). In addition to cytokines, immune cells also receive signals from antigens, and are therefore constantly integrating this complex information to drive immune responses (369). Therefore, immune cell density and phenotype is determined by cytokine networks. As we have already seen, there is significant immune system variation between individuals, and this occurs not only at the cellular level but also at the plasma protein level. This variance is explained by both inherited traits and nonheritable factors, with the latter accounting for the majority of the variation (333). Despite this variation, patterns emerge between immune cell composition and phenotype, and signalling protein levels in both health and disease (303). Cytokine signalling is usually regulated by negative feedback inhibition and epigenetic repression to maintain homeostasis; however, dysregulation can arise in a number of pathological states including autoimmunity and cancer (370, 371). In the most extreme situations immune system dysregulation can have devastating consequences. Cytokine release syndrome (CRS) is a toxicity of chimeric antigen receptor (CAR) T cell therapy in which excessive cytokine production and immune system hyperactivation drive a life-threatening inflammatory response (372). A similar phenomenon is thought to account for the multi-organ failure seen with the most severe cases of coronavirus disease 2019 (SARS-CoV-2) (373).

Normal and malignant lymphocytes are known to rely on cytokine signalling for growth and survival and a number of interleukins (IL) play key roles in B cell differentiation and ME

interactions (374-376). Patterns of cytokine dysregulation are reported in DLBCL and elevated levels of a number of cytokines including IL-6, IL-10 and TNF are associated with worse outcome (221, 377). IL-6 is known to be a growth factor for B-cells and promotes lymphoma development in murine models, whereas IL-10 is associated with immunosuppressive functions, which may be mediated through cells of myeloid origin (196). Polymorphisms in cytokine genes are associated with susceptibility to B-cell lymphoma and elevated IL-10 has been linked with increased AMC in DLBCL (196, 223, 224). The available data point to a role for cytokine dysregulation in lymphoma biology, but it remains unclear how cytokine levels are linked to immune system variation in DLBCL, and the AMC / ALC and their prognostic significance. Although IL-6 has been shown to be produced ectopically by lymphoma cells in murine models, and both IL-6 and IL-10 to be expressed by ABC DLBCL cell lines, the role of peripheral immune cells in cytokine dysregulation in DLBCL is not known (226, 378).

5.2 Aims

We aimed to assess cytokine overproduction in DLBCL, identify cytokine cellular origin, and to analyse cytokine signatures and their association with AMC/ALC, IPI, COO, molecular subtypes and peripheral blood immune cells.

5.3 Methods

5.3.1 Patient selection

Serum samples for cytokine measurements were accessed via the Barts Haemato-Oncology tissue bank for 64 different DLBCL patients collected at the time of diagnosis and prior to any treatment. An initial cohort of 34 were selected based on availability from those patients who also had PBMCs available. A second cohort of 30 were selected based on sample availability only. All serum samples from patients were confirmed to have DLBCL and were treated with RCHOP. Serum samples from 11 healthy donor controls were accessed via

the Barts tissue bank based on availability. All samples were stored frozen at -80°C. In addition, PBMC samples from 11 DLBCL patients were used in the intracellular cytokine staining mass cytometry (MC) experiments. Selection was based on those with remaining cells following the immunophenotyping studies detailed in chapter 4. The same 8 healthy donor PBMCs isolated from leucocyte cones used in the immunophenotyping study were used as controls.

5.3.2 Mesoscale discovery (MSD) electrochemiluminescence cytokine detection

The U-plex MSD platform was used to assay 20 cytokines in serum samples from 34 DLBCL patients and 11 healthy donors in duplicate. The 10 most deregulated cytokines were assayed as a confirmatory cohort in a further 30 DLBCL patients and the same 11 healthy donors in duplicate. The 20 cytokines assayed were selected based on the published literature in DLBCL as well as relevance to monocyte and lymphocyte biology (Table 5.1).

All samples were thawed at room temperature and assayed as detailed in chapter 2. Plates were read on the MESO Quickplex SQ 120 instrument and raw data exported from the MSD discovery workbench software. All cytokine measurements were performed in duplicate and reported in picograms per millilitre. For cytokine clustering, raw data were logarithmically transformed (log10) and standardised across all samples by the z-score as previously reported (379).

Table 5.1 Cytokines assayed by the mesoscale discovery (MSD) electrochemiluminescence platform. Plates 1A and 1B were run for the initial cohort of 34 DLBCL patients and 11 healthy donors. The 10 most deregulated cytokines were combined on plate 2 and assayed in a further 30 DLBCL patients and the same 11 controls. Greyed-out cytokines omitted on plate 2. IFN-γ, interferon gamma; IL, interleukin; IL-1RA, interleukin 1 receptor antagonist; TNF-α, tumour necrosis factor alpha; CCL, C-C motif chemokine ligand; MCP, monocyte chemotactic protein; M-CSF, macrophage colony stimulating factor; MDC, macrophage derived chemokine; MIP, macrophage inflammatory protein; CXCL, C-X-C motif chemokine ligand; SDF, stromal derived factor; VEGF, vascular endothelial growth factor.

Plate 1A	Plate 1B	Plate 2
IFN-γ	IL-16	IFN-γ
IL-10	IL-1RA	IL-10
IL-12p70	CCL2 (MCP-1)	IL-16
IL-13	CCL13 (MCP-4)	IL-1RA
IL-17A	CSF1 (M-CSF)	CSF1 (M-CSF)
IL-1β	CCL22(MDC)	CCL22 (MDC)
IL-2	CCL3 (MIP-1α)	CCL3 (MIP-1α)
IL-4	CCL4 (MIP-1β)	CCL4 (MIP-1β)
IL-6	CXCL12 (SDF-1a)	IL-6
TNF-α	VEGF	TNF-α

5.3.3 Intracellular cytokine staining by mass cytometry

PBMC samples were resuscitated from liquid nitrogen as described in chapter 2. Samples were prioritised for immunophenotyping but where sufficient cells were available intracellular cytokine staining was performed. Cells were rested overnight in a humidified incubator. Functional assays were performed in 96 well plates in a 250μl volume. For unstimulated wells, transport inhibitor cocktail was added only, and for stimulated wells either LPS or cell stimulation cocktail, plus transport inhibitor cocktail was added for a 6-hour period in a humidified incubator. Following this incubation, EDTA (ethylenediaminetetraacetic acid) was added to a concentration of 2mM for 15 minutes at room temperature and staining was carried out as previously described, using the 'cytokine' antibody panel.

5.4 Results

5.4.1 Patient characteristics

The characteristics of the patients included in the serum cytokine study are summarised in table 5.2. The median age at diagnosis was 62 (range, 31-84) with 38 of the 64 patients included over 60 years of age. Forty-six patients were in maintained complete remission at >24 months post completion of RCHOP (CR), 16 relapsed / refractory (R/R) within 12 months of initial therapy (R/R) and two relapsed after five years. The two patients with late relapse were included in the DLBCL cohort analysis but excluded from the CR v R/R comparisons. The cell of origin (COO) was available for 40 patients and diagnostic FBC for 45. The healthy donors were anonymised staff members, with no demographic data available.

Table 5.2 Patient characteristics for the serum cytokine study. COO, cell of origin; GCB, germinal centre B cell; IPI, international prognostic index; AMC, absolute monocyte count; ALC, absolute lymphocyte count.

Patient ID	Vial ID	Myeloid panel	T cell panel	Diagnosis	Outcome	COO	Age	IPI factors	Treatment	AMC (x 10^9/L)	ALC (x 10^9/L)
6518	s8276	Yes	Yes	DLBCL	Remission	GCB	72	1	RCHOP	0.5	2.0
6541	s8269	Yes	x	DLBCL	Relapse	Non_GCB	65	3	RCHOP	0.6	0.8
6561	s8259	Yes	Yes	DLBCL	Relapse	GCB	47	3	RCHOP	0.9	1.1
6609	s8302	x	x	DLBCL	Relapse	GCB	64	1	RCHOP	0.4	1.1
6623	s8364	Yes	Yes	DLBCL	Remission	Non_GCB	71	1	RCHOP	0.7	2.7
6634	s8323	x	x	DLBCL	Late Relapse	Non_GCB	72	1	RCHOP	0.6	1.5
6647	s8414	x	x	DLBCL	Remission	Unknown	82	3	RCHOP	0.8	2.3
6649	s8429	Yes	x	DLBCL	Relapse	GCB	61	4	RCHOP	0.7	0.7
6651	s8375	Yes	Yes	DLBCL	Remission	GCB	35	0	RCHOP	0.6	1.6
6657	s8354	Yes	Yes	DLBCL	Remission	GCB	58	3	RCHOP	0.2	0.4
6718	s8448	x	x	DLBCL	Remission	Unknown	55	0	RCHOP	0.7	1.8
6719	s8387	Yes	x	DLBCL	Remission	GCB	52	1	RCHOP	0.4	2.7
6722	s8443	Yes	x	DLBCL	Remission	Unknown	66	3	RCHOP	0.6	0.9
6746	s8467	x	x	DLBCL	Remission	Unknown	48	1	RCHOP	0.4	1.8
6778	s8293	x	x	DLBCL	Remission	Unknown	61	1	RCHOP	0.4	1.8
6797	s8381	Yes	Yes	DLBCL	Remission	GCB	58	1	RCHOP	0.4	0.9
6865	s8469	x	x	DLBCL	Remission	Unknown	61	3	RCHOP	0.7	1.1
6986	s8476	x	x	DLBCL	Remission	GCB	48	0	RCHOP	0.6	2.1
7140	s8608	Yes	Yes	DLBCL	Relapse	Unknown	67	3	RCHOP	x	x
7238	s8667	Yes	Yes	DLBCL	Remission	Unknown	69	1	RCHOP	x	x
7306	s8705	Yes	x	DLBCL	Remission	Non_GCB	72	3	RCHOP	x	x
7318	s8736	Yes	x	DLBCL	Remission	Non_GCB	57	3	RCHOP	x	x
7351	s8841	Yes	Yes	DLBCL	Remission	Unknown	84	1	RCHOP	x	x
7354	s8770	Yes	Yes	DLBCL	Remission	GCB	61	1	RCHOP	x	x
7355	s8748	x	x	DLBCL	Remission	Unknown	79	1	RCHOP	x	x
7368	s8724	Yes	Yes	DLBCL	Remission	GCB	57	1	RCHOP	x	x
7373	s8947	Yes	x	DLBCL	Remission	GCB	59	1	RCHOP	x	x
7374	s8948	Yes	x	DLBCL	Relapse	Unknown	32	2	RCHOP	x	x
7390	s9012	x	x	DLBCL	Remission	Unknown	61	2	RCHOP	x	x
7407	s8812	Yes	Yes	DLBCL	Remission	Non_GCB	67	3	RCHOP	x	x
7638	s9282	Yes	Yes	DLBCL	Relapse	Unknown	68	3	RCHOP	x	x
7676	s9354	x	x	DLBCL	Relapse	Non_GCB	79	4	RCHOP	x	x
7683	s9204	x	x	DLBCL	Remission	GCB	48	2	RCHOP	x	x
7789	s9440	x	x	DLBCL	Remission	Non_GCB	31	0	RCHOP	x	x
7838	s9478	x	x	DLBCL	Late Relapse	Non_GCB	79	3	RCHOP	x	x
7851	s9385	x	x	DLBCL	Remission	GCB	33	3	RCHOP	x	x
7889	s9492	Yes	Yes	DLBCL	Relapse	Non_GCB	79	4	RCHOP	x	x
8107	s9797	Yes	x	DLBCL	Remission	Non_GCB	79	5	RCHOP	0.8	1.9
8217	s9840	x	x	DLBCL	Remission	Non_GCB	64	1	RCHOP	0.6	1.2
8279	s9831	x	x	DLBCL	Remission	GCB	77	2	RCHOP	1.2	1.3
8397	s10089	x	x	DLBCL	Remission	Unknown	42	0	RCHOP	0.5	2.2
8400	s9932	x	x	DLBCL	Remission	Unknown	58	2	RCHOP	0.5	1.3
8449	s9993	x	x	DLBCL	Remission	Unknown	59	3	RCHOP	0.1	1.8
8479	s9988	Yes	Yes	DLBCL	Remission	Non_GCB	43	0	RCHOP	0.3	2.1
8681	s10306	x	x	DLBCL	Relapse	Non_GCB	60	3	RCHOP	0.4	0.4
8686	s10315	Yes	Yes	DLBCL	Remission	Non_GCB	78	3	RCHOP	0.6	1.7
8792	s10356	Yes	Yes	DLBCL	Remission	Non_GCB	77	2	RCHOP	1.2	1.3
9115	s10430	Yes	Yes	DLBCL	Remission	GCB	62	3	RCHOP	1.2	1.3
9253	s10481	x	x	DLBCL	Remission	Unknown	60	1	RCHOP	0.6	4
9311	s10510	Yes	Yes	DLBCL	Relapse	Unknown	69	3	RCHOP	2.0	2.7
9371	s10526	Yes	Yes	DLBCL	Remission	Non_GCB	80	4	RCHOP	0.4	1.4
9440	s10553	Yes	Yes	DLBCL	Remission	Non_GCB	48	2	RCHOP	0.2	0.9
9618	s10626	Yes	Yes	DLBCL	Relapse	Non_GCB	75	1	RCHOP	0.7	1.6
9974	s10741	Yes	Yes	DLBCL	Relapse	Non_GCB	39	2	RCHOP	1.9	6.8
10026	s10769	x	x	DLBCL	Remission	Unknown	73	1	RCHOP	0.5	1.3
10146	s10883	x	x	DLBCL	Remission	Unknown	62	3	RCHOP	1.8	1.6
10181	S10926	x	x	DLBCL	Remission	Unknown	63	4	RCHOP	0.7	0.4
10384	S11090	x	x	DLBCL	Remission	Unknown	55	0	RCHOP	0.4	2
10403	s11083	Yes	Yes	DLBCL	Remission	Non_GCB	75	1	RCHOP	0.3	1.7
10416	s11015	Yes	x	DLBCL	Relapse	Unknown	53	4	RCHOP	0.8	0.3
10647	s11226	x	x	DLBCL	Relapse	Non_GCB	70	5	RCHOP	0.7	0.3
10715	S11252BM	x	x	DLBCL	Remission	Unknown	43	0	RCHOP	0.7	2.4
10728	S11338PB	x	x	DLBCL	Remission	GCB	65	1	RCHOP	0.8	2.3
10900	s11454	x	Yes	DLBCL	Relapse	Non_GCB	82	4	RCHOP	0.7	1.0

5.4.2 Cytokine dysregulation in DLBCL

Initial measurement of the 20 cytokines on plates 1A and 1B identified cytokine dysregulation in DLBCL compared to the healthy donor cohort, which was more pronounced in the patients who went on to have R/R disease. The levels of IL-1β, IL-2, IL-4, IL-12p70, IL-13 and IL-17A were either undetectable or detected at low levels in all patients and healthy donors. The serum cytokine levels for all other measured analytes are summarised by mean cytokine concentration normalised to levels observed in the healthy control group, for all DLBCL patients, CR patients and R/R patients in figure 5.1. The 10 most deregulated cytokines were assayed on plate 2 in a second cohort of DLBCL patients and in the same 11 healthy donor samples. The individual measurements (mean of 2 replicates) for these 10 cytokines from all DLBCL patients and healthy donors are shown in figure 5.2. Comparison of healthy donor controls and DLBCL, and CR and R/R patients was performed by Mann-Whitney U-test. The median concentrations of eight of the analysed cytokines were elevated in DLBCL patients compared to healthy donors ($p<0.05$). Within the DLBCL patients, IL-1RA ($p=0.0166$), IL-6 ($p=0.0001$), IL-10 ($p=0.0112$), CCL3 ($p=0.0049$) and TNF ($p=0.0032$) were all significantly elevated at diagnosis in those patients who developed R/R disease with 12 months of RCHOP compared with those in maintained CR at 24 months.

Unsupervised clustering of cytokine levels across all samples clustered most of the DLBCL patients together based around broad patterns of cytokine expression, with the healthy donors and a small group of DLBCL patients with low cytokine levels clustering together (Figure 5.3). Consistent with cytokine dysregulation at diagnosis being most pronounced in patients who went on to develop R/R disease, these patients largely clustered together as indicated by the red bars in figure 5.3. Interestingly, the five cytokines significantly more elevated in the patients with R/R disease clustered together, suggesting coordinated patterns of cytokine expression in high-risk patients. To assess if this was a reflection of the COO, we compared the cytokine levels between GCB and non-GCB cases in the 40 patients with this information available. For the five cytokines increased in R/R patients, only IL-1RA was significantly different based on COO, being elevated in non-GCB ($p=0.0116$).

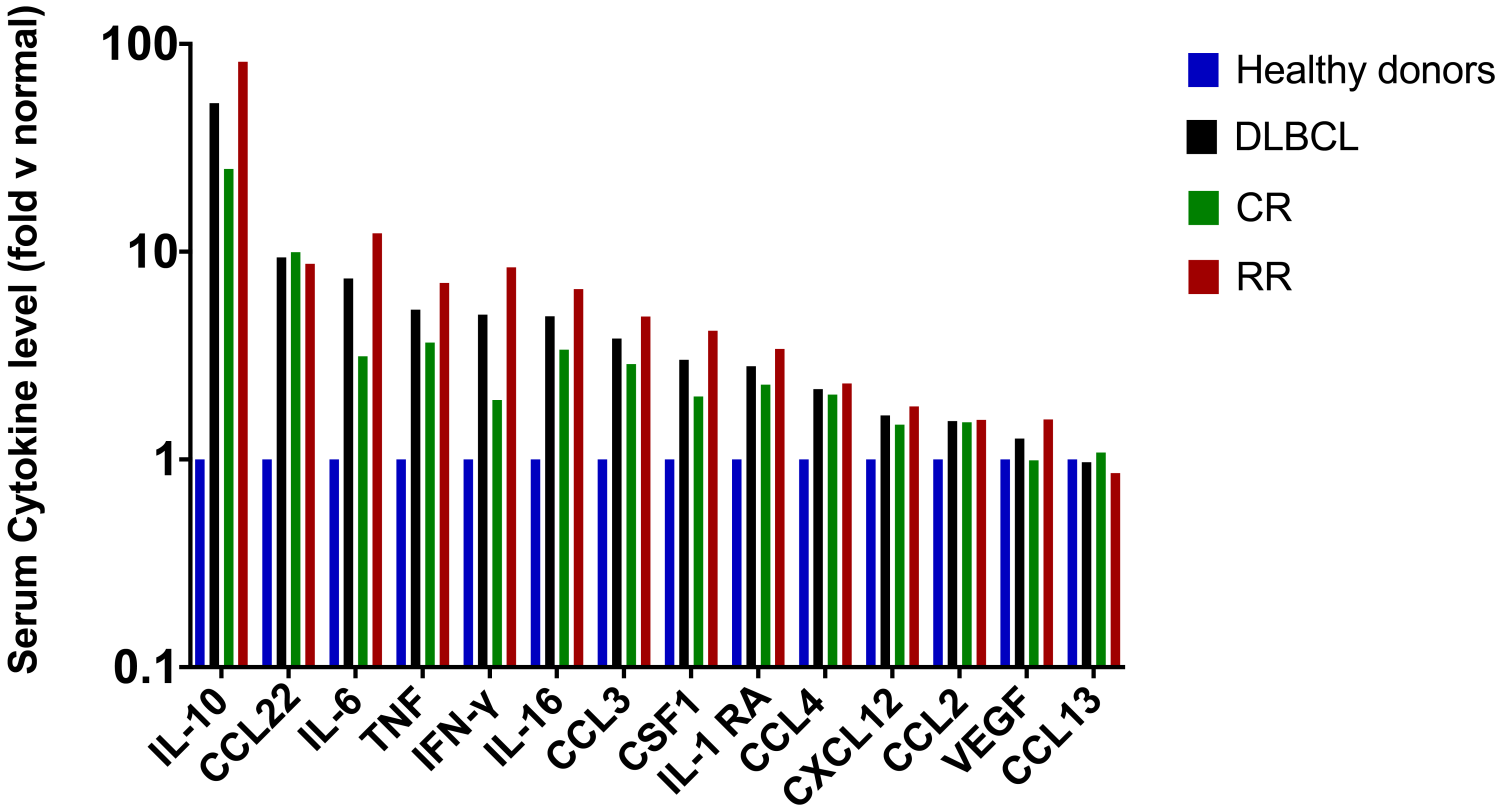

Figure 5.1 Serum cytokine levels in DLBCL (n=34). Cytokines are positioned left to right in order of highest to lowest fold elevation versus healthy donor controls (n=11). Bars represent mean normalised to controls. IL, interleukin; CCL, C-C motif chemokine ligand; TNF, tumour necrosis factor; IFN, interferon; CSF1, colony stimulating factor 1; RA, receptor antagonist; CXCL, C-X-C chemokine ligand; VEGF, vascular endothelial growth factor.

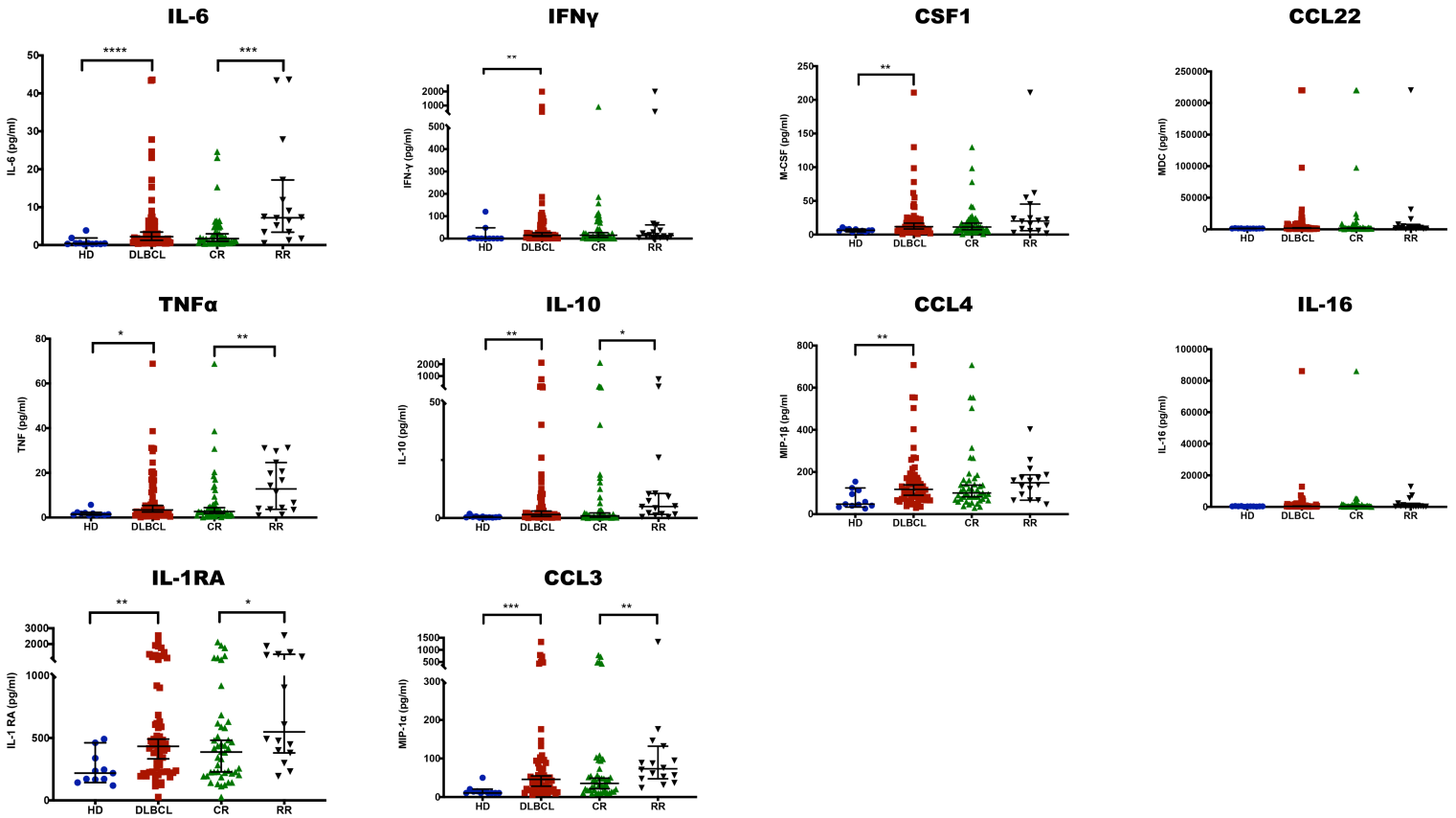

Figure 5.2 Individual serum Cytokine levels in DLBCL (n=64) compared with healthy donors (n=11). All patient samples take prior to treatment. Levels (pg/ml) indicate mean of 2 replicates. CR, complete remission maintained > 24 months post RCHOP (n=46); R/R, relapsed / refractory disease within 12 months of RCHOP (n=16). (Mann-Whitney U-test * $p<0.05$, ** $p<0.01$, *** $p<0.001$, **** $p< 0.0001$).

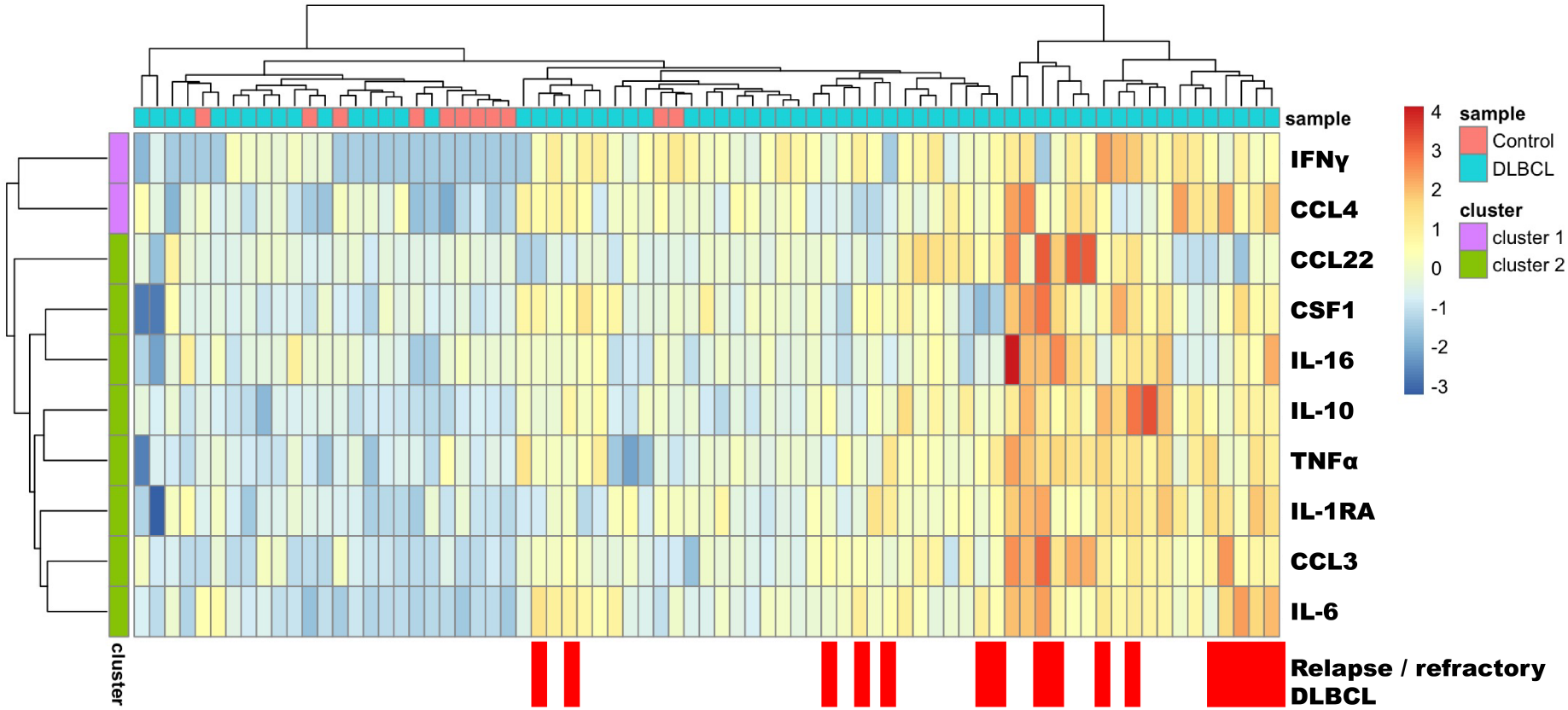

Figure 5.3 Unsupervised hierarchical clustering of all samples by cytokine levels. The top bar and dendrogram indicate sample type, either DLBCL (n=64) or healthy donor control (n=11). The left bar and dendrogram indicate cytokine clusters. The red bars at the bottom indicate cases that went on to have relapse / refractory disease. IFN, interferon; CCL, C-C chemokine ligand; CSF1, colony stimulating factor 1; IL, interleukin; TNF, tumour necrosis factor; RA, receptor antagonist.

5.4.3 Cytokine correlations

In order to identify co-deregulated immune cell and cytokine pathways in DLBCL with relevance to disease biology, we next used correlation analysis to assess the relationship of cytokine levels with IPI factors, AMC and ALC (figure 5.4). The five most deregulated cytokines at diagnosis in patients who went on to R/R disease all strongly positively correlated with each other ($p<0.000001$). They also positively correlated with LDH and total number of IPI factors ($p<0.00001$) but not age. IL-6 was positively correlated with the AMC ($p=0.014$), but levels of the other cytokines did not correlate with the AMC. CCL3, IL-10 and TNFα had negative correlations with the ALC ($p<0.05$). The AMC was positively correlated ($p=0.028$), and the ALC negatively correlated ($p=0.00013$) with the IPI factors. There was no correlation between AMC and ALC.

The gated percentage of monocytes and CD3 T cells both correlated positively with the AMC and ALC, respectively ($p<0.05$). The frequency of classical, intermediate and non-classical monocytes all positively correlated with the frequency of total monocytes ($p<0.05$). The AMC and the frequency of total, classical and intermediate monocytes all negatively correlated with the frequency of CD4 T cells ($p<0.05$). The monocyte clusters identified by FlowSOM to differentiate CR and R/R patients in chapter 4 correlated with monocyte subsets. Cluster 07, which had a classical phenotype and expressed CD206, correlated positively with classical and intermediate monocytes ($p<0.05$). Cluster 09, which had a suppressor phenotype, correlated positively with classical and intermediate monocytes and cluster 10, which had an intermediate phenotype correlated with both intermediate and non-classical monocytes ($p<0.05$). Cluster 07 correlated positively with both clusters 09 and 10 ($p<0.05$). There were no significant correlations between gated myeloid and T cell populations, or FlowSOM differentiating clusters with cytokine levels, consistent with a complex interplay between immune cells and signalling protein networks in driving the observed phenotypes.

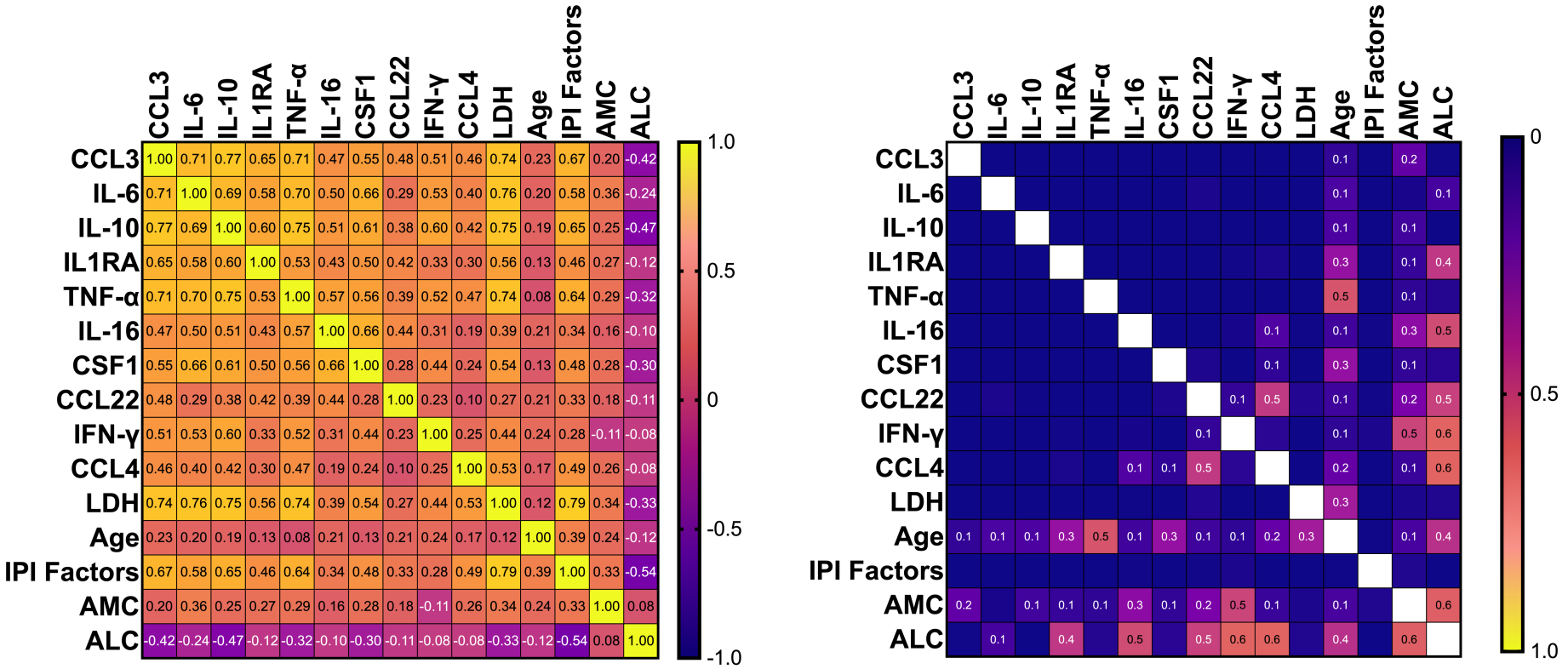

Figure 5.4 Correlation matrix of cytokine levels, LDH, age, IPI factors and AMC/ALC. Cell numbers indicate Spearman correlation coefficient, r (left) or p values (right). All significant correlations ($p<0.05$) unlabelled and coloured deep purple (right). CCL3/4/22, C-C motif chemokine ligand 3/4/22; IL, interleukin; RA, receptor antagonist; TNF, tumour necrosis factor; CSF1, colony stimulating factor 1; IFN, interferon; LDH, lactate dehydrogenase; IPI, international prognostic index; AMC, absolute monocyte count; ALC, absolute lymphocyte count.

5.4.4 Cellular origin of cytokines in DLBCL

To identify cytokine producing populations in DLBCL, we employed an intracellular cytokine staining MC protocol incorporating both lineage markers, to identify cell type, and cytokine / cytotoxicity markers, to identify the cellular source of cytokine production ('cytokine' panel, see table 2.1). PBMC samples from 11 DLBCL patients (table 5.3) with sufficient remaining cells following immunophenotyping were analysed across these experiments and compared with the same healthy donor control PBMCs isolated from leucocyte cones detailed in chapter 4. Analysis of the unstimulated samples identified monocytes to be the main cellular source of cytokine production with constitutive over expression of MIP-1α and IL-6 by monocytes in DLBCL (figure 5.5).

Table 5.3 Patients included in the intracellular MC cytokine staining study. Samples were either unstimulated or activated as detailed. LPS, bacterial lipopolysaccharide; PMA/I, phorbol 12-myristate 13-acetate / ionomycin.

Patient ID	Vial ID	Unstimulated	LPS	PMA/i
7065	R1959	x	Yes	x
7140	R5448	Yes	Yes	Yes
7189	R5749	x	Yes	x
7306	R6229	Yes	x	x
7374	R7219	x	Yes	x
7407	R6852	Yes	x	Yes
7851	R9081	x	Yes	x
8686	T3714	Yes	x	Yes
9311	T6450	x	Yes	x
9974	T8690	x	Yes	x
10146	T9596	Yes	Yes	Yes

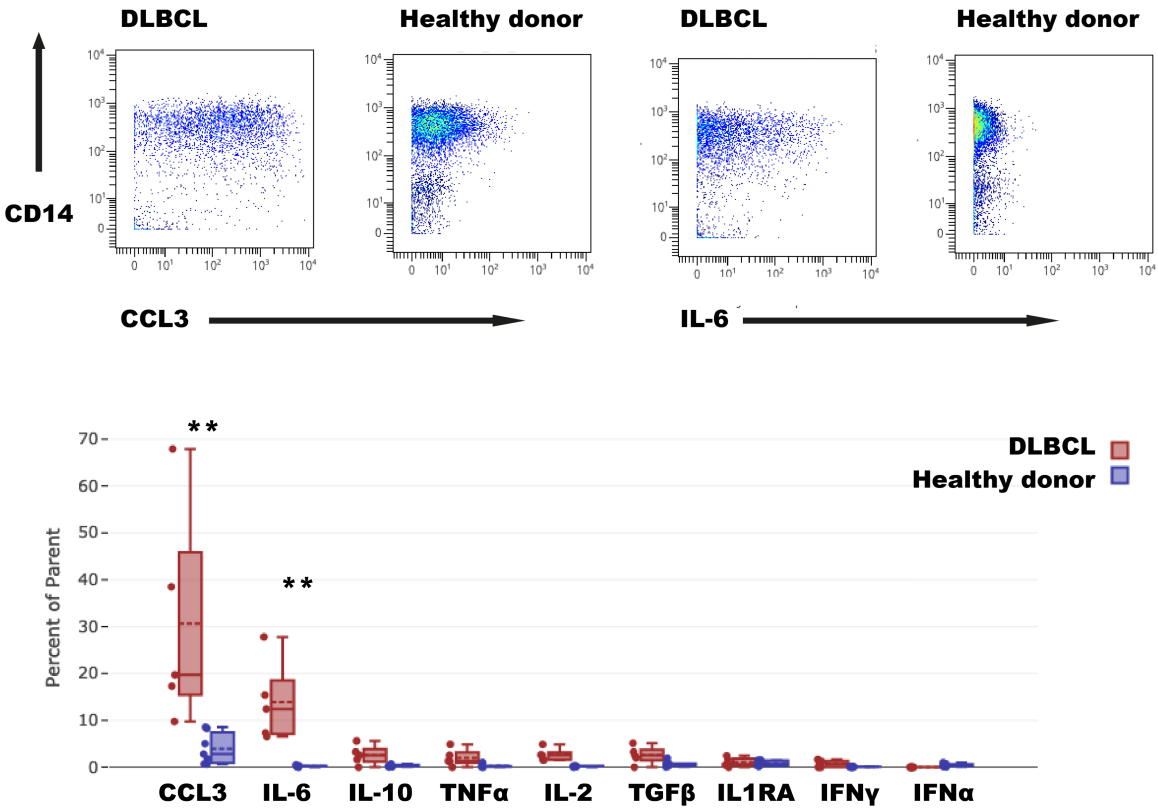

Figure 5.5 Gated percentage of unstimulated monocytes positive for indicated cytokines. Top, gated monocytes for one DLBCL patient and one health donor showing expression of MIP-1α and IL-6. Bottom, gated percentage of cytokine positive monocytes for all samples analysed (DLBCL, n=5, healthy donors n=7). CCL3, C-C chemokine ligand 3; IL, interleukin; TNF, tumour necrosis factor; TGF, transforming growth factor; RA, receptor antagonist; IFN, interferon. (Mann-Whitney U-test ** $p<0.01$).

The percentage of unstimulated monocytes positive for MIP-1α and IL-6 was increased in DLBCL compared with the healthy donors (p=0.0025). The DLBCL cytokine producing monocytes were all positive for both CCL3 and IL-6, with expression positively correlated, whereas healthy donor cytokine producing monocytes were positive only for CCL3 with minimal IL-6 production. There was also a trend to increased monocyte positivity for IL-10 and TNF, but these cytokines were secreted at low levels and did not reach significance. Cytokine production was predominantly by CD14+ classical monocytes.

Unstimulated cytokine production by T and NK cells was generally low, with less than 5% of cells positive, but despite this there were significantly increased percentages of IL-10, TNF, IFNγ and IL-2 positive T cells in DLBCL (p<0.05). Interestingly, the frequency of NK cells positive for CCL3 and IL-2 in DLBCL were increased, as were granzyme B and perforin positive NK cells suggestive of increased NK cell activation in DLBCL (p<0.05) (figures 5.6 and 5.7).

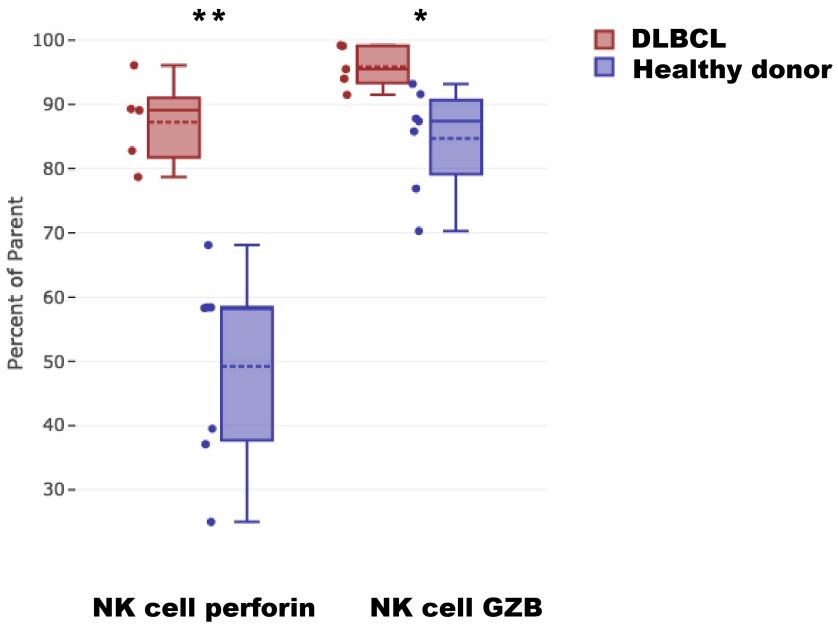

Figure 5.6 Gated percentage of NK cells positive for cytotoxic markers. Frequency of perforin and granzyme B (GZB) positive natural killer (NK) cells for all samples analysed (DLBCL, n=5, healthy donors, n=7). (Mann-Whitney U-test, * p<0.05, **p<0.01).

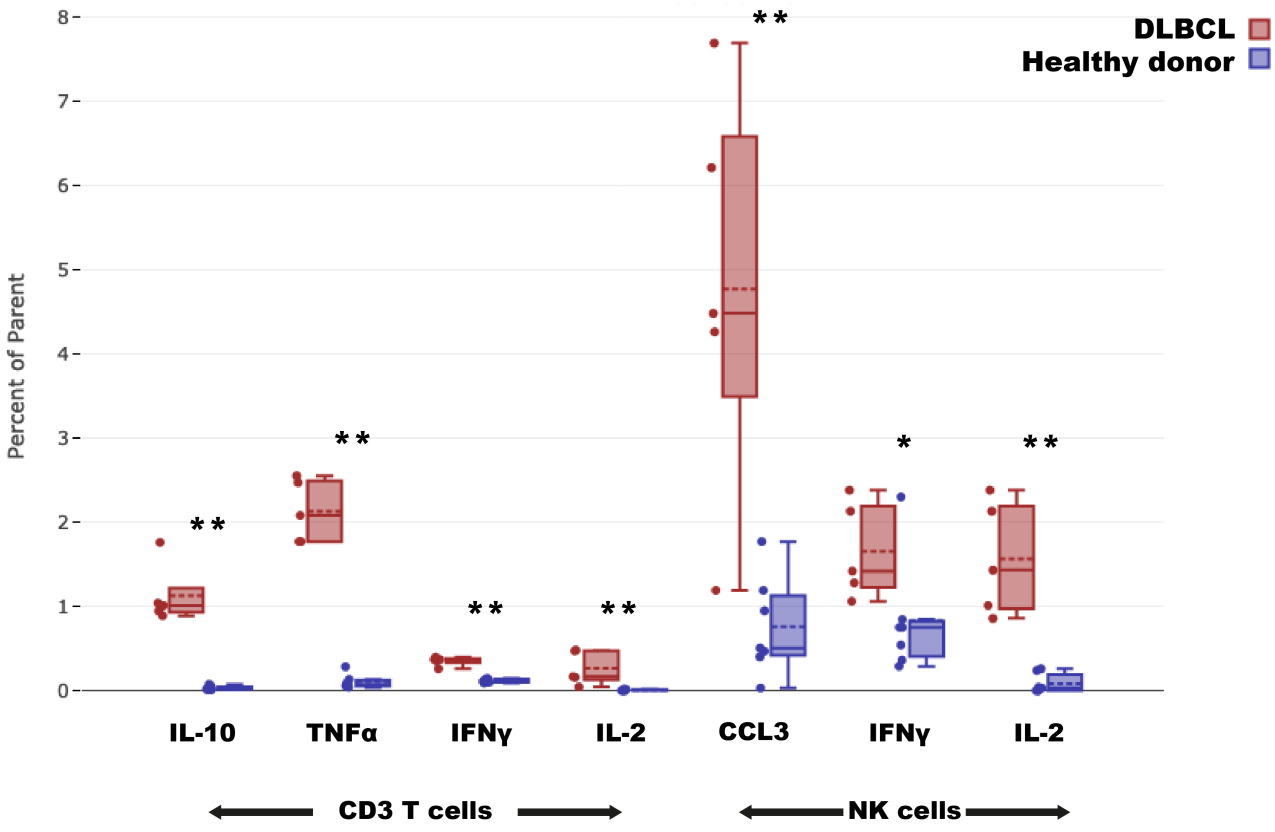

Figure 5.7 Gated percentage of T cell and NK cells positive for indicated cytokines. Frequency of cytokine positive CD3 T cells and NK cells for all samples analysed (DLBCL, n=5, healthy donors n=7). CCL3, C-C motif chemokine ligand 3; IL, interleukin; TNF, tumour necrosis factor; TGF, transforming growth factor; RA, receptor antagonist; IFN, interferon. (Mann-Whitney U-test, * $p<0.05$, **$p<0.01$).

To assess monocyte activation potential in DLBCL, we stimulated PBMC samples with bacterial lipopolysaccharide (LPS), a potent monocyte activator which acts through toll like receptor 4 (TLR4) and requires CD14 to activate downstream signalling via myeloid differentiation factor 88 (MYD88) (380). Both DLBCL and healthy donor monocytes responded to LPS stimulation with cytokine production, predominantly of CCL3, IL-6 and TNF (figure 5.8).

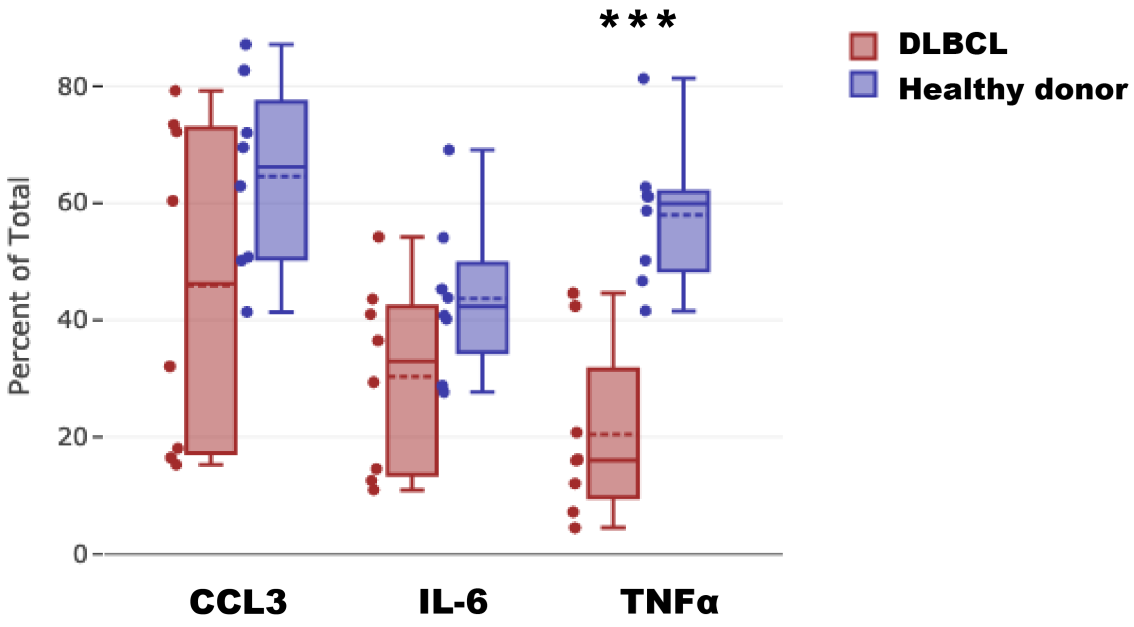

Figure 5.8 Gated percentage of monocytes positive for CCL3, IL-6 and TNF following LPS stimulation in DLBCL (n=8) and Healthy donors (n=8). CCL3, C-C motif chemokine ligand 3; IL-6, interleukin 6; TNF, tumour necrosis factor. (Mann-Whitney U-test, ***p<0.001).

Overall, the monocytes from DLBCL patients demonstrated blunted responses in terms of cytokine production with LPS stimulation compared to healthy donors. Comparing the percentage of cytokine positive monocytes for CCL3, IL-6 and TNF following LPS stimulation between DLBCL and healthy donors, there was an increased frequency of TNF positive monocytes in healthy donors (p=0.0006). There was a trend to an increased frequency of CCL3 and IL-6 expressing monocytes post stimulation in healthy donors, but this did not reach significance. There were seven healthy donor samples and two DLBCL samples that were analysed both unstimulated and following LPS stimulation. These paired samples were compared using the paired t test statistic. The mean differences in frequency of CCL3, IL-6 and TNF positive monocytes post LPS stimulation were all increased in healthy donors

(p<0.0001). There was no significant difference in expression of these cytokines post stimulation in the two DLBCL pairs.

Finally, we assessed T cell cytokine secretion in response to stimulation with PMA/ionomycin. We found no evidence of exhaustion, with robust cytokine production in DLBCL T cells, with coproduction of TNF and IFNγ, production of IL-2 and expression of the cytotoxic markers granzyme B and perforin. However, we did observe hypersensitivity of IL-2 and TNF production by T cells in DLBCL, most marked by CD4 T cells compared with healthy donors.

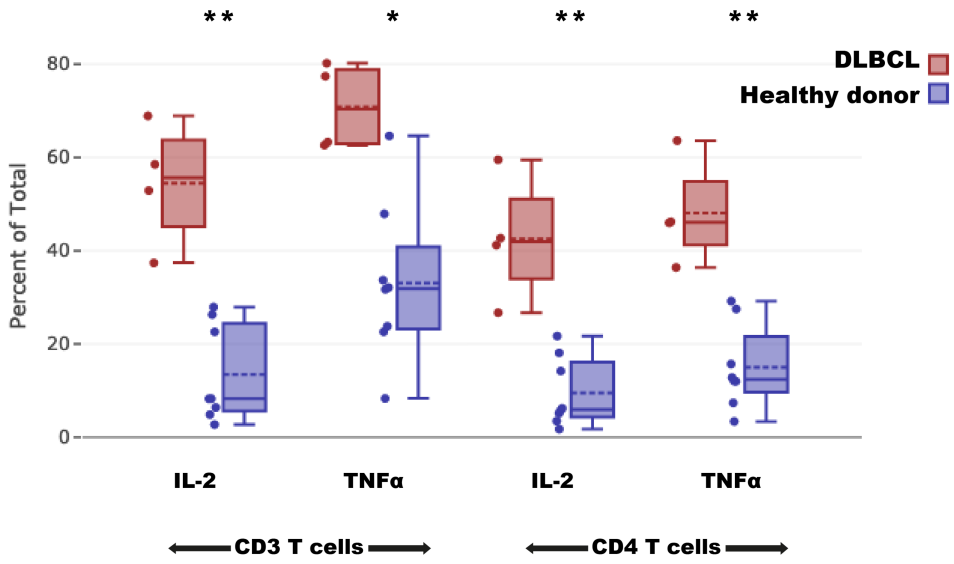

Figure 5.9 Gated percentage of T cells positive for IL-2 and TNF following PMA/ionomycin stimulation in DLBCL (n=4) and Healthy donors (n=8). IL-2, interleukin 2; TNF, tumour necrosis factor. (Mann-Whitney U-test, * p<0.05, **p<0.01).

5.4.5 Cytokines in molecular subtypes

A total of 24 patients included in the serum cytokines study had mutational data available as they were included in the genetic and functional drivers in DLBCL study (112). Seven patients could be identified as belonging to the EZB/C3/BCL2 group and nine to the MCD/C5/MYD88 group based on their mutational profiles (see section 1.3.3) (122-124). There were trends in the EZB/C3/BCL2 cases for decreased CCL3 and TNF levels and increased IL-10 and IL-1RA, and in the MCD/C5/MYD88 for decreased CCL3, TNF, IL-10 and IL-1RA, however no significant associations with cytokine levels were identified in the molecular subtypes in this small subset of patients.

5.5 Discussion

A number of previous studies have identified cytokine overproduction in DLBCL and associated specific cytokines with poor outcome (223, 226, 378). The overexpression of both IL-6 and IL-10 have been linked to the NFκB pathway, which is constitutively activated in ABC DLBCL, suggesting a lymphoma cell origin (378). These cytokines can then signal in an autocrine manner to stimulate B-cell survival through the JAK/STAT pathway. DLBCL cell lines and murine models have been demonstrated to express IL-6, and mutations inactivating the IL-6 negative regulator SOCS1 recurrently occur in DLBCL (124, 226). IL-10 receptor genes are also reported to amplified recurrently in DLBCL, with preclinical evidence supporting blockade of the IL-10 receptor as a therapeutic strategy (381). However, there are limited data on the association of cytokine dysregulation with the AMC and ALC and their role as prognostic indicators, as well as the role of peripheral blood immune cells in cytokine overproduction.

In this study we report overproduction of several cytokines in DLBCL, including IL-1RA, IL-6, IL-10, CCL3 and TNF, which were all significantly more increased at diagnosis in patients who were refractory to, or relapsed after RCHOP. Unsupervised clustering linked these five cytokines together and clustered a group of DLBCL patients together based on a pattern of generalised cytokine elevation at diagnosis, particularly across these five cytokines. Most of

the patients clustered in this group went on to fail frontline therapy. A small group of DLBCL patients clustered with most of the healthy controls, based on a pattern of low cytokine levels and all these patients achieved a maintained complete remission following RCHOP. The cytokines most elevated at diagnosis in patients who went on to R/R disease were independent of COO except for IL-1RA, which was increased in the non-GCB group. IL-1RA is an anti-inflammatory cytokine than binds the IL-1 receptor but does not activate intracellular signalling. Elevation of IL-1RA may represent a physiological response to constitutive activation of downstream signalling via MYD88, and it is interesting to note that 3 of the 4 patients in our cohort with the MYD88 mutation had elevated IL-1RA. It is also noteworthy that several cytokines are reported to be aberrantly epigenetically regulated in malignant disorders given that mutations in epigenetic regulators are frequently found in DLBCL (59, 382). In our cohort, four patients carried a mutation in the KMT2D (MLL2) gene, and all had widespread elevated cytokine levels.

IL-6 levels positively correlated with the AMC and IL-10, CCL3 and TNF all negatively correlated with the ALC. We identified unstimulated monocytes as the main peripheral blood cellular source of cytokines in DLBCL, with increased secretion of CCL3 and IL-6, suggesting a non-cell autonomous role for monocytes in the cytokine overproduction seen in this disease. This would suggest that elevated IL-6 may be a consequence of, rather than a driver for, the increased monocyte count observed in DLBCL. Although CSF1 is known to be a key cytokine in driving myeloid differentiation and monocyte production (383), and was elevated in our DLBCL cohort compared with controls, it did not have a significant association with AMC or monocyte frequency. We did, however, identify down regulation of CD184 (CXCR4) in the immunophenotyping study as a potential mechanism to increase the monocyte count in DLBCL by preventing bone marrow homing. Monocytes in DLBCL also had increased CCL3 production, which plays a role in myeloid differentiation and has been implicated in ME dysfunction in several malignancies, including haematologic (384). This would potentially support a positive feedback of monocyte derived CCL3 driving further monocyte production, although CCL3 did not correlate with AMC in our data. It did however, correlate negatively with ALC, and has been shown to both inhibit proliferation of primitive haematopoietic progenitor cells and activate proliferation of mature myeloid

progenitors, consistent with a role in mediating the relative monocytosis and lymphopenia in DLBCL (385).

In the stimulated experiments we observed attenuated cytokine production responses in DLBCL monocytes compared to healthy donor monocytes, which robustly upregulated secretion of IL-6, CCL3 and TNF. Due to the baseline cytokine over-production in DLBCL monocytes, only the frequency of TNF positive monocytes was significantly increased post stimulation in the healthy donor group compared with DLBCL. In the paired samples, the healthy donors significantly upregulated cytokine expression in response to LPS, whereas the DLBCL patients did not. Thus, we find evidence of cytokine overproduction by DLBCL monocytes but reduced ability to respond to stimuli, suggestive of a pattern of sustained activation resulting in a degree of exhaustion and dysfunction in DLBCL.

We observed increased positivity for several cytokines in T and NK cells in DLBCL, which was most marked for NK cell MIP-1α, although overall only low frequencies of these cells were cytokine positive in the unstimulated experiments. Most of the NK cells in the DLBCL samples were positive for the cytotoxic markers consistent with baseline NK activation. In the stimulated experiments, we found no evidence of peripheral T cell exhaustion with coproduction of IFNγ, IL-2 and TNF. The DLBCL cases demonstrated hypersensitivity to stimulation with increased frequency of cytokine positive cell compared to healthy donors, which was predominantly driven by CD4 T cells, including FoxP3 positive regulatory T cells.

Overall, we find cytokine dysregulation in DLBCL with outcome associations. We establish monocytes as playing a role in cytokine overproduction and infer possible links with the AMC / ALC and their prognostic nature. We find evidence to support poor monocyte responsiveness and possible exhaustion, with NK cell activation but no evidence of peripheral T cell exhaustion. The exaggerated responses of CD4 T cells to direct stimulation are consistent with underlying immune dysfunction and interesting given our observation that the costimulatory molecules CD27 and CD28 were down regulated in DLBCL.

Limitations of the study

As previously, the samples assayed in this work were all cryopreserved. Serum samples were used to assess peripheral blood cytokine levels and MC staining of PBMCs to assess cellular origin. While both serum and plasma samples have been assayed to measure cytokine levels, we choose serum purely based on availability. Differences in cytokine levels are reported between serum and plasma samples, largely because of coagulation, with levels generally increased when serum samples are used. This remains an accepted material to study cytokines, however and we were consistent throughout the study with both healthy donor and DLBCL samples. Cryopreservation is generally not considered an issue providing repeated freeze thaw cycles are avoided. Several factors can affect the levels of both serum and plasma cytokines including receptor binding, temperature degradation, urinary excretion and cellular breakdown (386). In addition, cytokines act in a paracrine manner and display variable levels during the day and therefore levels can be influenced by the timing of venepuncture. Serum cytokine levels can therefore be considered to provide an indirect estimate of cytokine activity in the peripheral blood and likely do not reflect activity in disease sites and in the bone marrow.

There was a significant overlap between the patients with PBMC and serum samples available, but some patients only had one or the other available for analysis. Most importantly though, since the PBMC samples were prioritised for the phenotyping arm of the study, many patients did not have enough available cells to be included in the cellular cytokine expression arm of the study. Finally, although we were able to use a health donor control group with serum samples, these samples did not have demographic data available and represented a population that was not age matched.

6. The tissue microenvironment in DLBCL

6.1 Introduction

Although the bulk of this work has focused on the peripheral blood immune compartment, DLBCL is primarily a disease of lymph node tissue, with approximately one third of patients having extra-nodal involvement, but primary extra-nodal or isolated bone marrow disease is much less frequent (75, 387, 388). The initial importance of the ME in DLBCL was highlighted in work by the Leukaemia/Lymphoma Molecular Profiling Project (LLMPP) in which two groups of patients were identified based on 'stromal' signatures from the non-malignant cells within diagnostic tissue biopsies (106). The two signatures were based on differential expression of genes associated with the immune ME and extracellular matrix (ECM), with each group associated with a distinct outcome. In addition, other gene expression profiling (GEP) studies have strengthened the evidence that the non-malignant component in the DLBCL tissue ME contributes to disease pathogenesis (154, 204, 210, 389). Several groups have applied single or dual marker immunohistochemistry (IHC) strategies to biopsy specimens to enumerate the non-malignant immune cells and distinguish functional subsets, often with inconsistent results (205-209, 211, 218). The recent genetic studies, which have opened the door to a new molecular classification in DLBCL, highlight recurrently mutated genes which establish a critical role for immune evasion in disease evolution (73). Recent years have also seen a move away from conventional cytotoxic chemotherapy, towards novel therapies based on harnessing the power of the immune system to improve outcomes, especially in the relapse setting (189, 280, 284, 285). Taken together, the current data support a key role for the tissue ME in disease biology and response to therapy, however, as with the peripheral blood compartment much of the basic immunology in terms of immune composition, including phenotypic and functional subsets, as well as spatial context remains understudied or lacking. We therefore hypothesised that single cell strategies such as MC and IMC could be applied to the complex tissue ME in DLBCL to further our existing knowledge and contribute to the deconvolution of immune subset heterogeneity.

6.2 Aims

Our aims for this study were to apply MC to diagnostic tissue suspensions in DLBCL to characterise the immune populations and develop an IMC pipeline to apply to FFPE tissue to facilitate in depth immune subset identification with spatial context.

6.3 Methods

6.3.1 Patient selection

Diagnostic tissue single cell suspensions (SCS) were accessed through the Barts tissue bank for five patients with DLBCL, all lymph node (LN) and five patients with reactive disorders, four LN and one tonsil (reactive lymph node / tonsil, RLNT). Samples were selected based on availability and all were collected prior to any therapy and cryopreserved in liquid nitrogen. All DLBCL patients were subsequently treated with RCHOP. For the IMC validation work, tonsil tissue was provided by Andrew Clear and Hodgkin lymphoma tissue by Dr Joseph Taylor. Two DLBCL tissue microarrays (TMAs), one constructed for a prior study (390) and one during this work to include 18 cases with PBMC phenotyping data and a balance between CR and R/R cases, have now been stained.

Table 6.1 Patients with tissue suspensions for mass cytometry experiments. LN, lymph node; RCHOP, rituximab, cyclophosphamide, doxorubicin, vincristine, prednisolone.

Patient ID	Vial ID	Diagnosis	Tissue	Treatment	Outcome
6719	R3153	DLBCL	LN	RCHOP	Remission
10085	T8477	DLBCL	LN	RCHOP	Relapse
10115	T9041	DLBCL	LN	RCHOP	Remission
10344	C0447	DLBCL	LN	RCHOP	Relapse
10403	C0572	DLBCL	LN	RCHOP	Remission
NA	T9611	Reactive	LN	NA	NA
NA	C0939	Reactive	LN	NA	NA
NA	C1587	Reactive	LN	NA	NA
NA	C1130	Reactive	LN	NA	NA
NA	C1171	Reactive	Tonsil	NA	NA

6.3.2 Mass cytometry staining

SCS were resuscitated from liquid nitrogen storage and stained as previously described. Samples were stained in 5ml polypropylene falcon tubes and acquired in 2 batches, with one of the RLNT samples being acquired with both batches to ensure consistency between runs. The SCS samples were stained with the 'lymph node' panel, which was based on the 'T-cell' panel given previous work in our laboratory had shown T cells to be the predominant viable cells in these samples, suggesting the malignant cells and myeloid populations identifiable on FFPE tissues did not survive the processing and cryopreservation. For functional studies, SCS were rested overnight in 12-well plates in a humidified incubator and stimulated with PMA/ionomycin with transport inhibitors in a 500μl volume and stained with the 'cytokine' panel to assess T cell cytokine production.

6.3.3 Imaging mass cytometry staining

Individual tissue sections or TMA sections were stained as described in section 2.4 for IHC and IMC to optimise an antibody panel to interrogate the tissue ME in both DLBCL and Hodgkin lymphoma. Samples were selected based on prior IHC characterisation for the

specific antibodies under validation. In total, two DLBCL TMAs, labelled TMA 2018 and TMA 2020, one Hodgkin lymphoma TMA and one reactive TMA have now been stained as part of the experimental work of this thesis, however data acquisition and analysis are ongoing and therefore only details of the validated panel are presented here.

6.4 Results

6.4.1 Patient characteristics

SCS were only available for five DLBCL cases at diagnosis and all received RCHOP. The median age at diagnosis was 55 (range, 50-67). Two relapsed within 12-months of RCHOP and the remaining three achieved prolonged remission. There were five RLNT tonsil cases consisting of four LN and one tonsil. A malignant diagnosis was excluded in all cases, and they received no specific therapy other than antibiotics following biopsy. No further demographic details were available. See table 6.1.

6.4.2 T cell microenvironment in DLBCL tissue

Interrogation of the ME in the SCS samples focused on the T cell compartment. Although the diagnostic histology reports confirmed the presence of predominantly malignant cells but also myeloid and T cells, previous work from our laboratory had demonstrated T cells to be the predominant viable cell type in these samples, which was confirmed in our work. Data were processed as previously described and gated to live CD45+ CD3+ single events prior to further analysis. The samples were acquired in two batches with cells from the reactive donor T9611 included in both for quality control (figure 6.1).

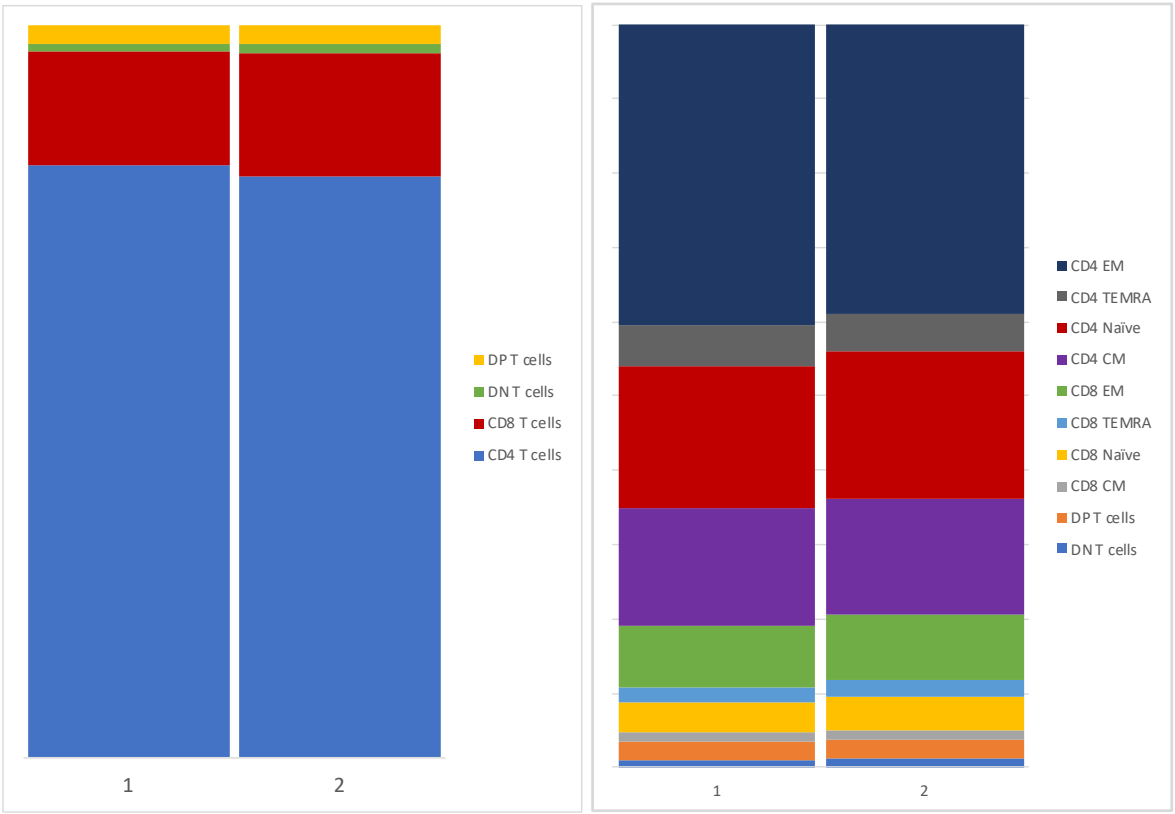

Figure 6.1 Gated percentages of T cell subsets for RNLT donor T9611 for each of two MC batches. An aliquot of single cell suspension (SCS) from donor T9611 was aquired with each batch of SCS samples, with the results of each T9611 control showing comparable results, indicating staining consitency between batch runs. DP, double positive; DN, double negative; EM, effector memory; TEMRA, T effector memory RA; CM, central memory

As before, data were analysed with manual gating (figure 4.4) and with opt-SNE dimensionality reduction and FlowSOM clustering. Data from all 10 SCS were gated into T cell subsets and are summarised in figure 6.2. The effector memory populations could be further gated to EM1 – EM4 based on expression of CD27 and CD28 (347). CD4 T cells were the predominant cell type in both RNLT and DLBCL but with a skew in the CD4:CD8 ratio in DLBCL with a relative decrease in median CD4 T percentage (57.6 v 79.3, p=0.032) and an increased CD8 percentage (33.2 v 16.8, p=ns). In the subset analysis, CD4 naïve T cells were reduced as a percentage of T cells and CD8 effector memory (EM) increased in DLBCL as compared with RNLT (p=0.0317). Differential abundance (DA) analysis with EdgeR revealed similar results with significant fold change decreases in CD4 naïve T cells and increases in

CD8 EM subsets EM1 and EM4, CD8 central memory (CM) and natural killer T (NKT) cells in DLBCL, however NKT cells were present at low frequencies in all samples (figure 6.3).

Overall, the gating analysis identified a skew towards a reduced CD4:CD8 ratio compared to reactive tissues, with a shift in differentiation away from naïve and towards an EM phenotype in both CD4 and CD8 T cells in DLBCL. We next performed FlowSOM clustering of the CD3 T cells in all samples, using all the T cell and checkpoint markers to further interrogate these subsets. We identified 25 T cell clusters, each representing a phenotypic subset, which are shown by colour overlay on to an opt-SNE map (figure 6.4). DA analysis of the clusters identified six T cell subsets present in increased abundance in DLBCL tissues compared with RLNT. The clusters represent three CD4 T, one CD8 T, one double negative (DN) and one double positive (DP) T cell subsets. Cluster 06 had the phenotype of regulatory T cells (Treg), with CD25 and FoxP3 expression and low CD127 expression. The cluster also expressed PD-1 consistent with a suppressive Treg population. Clusters 10 and 12 had similar CD4 EM4 phenotypes with expression of T-bet and the activation markers CD38 and CD134 (OX40). Although both clusters expressed PD-1, they were distinguished by higher expression on cluster 10. Cluster 11 had a CD8 EM1 phenotype consistent with the gating analysis and expressed both inhibitory checkpoints PD-1 and TIM-3 (CD366). The DN population, cluster 13 also expressed PD-1 and the DP population, cluster 15 expressed the activation marker CD38. The median expression levels of all antigens analysed for each T cell cluster are shown in the heatmap (figure 6.6).

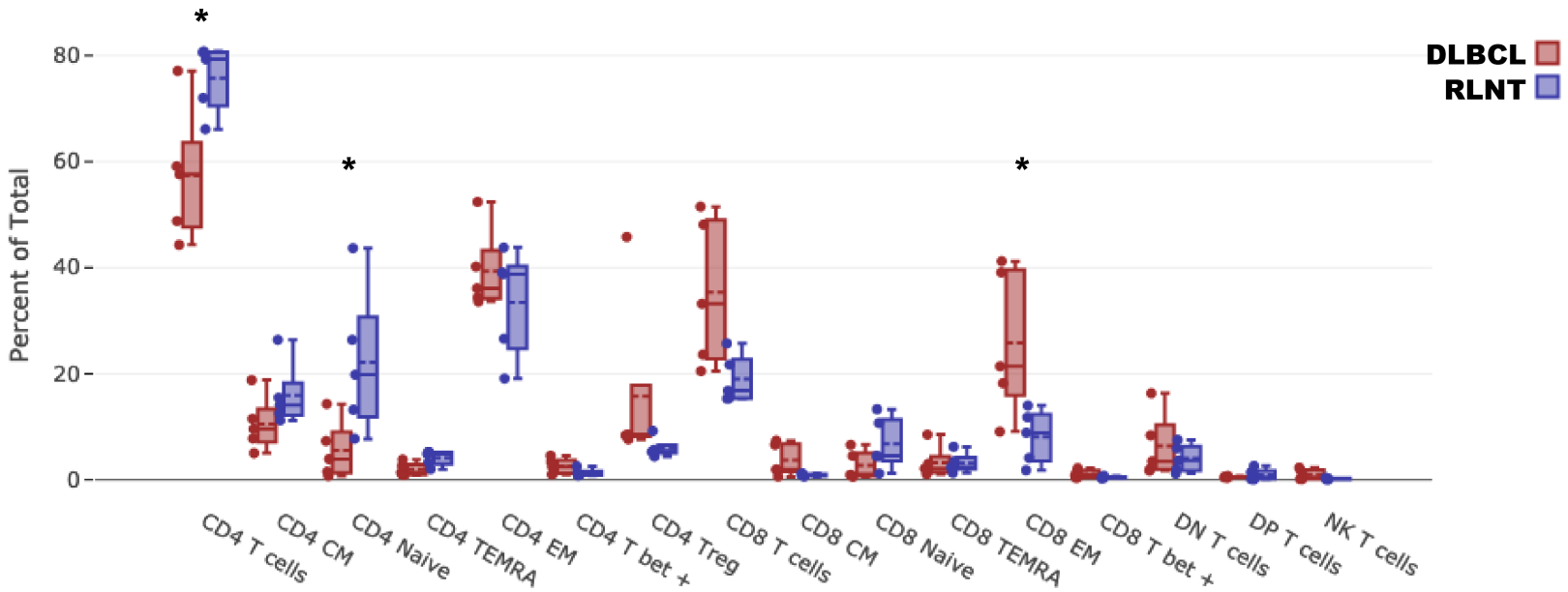

Figure 6.2 Gating derived frequencies of T cell subsets for all DLBCL (n=5) and RLNT controls (n=5).CM, central memory; TEMRA, T effector memory RA, EM, effector memory; Treg, regulatory T cells; DN, double negative; DP, double positive; DN, double negative; NKT, natural killer T; RNLT, reactive lymph node and tonsil. (Mann-Whitney U-test, * $p<0.05$)

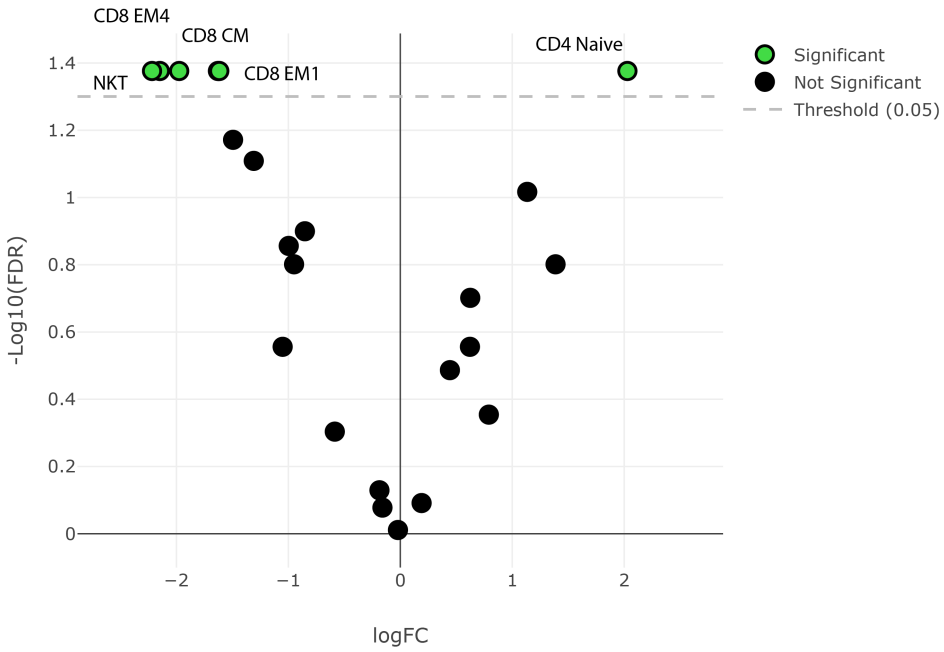

Figure 6.3 Differential abundance analysis of gated T cell subsets between DLBCL (n=5) and RLNT (n=5). Volcano plot showing false discovery rate (FDR) against fold change (FC) of T cell subsets between DLBCL and reactive lymph node and tonsil (RNLT) controls. Left of centre indicates population increased in DLBCL, right increased in RLNT, green indicates statistical significance (FDR<0.05).

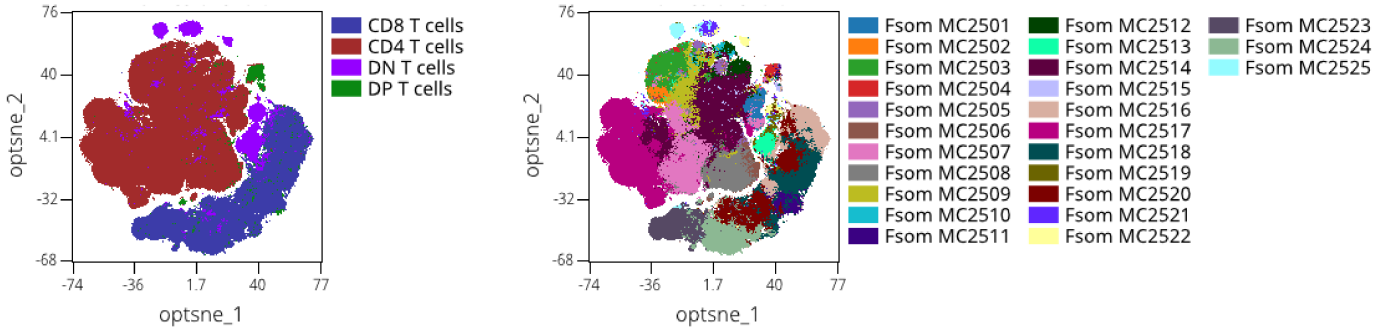

Figure 6.4 Dimensionality reduction with opt-SNE for all DLBCL (n=5) and RNLT (n=5). Maps are coloured by gated populations (left) and FlowSOM clusters (right).

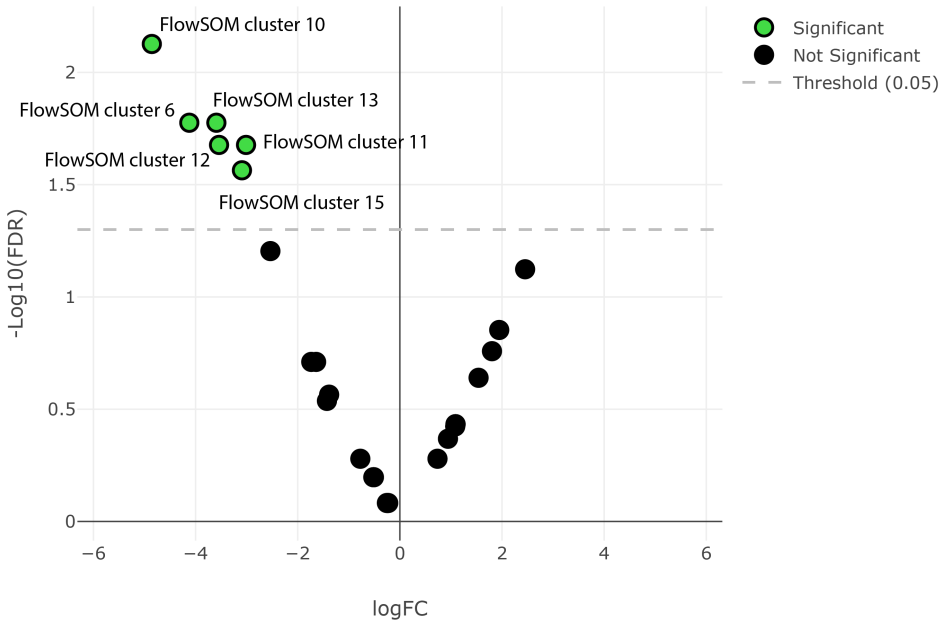

Figure 6.5 Differential abundance analysis of FlowSOM T cell clusters between DLBCL (n=5) and RLNT (n=5). Volcano plot showing false discovery rate (FDR) against fold change (FC) of T cell subsets between DLBCL and reactive lymph node and tonsil (RNLT) controls. Left of centre indicates population increased in DLBCL, right increased in RLNT, green indicates statistical significance (FDR<0.05).

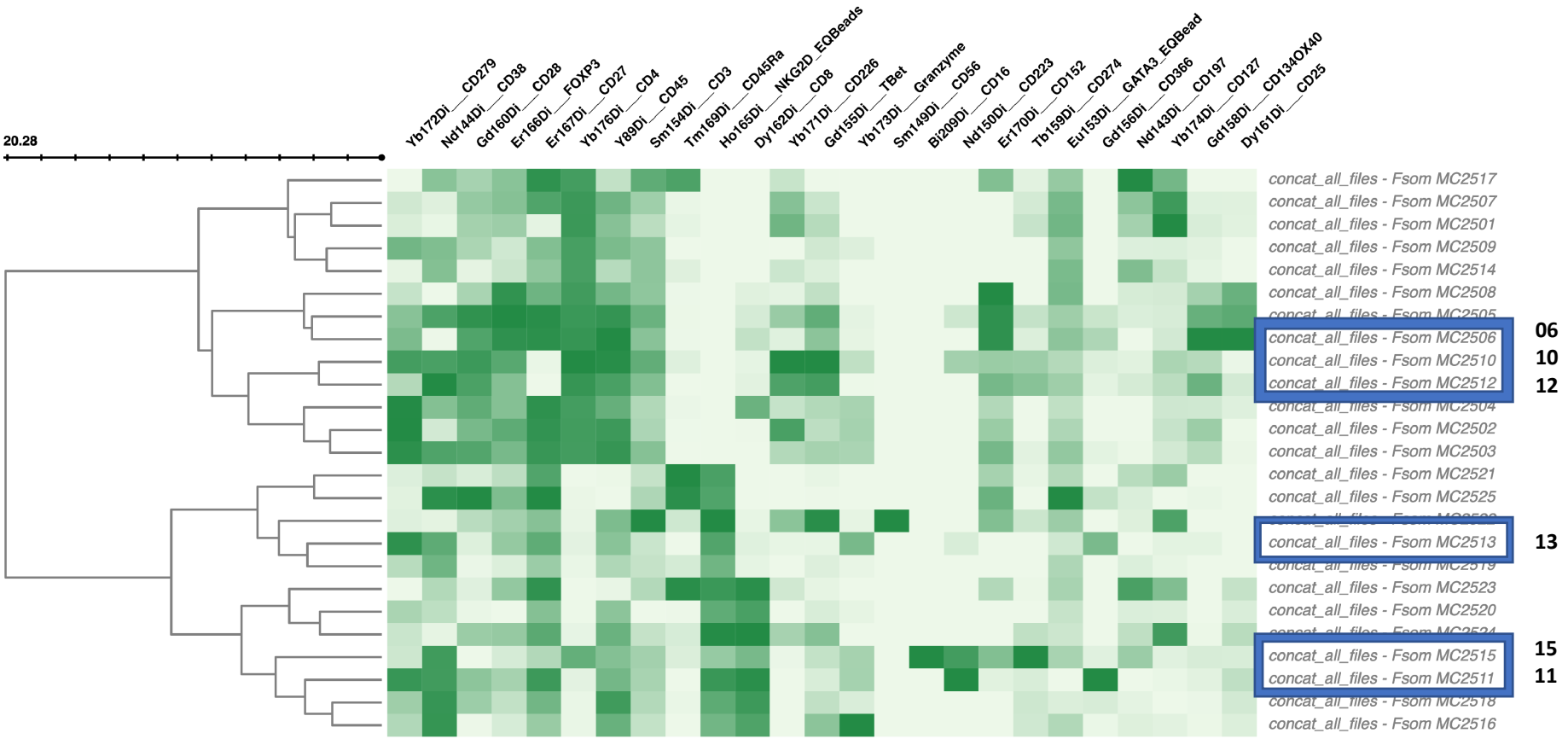

Figure 6.6 Heatmap of antigen expression for FlowSOM T cell clusters. Median expression of all analysed markers (columns) for each FlowSOM cluster (row). Clusters 6, 10, 11, 12, 12 and 15 were present in increased abundance in DLBCL compared with RLNT.

6.4.3 T cell function in DLBCL microenvironment

The cytokine producing ability of the T cells in the DLBCL microenvironment was assessed in response to stimulation with PMA/ionomycin. We found no evidence of CD8 T cell exhaustion in DLBCL in terms of cytokine production, with similar frequencies of cells positive for IFNγ and TNF in response to stimulation when compared with RLNT. They were also able to produce IL-2, with a trend to reduced production. There were increased frequencies of granzyme B and perforin positive CD8 T cells in lymph node tissue in DLBCL (figure 6.7). Although the CD4 T cells in the DLBCL ME were able to produce cytokines in response to stimulation, there were some features consistent with exhaustion. There were significantly less IL-2 and TNF positive CD4 T cells compared to reactive controls ($p<0.05$) (figure 6.8). There were no differences in ability to produce IFNγ and IL-10. Overall, there were relatively few T cells positive for IL-10 in both the DLBCL and reactive groups, most likely due to the shorter stimulation period of 6 hours.

In summary we found no evidence of CD8 T cell exhaustion, with robust cytokine production observed post stimulation. The finding of an increased frequency of CD8 T cells positive for the markers of cytotoxicity is also consistent with a lack of exhaustion and suggestive of an increased baseline of activation in this compartment. Within the CD4 T cells we identified blunted responses in terms of IL-2 and TNF production compared with RLNT, suggestive of a level of exhaustion in this compartment. Interestingly, we found the opposite in the peripheral blood CD4 T cell compartment with an exaggerated IL-2 and TNF response to stimulation.

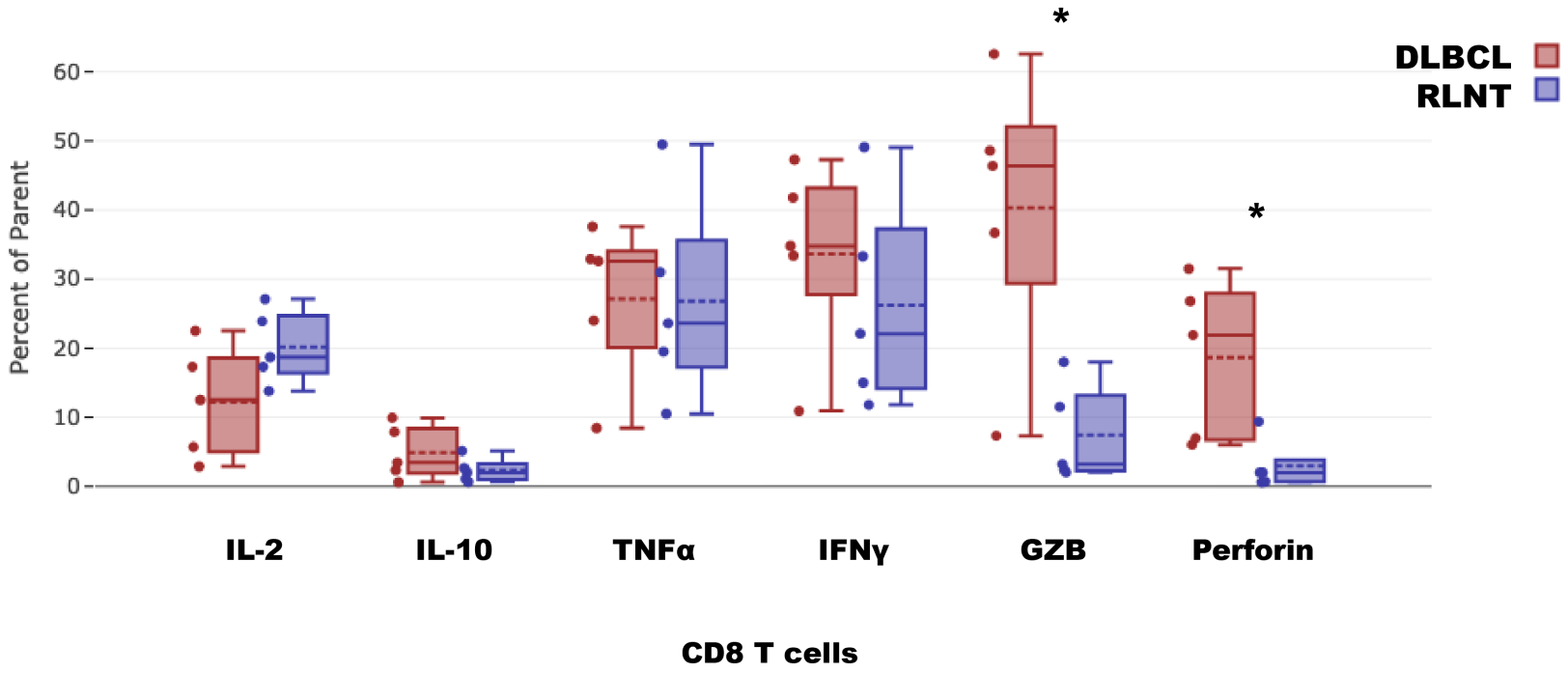

Figure 6.7 Gated percentage of CD8 T cells positive for the indicated cytokines and cytotoxic markers following PMA/ionomycin stimulation in SCS from DLBCL (n=5) and RLNT (n=5). Granzyme B (GZB) and perforin positive CD8 T cells were increased in DLBCL compared with RLNT following stimulation. IL, interleukin; TNF, tumour necrosis factor; IFN, interferon. (Mann-Whitney U-test, * $p<0.05$).

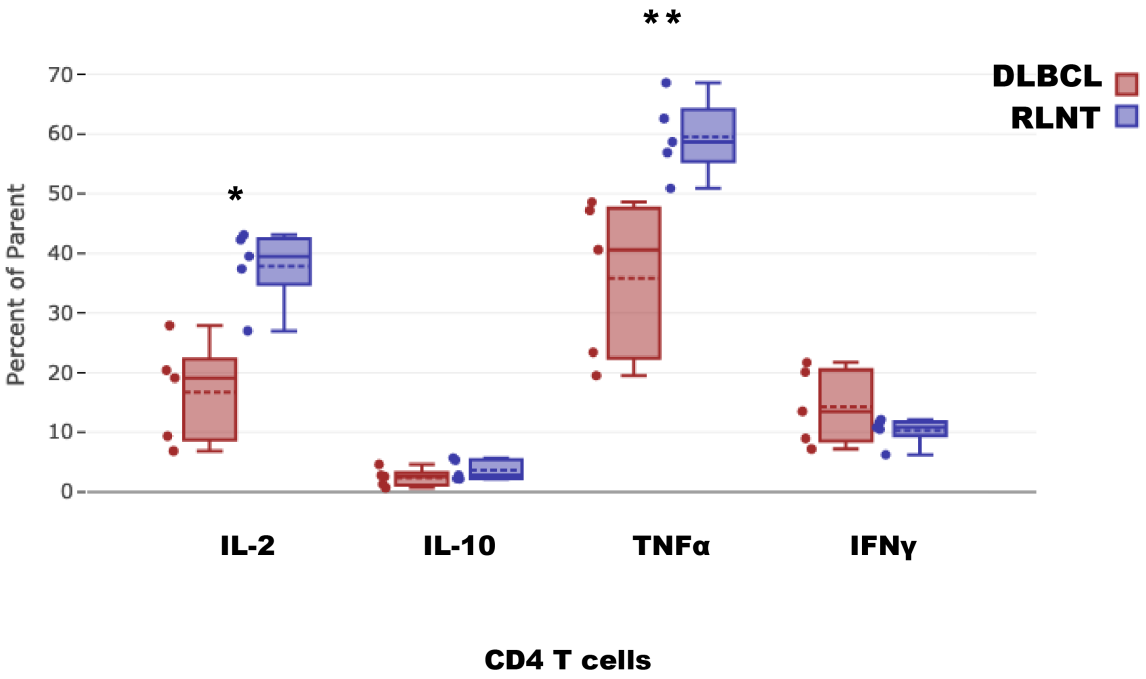

Figure 6.8 Gated percentage of CD4 T cells positive for indicated cytokines following PMA/ionomycin stimulation in SCS from DLBCL (n=5) and RLNT (n=5). IL-2 and TNF positive CD4 T cells were decreased in DLBCL compared with RNLT following stimulation. IL, interleukin; IFN, interferon. (Mann-Whitney U-test, * $p<0.05$, ** $p<0.01$).

6.4.4 Imaging mass cytometry panel optimisation

During the experimental work for this thesis a protocol and antibody panel for imaging mass cytometry (IMC) were optimised to characterise the infiltrating immune populations in the tissue ME of DLBCL and Hodgkin lymphoma. IMC is a relatively recent adaptation of MC for high dimensional profiling of tissue sections. This has been applied to both malignant and non-malignant tissues to characterise tissue architecture and immune cell subpopulations, facilitating analysis with spatial context (301, 391, 392). However, as yet there remains limited published data applying IMC to lymphoma tissues (316). The panel of antibodies was designed to be complimentary to the work already presented in this thesis and that of a parallel project on Hodgkin lymphoma (figure 6.9).

Leucocytes / nuclear markers	
CD45	Leucocyte common antigen
Histone H3	Nuclear marker
Iridium	DNA marker
Ki67	Proliferation marker

Tissue architecture and blood vessels	
αSMA	alpha smooth muscle actin
Collagen 1	ECM protein
CD31	Endothelial cells
CD34	Endothelial cells

T and NK cells	
CD3	T cells
CD4	CD4+ T cells
CD8a	CD8+ T cells
CD45RA	Naïve cells
FoxP3	Treg transcription factor
T-bet	T helper (TH1) transcription factor
Granzyme B	Cytotoxicity
CD16	Fcγ Receptor III, NK cells

Myeloid cells	
CD11c	Complement receptor, Monocytes, DCs
CD14	LPS receptor, Monocytes / Macrophages
CD16	Fcγ Receptor III, Monocyte subsets
CD68	Myeloid cells
CD163	Scavenger receptor
CD206 (MMR)	Macrophage mannose receptor
CX3CR1	Chemotaxis, myeloid subsets
HLA-DR	Antigen presentation (MHC-II)

Immune checkpoint molecules	
B7H4	Negative regulator of T cell immunity
PD-1	Immune checkpoint
PD-L1	Immune checkpoint
LAG-3	Immune checkpoint
TIM-3	Immune checkpoint

B-cell / Tumour Markers	
CD20	B cells, DLBCL
CD30	Hodgkin's cells
MUM1/IRF4	Expressed by ABC DLBCL
CD10	GC B cells
HLA-DR	Antigen presentation (MHC-II)

Figure 6.9 Optimised antibody panel for imaging mass cytometry. SMA, smooth muscle actin; PD-1, programmed death 1; PD-L1, programmed death ligand 1; LAG-3, lymphocyte activation gene 3; TIM-3, T cell immunoglobulin and mucin domain-containing protein 3; Macrophage mannose receptor; MUM1, multiple myeloma oncogene 1; IRF4, interferon regulatory factor 4; HLA, human leucocyte antigen.

The above panel has been used to stain DLBCL, Hodgkin lymphoma and reactive TMAs with acquisition and data analysis ongoing. Representative images are shown for selected antibodies on tonsil (figure 6.10), DLBCL (figure 6.11) and Hodgkin lymphoma (figure 6.12) tissues. As part of a collaboration, my colleague Dr Joseph Taylor developed a multiplex imaging analysis pipeline for use with both multiplex IHC and IMC data. This involved designing a customised application for the Visiopharm analysis software to perform cell segmentation on multiplexed tissues using a composite of the cell surface markers for cell boundaries and a composite of intracellular markers to define individual cells. Data can then be exported for further analysis with dimensionality reduction and clustering as for MC data with spatial context retained for further modelling analysis (figure 6.13).

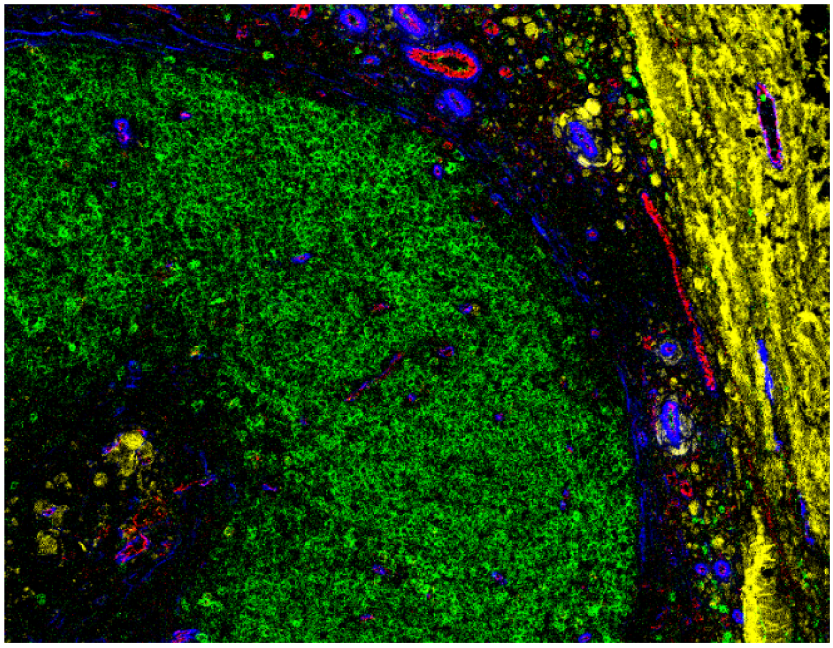

Figure 6.10 Tonsil stained with IMC panel. The image shows a 'false colour' representation of alpha-SMA (blue), CD31 (red), collagen 1 (yellow) and CD10 (green) highlighting the germinal centre B cells (green), vasculature (blue/red) and collagen (yellow).

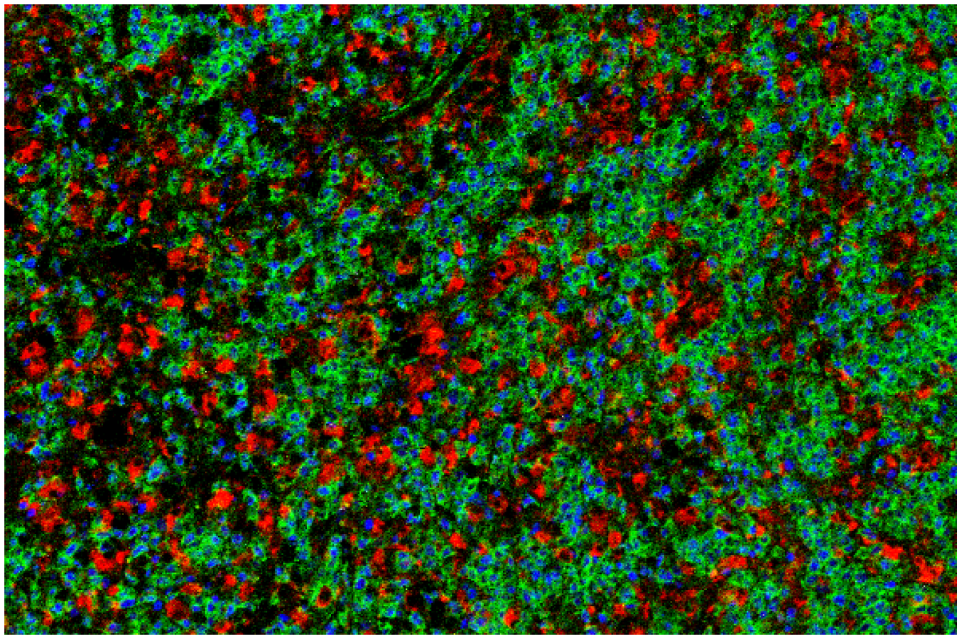

Figure 6.11 DLBCL lymph node stained with IMC panel. The image shows CD20 (green) and ki67 (blue) highlighting the proliferating lymphoma cells and CD68 (red) highlighting the macrophages.

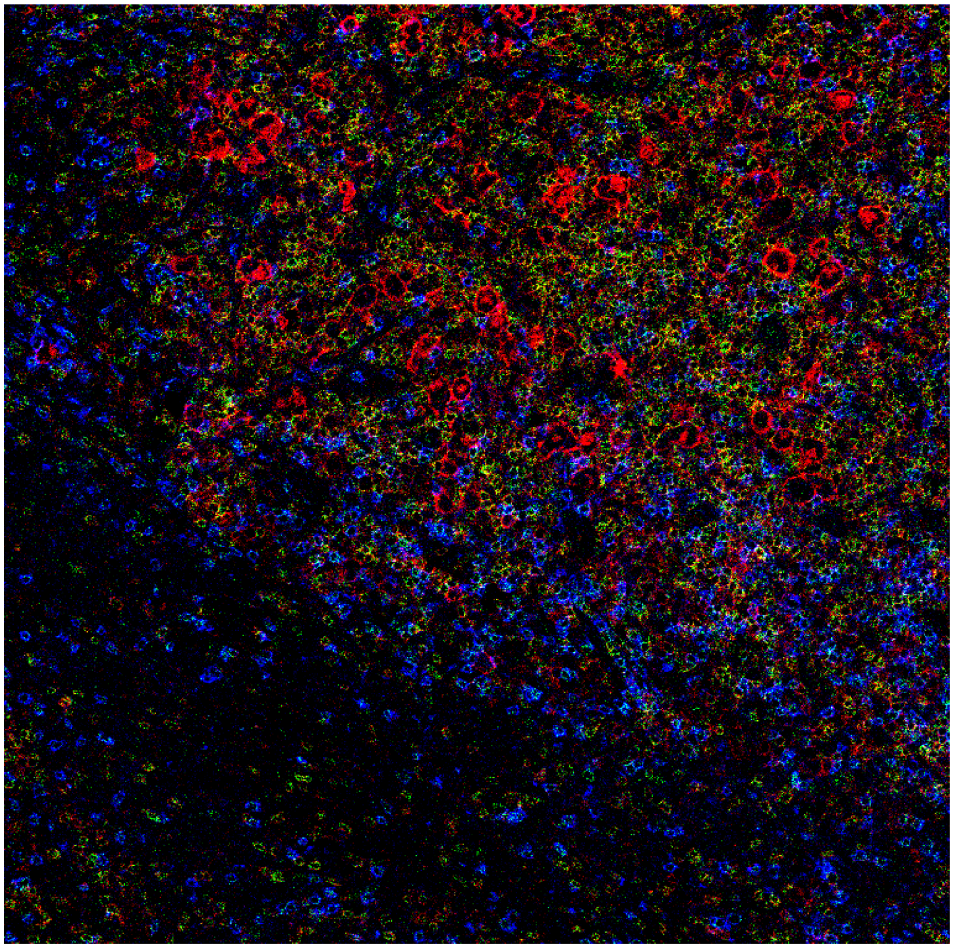

Figure 6.12 Hodgkin lymphoma lymph node stained with IMC panel. The image highlights the large Hodgkin's cells which are CD4 positive (red), the surrounding CD3 (green) CD4 dual positive T cells and the CD8 (blue) T cells which are largely excluded from the tumour area.

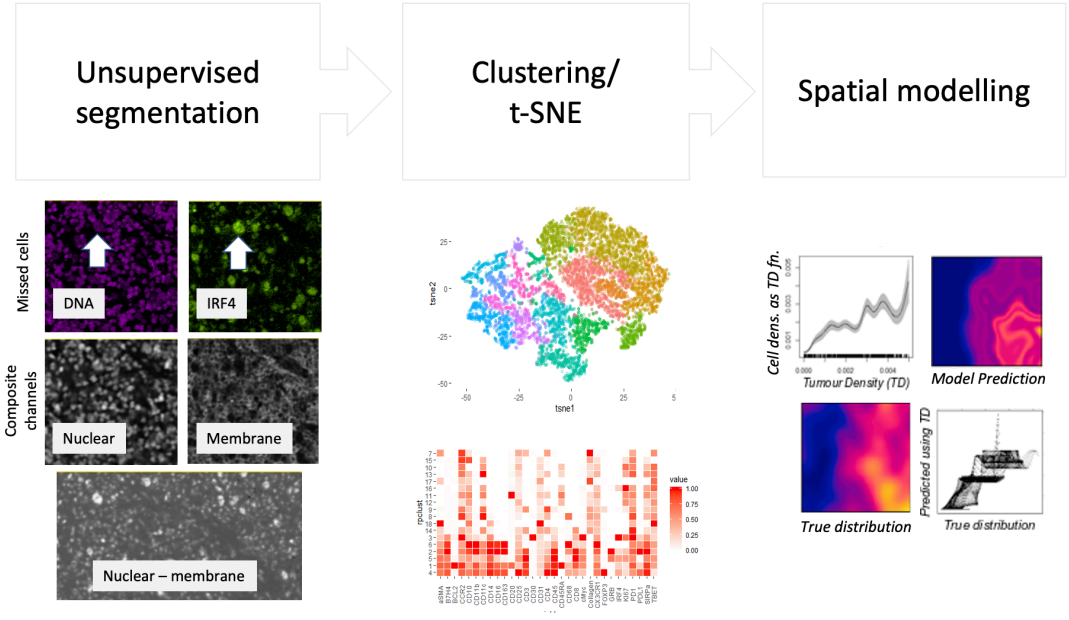

Figure 6.13 Analysis pipeline for IMC data. Figure provided by Dr J Taylor. Following acquisition, data are exported as stacked TIFFs and uploaded to Visiopharm for cell segmentation based on membrane and intracellular markers. Segmented data can then be analysed with downstream clustering and dimensionality reduction algorithms. Spatial modelling can be performed to assess whether the distribution of one cell type (immune subsets) can be predicted from the density of another (tumour cells).

6.5 Discussion

The tissue immune ME in DLBCL shows significant heterogeneity between individual cases but the non-malignant compartment has been used to define subgroups and associates with outcome in histological and gene expression profiling studies (106, 205, 211). Immune evasion is a key component in disease biology, highlighted by recurrent genetic and epigenetic bases of escape from immune detection (74). However, in depth characterisation of immune subsets at a single cell level is largely lacking from the published data with recent studies focusing on the genomic landscape.

Most patients are diagnosed with a lymph node or tissue biopsy which is formalin fixed and paraffin embedded (FFPE) with the result that many studies investigating the ME have focused on histological approaches. Also, in recent years there has been a dramatic increase in the use of core needle biopsies over excisional approaches for diagnostics with the result that less tissue is available for research studies. In contrast to the number of peripheral blood samples, we were able to identify only five DLBCL tissues SCS for analysis with MC with a similar number of reactive control tissues. In this group we focused our analysis on the CD3 T cell compartment as this was the predominant viable cell type in these samples. We identified a skew in CD4:CD8 ratio with a relative decrease in CD4 T cells and increase in CD8 T cells in DLBCL, with a trend for this to be more pronounced in the cases that went on to relapse. The data also demonstrated an increase in differentiation of the DLBCL T cell subsets with reduced naïve and increased effector memory (EM) populations, which again showed a trend to being more pronounced in the relapse cases and similar to the pattern in the peripheral blood. The clustering analysis identified a Treg subset with high expression of PD-1, consistent with suppressive function as being increased in abundance in the DLBCL samples. The differentiating CD8 T cell cluster more abundant in DLBCL also expressed inhibitory checkpoint molecules associated with limiting immune responses, with a recent profiling study associating a high proportion of checkpoint positive T cells with adverse outcome (154). We also found increased abundance of a DN cluster and a DP cluster of T cells which have both been associated with immunoregulatory functions and immune tolerance, but overall, these cells were present at low frequencies (393, 394).

In the functional work, we found that CD8 T cells in the DLBCL ME remained fully capable of cytokine production with similar frequencies of positive cells as the reactive tissues and increased cells positive for the cytotoxic markers. The increase in granzyme b and perforin positive CD8 T cells may reflect a generalised immune dysfunction or activated state, with an increase in activated CD8 T cells associated with autoimmune diseases (395). The CD4 T cell compartment did demonstrate some features consistent with exhaustion with reduced cytokine positive cells compared with the reactive controls. In contrast, we found hyperresponsiveness of CD4 T cells in the peripheral blood in terms of cytokine production following stimulation.

Finally, we established a broad immune panel of antibodies to characterise the lymphoma tissue ME in high dimension at the single cell level with imaging mass cytometry, and in collaboration with colleagues develop an analysis pipeline for the data. The results from this work are not yet available and will form part of the future work associated with this project, discussed further in the final chapter.

These data support a suppressive tissue ME in DLBCL with increased differentiation, an increased abundance of Tregs as well as expression of immune checkpoint molecules by the infiltrating cytotoxic T cells. Although the CD8 T cells remain functional in response to stimuli, the immunosuppressive ME and / or lymphoma immune evasion likely hinder their effectiveness. This would also provide a rationale for targeting the suppressive ME alongside immune effector approaches including CAR-T cell therapy to maximise efficacy.

Limitations of the study

Unlike the PBMC samples in our earlier study, the tissue processing and / or cryopreservation affected the lymph node SCS populations, with relatively few malignant cells and only rare myeloid cells identified following analysis. These populations are clearly observed by IHC and IMC and therefore are likely lost due to technical variation introduced by the sample processing and storage. In recent years radiological core biopsies have been increasingly employed for diagnostic sampling with the result that SCS are now infrequently available with only 5 DLBCL cases available, limited the conclusions we can draw from this work and precluding any outcome assessment. As with the previous studies, the lack of CMV status for all patients and demographics data for the control group were considered limiting factors.

Finally, although the IMC experimental work has completed, the analysis of this data remains ongoing and cannot be considered in the conclusions presented in this work. Many of the patients in the IMC study overlap with the PBMC and serum samples and therefore when this data is available, we will have a more complete immune cell and cytokine landscape for our cohort of DLBCL patients.

7. Discussion

DLBCL is a curable disease, but great heterogeneity is seen in disease biology, clinical behaviour and outcome following standard therapy. Although in the region of 60-65% of patients treated with RCHOP can expect long-term survival there remain several unmet needs including improved prognostic and predictive tools; a widely available, clinically useful novel classification system to capture targetable molecular heterogeneity; a risk adapted approach to facilitate precision medicine and limit unnecessary toxicity; improved frontline options for older patients and those where comorbidities prevent use of RCHOP; improved options for patients with relapsed / refractory disease; appropriate sequencing of novel agents during an individual patient's disease course. Many of these issues have been extensively explored in translational research studies and / or are currently being addressed in the context of clinical trials. Notably, the recent genomic landscape studies have offered new insights into genetic heterogeneity, with reproducible molecular subtypes of DLBCL identified in independent studies with recurrent targetable lesions (122-124). The knowledge generated from these studies is now being used to develop novel systems of classification, with the caveats that a significant minority of patients remain unclassified and, at least at present, most patients will not have their tumour profiled in such depth to allow subtype assignment (73, 74). Nevertheless, these studies represent a landmark in refining the molecular heterogeneity of DLBCL. In the clinical setting, the RCHOP-X model of adding a novel agent to standard therapy has as yet failed to demonstrate superiority for agents including bortezomib, ibrutinib and lenalidomide but with results for the addition of polatuzumab awaited (118, 243, 244, 280). Novel chemotherapy-free approaches are also being investigated in the frontline setting for older and unfit patients with studies ongoing (280). Again, there has been remarkable progress in developing several targeted therapies for DLBCL patients, particularly in the relapse setting, with CAR-T cells and polatuzumab combinations now approved for patients in the UK. In terms of prognostication, the clinical tools based around the international prognostic index (IPI) remain in use but fail to clearly identify the highest risk patients. The concept of using the peripheral blood monocyte and lymphocyte counts as prognostic markers has been reported in several studies and is consistent with the transcriptomic data highlighting the relevance of ME biology in DLBCL

(106, 191-193, 204). These findings are also complementary to the interests of our laboratory and were the starting point for the conceptualisation of this work.

7.1 Data summary and interpretation

We identify the absolute monocyte count (AMC) as being increased and the absolute lymphocyte count (ALC) decreased in DLBCL compared with controls, but no clear correlation between the two counts. We also confirm the prior finding that AMC high and ALC low associate with worse outcome, with the presence of both a poor prognostic factor at diagnosis that can further stratify the highest risk patients identified with the clinical prognostic tools. Given these findings, together with the fact that many of the basics of the human immune system in health and disease remain incompletely understood, we focused the bulk of our experimental work on characterisation of the peripheral blood immune compartment in DLBCL.

We identified an increased frequency of intermediate and non-classical monocytes in DLBCL and significant heterogeneity within the classical monocytes, with a continuum seen across populations and with expression of antigen markers. We also found consistently reduced expression of CD184 (CXCR4) on the myeloid populations in DLBCL. This could feasibly represent a mechanism explaining the relative monocytosis we observed given that inhibition CD184 with plerixafor is known to mobilise cells expressing this receptor from the bone marrow (BM) niche, with expression of CD184 associated with BM homing (396). The reduced expression of CD86 we observed on classical monocytes in DLBCL would support a role in limiting T cell immune responses due to its key role in costimulatory signalling. The clustering analysis identified three monocyte subsets in DLBCL associated with subsequent relapse. One of these had a phenotype consistent with that described for myeloid derived suppressor cells (MDSC), with low HLA-DR and positivity for CD163, which is associated with IL-10 polarised myeloid populations and IL-6 driven pro-tumoral function (194, 340, 353). Both cytokines were elevated in our DLBCL cohort. Another cluster expressed CD206, which has documented roles in both T cell suppression and tumour support (354). Both populations highly expressed CD192 (CCR2), which mediates monocyte recruitment,

another potential mechanism to explain the relative monocytosis we observed. However, both ligands for this receptor analysed in this study, CCL2 (MCP-1) and CCL13 (MCP-4), were only moderately elevated and not associated with outcome.

Interrogating the T cell landscape, we found a generalised reduction in frequency across several subsets in DLBCL, with significantly reduced CD4 effector memory 1 (EM1) and CD8 central memory (CM) T cells, with an increase in CD8 T effector memory RA (TEMRA) consistent with increased activation and differentiation. Further support for T cell activation was provided by the finding of an increased frequency of CD4 T cells with a T_H1 phenotype. There was a reduced frequency of CD3 T cells at diagnosis in patients who went on to fail RCHOP, compared to those who did not, consistent with the adverse nature of ALC low. These patients also had reduced frequency of the CD8 TEMRA, such that although this subset was increased in DLBCL compared to controls, within the DLBCL cohort the highest frequencies were seen in patients achieving sustained remission with RCHOP. The increase in CD8 TEMRA may reflect a response to chronic antigen stimulation and immune activation in DLBCL, with the highest risk patients less able to respond. However, it is also notable that increased CD8 TEMRA and decreased CD4 EM1 have been associated with aging (348). We also report increased CD8 EM3 with a T_C1 phenotype and PD-1 expression in DLBCL patients who went on to relapse. These cells represent a differentiated effector population, and while the PD-1 expression could represent activation, it also provides a base for inhibitory signalling. Perhaps most strikingly in the T cell compartment, we observed widespread reduced expression of CD27 and CD28 on T and NK cells compared to controls, and this finding was most pronounced in patients who went on to relapse. Given that CD27 and CD28 are critical to T cell immune responses, and without signals from these molecules T cells become refractory to further stimuli, this represents a potentially critical disruption to anti-tumour immune responses. Our data are therefore consistent with a reduced frequency of T cells in the peripheral ME being an adverse prognostic factor, with increased T cell differentiation and activation seen, together with bases of immune suppression from both the myeloid and T cell compartments, likely resulting in a dysfunctional immune response.

To establish the relationship between the immune cell landscape and the cytokine dysregulation reported in DLBCL, we assessed the levels of a number of cytokines and found that CD14 monocytes were the main cellular source of peripheral blood cytokines. In accordance with published studies, we found widespread cytokine elevations in DLBCL with significantly increased levels of IL-1RA, IL-6, IL-10, CCL3 and TNF at diagnosis in the patients who went on to relapse. IL-6 is known to be a potent growth factor for both normal and malignant B cells, with murine models of B-NHL demonstrating both a critical role in lymphomagenesis for IL-6 and its production by the lymphoma cells (226, 376, 397). We confirm the adverse prognostic nature of elevated IL-6 in DLBCL and establish a non-cell autonomous role for monocyte derived IL-6 in DLBCL. Interestingly, unpublished data from our laboratory in a mouse model of aggressive MYC driven lymphoma demonstrated that high levels of IL-6 were associated with disease progression and that inhibition of the CSF-1 receptor (CSF-1R / M-CSF receptor) resulted in reduced lymphoma burden and reduced IL-6 levels. In this model, CSF-1R inhibition also resulted in reduced monocytes and macrophages, with no effect of normal B and T cells. No direct effect of CSF-1R inhibition was observed on lymphoma cells, suggesting the efficacy to be mediated through myeloid cell depletion. Consistent with these findings, we report increased IL-6 in DLBCL, IL-6 as an adverse prognostic factor as well as increased production of IL-6 by unstimulated DLBCL monocytes. We also identified elevated CCL3 levels in DLBCL, associated them with poor outcome and established monocytes as the main peripheral cellular source. CCL3 correlated negatively with the ALC consistent with its known role in ME dysfunction (384). We also observed a reduced ability to upregulate cytokine production in response to stimulation in DLBCL monocytes, suggestive of deregulated cytokine production but a limited capacity to respond to immune challenges. In the lymphocyte compartment, we report NK cell activation in DLBCL and find no evidence of peripheral T cell exhaustion, with robust cytokine responses to stimuli. We did observe hypersensitivity of the CD4 T cells to stimulation, with increased IL-2 and TNF responses, consistent with retained cytokine producing capacity but in the context of a dysfunctional immune response.

In addition to the peripheral microenvironment, we also characterised the lymph node T cell compartment finding a skew towards reduced CD4 T cells and increased CD8 when compared to reactive tissues, consistent with a recently published study (398). Similar to our

findings in the peripheral blood T cell compartment, we also identified evidence of increased differentiation, with reduced naïve CD4 and increased effector memory CD8 subsets. The clustering analysis discovered increased abundance of PD-1 positive regulatory T cells and immune checkpoint expressing CD8 T cells in DLBCL. The functional work demonstrated no evidence of CD8 exhaustion in terms of cytokine production, with increased frequencies of cytotoxic marker positive cells. There were some features of exhaustion in the CD4 T cells, with attenuated cytokine responses, in contrast to the peripheral blood CD4 T cell response to activation. Although we were only able to analyse a small number of cases due to the rarity of single cell suspension (SCS) material, our data are suggestive of an activated and differentiated T cell ME, with increased regulatory T cells and checkpoint marker expression. Taken together and considered with the frequent immune evasion strategies employed by the lymphoma cell, such as loss of MHC molecule expression, these findings support a suppressive microenvironment, with increased cytotoxic CD8 T cells with functional potential, which are unable to recognise and eradicate the lymphoma cells.

7.2 Limitations of the study

Although our findings reveal key insights into the peripheral blood immune landscape in DLBCL, they must be interpreted in the light of the limitations of this study. We profiled the immune cells in blood samples from 42 DLBCL patients with the 'myeloid' panel and 32 with the 'T cell' panel with mass cytometry (MC), a high parameter technology only applied to a very limited number of DLBCL cases in the published literature (335). However, as we have seen DLBCL is a disease of biological heterogeneity and as such, requires large cohorts for meaningful conclusions to be drawn, especially when data are viewed in the context of outcome, cell of origin (COO) subgroups or genomic aberrations. The predominant focus of this work was the peripheral blood immune cell composition in DLBCL and thus the available samples were prioritised for these experiments. This did result in only a limited number of samples having enough cells available for the cytokine staining experiments. While we observed significant differences between DLBCL and healthy donors, the limited sample size of these experiments precluded assessment of differences in cytokine producing monocytes

between outcome groups. In contrast to diagnostic biopsy tissue, peripheral blood represents a relatively easy sample to obtain and usually yields sufficient viable cells for meaningful analysis, therefore larger studies in the future are entirely feasible for both the immunophenotyping and functional work.

All of the samples used for this work were cryopreserved and the blood samples stored as peripheral blood mononuclear cells (PBMCs), potentially introducing technical variation with implications for discovery of biological variation. In terms of cryopreservation, our study design would not have supported using freshly stained cells from DLBCL patients and would have resulted in many more experimental batches, another potential source of technical variation. To validate our method, we stained a healthy control PBMC sample immediately following isolation, having never been cryopreserved and again repeatedly over the course of the study with comparable results. While other groups have reported effects of cryopreservation on immune cell populations, we did not observe this and could identify expected cell subsets with consistency between the fresh and frozen samples (399). This healthy donor was also stained and acquired with each experiment and used for quality control in assessing potential batch effect. In order to analyse sufficient numbers of samples, future studies would almost certainly face the requirement for cryopreservation and batch acquisition.

The SCS samples we analysed in this study did seem to suffer from technical variation with the main viable cell being CD3 T cells, however examination of corresponding formalin fixed paraffin embedded (FFPE) tissue blocks revealed the presence of abundant malignant B cell and the presence of myeloid cells. Other groups have reported similar issues with tissue suspensions and identified the specific method and enzymes used for tissue digestion as key factors in sample preparation (400). SCS also represent a rare tissue due to the nature of their acquisition and preparation. However, the advent of multiplex tissue analysis applicable to both FFPE and fresh frozen tissues has somewhat circumvented this issue and we are currently addressing this with in depth characterisation of the lymphoma tissue ME in our ongoing imaging mass cytometry (IMC) study.

Although demographic information was not available for the control groups used in this study, these samples still provided a useful baseline against which to assess the immune and cytokine landscape in DLBCL. The PBMCs were isolated from leucocyte cones from healthy blood donors and the serum samples from staff members, almost certainly representing much younger age groups than our patient cohort. In addition to the demographics of our controls, cytomegalovirus (CMV) status was not available for our control or patient cohorts. While this information was not deemed essential to the study, CMV is known to influence an individual's immune cell composition and response to immunological challenges (333).

7.3 Future work

With direct reference to our study rationale, there remains much we do not known about the basics of the immune system in DLBCL and how and why this differs from healthy individuals. We have used MC to broadly capture the immune system heterogeneity in health and DLBCL, increasing our understanding of the landscape and analysing many millions of cells, but in a relatively small cohort overall. Therefore, to build on the work we have presented in this thesis, we suggest immune monitoring approaches as critical to improving our knowledge of immune system variation in DLBCL. This would likely be best achieved as a sub-study associated with a large-scale clinical trial in which peripheral blood samples could be collected from large numbers of patients and at time points throughout frontline therapy and at progression / relapse in those not cured by initial therapy. During the course of the current study, a lyophilised antibody master-mix to facilitate delineation of 37 immune populations with automated analysis software for rapid preliminary analysis, has become commercially available (401). Having run preliminary samples with this assay, we suggest this would be an ideal starting point for any such large-scale study, with a number of channels available for addition targets to be added. For comparison the recent genomic studies have captured hundreds to thousands of cases. Given the diversity of immune cells in the peripheral blood it is likely that similar numbers of cases will need to be studied to fully understand this compartment.

In regard to some of the specific findings of this work, IL-6 appears to be critical to lymphoma biology, with our study identifying peripheral blood monocytes as a cellular source. Other work has indicated the lymphoma cell as a source of IL-6, with the dual production by the tumour and the ME perhaps highlighting its importance in lymphoma survival. Other cells, such as macrophages, in the tissue ME may also be important cellular sources and this remains to be defined in future work. It would also be of interest to monitor IL-6 levels to assess their potential as a biomarker of disease activity, the IL-6 response to immune targeting therapies such as disruption of the CD47 pathway and the activity of IL-6 inhibition in preclinical disease models. The other cytokine identified to be elevated and over produced by monocytes in DLBCL was CCL3, with one report suggesting that BCR activation in ABC DLBCL results in lymphoma secretion of this cytokine (402). The direct impact of CCL3 on DLBCL cells and other cellular sources of origin remain to be defined, however as for IL-6, the existing data and our findings support a key role in lymphoma biology which warrants further study. The findings of decreased expression of CD184 (CXCR4) on all myeloid populations and the global reductions in CD27 and CD28 expression on T cell subsets also warrant confirmation and further exploration as potential biomarkers of disease, with CD27 and CD28 downregulation more prominent in cases that subsequently relapsed.

Finally, although this work focused on peripheral blood immune cells, there are abundant tumour infiltrating immune cells in DLBCL. We have developed a protocol and analysis pipeline for IMC to be applied to lymphoma tissues with the primary aim of characterising the immune cell populations and phenotypes in high dimension. The experimental work and data acquisition for this is now largely complete with the analysis still ongoing. This work will facilitate confirmation of our findings in the T cell compartment of SCS tissues and allow detailed study of the myeloid compartment together with the spatial context of the immune cell and tumour populations. We will also use this data to correlate paired information from the overlapping cases presented in this work.

7.4 Concluding statement

We have presented confirmation of the prognostic nature of AMC and ALC in DLBCL, together with a detailed immunophenotypic characterisation of these cells and their subset frequencies. We identify potential mechanisms to account for the relative monocytosis observed in DLBCL, including increased IL-6 and reduced CD184 (CXCR4) expression. We find a number of cytokines to be associated with relapsed DLBCL and identify CD14 monocytes as key cellular sources of two of these, IL-6 and MIP-1α. We report several potential peripheral blood biomarkers which warrant further study, including the above cytokines, CD184 (CXCR4) expression on myeloid populations and CD27 and CD28 expression on T cells. In the lymph node T cell analysis, we find limited evidence of T cell exhaustion, with only the CD4 T cell compartment demonstrating reduced cytokine producing capability. However, we identify increased T cell differentiation, similar to the peripheral blood, and multiple potential bases of immune suppression, including increased regulatory T cell with PD-1 expression and cytotoxic T cell with immune checkpoint expression. We have already established a complementary approach to study the tissue immune composition with IMC which will facilitate unprecedented characterisation of the DLBCL immune microenvironment.

8. Meeting Abstracts

Truelove E, Taylor J, Seymour F, Clear AJ, Calaminici M, Gribben JG. **Disease and outcome associated immune signatures at diagnosis in diffuse large B cell lymphoma (DLBCL).** EHA 2021 submitted.

Truelove E, Taylor J, Clear AJ, Calaminici M, Gribben JG. **Immune system deregulation predicts outcome in diffuse large B cell lymphoma (DLBCL).** Blood. 2020; 136(suppl. 1): 33-34

Taylor J, Clear AJ, **Truelove E**, Calaminici M, Gribben JG. **Beyond exhaustion: The PDL1-PD1 axis shapes the classical Hodgkin lymphoma microenvironment.** Blood. 2019; 134(suppl. 1): 658

Truelove E, Seymour F, Taylor J, Clear AJ, Calaminici M, Gribben JG. **The immune microenvironment in diffuse large B cell lymphoma is characterised by an immunosuppressive shift in T cell subsets.** Blood. 2019; 134(suppl. 1): 5240

Truelove E, Seymour F, Matthews J, Gribben JG. **Deep phenotypic analysis reveals a monocyte subpopulation predictive of relapse in diffuse large B cell lymphoma.** Blood. 2018; 132(suppl. 1): 2863

9. References

1. Swerdlow SH, Campo E, Pileri SA, Harris NL, Stein H, Siebert R, et al. The 2016 revision of the World Health Organization classification of lymphoid neoplasms. Blood. 2016;127(20):2375-90.
2. Lawrence MS, Stojanov P, Polak P, Kryukov GV, Cibulskis K, Sivachenko A, et al. Mutational heterogeneity in cancer and the search for new cancer-associated genes. Nature. 2013;499(7457):214-8.
3. Shaffer AL, 3rd, Young RM, Staudt LM. Pathogenesis of human B cell lymphomas. Annu Rev Immunol. 2012;30:565-610.
4. Quail DF, Joyce JA. Microenvironmental regulation of tumor progression and metastasis. Nature medicine. 2013;19(11):1423-37.
5. Burger JA, Wiestner A. Targeting B cell receptor signalling in cancer: preclinical and clinical advances. Nat Rev Cancer. 2018;18(3):148-67.
6. Melchers F. Checkpoints that control B cell development. J Clin Invest. 2015;125(6):2203-10.
7. LeBien TW, Tedder TF. B lymphocytes: how they develop and function. Blood. 2008;112(5):1570-80.
8. Brack C, Hirama M, Lenhard-Schuller R, Tonegawa S. A complete immunoglobulin gene is created by somatic recombination. Cell. 1978;15(1):1-14.
9. Tonegawa S. Somatic generation of antibody diversity. Nature. 1983;302(5909):575-81.
10. Chi X, Li Y, Qiu X. V(D)J recombination, somatic hypermutation and class switch recombination of immunoglobulins: mechanism and regulation. Immunology. 2020;160(3):233-47.
11. Schatz DG, Ji Y. Recombination centres and the orchestration of V(D)J recombination. Nat Rev Immunol. 2011;11(4):251-63.
12. Mills KD, Ferguson DO, Alt FW. The role of DNA breaks in genomic instability and tumorigenesis. Immunol Rev. 2003;194:77-95.
13. van Gent DC, Ramsden DA, Gellert M. The RAG1 and RAG2 proteins establish the 12/23 rule in V(D)J recombination. Cell. 1996;85(1):107-13.
14. Lewis SM. The mechanism of V(D)J joining: lessons from molecular, immunological, and comparative analyses. Adv Immunol. 1994;56:27-150.
15. Cobb RM, Oestreich KJ, Osipovich OA, Oltz EM. Accessibility control of V(D)J recombination. Adv Immunol. 2006;91:45-109.
16. Cook GP, Tomlinson IM. The human immunoglobulin VH repertoire. Immunol Today. 1995;16(5):237-42.
17. Rajewsky K. Clonal selection and learning in the antibody system. Nature. 1996;381(6585):751-8.
18. Alt FW, Rathbun G, Oltz E, Taccioli G, Shinkai Y. Function and control of recombination-activating gene activity. Ann N Y Acad Sci. 1992;651:277-94.
19. Brauninger A, Goossens T, Rajewsky K, Kuppers R. Regulation of immunoglobulin light chain gene rearrangements during early B cell development in the human. Eur J Immunol. 2001;31(12):3631-7.
20. Pieper K, Grimbacher B, Eibel H. B-cell biology and development. J Allergy Clin Immunol. 2013;131(4):959-71.

21. Nutt SL, Hodgkin PD, Tarlinton DM, Corcoran LM. The generation of antibody-secreting plasma cells. Nat Rev Immunol. 2015;15(3):160-71.
22. Victora GD, Nussenzweig MC. Germinal centers. Annu Rev Immunol. 2012;30:429-57.
23. Mesin L, Ersching J, Victora GD. Germinal Center B Cell Dynamics. Immunity. 2016;45(3):471-82.
24. Kuppers R. Mechanisms of B-cell lymphoma pathogenesis. Nat Rev Cancer. 2005;5(4):251-62.
25. Basso K, Dalla-Favera R. Germinal centres and B cell lymphomagenesis. Nat Rev Immunol. 2015;15(3):172-84.
26. Stavnezer J, Guikema JE, Schrader CE. Mechanism and regulation of class switch recombination. Annu Rev Immunol. 2008;26:261-92.
27. Roco JA, Mesin L, Binder SC, Nefzger C, Gonzalez-Figueroa P, Canete PF, et al. Class-Switch Recombination Occurs Infrequently in Germinal Centers. Immunity. 2019;51(2):337-50 e7.
28. Pasqualucci L, Bhagat G, Jankovic M, Compagno M, Smith P, Muramatsu M, et al. AID is required for germinal center-derived lymphomagenesis. Nat Genet. 2008;40(1):108-12.
29. Di Noia JM, Neuberger MS. Molecular mechanisms of antibody somatic hypermutation. Annu Rev Biochem. 2007;76:1-22.
30. Boboila C, Yan C, Wesemann DR, Jankovic M, Wang JH, Manis J, et al. Alternative end-joining catalyzes class switch recombination in the absence of both Ku70 and DNA ligase 4. J Exp Med. 2010;207(2):417-27.
31. MacLennan IC. Germinal centers. Annu Rev Immunol. 1994;12:117-39.
32. De Silva NS, Klein U. Dynamics of B cells in germinal centres. Nat Rev Immunol. 2015;15(3):137-48.
33. Victora GD, Schwickert TA, Fooksman DR, Kamphorst AO, Meyer-Hermann M, Dustin ML, et al. Germinal center dynamics revealed by multiphoton microscopy with a photoactivatable fluorescent reporter. Cell. 2010;143(4):592-605.
34. Seifert M, Scholtysik R, Kuppers R. Origin and pathogenesis of B cell lymphomas. Methods Mol Biol. 2013;971:1-25.
35. Peters A, Storb U. Somatic hypermutation of immunoglobulin genes is linked to transcription initiation. Immunity. 1996;4(1):57-65.
36. Muramatsu M, Kinoshita K, Fagarasan S, Yamada S, Shinkai Y, Honjo T. Class switch recombination and hypermutation require activation-induced cytidine deaminase (AID), a potential RNA editing enzyme. Cell. 2000;102(5):553-63.
37. Pasqualucci L, Dalla-Favera R. Genetics of diffuse large B-cell lymphoma. Blood. 2018;131(21):2307-19.
38. Pilzecker B, Jacobs H. Mutating for Good: DNA Damage Responses During Somatic Hypermutation. Front Immunol. 2019;10:438.
39. Rada C, Di Noia JM, Neuberger MS. Mismatch recognition and uracil excision provide complementary paths to both Ig switching and the A/T-focused phase of somatic mutation. Mol Cell. 2004;16(2):163-71.
40. Di Noia J, Neuberger MS. Altering the pathway of immunoglobulin hypermutation by inhibiting uracil-DNA glycosylase. Nature. 2002;419(6902):43-8.
41. Jansen JG, Langerak P, Tsaalbi-Shtylik A, van den Berk P, Jacobs H, de Wind N. Strand-biased defect in C/G transversions in hypermutating immunoglobulin genes in Rev1-deficient mice. J Exp Med. 2006;203(2):319-23.

42. Zeng X, Winter DB, Kasmer C, Kraemer KH, Lehmann AR, Gearhart PJ. DNA polymerase eta is an A-T mutator in somatic hypermutation of immunoglobulin variable genes. Nat Immunol. 2001;2(6):537-41.
43. Pasqualucci L, Neumeister P, Goossens T, Nanjangud G, Chaganti RS, Kuppers R, et al. Hypermutation of multiple proto-oncogenes in B-cell diffuse large-cell lymphomas. Nature. 2001;412(6844):341-6.
44. Calado DP, Sasaki Y, Godinho SA, Pellerin A, Kochert K, Sleckman BP, et al. The cell-cycle regulator c-Myc is essential for the formation and maintenance of germinal centers. Nat Immunol. 2012;13(11):1092-100.
45. Dominguez-Sola D, Victora GD, Ying CY, Phan RT, Saito M, Nussenzweig MC, et al. The proto-oncogene MYC is required for selection in the germinal center and cyclic reentry. Nat Immunol. 2012;13(11):1083-91.
46. Ying CY, Dominguez-Sola D, Fabi M, Lorenz IC, Hussein S, Bansal M, et al. MEF2B mutations lead to deregulated expression of the oncogene BCL6 in diffuse large B cell lymphoma. Nat Immunol. 2013;14(10):1084-92.
47. Pasqualucci L, Migliazza A, Basso K, Houldsworth J, Chaganti RS, Dalla-Favera R. Mutations of the BCL6 proto-oncogene disrupt its negative autoregulation in diffuse large B-cell lymphoma. Blood. 2003;101(8):2914-23.
48. Basso K, Schneider C, Shen Q, Holmes AB, Setty M, Leslie C, et al. BCL6 positively regulates AID and germinal center gene expression via repression of miR-155. J Exp Med. 2012;209(13):2455-65.
49. Basso K, Saito M, Sumazin P, Margolin AA, Wang K, Lim WK, et al. Integrated biochemical and computational approach identifies BCL6 direct target genes controlling multiple pathways in normal germinal center B cells. Blood. 2010;115(5):975-84.
50. Ci W, Polo JM, Cerchietti L, Shaknovich R, Wang L, Yang SN, et al. The BCL6 transcriptional program features repression of multiple oncogenes in primary B cells and is deregulated in DLBCL. Blood. 2009;113(22):5536-48.
51. Cattoretti G, Pasqualucci L, Ballon G, Tam W, Nandula SV, Shen Q, et al. Deregulated BCL6 expression recapitulates the pathogenesis of human diffuse large B cell lymphomas in mice. Cancer Cell. 2005;7(5):445-55.
52. Dent AL, Shaffer AL, Yu X, Allman D, Staudt LM. Control of inflammation, cytokine expression, and germinal center formation by BCL-6. Science. 1997;276(5312):589-92.
53. Cao R, Wang L, Wang H, Xia L, Erdjument-Bromage H, Tempst P, et al. Role of histone H3 lysine 27 methylation in Polycomb-group silencing. Science. 2002;298(5595):1039-43.
54. Czermin B, Melfi R, McCabe D, Seitz V, Imhof A, Pirrotta V. Drosophila enhancer of Zeste/ESC complexes have a histone H3 methyltransferase activity that marks chromosomal Polycomb sites. Cell. 2002;111(2):185-96.
55. Beguelin W, Popovic R, Teater M, Jiang Y, Bunting KL, Rosen M, et al. EZH2 is required for germinal center formation and somatic EZH2 mutations promote lymphoid transformation. Cancer Cell. 2013;23(5):677-92.
56. Caganova M, Carrisi C, Varano G, Mainoldi F, Zanardi F, Germain PL, et al. Germinal center dysregulation by histone methyltransferase EZH2 promotes lymphomagenesis. J Clin Invest. 2013;123(12):5009-22.
57. Willis SN, Good-Jacobson KL, Curtis J, Light A, Tellier J, Shi W, et al. Transcription factor IRF4 regulates germinal center cell formation through a B cell-intrinsic mechanism. J Immunol. 2014;192(7):3200-6.

58. Basso K, Klein U, Niu H, Stolovitzky GA, Tu Y, Califano A, et al. Tracking CD40 signaling during germinal center development. Blood. 2004;104(13):4088-96.
59. Yang H, Green MR. Epigenetic Programing of B-Cell Lymphoma by BCL6 and Its Genetic Deregulation. Front Cell Dev Biol. 2019;7:272.
60. Saito M, Gao J, Basso K, Kitagawa Y, Smith PM, Bhagat G, et al. A signaling pathway mediating downregulation of BCL6 in germinal center B cells is blocked by BCL6 gene alterations in B cell lymphoma. Cancer Cell. 2007;12(3):280-92.
61. Cardenas MG, Oswald E, Yu W, Xue F, MacKerell AD, Jr., Melnick AM. The Expanding Role of the BCL6 Oncoprotein as a Cancer Therapeutic Target. Clinical cancer research : an official journal of the American Association for Cancer Research. 2017;23(4):885-93.
62. Sciammas R, Shaffer AL, Schatz JH, Zhao H, Staudt LM, Singh H. Graded expression of interferon regulatory factor-4 coordinates isotype switching with plasma cell differentiation. Immunity. 2006;25(2):225-36.
63. Akkaya M, Kwak K, Pierce SK. B cell memory: building two walls of protection against pathogens. Nat Rev Immunol. 2020;20(4):229-38.
64. Reimold AM, Iwakoshi NN, Manis J, Vallabhajosyula P, Szomolanyi-Tsuda E, Gravallese EM, et al. Plasma cell differentiation requires the transcription factor XBP-1. Nature. 2001;412(6844):300-7.
65. Cerhan JR, Kricker A, Paltiel O, Flowers CR, Wang SS, Monnereau A, et al. Medical history, lifestyle, family history, and occupational risk factors for diffuse large B-cell lymphoma: the InterLymph Non-Hodgkin Lymphoma Subtypes Project. J Natl Cancer Inst Monogr. 2014;2014(48):15-25.
66. Cerhan JR, Slager SL. Familial predisposition and genetic risk factors for lymphoma. Blood. 2015;126(20):2265-73.
67. Cerhan JR, Berndt SI, Vijai J, Ghesquieres H, McKay J, Wang SS, et al. Genome-wide association study identifies multiple susceptibility loci for diffuse large B cell lymphoma. Nat Genet. 2014;46(11):1233-8.
68. Feugier P, Van Hoof A, Sebban C, Solal-Celigny P, Bouabdallah R, Ferme C, et al. Long-term results of the R-CHOP study in the treatment of elderly patients with diffuse large B-cell lymphoma: a study by the Groupe d'Etude des Lymphomes de l'Adulte. J Clin Oncol. 2005;23(18):4117-26.
69. Chaganti S, Illidge T, Barrington S, McKay P, Linton K, Cwynarski K, et al. Guidelines for the management of diffuse large B-cell lymphoma. Br J Haematol. 2016;174(1):43-56.
70. Alizadeh AA, Eisen MB, Davis RE, Ma C, Lossos IS, Rosenwald A, et al. Distinct types of diffuse large B-cell lymphoma identified by gene expression profiling. Nature. 2000;403(6769):503-11.
71. Rosenwald A, Wright G, Chan WC, Connors JM, Campo E, Fisher RI, et al. The use of molecular profiling to predict survival after chemotherapy for diffuse large-B-cell lymphoma. N Engl J Med. 2002;346(25):1937-47.
72. Kuppers R, Klein U, Hansmann ML, Rajewsky K. Cellular origin of human B-cell lymphomas. N Engl J Med. 1999;341(20):1520-9.
73. Ennishi D, Hsi ED, Steidl C, Scott DW. Toward a New Molecular Taxonomy of Diffuse Large B-cell Lymphoma. Cancer Discov. 2020;10(9):1267-81.
74. Wright GW, Huang DW, Phelan JD, Coulibaly ZA, Roulland S, Young RM, et al. A Probabilistic Classification Tool for Genetic Subtypes of Diffuse Large B Cell Lymphoma with Therapeutic Implications. Cancer Cell. 2020;37(4):551-68 e14.

75. Tilly H, Gomes da Silva M, Vitolo U, Jack A, Meignan M, Lopez-Guillermo A, et al. Diffuse large B-cell lymphoma (DLBCL): ESMO Clinical Practice Guidelines for diagnosis, treatment and follow-up. Ann Oncol. 2015;26 Suppl 5:v116-25.
76. Caimi PF, Hill BT, Hsi ED, Smith MR. Clinical approach to diffuse large B cell lymphoma. Blood Rev. 2016;30(6):477-91.
77. Colomo L, Lopez-Guillermo A, Perales M, Rives S, Martinez A, Bosch F, et al. Clinical impact of the differentiation profile assessed by immunophenotyping in patients with diffuse large B-cell lymphoma. Blood. 2003;101(1):78-84.
78. Gascoyne RD, Adomat SA, Krajewski S, Krajewska M, Horsman DE, Tolcher AW, et al. Prognostic significance of Bcl-2 protein expression and Bcl-2 gene rearrangement in diffuse aggressive non-Hodgkin's lymphoma. Blood. 1997;90(1):244-51.
79. Skinnider BF, Horsman DE, Dupuis B, Gascoyne RD. Bcl-6 and Bcl-2 protein expression in diffuse large B-cell lymphoma and follicular lymphoma: correlation with 3q27 and 18q21 chromosomal abnormalities. Hum Pathol. 1999;30(7):803-8.
80. de Leval L, Ferry JA, Falini B, Shipp M, Harris NL. Expression of bcl-6 and CD10 in primary mediastinal large B-cell lymphoma: evidence for derivation from germinal center B cells? Am J Surg Pathol. 2001;25(10):1277-82.
81. Savage KJ, Monti S, Kutok JL, Cattoretti G, Neuberg D, De Leval L, et al. The molecular signature of mediastinal large B-cell lymphoma differs from that of other diffuse large B-cell lymphomas and shares features with classical Hodgkin lymphoma. Blood. 2003;102(12):3871-9.
82. Shipp MA, Ross KN, Tamayo P, Weng AP, Kutok JL, Aguiar RC, et al. Diffuse large B-cell lymphoma outcome prediction by gene-expression profiling and supervised machine learning. Nature medicine. 2002;8(1):68-74.
83. Young RM, Shaffer AL, 3rd, Phelan JD, Staudt LM. B-cell receptor signaling in diffuse large B-cell lymphoma. Semin Hematol. 2015;52(2):77-85.
84. Hans CP, Weisenburger DD, Greiner TC, Gascoyne RD, Delabie J, Ott G, et al. Confirmation of the molecular classification of diffuse large B-cell lymphoma by immunohistochemistry using a tissue microarray. Blood. 2004;103(1):275-82.
85. Coutinho R, Clear AJ, Owen A, Wilson A, Matthews J, Lee A, et al. Poor concordance among nine immunohistochemistry classifiers of cell-of-origin for diffuse large B-cell lymphoma: implications for therapeutic strategies. Clinical cancer research : an official journal of the American Association for Cancer Research. 2013;19(24):6686-95.
86. de Jong D, Rosenwald A, Chhanabhai M, Gaulard P, Klapper W, Lee A, et al. Immunohistochemical prognostic markers in diffuse large B-cell lymphoma: validation of tissue microarray as a prerequisite for broad clinical applications--a study from the Lunenburg Lymphoma Biomarker Consortium. J Clin Oncol. 2007;25(7):805-12.
87. Aukema SM, Siebert R, Schuuring E, van Imhoff GW, Kluin-Nelemans HC, Boerma EJ, et al. Double-hit B-cell lymphomas. Blood. 2011;117(8):2319-31.
88. Johnson NA, Slack GW, Savage KJ, Connors JM, Ben-Neriah S, Rogic S, et al. Concurrent expression of MYC and BCL2 in diffuse large B-cell lymphoma treated with rituximab plus cyclophosphamide, doxorubicin, vincristine, and prednisone. J Clin Oncol. 2012;30(28):3452-9.
89. Hu S, Xu-Monette ZY, Tzankov A, Green T, Wu L, Balasubramanyam A, et al. MYC/BCL2 protein coexpression contributes to the inferior survival of activated B-cell subtype of diffuse large B-cell lymphoma and demonstrates high-risk gene expression

signatures: a report from The International DLBCL Rituximab-CHOP Consortium Program. Blood. 2013;121(20):4021-31; quiz 250.
90. Friedberg JW. How I treat double-hit lymphoma. Blood. 2017;130(5):590-6.
91. Rosenwald A, Bens S, Advani R, Barrans S, Copie-Bergman C, Elsensohn MH, et al. Prognostic Significance of MYC Rearrangement and Translocation Partner in Diffuse Large B-Cell Lymphoma: A Study by the Lunenburg Lymphoma Biomarker Consortium. J Clin Oncol. 2019;37(35):3359-68.
92. Cheson BD, Fisher RI, Barrington SF, Cavalli F, Schwartz LH, Zucca E, et al. Recommendations for initial evaluation, staging, and response assessment of Hodgkin and non-Hodgkin lymphoma: the Lugano classification. J Clin Oncol. 2014;32(27):3059-68.
93. Khan AB, Barrington SF, Mikhaeel NG, Hunt AA, Cameron L, Morris T, et al. PET-CT staging of DLBCL accurately identifies and provides new insight into the clinical significance of bone marrow involvement. Blood. 2013;122(1):61-7.
94. International Non-Hodgkin's Lymphoma Prognostic Factors P. A predictive model for aggressive non-Hodgkin's lymphoma. N Engl J Med. 1993;329(14):987-94.
95. Sehn LH, Berry B, Chhanabhai M, Fitzgerald C, Gill K, Hoskins P, et al. The revised International Prognostic Index (R-IPI) is a better predictor of outcome than the standard IPI for patients with diffuse large B-cell lymphoma treated with R-CHOP. Blood. 2007;109(5):1857-61.
96. Zhou Z, Sehn LH, Rademaker AW, Gordon LI, Lacasce AS, Crosby-Thompson A, et al. An enhanced International Prognostic Index (NCCN-IPI) for patients with diffuse large B-cell lymphoma treated in the rituximab era. Blood. 2014;123(6):837-42.
97. Ruppert AS, Dixon JG, Salles G, Wall A, Cunningham D, Poeschel V, et al. International prognostic indices in diffuse large B-cell lymphoma: a comparison of IPI, R-IPI, and NCCN-IPI. Blood. 2020;135(23):2041-8.
98. Gleeson M, Counsell N, Cunningham D, Lawrie A, Clifton-Hadley L, Hawkes E, et al. Prognostic indices in diffuse large B-cell lymphoma in the rituximab era: an analysis of the UK National Cancer Research Institute R-CHOP 14 versus 21 phase 3 trial. Br J Haematol. 2020.
99. Kurtz DM. Prognostication with circulating tumor DNA: is it ready for prime time? Hematology Am Soc Hematol Educ Program. 2019;2019(1):47-52.
100. Kurtz DM, Esfahani MS, Scherer F, Soo J, Jin MC, Liu CL, et al. Dynamic Risk Profiling Using Serial Tumor Biomarkers for Personalized Outcome Prediction. Cell. 2019;178(3):699-713 e19.
101. Kurtz DM, Scherer F, Jin MC, Soo J, Craig AFM, Esfahani MS, et al. Circulating Tumor DNA Measurements As Early Outcome Predictors in Diffuse Large B-Cell Lymphoma. J Clin Oncol. 2018;36(28):2845-53.
102. Scherer F, Kurtz DM, Newman AM, Stehr H, Craig AF, Esfahani MS, et al. Distinct biological subtypes and patterns of genome evolution in lymphoma revealed by circulating tumor DNA. Sci Transl Med. 2016;8(364):364ra155.
103. Kuppers R, Dalla-Favera R. Mechanisms of chromosomal translocations in B cell lymphomas. Oncogene. 2001;20(40):5580-94.
104. Victora GD, Dominguez-Sola D, Holmes AB, Deroubaix S, Dalla-Favera R, Nussenzweig MC. Identification of human germinal center light and dark zone cells and their relationship to human B-cell lymphomas. Blood. 2012;120(11):2240-8.
105. Scott DW, Mottok A, Ennishi D, Wright GW, Farinha P, Ben-Neriah S, et al. Prognostic Significance of Diffuse Large B-Cell Lymphoma Cell of Origin Determined by Digital Gene

Expression in Formalin-Fixed Paraffin-Embedded Tissue Biopsies. J Clin Oncol. 2015;33(26):2848-56.
106. Lenz G, Wright G, Dave SS, Xiao W, Powell J, Zhao H, et al. Stromal gene signatures in large-B-cell lymphomas. N Engl J Med. 2008;359(22):2313-23.
107. Scott DW, King RL, Staiger AM, Ben-Neriah S, Jiang A, Horn H, et al. High-grade B-cell lymphoma with MYC and BCL2 and/or BCL6 rearrangements with diffuse large B-cell lymphoma morphology. Blood. 2018;131(18):2060-4.
108. Ennishi D, Mottok A, Ben-Neriah S, Shulha HP, Farinha P, Chan FC, et al. Genetic profiling of MYC and BCL2 in diffuse large B-cell lymphoma determines cell-of-origin-specific clinical impact. Blood. 2017;129(20):2760-70.
109. Iqbal J, Meyer PN, Smith LM, Johnson NA, Vose JM, Greiner TC, et al. BCL2 predicts survival in germinal center B-cell-like diffuse large B-cell lymphoma treated with CHOP-like therapy and rituximab. Clinical cancer research : an official journal of the American Association for Cancer Research. 2011;17(24):7785-95.
110. Pasqualucci L, Dominguez-Sola D, Chiarenza A, Fabbri G, Grunn A, Trifonov V, et al. Inactivating mutations of acetyltransferase genes in B-cell lymphoma. Nature. 2011;471(7337):189-95.
111. Morin RD, Johnson NA, Severson TM, Mungall AJ, An J, Goya R, et al. Somatic mutations altering EZH2 (Tyr641) in follicular and diffuse large B-cell lymphomas of germinal-center origin. Nat Genet. 2010;42(2):181-5.
112. Reddy A, Zhang J, Davis NS, Moffitt AB, Love CL, Waldrop A, et al. Genetic and Functional Drivers of Diffuse Large B Cell Lymphoma. Cell. 2017;171(2):481-94 e15.
113. Muppidi JR, Schmitz R, Green JA, Xiao W, Larsen AB, Braun SE, et al. Loss of signalling via Galpha13 in germinal centre B-cell-derived lymphoma. Nature. 2014;516(7530):254-8.
114. Lenz G, Wright GW, Emre NC, Kohlhammer H, Dave SS, Davis RE, et al. Molecular subtypes of diffuse large B-cell lymphoma arise by distinct genetic pathways. Proc Natl Acad Sci U S A. 2008;105(36):13520-5.
115. Calado DP, Zhang B, Srinivasan L, Sasaki Y, Seagal J, Unitt C, et al. Constitutive canonical NF-kappaB activation cooperates with disruption of BLIMP1 in the pathogenesis of activated B cell-like diffuse large cell lymphoma. Cancer Cell. 2010;18(6):580-9.
116. Scott DW, Wright GW, Williams PM, Lih CJ, Walsh W, Jaffe ES, et al. Determining cell-of-origin subtypes of diffuse large B-cell lymphoma using gene expression in formalin-fixed paraffin-embedded tissue. Blood. 2014;123(8):1214-7.
117. Care MA, Barrans S, Worrillow L, Jack A, Westhead DR, Tooze RM. A microarray platform-independent classification tool for cell of origin class allows comparative analysis of gene expression in diffuse large B-cell lymphoma. PloS one. 2013;8(2):e55895.
118. Davies A, Cummin TE, Barrans S, Maishman T, Mamot C, Novak U, et al. Gene-expression profiling of bortezomib added to standard chemoimmunotherapy for diffuse large B-cell lymphoma (REMoDL-B): an open-label, randomised, phase 3 trial. Lancet Oncol. 2019;20(5):649-62.
119. Ennishi D, Jiang A, Boyle M, Collinge B, Grande BM, Ben-Neriah S, et al. Double-Hit Gene Expression Signature Defines a Distinct Subgroup of Germinal Center B-Cell-Like Diffuse Large B-Cell Lymphoma. J Clin Oncol. 2019;37(3):190-201.
120. Sha C, Barrans S, Cucco F, Bentley MA, Care MA, Cummin T, et al. Molecular High-Grade B-Cell Lymphoma: Defining a Poor-Risk Group That Requires Different Approaches to Therapy. J Clin Oncol. 2019;37(3):202-12.

121. Hilton LK, Tang J, Ben-Neriah S, Alcaide M, Jiang A, Grande BM, et al. The double-hit signature identifies double-hit diffuse large B-cell lymphoma with genetic events cryptic to FISH. Blood. 2019;134(18):1528-32.
122. Chapuy B, Stewart C, Dunford AJ, Kim J, Kamburov A, Redd RA, et al. Molecular subtypes of diffuse large B cell lymphoma are associated with distinct pathogenic mechanisms and outcomes. Nature medicine. 2018;24(5):679-90.
123. Schmitz R, Wright GW, Huang DW, Johnson CA, Phelan JD, Wang JQ, et al. Genetics and Pathogenesis of Diffuse Large B-Cell Lymphoma. N Engl J Med. 2018;378(15):1396-407.
124. Lacy SE, Barrans SL, Beer PA, Painter D, Smith AG, Roman E, et al. Targeted sequencing in DLBCL, molecular subtypes, and outcomes: a Haematological Malignancy Research Network report. Blood. 2020;135(20):1759-71.
125. Araf S, Korfi K, Bewicke-Copley F, Wang J, Cogliatti S, Kumar E, et al. Genetic heterogeneity highlighted by differential FDG-PET response in diffuse large B-cell lymphoma. Haematologica. 2020;105(6):318-21.
126. Ryan RJ, Drier Y, Whitton H, Cotton MJ, Kaur J, Issner R, et al. Detection of Enhancer-Associated Rearrangements Reveals Mechanisms of Oncogene Dysregulation in B-cell Lymphoma. Cancer Discov. 2015;5(10):1058-71.
127. Mathelier A, Lefebvre C, Zhang AW, Arenillas DJ, Ding J, Wasserman WW, et al. Cis-regulatory somatic mutations and gene-expression alteration in B-cell lymphomas. Genome Biol. 2015;16:84.
128. Davis RE, Ngo VN, Lenz G, Tolar P, Young RM, Romesser PB, et al. Chronic active B-cell-receptor signalling in diffuse large B-cell lymphoma. Nature. 2010;463(7277):88-92.
129. Ngo VN, Young RM, Schmitz R, Jhavar S, Xiao W, Lim KH, et al. Oncogenically active MYD88 mutations in human lymphoma. Nature. 2011;470(7332):115-9.
130. Knittel G, Liedgens P, Korovkina D, Seeger JM, Al-Baldawi Y, Al-Maarri M, et al. B-cell-specific conditional expression of Myd88p.L252P leads to the development of diffuse large B-cell lymphoma in mice. Blood. 2016;127(22):2732-41.
131. Young RM, Wu T, Schmitz R, Dawood M, Xiao W, Phelan JD, et al. Survival of human lymphoma cells requires B-cell receptor engagement by self-antigens. Proc Natl Acad Sci U S A. 2015;112(44):13447-54.
132. Wilson WH, Young RM, Schmitz R, Yang Y, Pittaluga S, Wright G, et al. Targeting B cell receptor signaling with ibrutinib in diffuse large B cell lymphoma. Nature medicine. 2015;21(8):922-6.
133. Jain N, Hartert K, Tadros S, Fiskus W, Havranek O, Ma MCJ, et al. Targetable genetic alterations of TCF4 (E2-2) drive immunoglobulin expression in diffuse large B cell lymphoma. Sci Transl Med. 2019;11(497).
134. Challa-Malladi M, Lieu YK, Califano O, Holmes AB, Bhagat G, Murty VV, et al. Combined genetic inactivation of beta2-Microglobulin and CD58 reveals frequent escape from immune recognition in diffuse large B cell lymphoma. Cancer Cell. 2011;20(6):728-40.
135. Chapuy B, Roemer MG, Stewart C, Tan Y, Abo RP, Zhang L, et al. Targetable genetic features of primary testicular and primary central nervous system lymphomas. Blood. 2016;127(7):869-81.
136. Ennishi D, Healy S, Bashashati A, Saberi S, Hother C, Mottok A, et al. TMEM30A loss-of-function mutations drive lymphomagenesis and confer therapeutically exploitable vulnerability in B-cell lymphoma. Nature medicine. 2020;26(4):577-88.

137. Saito M, Novak U, Piovan E, Basso K, Sumazin P, Schneider C, et al. BCL6 suppression of BCL2 via Miz1 and its disruption in diffuse large B cell lymphoma. Proc Natl Acad Sci U S A. 2009;106(27):11294-9.
138. McCabe MT, Graves AP, Ganji G, Diaz E, Halsey WS, Jiang Y, et al. Mutation of A677 in histone methyltransferase EZH2 in human B-cell lymphoma promotes hypertrimethylation of histone H3 on lysine 27 (H3K27). Proc Natl Acad Sci U S A. 2012;109(8):2989-94.
139. Beguelin W, Teater M, Meydan C, Hoehn KB, Phillip JM, Soshnev AA, et al. Mutant EZH2 Induces a Pre-malignant Lymphoma Niche by Reprogramming the Immune Response. Cancer Cell. 2020;37(5):655-73 e11.
140. Ennishi D, Takata K, Beguelin W, Duns G, Mottok A, Farinha P, et al. Molecular and Genetic Characterization of MHC Deficiency Identifies EZH2 as Therapeutic Target for Enhancing Immune Recognition. Cancer Discov. 2019;9(4):546-63.
141. Zhang J, Dominguez-Sola D, Hussein S, Lee JE, Holmes AB, Bansal M, et al. Disruption of KMT2D perturbs germinal center B cell development and promotes lymphomagenesis. Nature medicine. 2015;21(10):1190-8.
142. Zhang J, Vlasevska S, Wells VA, Nataraj S, Holmes AB, Duval R, et al. The CREBBP Acetyltransferase Is a Haploinsufficient Tumor Suppressor in B-cell Lymphoma. Cancer Discov. 2017;7(3):322-37.
143. Jiang Y, Ortega-Molina A, Geng H, Ying HY, Hatzi K, Parsa S, et al. CREBBP Inactivation Promotes the Development of HDAC3-Dependent Lymphomas. Cancer Discov. 2017;7(1):38-53.
144. Brescia P, Schneider C, Holmes AB, Shen Q, Hussein S, Pasqualucci L, et al. MEF2B Instructs Germinal Center Development and Acts as an Oncogene in B Cell Lymphomagenesis. Cancer Cell. 2018;34(3):453-65 e9.
145. Boice M, Salloum D, Mourcin F, Sanghvi V, Amin R, Oricchio E, et al. Loss of the HVEM Tumor Suppressor in Lymphoma and Restoration by Modified CAR-T Cells. Cell. 2016;167(2):405-18 e13.
146. Pfeifer M, Grau M, Lenze D, Wenzel SS, Wolf A, Wollert-Wulf B, et al. PTEN loss defines a PI3K/AKT pathway-dependent germinal center subtype of diffuse large B-cell lymphoma. Proc Natl Acad Sci U S A. 2013;110(30):12420-5.
147. Yuan J, Wright G, Rosenwald A, Steidl C, Gascoyne RD, Connors JM, et al. Identification of Primary Mediastinal Large B-cell Lymphoma at Nonmediastinal Sites by Gene Expression Profiling. Am J Surg Pathol. 2015;39(10):1322-30.
148. Dominguez PM, Ghamlouch H, Rosikiewicz W, Kumar P, Beguelin W, Fontan L, et al. TET2 Deficiency Causes Germinal Center Hyperplasia, Impairs Plasma Cell Differentiation, and Promotes B-cell Lymphomagenesis. Cancer Discov. 2018;8(12):1632-53.
149. Celeste A, Petersen S, Romanienko PJ, Fernandez-Capetillo O, Chen HT, Sedelnikova OA, et al. Genomic instability in mice lacking histone H2AX. Science. 2002;296(5569):922-7.
150. Wright GW, Wilson WH, Staudt LM. Genetics of Diffuse Large B-Cell Lymphoma. N Engl J Med. 2018;379(5):493-4.
151. Sandhu SK, Fassan M, Volinia S, Lovat F, Balatti V, Pekarsky Y, et al. B-cell malignancies in microRNA Emu-miR-17~92 transgenic mice. Proc Natl Acad Sci U S A. 2013;110(45):18208-13.
152. Mihailovich M, Bremang M, Spadotto V, Musiani D, Vitale E, Varano G, et al. miR-17-92 fine-tunes MYC expression and function to ensure optimal B cell lymphoma growth. Nat Commun. 2015;6:8725.

153. Fowler NH, Cheah CY, Gascoyne RD, Gribben J, Neelapu SS, Ghia P, et al. Role of the tumor microenvironment in mature B-cell lymphoid malignancies. Haematologica. 2016;101(5):531-40.
154. Autio M, Leivonen SK, Bruck O, Mustjoki S, Meszaros Jorgensen J, Karjalainen-Lindsberg ML, et al. Immune cell constitution in the tumor microenvironment predicts the outcome in diffuse large B-cell lymphoma. Haematologica. 2021;106(3):718-29.
155. Scott DW, Gascoyne RD. The tumour microenvironment in B cell lymphomas. Nat Rev Cancer. 2014;14(8):517-34.
156. Tweeddale ME, Lim B, Jamal N, Robinson J, Zalcberg J, Lockwood G, et al. The presence of clonogenic cells in high-grade malignant lymphoma: a prognostic factor. Blood. 1987;69(5):1307-14.
157. Schreiber RD, Old LJ, Smyth MJ. Cancer immunoediting: integrating immunity's roles in cancer suppression and promotion. Science. 2011;331(6024):1565-70.
158. Schuler F, Hirt C, Dolken G. Chromosomal translocation t(14;18) in healthy individuals. Semin Cancer Biol. 2003;13(3):203-9.
159. Sehn LH, Salles G. Diffuse Large B-Cell Lymphoma. N Engl J Med. 2021;384(9):842-58.
160. Kotlov N, Bagaev A, Revuelta MV, Phillip JM, Cacciapuoti MT, Antysheva Z, et al. Clinical and Biological Subtypes of B-cell Lymphoma Revealed by Microenvironmental Signatures. Cancer Discov. 2021;11(6):1468-89.
161. Zitvogel L, Apetoh L, Ghiringhelli F, Kroemer G. Immunological aspects of cancer chemotherapy. Nat Rev Immunol. 2008;8(1):59-73.
162. Heath WR, Carbone FR. Cross-presentation in viral immunity and self-tolerance. Nat Rev Immunol. 2001;1(2):126-34.
163. Ansell SM. Fundamentals of immunology for understanding immunotherapy for lymphoma. Hematology Am Soc Hematol Educ Program. 2020;2020(1):585-9.
164. Courtney AH, Lo WL, Weiss A. TCR Signaling: Mechanisms of Initiation and Propagation. Trends Biochem Sci. 2018;43(2):108-23.
165. Murakami N, Riella LV. Co-inhibitory pathways and their importance in immune regulation. Transplantation. 2014;98(1):3-14.
166. de Charette M, Houot R. Hide or defend, the two strategies of lymphoma immune evasion: potential implications for immunotherapy. Haematologica. 2018;103(8):1256-68.
167. Yoshihama S, Roszik J, Downs I, Meissner TB, Vijayan S, Chapuy B, et al. NLRC5/MHC class I transactivator is a target for immune evasion in cancer. Proc Natl Acad Sci U S A. 2016;113(21):5999-6004.
168. Rimsza LM, Roberts RA, Campo E, Grogan TM, Bea S, Salaverria I, et al. Loss of major histocompatibility class II expression in non-immune-privileged site diffuse large B-cell lymphoma is highly coordinated and not due to chromosomal deletions. Blood. 2006;107(3):1101-7.
169. Rimsza LM, Roberts RA, Miller TP, Unger JM, LeBlanc M, Braziel RM, et al. Loss of MHC class II gene and protein expression in diffuse large B-cell lymphoma is related to decreased tumor immunosurveillance and poor patient survival regardless of other prognostic factors: a follow-up study from the Leukemia and Lymphoma Molecular Profiling Project. Blood. 2004;103(11):4251-8.
170. Riemersma SA, Jordanova ES, Schop RF, Philippo K, Looijenga LH, Schuuring E, et al. Extensive genetic alterations of the HLA region, including homozygous deletions of HLA class II genes in B-cell lymphomas arising in immune-privileged sites. Blood. 2000;96(10):3569-77.

171. Steidl C, Shah SP, Woolcock BW, Rui L, Kawahara M, Farinha P, et al. MHC class II transactivator CIITA is a recurrent gene fusion partner in lymphoid cancers. Nature. 2011;471(7338):377-81.
172. Mondello P, Tadros S, Teater M, Fontan L, Chang AY, Jain N, et al. Selective Inhibition of HDAC3 Targets Synthetic Vulnerabilities and Activates Immune Surveillance in Lymphoma. Cancer Discov. 2020;10(3):440-59.
173. Wilkinson ST, Vanpatten KA, Fernandez DR, Brunhoeber P, Garsha KE, Glinsmann-Gibson BJ, et al. Partial plasma cell differentiation as a mechanism of lost major histocompatibility complex class II expression in diffuse large B-cell lymphoma. Blood. 2012;119(6):1459-67.
174. Greaves P, Gribben JG. The role of B7 family molecules in hematologic malignancy. Blood. 2013;121(5):734-44.
175. Stopeck AT, Gessner A, Miller TP, Hersh EM, Johnson CS, Cui H, et al. Loss of B7.2 (CD86) and intracellular adhesion molecule 1 (CD54) expression is associated with decreased tumor-infiltrating T lymphocytes in diffuse B-cell large-cell lymphoma. Clinical cancer research : an official journal of the American Association for Cancer Research. 2000;6(10):3904-9.
176. Perini GF, Ribeiro GN, Pinto Neto JV, Campos LT, Hamerschlak N. BCL-2 as therapeutic target for hematological malignancies. J Hematol Oncol. 2018;11(1):65.
177. Peter ME, Hadji A, Murmann AE, Brockway S, Putzbach W, Pattanayak A, et al. The role of CD95 and CD95 ligand in cancer. Cell Death Differ. 2015;22(5):885-6.
178. van Eijk M, Defrance T, Hennino A, de Groot C. Death-receptor contribution to the germinal-center reaction. Trends Immunol. 2001;22(12):677-82.
179. Markovic O, Marisavljevic D, Cemerikic V, Perunicic M, Savic S, Filipovic B, et al. Clinical and prognostic significance of apoptotic profile in patients with newly diagnosed nodal diffuse large B-cell lymphoma (DLBCL). Eur J Haematol. 2011;86(3):246-55.
180. Casey SC, Baylot V, Felsher DW. The MYC oncogene is a global regulator of the immune response. Blood. 2018;131(18):2007-15.
181. Keir ME, Butte MJ, Freeman GJ, Sharpe AH. PD-1 and its ligands in tolerance and immunity. Annu Rev Immunol. 2008;26:677-704.
182. Kiyasu J, Miyoshi H, Hirata A, Arakawa F, Ichikawa A, Niino D, et al. Expression of programmed cell death ligand 1 is associated with poor overall survival in patients with diffuse large B-cell lymphoma. Blood. 2015;126(19):2193-201.
183. Georgiou K, Chen L, Berglund M, Ren W, de Miranda NF, Lisboa S, et al. Genetic basis of PD-L1 overexpression in diffuse large B-cell lymphomas. Blood. 2016;127(24):3026-34.
184. Gravelle P, Burroni B, Pericart S, Rossi C, Bezombes C, Tosolini M, et al. Mechanisms of PD-1/PD-L1 expression and prognostic relevance in non-Hodgkin lymphoma: a summary of immunohistochemical studies. Oncotarget. 2017;8(27):44960-75.
185. Hude I, Sasse S, Engert A, Brockelmann PJ. The emerging role of immune checkpoint inhibition in malignant lymphoma. Haematologica. 2017;102(1):30-42.
186. Godfrey J, Tumuluru S, Bao R, Leukam M, Venkataraman G, Phillip J, et al. PD-L1 gene alterations identify a subset of diffuse large B-cell lymphoma harboring a T-cell-inflamed phenotype. Blood. 2019;133(21):2279-90.
187. Petrova PS, Viller NN, Wong M, Pang X, Lin GH, Dodge K, et al. TTI-621 (SIRPalphaFc): A CD47-Blocking Innate Immune Checkpoint Inhibitor with Broad Antitumor Activity and Minimal Erythrocyte Binding. Clinical cancer research : an official journal of the American Association for Cancer Research. 2017;23(4):1068-79.

188. Chao MP, Alizadeh AA, Tang C, Myklebust JH, Varghese B, Gill S, et al. Anti-CD47 antibody synergizes with rituximab to promote phagocytosis and eradicate non-Hodgkin lymphoma. Cell. 2010;142(5):699-713.
189. Advani R, Flinn I, Popplewell L, Forero A, Bartlett NL, Ghosh N, et al. CD47 Blockade by Hu5F9-G4 and Rituximab in Non-Hodgkin's Lymphoma. N Engl J Med. 2018;379(18):1711-21.
190. Tseng D, Volkmer JP, Willingham SB, Contreras-Trujillo H, Fathman JW, Fernhoff NB, et al. Anti-CD47 antibody-mediated phagocytosis of cancer by macrophages primes an effective antitumor T-cell response. Proc Natl Acad Sci U S A. 2013;110(27):11103-8.
191. Wilcox RA, Ristow K, Habermann TM, Inwards DJ, Micallef IN, Johnston PB, et al. The absolute monocyte and lymphocyte prognostic score predicts survival and identifies high-risk patients in diffuse large-B-cell lymphoma. Leukemia. 2011;25(9):1502-9.
192. Li ZM, Huang JJ, Xia Y, Sun J, Huang Y, Wang Y, et al. Blood lymphocyte-to-monocyte ratio identifies high-risk patients in diffuse large B-cell lymphoma treated with R-CHOP. PloS one. 2012;7(7):e41658.
193. Katoh D, Ochi Y, Yabushita T, Ono Y, Hiramoto N, Yoshioka S, et al. Peripheral Blood Lymphocyte-to-Monocyte Ratio at Relapse Predicts Outcome for Patients With Relapsed or Refractory Diffuse Large B-cell Lymphoma in the Rituximab Era. Clinical lymphoma, myeloma & leukemia. 2017;17(12):e91-e7.
194. Azzaoui I, Uhel F, Rossille D, Pangault C, Dulong J, Le Priol J, et al. T-cell defect in diffuse large B-cell lymphomas involves expansion of myeloid-derived suppressor cells. Blood. 2016;128(8):1081-92.
195. Lin Y, Gustafson MP, Bulur PA, Gastineau DA, Witzig TE, Dietz AB. Immunosuppressive CD14+HLA-DR(low)/- monocytes in B-cell non-Hodgkin lymphoma. Blood. 2011;117(3):872-81.
196. Xiu B, Lin Y, Grote DM, Ziesmer SC, Gustafson MP, Maas ML, et al. IL-10 induces the development of immunosuppressive CD14(+)HLA-DR(low/-) monocytes in B-cell non-Hodgkin lymphoma. Blood cancer journal. 2015;5:e328.
197. Mueller CG, Boix C, Kwan WH, Daussy C, Fournier E, Fridman WH, et al. Critical role of monocytes to support normal B cell and diffuse large B cell lymphoma survival and proliferation. J Leukoc Biol. 2007;82(3):567-75.
198. Roussel M, Irish JM, Menard C, Lhomme F, Tarte K, Fest T. Regulatory myeloid cells: an underexplored continent in B-cell lymphomas. Cancer Immunol Immunother. 2017;66(8):1103-11.
199. Kusano Y, Yokoyama M, Terui Y, Nishimura N, Mishima Y, Ueda K, et al. Low absolute peripheral blood CD4+ T-cell count predicts poor prognosis in R-CHOP-treated patients with diffuse large B-cell lymphoma. Blood cancer journal. 2017;7(5):e561.
200. Amini RM, Enblad G, Hollander P, Laszlo S, Eriksson E, Ayoola Gustafsson K, et al. Altered profile of immune regulatory cells in the peripheral blood of lymphoma patients. BMC Cancer. 2019;19(1):316.
201. Chang C, Wu SY, Kang YW, Lin KP, Chen TY, Medeiros LJ, et al. High levels of regulatory T cells in blood are a poor prognostic factor in patients with diffuse large B-cell lymphoma. American journal of clinical pathology. 2015;144(6):935-44.
202. Dehghani M, Kalani M, Golmoghaddam H, Ramzi M, Arandi N. Aberrant peripheral blood CD4(+) CD25(+) FOXP3(+) regulatory T cells/T helper-17 number is associated with the outcome of patients with lymphoma. Cancer Immunol Immunother. 2020;69(9):1917-28.

203. Battella S, Cox MC, La Scaleia R, Di Napoli A, Di Landro F, Porzia A, et al. Peripheral blood T cell alterations in newly diagnosed diffuse large B cell lymphoma patients and their long-term dynamics upon rituximab-based chemoimmunotherapy. Cancer Immunol Immunother. 2017;66(10):1295-306.
204. Monti S, Savage KJ, Kutok JL, Feuerhake F, Kurtin P, Mihm M, et al. Molecular profiling of diffuse large B-cell lymphoma identifies robust subtypes including one characterized by host inflammatory response. Blood. 2005;105(5):1851-61.
205. Coutinho R, Clear AJ, Mazzola E, Owen A, Greaves P, Wilson A, et al. Revisiting the immune microenvironment of diffuse large B-cell lymphoma using a tissue microarray and immunohistochemistry: robust semi-automated analysis reveals CD3 and FoxP3 as potential predictors of response to R-CHOP. Haematologica. 2015;100(3):363-9.
206. Kridel R, Steidl C, Gascoyne RD. Tumor-associated macrophages in diffuse large B-cell lymphoma. Haematologica. 2015;100(2):143-5.
207. Nam SJ, Go H, Paik JH, Kim TM, Heo DS, Kim CW, et al. An increase of M2 macrophages predicts poor prognosis in patients with diffuse large B-cell lymphoma treated with rituximab, cyclophosphamide, doxorubicin, vincristine and prednisone. Leukemia & lymphoma. 2014;55(11):2466-76.
208. Wada N, Zaki MA, Hori Y, Hashimoto K, Tsukaguchi M, Tatsumi Y, et al. Tumour-associated macrophages in diffuse large B-cell lymphoma: a study of the Osaka Lymphoma Study Group. Histopathology. 2012;60(2):313-9.
209. Meyer PN, Fu K, Greiner T, Smith L, Delabie J, Gascoyne R, et al. The stromal cell marker SPARC predicts for survival in patients with diffuse large B-cell lymphoma treated with rituximab. American journal of clinical pathology. 2011;135(1):54-61.
210. Staiger AM, Altenbuchinger M, Ziepert M, Kohler C, Horn H, Huttner M, et al. A novel lymphoma-associated macrophage interaction signature (LAMIS) provides robust risk prognostication in diffuse large B-cell lymphoma clinical trial cohorts of the DSHNHL. Leukemia. 2020;34(2):543-52.
211. Riihijarvi S, Fiskvik I, Taskinen M, Vajavaara H, Tikkala M, Yri O, et al. Prognostic influence of macrophages in patients with diffuse large B-cell lymphoma: a correlative study from a Nordic phase II trial. Haematologica. 2015;100(2):238-45.
212. Clynes RA, Towers TL, Presta LG, Ravetch JV. Inhibitory Fc receptors modulate in vivo cytotoxicity against tumor targets. Nature medicine. 2000;6(4):443-6.
213. Glennie MJ, French RR, Cragg MS, Taylor RP. Mechanisms of killing by anti-CD20 monoclonal antibodies. Molecular immunology. 2007;44(16):3823-37.
214. Lim SH, Beers SA, French RR, Johnson PW, Glennie MJ, Cragg MS. Anti-CD20 monoclonal antibodies: historical and future perspectives. Haematologica. 2010;95(1):135-43.
215. Kim DH, Jung HD, Kim JG, Lee JJ, Yang DH, Park YH, et al. FCGR3A gene polymorphisms may correlate with response to frontline R-CHOP therapy for diffuse large B-cell lymphoma. Blood. 2006;108(8):2720-5.
216. Mellor JD, Brown MP, Irving HR, Zalcberg JR, Dobrovic A. A critical review of the role of Fc gamma receptor polymorphisms in the response to monoclonal antibodies in cancer. J Hematol Oncol. 2013;6:1.
217. Nakamura K, Casey M, Oey H, Vari F, Stagg J, Gandhi MK, et al. Targeting an adenosine-mediated "don't eat me signal" augments anti-lymphoma immunity by anti-CD20 monoclonal antibody. Leukemia. 2020;34(10):2708-21.

218. Keane C, Gill D, Vari F, Cross D, Griffiths L, Gandhi M. CD4(+) tumor infiltrating lymphocytes are prognostic and independent of R-IPI in patients with DLBCL receiving R-CHOP chemo-immunotherapy. Am J Hematol. 2013;88(4):273-6.
219. Keane C, Vari F, Hertzberg M, Cao KA, Green MR, Han E, et al. Ratios of T-cell immune effectors and checkpoint molecules as prognostic biomarkers in diffuse large B-cell lymphoma: a population-based study. Lancet Haematol. 2015;2(10):e445-55.
220. Charbonneau B, Maurer MJ, Ansell SM, Slager SL, Fredericksen ZS, Ziesmer SC, et al. Pretreatment circulating serum cytokines associated with follicular and diffuse large B-cell lymphoma: a clinic-based case-control study. Cytokine. 2012;60(3):882-9.
221. Pauly F, Fjorden K, Leppa S, Holte H, Bjorkholm M, Fluge O, et al. Plasma immunoprofiling of patients with high-risk diffuse large B-cell lymphoma: a Nordic Lymphoma Group study. Blood cancer journal. 2016;6(11):e501.
222. Zhong H, Chen J, Cheng S, Chen S, Shen R, Shi Q, et al. Prognostic nomogram incorporating inflammatory cytokines for overall survival in patients with aggressive non-Hodgkin's lymphoma. EBioMedicine. 2019;41:167-74.
223. Gupta M, Han JJ, Stenson M, Maurer M, Wellik L, Hu G, et al. Elevated serum IL-10 levels in diffuse large B-cell lymphoma: a mechanism of aberrant JAK2 activation. Blood. 2012;119(12):2844-53.
224. Rothman N, Skibola CF, Wang SS, Morgan G, Lan Q, Smith MT, et al. Genetic variation in TNF and IL10 and risk of non-Hodgkin lymphoma: a report from the InterLymph Consortium. Lancet Oncol. 2006;7(1):27-38.
225. Cunningham LM, Chapman C, Dunstan R, Bell MC, Joske DJ. Polymorphisms in the interleukin 10 gene promoter are associated with susceptibility to aggressive non-Hodgkin's lymphoma. Leukemia & lymphoma. 2003;44(2):251-5.
226. Hashwah H, Bertram K, Stirm K, Stelling A, Wu CT, Kasser S, et al. The IL-6 signaling complex is a critical driver, negative prognostic factor, and therapeutic target in diffuse large B-cell lymphoma. EMBO Mol Med. 2019;11(10):e10576.
227. Yang L, Pang Y, Moses HL. TGF-beta and immune cells: an important regulatory axis in the tumor microenvironment and progression. Trends Immunol. 2010;31(6):220-7.
228. Taylor JG, Gribben JG. Microenvironment abnormalities and lymphomagenesis: Immunological aspects. Semin Cancer Biol. 2015;34:36-45.
229. Coiffier B, Thieblemont C, Van Den Neste E, Lepeu G, Plantier I, Castaigne S, et al. Long-term outcome of patients in the LNH-98.5 trial, the first randomized study comparing rituximab-CHOP to standard CHOP chemotherapy in DLBCL patients: a study by the Groupe d'Etudes des Lymphomes de l'Adulte. Blood. 2010;116(12):2040-5.
230. Pfreundschuh M, Trumper L, Osterborg A, Pettengell R, Trneny M, Imrie K, et al. CHOP-like chemotherapy plus rituximab versus CHOP-like chemotherapy alone in young patients with good-prognosis diffuse large-B-cell lymphoma: a randomised controlled trial by the MabThera International Trial (MInT) Group. Lancet Oncol. 2006;7(5):379-91.
231. Sehn LH, Donaldson J, Chhanabhai M, Fitzgerald C, Gill K, Klasa R, et al. Introduction of combined CHOP plus rituximab therapy dramatically improved outcome of diffuse large B-cell lymphoma in British Columbia. J Clin Oncol. 2005;23(22):5027-33.
232. Cunningham D, Hawkes EA, Jack A, Qian W, Smith P, Mouncey P, et al. Rituximab plus cyclophosphamide, doxorubicin, vincristine, and prednisolone in patients with newly diagnosed diffuse large B-cell non-Hodgkin lymphoma: a phase 3 comparison of dose intensification with 14-day versus 21-day cycles. Lancet. 2013;381(9880):1817-26.

233. Pfreundschuh M, Schubert J, Ziepert M, Schmits R, Mohren M, Lengfelder E, et al. Six versus eight cycles of bi-weekly CHOP-14 with or without rituximab in elderly patients with aggressive CD20+ B-cell lymphomas: a randomised controlled trial (RICOVER-60). Lancet Oncol. 2008;9(2):105-16.
234. Stiff PJ, Unger JM, Cook JR, Constine LS, Couban S, Stewart DA, et al. Autologous transplantation as consolidation for aggressive non-Hodgkin's lymphoma. N Engl J Med. 2013;369(18):1681-90.
235. Delarue R, Tilly H, Mounier N, Petrella T, Salles G, Thieblemont C, et al. Dose-dense rituximab-CHOP compared with standard rituximab-CHOP in elderly patients with diffuse large B-cell lymphoma (the LNH03-6B study): a randomised phase 3 trial. Lancet Oncol. 2013;14(6):525-33.
236. Gang AO, Strom C, Pedersen M, d'Amore F, Pedersen LM, Bukh A, et al. R-CHOEP-14 improves overall survival in young high-risk patients with diffuse large B-cell lymphoma compared with R-CHOP-14. A population-based investigation from the Danish Lymphoma Group. Ann Oncol. 2012;23(1):147-53.
237. Pedersen MO, Gang AO, Brown P, Pedersen M, Knudsen H, Nielsen SL, et al. Real world data on young patients with high-risk diffuse large B-cell lymphoma treated with R-CHOP or R-CHOEP - MYC, BCL2 and BCL6 as prognostic biomarkers. PloS one. 2017;12(10):e0186983.
238. Wasterlid T, Hartman L, Szekely E, Jerkeman M. Impact on survival of addition of etoposide to primary chemotherapy in diffuse large B-cell lymphoma: a Swedish Lymphoma Registry study. Hematol Oncol. 2017;35(2):151-7.
239. Recher C, Coiffier B, Haioun C, Molina TJ, Ferme C, Casasnovas O, et al. Intensified chemotherapy with ACVBP plus rituximab versus standard CHOP plus rituximab for the treatment of diffuse large B-cell lymphoma (LNH03-2B): an open-label randomised phase 3 trial. Lancet. 2011;378(9806):1858-67.
240. Bartlett NL, Wilson WH, Jung SH, Hsi ED, Maurer MJ, Pederson LD, et al. Dose-Adjusted EPOCH-R Compared With R-CHOP as Frontline Therapy for Diffuse Large B-Cell Lymphoma: Clinical Outcomes of the Phase III Intergroup Trial Alliance/CALGB 50303. J Clin Oncol. 2019;37(21):1790-9.
241. McMillan AK, Phillips EH, Kirkwood AA, Barrans S, Burton C, Rule S, et al. Favourable outcomes for high-risk diffuse large B-cell lymphoma (IPI 3-5) treated with front-line R-CODOX-M/R-IVAC chemotherapy: results of a phase 2 UK NCRI trial. Ann Oncol. 2020;31(9):1251-9.
242. Vitolo U, Trneny M, Belada D, Burke JM, Carella AM, Chua N, et al. Obinutuzumab or Rituximab Plus Cyclophosphamide, Doxorubicin, Vincristine, and Prednisone in Previously Untreated Diffuse Large B-Cell Lymphoma. J Clin Oncol. 2017;35(31):3529-37.
243. Nowakowski GS, Chiappella A, Gascoyne RD, Scott DW, Zhang Q, Jurczak W, et al. ROBUST: A Phase III Study of Lenalidomide Plus R-CHOP Versus Placebo Plus R-CHOP in Previously Untreated Patients With ABC-Type Diffuse Large B-Cell Lymphoma. J Clin Oncol. 2021:JCO2001366.
244. Younes A, Sehn LH, Johnson P, Zinzani PL, Hong X, Zhu J, et al. Randomized Phase III Trial of Ibrutinib and Rituximab Plus Cyclophosphamide, Doxorubicin, Vincristine, and Prednisone in Non-Germinal Center B-Cell Diffuse Large B-Cell Lymphoma. J Clin Oncol. 2019;37(15):1285-95.
245. Sehn LH, Martelli M, Trneny M, Liu W, Bolen CR, Knapp A, et al. A randomized, open-label, Phase III study of obinutuzumab or rituximab plus CHOP in patients with previously

untreated diffuse large B-Cell lymphoma: final analysis of GOYA. J Hematol Oncol. 2020;13(1):71.
246. Chanan-Khan AA, Cheson BD. Lenalidomide for the treatment of B-cell malignancies. J Clin Oncol. 2008;26(9):1544-52.
247. Gribben JG, Fowler N, Morschhauser F. Mechanisms of Action of Lenalidomide in B-Cell Non-Hodgkin Lymphoma. J Clin Oncol. 2015;33(25):2803-11.
248. Nowakowski GS, LaPlant B, Macon WR, Reeder CB, Foran JM, Nelson GD, et al. Lenalidomide combined with R-CHOP overcomes negative prognostic impact of non-germinal center B-cell phenotype in newly diagnosed diffuse large B-Cell lymphoma: a phase II study. J Clin Oncol. 2015;33(3):251-7.
249. Thieblemont C, Tilly H, Gomes da Silva M, Casasnovas RO, Fruchart C, Morschhauser F, et al. Lenalidomide Maintenance Compared With Placebo in Responding Elderly Patients With Diffuse Large B-Cell Lymphoma Treated With First-Line Rituximab Plus Cyclophosphamide, Doxorubicin, Vincristine, and Prednisone. J Clin Oncol. 2017;35(22):2473-81.
250. McKay P, Wilson MR, Chaganti S, Smith J, Fox CP, Cwynarski K, et al. The prevention of central nervous system relapse in diffuse large B-cell lymphoma: a British Society for Haematology good practice paper. Br J Haematol. 2020;190(5):708-14.
251. Peyrade F, Jardin F, Thieblemont C, Thyss A, Emile JF, Castaigne S, et al. Attenuated immunochemotherapy regimen (R-miniCHOP) in elderly patients older than 80 years with diffuse large B-cell lymphoma: a multicentre, single-arm, phase 2 trial. Lancet Oncol. 2011;12(5):460-8.
252. Fields PA, Townsend W, Webb A, Counsell N, Pocock C, Smith P, et al. De novo treatment of diffuse large B-cell lymphoma with rituximab, cyclophosphamide, vincristine, gemcitabine, and prednisolone in patients with cardiac comorbidity: a United Kingdom National Cancer Research Institute trial. J Clin Oncol. 2014;32(4):282-7.
253. Gisselbrecht C, Glass B, Mounier N, Singh Gill D, Linch DC, Trneny M, et al. Salvage regimens with autologous transplantation for relapsed large B-cell lymphoma in the rituximab era. J Clin Oncol. 2010;28(27):4184-90.
254. Maurer MJ, Ghesquieres H, Jais JP, Witzig TE, Haioun C, Thompson CA, et al. Event-free survival at 24 months is a robust end point for disease-related outcome in diffuse large B-cell lymphoma treated with immunochemotherapy. J Clin Oncol. 2014;32(10):1066-73.
255. Larouche JF, Berger F, Chassagne-Clement C, Ffrench M, Callet-Bauchu E, Sebban C, et al. Lymphoma recurrence 5 years or later following diffuse large B-cell lymphoma: clinical characteristics and outcome. J Clin Oncol. 2010;28(12):2094-100.
256. Philip T, Guglielmi C, Hagenbeek A, Somers R, Van der Lelie H, Bron D, et al. Autologous bone marrow transplantation as compared with salvage chemotherapy in relapses of chemotherapy-sensitive non-Hodgkin's lymphoma. N Engl J Med. 1995;333(23):1540-5.
257. Hoppe BS, Moskowitz CH, Zhang Z, Maragulia JC, Rice RD, Reiner AS, et al. The role of FDG-PET imaging and involved field radiotherapy in relapsed or refractory diffuse large B-cell lymphoma. Bone Marrow Transplant. 2009;43(12):941-8.
258. Sauter CS, Matasar MJ, Meikle J, Schoder H, Ulaner GA, Migliacci JC, et al. Prognostic value of FDG-PET prior to autologous stem cell transplantation for relapsed and refractory diffuse large B-cell lymphoma. Blood. 2015;125(16):2579-81.
259. Thieblemont C, Briere J, Mounier N, Voelker HU, Cuccuini W, Hirchaud E, et al. The germinal center/activated B-cell subclassification has a prognostic impact for response to

salvage therapy in relapsed/refractory diffuse large B-cell lymphoma: a bio-CORAL study. J Clin Oncol. 2011;29(31):4079-87.
260. Crump M, Kuruvilla J, Couban S, MacDonald DA, Kukreti V, Kouroukis CT, et al. Randomized comparison of gemcitabine, dexamethasone, and cisplatin versus dexamethasone, cytarabine, and cisplatin chemotherapy before autologous stem-cell transplantation for relapsed and refractory aggressive lymphomas: NCIC-CTG LY.12. J Clin Oncol. 2014;32(31):3490-6.
261. Mounier N, Canals C, Gisselbrecht C, Cornelissen J, Foa R, Conde E, et al. High-dose therapy and autologous stem cell transplantation in first relapse for diffuse large B cell lymphoma in the rituximab era: an analysis based on data from the European Blood and Marrow Transplantation Registry. Biol Blood Marrow Transplant. 2012;18(5):788-93.
262. van Imhoff GW, McMillan A, Matasar MJ, Radford J, Ardeshna KM, Kuliczkowski K, et al. Ofatumumab Versus Rituximab Salvage Chemoimmunotherapy in Relapsed or Refractory Diffuse Large B-Cell Lymphoma: The ORCHARRD Study. J Clin Oncol. 2017;35(5):544-51.
263. Friedberg JW. Relapsed/refractory diffuse large B-cell lymphoma. Hematology Am Soc Hematol Educ Program. 2011;2011:498-505.
264. Ardeshna KM, Kakouros N, Qian W, Powell MG, Saini N, D'Sa S, et al. Conventional second-line salvage chemotherapy regimens are not warranted in patients with malignant lymphomas who have progressive disease after first-line salvage therapy regimens. Br J Haematol. 2005;130(3):363-72.
265. Elstrom RL, Martin P, Ostrow K, Barrientos J, Chadburn A, Furman R, et al. Response to second-line therapy defines the potential for cure in patients with recurrent diffuse large B-cell lymphoma: implications for the development of novel therapeutic strategies. Clinical lymphoma, myeloma & leukemia. 2010;10(3):192-6.
266. Crump M, Neelapu SS, Farooq U, Van Den Neste E, Kuruvilla J, Westin J, et al. Outcomes in refractory diffuse large B-cell lymphoma: results from the international SCHOLAR-1 study. Blood. 2017;130(16):1800-8.
267. van Kampen RJ, Canals C, Schouten HC, Nagler A, Thomson KJ, Vernant JP, et al. Allogeneic stem-cell transplantation as salvage therapy for patients with diffuse large B-cell non-Hodgkin's lymphoma relapsing after an autologous stem-cell transplantation: an analysis of the European Group for Blood and Marrow Transplantation Registry. J Clin Oncol. 2011;29(10):1342-8.
268. Truelove E, Fox C, Robinson S, Pearce R, Perry J, Kirkland K, et al. Carmustine, etoposide, cytarabine, and melphalan (BEAM)-campath allogeneic stem cell transplantation for aggressive non-hodgkin lymphoma: an analysis of outcomes from the British Society of Blood and Marrow Transplantation. Biol Blood Marrow Transplant. 2015;21(3):483-8.
269. Fenske TS, Ahn KW, Graff TM, DiGilio A, Bashir Q, Kamble RT, et al. Allogeneic transplantation provides durable remission in a subset of DLBCL patients relapsing after autologous transplantation. Br J Haematol. 2016;174(2):235-48.
270. Tran E, Longo DL, Urba WJ. A Milestone for CAR T Cells. N Engl J Med. 2017;377(26):2593-6.
271. Neelapu SS, Locke FL, Bartlett NL, Lekakis LJ, Miklos DB, Jacobson CA, et al. Axicabtagene Ciloleucel CAR T-Cell Therapy in Refractory Large B-Cell Lymphoma. N Engl J Med. 2017;377(26):2531-44.
272. Schuster SJ, Bishop MR, Tam CS, Waller EK, Borchmann P, McGuirk JP, et al. Tisagenlecleucel in Adult Relapsed or Refractory Diffuse Large B-Cell Lymphoma. N Engl J Med. 2019;380(1):45-56.

273. Locke FL, Ghobadi A, Jacobson CA, Miklos DB, Lekakis LJ, Oluwole OO, et al. Long-term safety and activity of axicabtagene ciloleucel in refractory large B-cell lymphoma (ZUMA-1): a single-arm, multicentre, phase 1-2 trial. Lancet Oncol. 2019;20(1):31-42.
274. Barton S, Hawkes EA, Cunningham D, Peckitt C, Chua S, Wotherspoon A, et al. Rituximab, Gemcitabine, Cisplatin and Methylprednisolone (R-GEM-P) is an effective regimen in relapsed diffuse large B-cell lymphoma. Eur J Haematol. 2015;94(3):219-26.
275. Mounier N, El Gnaoui T, Tilly H, Canioni D, Sebban C, Casasnovas RO, et al. Rituximab plus gemcitabine and oxaliplatin in patients with refractory/relapsed diffuse large B-cell lymphoma who are not candidates for high-dose therapy. A phase II Lymphoma Study Association trial. Haematologica. 2013;98(11):1726-31.
276. Eyre TA, Linton KM, Rohman P, Kothari J, Cwynarski K, Ardeshna K, et al. Results of a multicentre UK-wide retrospective study evaluating the efficacy of pixantrone in relapsed, refractory diffuse large B cell lymphoma. Br J Haematol. 2016;173(6):896-904.
277. Sehn LH, Herrera AF, Flowers CR, Kamdar MK, McMillan A, Hertzberg M, et al. Polatuzumab Vedotin in Relapsed or Refractory Diffuse Large B-Cell Lymphoma. J Clin Oncol. 2020;38(2):155-65.
278. Jurczak W, Zinzani PL, Gaidano G, Goy A, Provencio M, Nagy Z, et al. Phase IIa study of the CD19 antibody MOR208 in patients with relapsed or refractory B-cell non-Hodgkin's lymphoma. Ann Oncol. 2018;29(5):1266-72.
279. Salles G, Duell J, Gonzalez Barca E, Tournilhac O, Jurczak W, Liberati AM, et al. Tafasitamab plus lenalidomide in relapsed or refractory diffuse large B-cell lymphoma (L-MIND): a multicentre, prospective, single-arm, phase 2 study. Lancet Oncol. 2020;21(7):978-88.
280. Maddocks K. Novel targets in aggressive lymphoma. Hematology Am Soc Hematol Educ Program. 2020;2020(1):101-6.
281. Kahl BS, Hamadani M, Radford J, Carlo-Stella C, Caimi P, Reid E, et al. A Phase I Study of ADCT-402 (Loncastuximab Tesirine), a Novel Pyrrolobenzodiazepine-Based Antibody-Drug Conjugate, in Relapsed/Refractory B-Cell Non-Hodgkin Lymphoma. Clinical cancer research : an official journal of the American Association for Cancer Research. 2019;25(23):6986-94.
282. Abramson JS, Palomba ML, Gordon LI, Lunning MA, Wang M, Arnason J, et al. Lisocabtagene maraleucel for patients with relapsed or refractory large B-cell lymphomas (TRANSCEND NHL 001): a multicentre seamless design study. Lancet. 2020;396(10254):839-52.
283. Yeku OO, Purdon TJ, Koneru M, Spriggs D, Brentjens RJ. Armored CAR T cells enhance antitumor efficacy and overcome the tumor microenvironment. Sci Rep. 2017;7(1):10541.
284. Chong EA, Porter DL. Immunotherapy with cells (article not eligible for CME credit). Hematology Am Soc Hematol Educ Program. 2020;2020(1):590-7.
285. Choi Y, Diefenbach CS. Immunotherapy with drugs. Hematology Am Soc Hematol Educ Program. 2020;2020(1):598-605.
286. van der Horst HJ, de Jonge AV, Hiemstra IH, Gelderloos AT, Berry D, Hijmering NJ, et al. Epcoritamab induces potent anti-tumor activity against malignant B-cells from patients with DLBCL, FL and MCL, irrespective of prior CD20 monoclonal antibody treatment. Blood cancer journal. 2021;11(2):38.
287. Dubovsky JA, Beckwith KA, Natarajan G, Woyach JA, Jaglowski S, Zhong Y, et al. Ibrutinib is an irreversible molecular inhibitor of ITK driving a Th1-selective pressure in T lymphocytes. Blood. 2013;122(15):2539-49.

288. Goy A, Ramchandren R, Ghosh N, Munoz J, Morgan DS, Dang NH, et al. Ibrutinib plus lenalidomide and rituximab has promising activity in relapsed/refractory non-germinal center B-cell-like DLBCL. Blood. 2019;134(13):1024-36.
289. Zelenetz AD, Salles G, Mason KD, Casulo C, Le Gouill S, Sehn LH, et al. Venetoclax plus R- or G-CHOP in non-Hodgkin lymphoma: results from the CAVALLI phase 1b trial. Blood. 2019;133(18):1964-76.
290. Amengual JE. Can we use epigenetics to prime chemoresistant lymphomas? Hematology Am Soc Hematol Educ Program. 2020;2020(1):85-94.
291. De S, Shaknovich R, Riester M, Elemento O, Geng H, Kormaksson M, et al. Aberration in DNA methylation in B-cell lymphomas has a complex origin and increases with disease severity. PLoS Genet. 2013;9(1):e1003137.
292. Clozel T, Yang S, Elstrom RL, Tam W, Martin P, Kormaksson M, et al. Mechanism-based epigenetic chemosensitization therapy of diffuse large B-cell lymphoma. Cancer Discov. 2013;3(9):1002-19.
293. Beguelin W, Teater M, Gearhart MD, Calvo Fernandez MT, Goldstein RL, Cardenas MG, et al. EZH2 and BCL6 Cooperate to Assemble CBX8-BCOR Complex to Repress Bivalent Promoters, Mediate Germinal Center Formation and Lymphomagenesis. Cancer Cell. 2016;30(2):197-213.
294. Yang H, Green MR. Harnessing lymphoma epigenetics to improve therapies. Hematology Am Soc Hematol Educ Program. 2020;2020(1):95-100.
295. Brudno JN, Somerville RP, Shi V, Rose JJ, Halverson DC, Fowler DH, et al. Allogeneic T Cells That Express an Anti-CD19 Chimeric Antigen Receptor Induce Remissions of B-Cell Malignancies That Progress After Allogeneic Hematopoietic Stem-Cell Transplantation Without Causing Graft-Versus-Host Disease. J Clin Oncol. 2016;34(10):1112-21.
296. Qasim W, Zhan H, Samarasinghe S, Adams S, Amrolia P, Stafford S, et al. Molecular remission of infant B-ALL after infusion of universal TALEN gene-edited CAR T cells. Sci Transl Med. 2017;9(374).
297. Bandura DR, Baranov VI, Ornatsky OI, Antonov A, Kinach R, Lou X, et al. Mass cytometry: technique for real time single cell multitarget immunoassay based on inductively coupled plasma time-of-flight mass spectrometry. Anal Chem. 2009;81(16):6813-22.
298. Leipold MD, Newell EW, Maecker HT. Multiparameter Phenotyping of Human PBMCs Using Mass Cytometry. Methods Mol Biol. 2015;1343:81-95.
299. Bendall SC, Nolan GP, Roederer M, Chattopadhyay PK. A deep profiler's guide to cytometry. Trends Immunol. 2012;33(7):323-32.
300. Giesen C, Wang HA, Schapiro D, Zivanovic N, Jacobs A, Hattendorf B, et al. Highly multiplexed imaging of tumor tissues with subcellular resolution by mass cytometry. Nat Methods. 2014;11(4):417-22.
301. Schapiro D, Jackson HW, Raghuraman S, Fischer JR, Zanotelli VRT, Schulz D, et al. histoCAT: analysis of cell phenotypes and interactions in multiplex image cytometry data. Nat Methods. 2017;14(9):873-6.
302. Berthel A, Zoernig I, Valous NA, Kahlert C, Klupp F, Ulrich A, et al. Detailed resolution analysis reveals spatial T cell heterogeneity in the invasive margin of colorectal cancer liver metastases associated with improved survival. Oncoimmunology. 2017;6(3):e1286436.
303. Lakshmikanth T, Muhammad SA, Olin A, Chen Y, Mikes J, Fagerberg L, et al. Human Immune System Variation during 1 Year. Cell Rep. 2020;32(3):107923.

304. Takahashi C, Au-Yeung A, Fuh F, Ramirez-Montagut T, Bolen C, Mathews W, et al. Mass cytometry panel optimization through the designed distribution of signal interference. Cytometry A. 2017;91(1):39-47.
305. Sumatoh HR, Teng KW, Cheng Y, Newell EW. Optimization of mass cytometry sample cryopreservation after staining. Cytometry A. 2017;91(1):48-61.
306. Hedley BD, Keeney M. Technical issues: flow cytometry and rare event analysis. Int J Lab Hematol. 2013;35(3):344-50.
307. Weber LM, Robinson MD. Comparison of clustering methods for high-dimensional single-cell flow and mass cytometry data. Cytometry A. 2016;89(12):1084-96.
308. Saeys Y, Van Gassen S, Lambrecht BN. Computational flow cytometry: helping to make sense of high-dimensional immunology data. Nat Rev Immunol. 2016;16(7):449-62.
309. Kimball AK, Oko LM, Bullock BL, Nemenoff RA, van Dyk LF, Clambey ET. A Beginner's Guide to Analyzing and Visualizing Mass Cytometry Data. J Immunol. 2018;200(1):3-22.
310. Amir el AD, Davis KL, Tadmor MD, Simonds EF, Levine JH, Bendall SC, et al. viSNE enables visualization of high dimensional single-cell data and reveals phenotypic heterogeneity of leukemia. Nat Biotechnol. 2013;31(6):545-52.
311. Levine JH, Simonds EF, Bendall SC, Davis KL, Amir el AD, Tadmor MD, et al. Data-Driven Phenotypic Dissection of AML Reveals Progenitor-like Cells that Correlate with Prognosis. Cell. 2015;162(1):184-97.
312. Van Gassen S, Callebaut B, Van Helden MJ, Lambrecht BN, Demeester P, Dhaene T, et al. FlowSOM: Using self-organizing maps for visualization and interpretation of cytometry data. Cytometry A. 2015;87(7):636-45.
313. Belkina AC, Ciccolella CO, Anno R, Halpert R, Spidlen J, Snyder-Cappione JE. Automated optimized parameters for T-distributed stochastic neighbor embedding improve visualization and analysis of large datasets. Nat Commun. 2019;10(1):5415.
314. Robinson MD, McCarthy DJ, Smyth GK. edgeR: a Bioconductor package for differential expression analysis of digital gene expression data. Bioinformatics. 2010;26(1):139-40.
315. Tusher VG, Tibshirani R, Chu G. Significance analysis of microarrays applied to the ionizing radiation response. Proc Natl Acad Sci U S A. 2001;98(9):5116-21.
316. Bruggner RV, Bodenmiller B, Dill DL, Tibshirani RJ, Nolan GP. Automated identification of stratifying signatures in cellular subpopulations. Proc Natl Acad Sci U S A. 2014;111(26):E2770-7.
317. Finck R, Simonds EF, Jager A, Krishnaswamy S, Sachs K, Fantl W, et al. Normalization of mass cytometry data with bead standards. Cytometry A. 2013;83(5):483-94.
318. Lun ATL, Richard AC, Marioni JC. Testing for differential abundance in mass cytometry data. Nat Methods. 2017;14(7):707-9.
319. Keane C, Tobin J, Talaulikar D, Green M, Crooks P, Jain S, et al. A high LDH to absolute lymphocyte count ratio in patients with DLBCL predicts for a poor intratumoral immune response and inferior survival. Oncotarget. 2018;9(34):23620-7.
320. Schuster SJ, Svoboda J, Chong EA, Nasta SD, Mato AR, Anak O, et al. Chimeric Antigen Receptor T Cells in Refractory B-Cell Lymphomas. N Engl J Med. 2017;377(26):2545-54.
321. Jager KJ, van Dijk PC, Zoccali C, Dekker FW. The analysis of survival data: the Kaplan-Meier method. Kidney Int. 2008;74(5):560-5.
322. Kim DH, Baek JH, Chae YS, Kim YK, Kim HJ, Park YH, et al. Absolute lymphocyte counts predicts response to chemotherapy and survival in diffuse large B-cell lymphoma. Leukemia. 2007;21(10):2227-30.

323. Porrata LF, Inwards DJ, Ansell SM, Micallef IN, Johnston PB, Hogan WJ, et al. New-onset lymphopenia assessed during routine follow-up is a risk factor for relapse postautologous peripheral blood hematopoietic stem cell transplantation in patients with diffuse large B-cell lymphoma. Biol Blood Marrow Transplant. 2010;16(3):376-83.
324. Wang J, Gao K, Lei W, Dong L, Xuan Q, Feng M, et al. Lymphocyte-to-monocyte ratio is associated with prognosis of diffuse large B-cell lymphoma: correlation with CD163 positive M2 type tumor-associated macrophages, not PD-1 positive tumor-infiltrating lymphocytes. Oncotarget. 2017;8(3):5414-25.
325. Wilcox RA, Wada DA, Ziesmer SC, Elsawa SF, Comfere NI, Dietz AB, et al. Monocytes promote tumor cell survival in T-cell lymphoproliferative disorders and are impaired in their ability to differentiate into mature dendritic cells. Blood. 2009;114(14):2936-44.
326. Long KB, Beatty GL. Harnessing the antitumor potential of macrophages for cancer immunotherapy. Oncoimmunology. 2013;2(12):e26860.
327. Wilcox RA, Feldman AL, Wada DA, Yang ZZ, Comfere NI, Dong H, et al. B7-H1 (PD-L1, CD274) suppresses host immunity in T-cell lymphoproliferative disorders. Blood. 2009;114(10):2149-58.
328. He B, Chadburn A, Jou E, Schattner EJ, Knowles DM, Cerutti A. Lymphoma B cells evade apoptosis through the TNF family members BAFF/BLyS and APRIL. J Immunol. 2004;172(5):3268-79.
329. Kim DH, Kim JG, Sohn SK, Sung WJ, Suh JS, Lee KS, et al. Clinical impact of early absolute lymphocyte count after allogeneic stem cell transplantation. Br J Haematol. 2004;125(2):217-24.
330. Porrata LF, Gertz MA, Inwards DJ, Litzow MR, Lacy MQ, Tefferi A, et al. Early lymphocyte recovery predicts superior survival after autologous hematopoietic stem cell transplantation in multiple myeloma or non-Hodgkin lymphoma. Blood. 2001;98(3):579-85.
331. Gordan LN, Sugrue MW, Lynch JW, Williams KD, Khan SA, Moreb JS. Correlation of early lymphocyte recovery and progression-free survival after autologous stem-cell transplant in patients with Hodgkin's and non-Hodgkin's Lymphoma. Bone Marrow Transplant. 2003;31(11):1009-13.
332. Carella AM, de Souza CA, Luminari S, Marcheselli L, Chiappella A, di Rocco A, et al. Prognostic role of gender in diffuse large B-cell lymphoma treated with rituximab containing regimens: a Fondazione Italiana Linfomi/Grupo de Estudos em Molestias Onco-Hematologicas retrospective study. Leukemia & lymphoma. 2013;54(1):53-7.
333. Brodin P, Davis MM. Human immune system variation. Nat Rev Immunol. 2017;17(1):21-9.
334. Hartmann FJ, Babdor J, Gherardini PF, Amir ED, Jones K, Sahaf B, et al. Comprehensive Immune Monitoring of Clinical Trials to Advance Human Immunotherapy. Cell Rep. 2019;28(3):819-31 e4.
335. Ferrant J, Lhomme F, Le Gallou S, Irish JM, Roussel M. Circulating Myeloid Regulatory Cells: Promising Biomarkers in B-Cell Lymphomas. Front Immunol. 2020;11:623993.
336. Sallusto F, Geginat J, Lanzavecchia A. Central memory and effector memory T cell subsets: function, generation, and maintenance. Annu Rev Immunol. 2004;22:745-63.
337. Takahashi T, Tagami T, Yamazaki S, Uede T, Shimizu J, Sakaguchi N, et al. Immunologic self-tolerance maintained by CD25(+)CD4(+) regulatory T cells constitutively expressing cytotoxic T lymphocyte-associated antigen 4. J Exp Med. 2000;192(2):303-10.
338. Szabo SJ, Kim ST, Costa GL, Zhang X, Fathman CG, Glimcher LH. A novel transcription factor, T-bet, directs Th1 lineage commitment. Cell. 2000;100(6):655-69.

339. Ong SM, Teng K, Newell E, Chen H, Chen J, Loy T, et al. A Novel, Five-Marker Alternative to CD16-CD14 Gating to Identify the Three Human Monocyte Subsets. Front Immunol. 2019;10:1761.
340. Roussel M, Ferrell PB, Jr., Greenplate AR, Lhomme F, Le Gallou S, Diggins KE, et al. Mass cytometry deep phenotyping of human mononuclear phagocytes and myeloid-derived suppressor cells from human blood and bone marrow. J Leukoc Biol. 2017;102(2):437-47.
341. Villani AC, Satija R, Reynolds G, Sarkizova S, Shekhar K, Fletcher J, et al. Single-cell RNA-seq reveals new types of human blood dendritic cells, monocytes, and progenitors. Science. 2017;356(6335).
342. Hamers AAJ, Dinh HQ, Thomas GD, Marcovecchio P, Blatchley A, Nakao CS, et al. Human Monocyte Heterogeneity as Revealed by High-Dimensional Mass Cytometry. Arterioscler Thromb Vasc Biol. 2019;39(1):25-36.
343. Chevrier S, Levine JH, Zanotelli VRT, Silina K, Schulz D, Bacac M, et al. An Immune Atlas of Clear Cell Renal Cell Carcinoma. Cell. 2017;169(4):736-49 e18.
344. Lavin Y, Kobayashi S, Leader A, Amir ED, Elefant N, Bigenwald C, et al. Innate Immune Landscape in Early Lung Adenocarcinoma by Paired Single-Cell Analyses. Cell. 2017;169(4):750-65 e17.
345. Becht E, McInnes L, Healy J, Dutertre CA, Kwok IWH, Ng LG, et al. Dimensionality reduction for visualizing single-cell data using UMAP. Nat Biotechnol. 2018.
346. Chen H, Lau MC, Wong MT, Newell EW, Poidinger M, Chen J. Cytofkit: A Bioconductor Package for an Integrated Mass Cytometry Data Analysis Pipeline. PLoS Comput Biol. 2016;12(9):e1005112.
347. Romero P, Zippelius A, Kurth I, Pittet MJ, Touvrey C, Iancu EM, et al. Four functionally distinct populations of human effector-memory CD8+ T lymphocytes. J Immunol. 2007;178(7):4112-9.
348. Koch S, Larbi A, Derhovanessian E, Ozcelik D, Naumova E, Pawelec G. Multiparameter flow cytometric analysis of CD4 and CD8 T cell subsets in young and old people. Immun Ageing. 2008;5:6.
349. Wagar LE, Bolen CR, Sigal N, Lopez Angel CJ, Guan L, Kirkpatrick BD, et al. Increased T Cell Differentiation and Cytolytic Function in Bangladeshi Compared to American Children. Front Immunol. 2019;10:2239.
350. Bengsch B, Ohtani T, Khan O, Setty M, Manne S, O'Brien S, et al. Epigenomic-Guided Mass Cytometry Profiling Reveals Disease-Specific Features of Exhausted CD8 T Cells. Immunity. 2018;48(5):1029-45 e5.
351. Michlmayr D, Pak TR, Rahman AH, Amir ED, Kim EY, Kim-Schulze S, et al. Comprehensive innate immune profiling of chikungunya virus infection in pediatric cases. Mol Syst Biol. 2018;14(8):e7862.
352. Shi C, Pamer EG. Monocyte recruitment during infection and inflammation. Nat Rev Immunol. 2011;11(11):762-74.
353. Shiraishi D, Fujiwara Y, Horlad H, Saito Y, Iriki T, Tsuboki J, et al. CD163 Is Required for Protumoral Activation of Macrophages in Human and Murine Sarcoma. Cancer Res. 2018;78(12):3255-66.
354. Haque A, Moriyama M, Kubota K, Ishiguro N, Sakamoto M, Chinju A, et al. CD206(+) tumor-associated macrophages promote proliferation and invasion in oral squamous cell carcinoma via EGF production. Sci Rep. 2019;9(1):14611.

355. Singhal S, Stadanlick J, Annunziata MJ, Rao AS, Bhojnagarwala PS, O'Brien S, et al. Human tumor-associated monocytes/macrophages and their regulation of T cell responses in early-stage lung cancer. Sci Transl Med. 2019;11(479).
356. Olingy CE, Dinh HQ, Hedrick CC. Monocyte heterogeneity and functions in cancer. J Leukoc Biol. 2019;106(2):309-22.
357. Larbi A, Fulop T. From "truly naive" to "exhausted senescent" T cells: when markers predict functionality. Cytometry A. 2014;85(1):25-35.
358. Martin MD, Badovinac VP. Defining Memory CD8 T Cell. Front Immunol. 2018;9:2692.
359. Reading JL, Galvez-Cancino F, Swanton C, Lladser A, Peggs KS, Quezada SA. The function and dysfunction of memory CD8(+) T cells in tumor immunity. Immunol Rev. 2018;283(1):194-212.
360. Willinger T, Freeman T, Hasegawa H, McMichael AJ, Callan MF. Molecular signatures distinguish human central memory from effector memory CD8 T cell subsets. J Immunol. 2005;175(9):5895-903.
361. Jacquemont L, Tilly G, Yap M, Doan-Ngoc TM, Danger R, Guerif P, et al. Terminally Differentiated Effector Memory CD8(+) T Cells Identify Kidney Transplant Recipients at High Risk of Graft Failure. J Am Soc Nephrol. 2020;31(4):876-91.
362. Lord GM, Rao RM, Choe H, Sullivan BM, Lichtman AH, Luscinskas FW, et al. T-bet is required for optimal proinflammatory CD4+ T-cell trafficking. Blood. 2005;106(10):3432-9.
363. Wan YY, Flavell RA. How diverse--CD4 effector T cells and their functions. J Mol Cell Biol. 2009;1(1):20-36.
364. Hendriks J, Gravestein LA, Tesselaar K, van Lier RA, Schumacher TN, Borst J. CD27 is required for generation and long-term maintenance of T cell immunity. Nat Immunol. 2000;1(5):433-40.
365. Lenschow DJ, Walunas TL, Bluestone JA. CD28/B7 system of T cell costimulation. Annu Rev Immunol. 1996;14:233-58.
366. Turaj AH, Hussain K, Cox KL, Rose-Zerilli MJJ, Testa J, Dahal LN, et al. Antibody Tumor Targeting Is Enhanced by CD27 Agonists through Myeloid Recruitment. Cancer Cell. 2017;32(6):777-91 e6.
367. Metcalf D. Hematopoietic cytokines. Blood. 2008;111(2):485-91.
368. Altan-Bonnet G, Mukherjee R. Cytokine-mediated communication: a quantitative appraisal of immune complexity. Nat Rev Immunol. 2019;19(4):205-17.
369. Eizenberg-Magar I, Rimer J, Zaretsky I, Lara-Astiaso D, Reich-Zeliger S, Friedman N. Diverse continuum of CD4(+) T-cell states is determined by hierarchical additive integration of cytokine signals. Proc Natl Acad Sci U S A. 2017;114(31):E6447-E56.
370. Mortier E, Ma A, Malynn BA, Neurath MF. Editorial: Modulating Cytokines as Treatment for Autoimmune Diseases and Cancer. Front Immunol. 2020;11:608636.
371. Villagra A, Sotomayor EM, Seto E. Histone deacetylases and the immunological network: implications in cancer and inflammation. Oncogene. 2010;29(2):157-73.
372. Fajgenbaum DC, June CH. Cytokine Storm. N Engl J Med. 2020;383(23):2255-73.
373. Ragab D, Salah Eldin H, Taeimah M, Khattab R, Salem R. The COVID-19 Cytokine Storm; What We Know So Far. Front Immunol. 2020;11:1446.
374. Deenick EK, Avery DT, Chan A, Berglund LJ, Ives ML, Moens L, et al. Naive and memory human B cells have distinct requirements for STAT3 activation to differentiate into antibody-secreting plasma cells. J Exp Med. 2013;210(12):2739-53.

375. Lu X, Nechushtan H, Ding F, Rosado MF, Singal R, Alizadeh AA, et al. Distinct IL-4-induced gene expression, proliferation, and intracellular signaling in germinal center B-cell-like and activated B-cell-like diffuse large-cell lymphomas. Blood. 2005;105(7):2924-32.
376. Rutsch S, Neppalli VT, Shin DM, DuBois W, Morse HC, 3rd, Goldschmidt H, et al. IL-6 and MYC collaborate in plasma cell tumor formation in mice. Blood. 2010;115(9):1746-54.
377. Giachelia M, Voso MT, Tisi MC, Martini M, Bozzoli V, Massini G, et al. Interleukin-6 plasma levels are modulated by a polymorphism in the NF-kappaB1 gene and are associated with outcome following rituximab-combined chemotherapy in diffuse large B-cell non-Hodgkin lymphoma. Leukemia & lymphoma. 2012;53(3):411-6.
378. Lam LT, Wright G, Davis RE, Lenz G, Farinha P, Dang L, et al. Cooperative signaling through the signal transducer and activator of transcription 3 and nuclear factor-{kappa}B pathways in subtypes of diffuse large B-cell lymphoma. Blood. 2008;111(7):3701-13.
379. Yan XJ, Dozmorov I, Li W, Yancopoulos S, Sison C, Centola M, et al. Identification of outcome-correlated cytokine clusters in chronic lymphocytic leukemia. Blood. 2011;118(19):5201-10.
380. Kawasaki T, Kawai T. Toll-like receptor signaling pathways. Front Immunol. 2014;5:461.
381. Beguelin W, Sawh S, Chambwe N, Chan FC, Jiang Y, Choo JW, et al. IL10 receptor is a novel therapeutic target in DLBCLs. Leukemia. 2015;29(8):1684-94.
382. Yasmin R, Siraj S, Hassan A, Khan AR, Abbasi R, Ahmad N. Epigenetic regulation of inflammatory cytokines and associated genes in human malignancies. Mediators Inflamm. 2015;2015:201703.
383. Mossadegh-Keller N, Sarrazin S, Kandalla PK, Espinosa L, Stanley ER, Nutt SL, et al. M-CSF instructs myeloid lineage fate in single haematopoietic stem cells. Nature. 2013;497(7448):239-43.
384. Staversky RJ, Byun DK, Georger MA, Zaffuto BJ, Goodman A, Becker MW, et al. The Chemokine CCL3 Regulates Myeloid Differentiation and Hematopoietic Stem Cell Numbers. Sci Rep. 2018;8(1):14691.
385. Broxmeyer HE, Sherry B, Lu L, Cooper S, Oh KO, Tekamp-Olson P, et al. Enhancing and suppressing effects of recombinant murine macrophage inflammatory proteins on colony formation in vitro by bone marrow myeloid progenitor cells. Blood. 1990;76(6):1110-6.
386. Jason J, Archibald LK, Nwanyanwu OC, Byrd MG, Kazembe PN, Dobbie H, et al. Comparison of serum and cell-specific cytokines in humans. Clin Diagn Lab Immunol. 2001;8(6):1097-103.
387. Castillo JJ, Winer ES, Olszewski AJ. Sites of extranodal involvement are prognostic in patients with diffuse large B-cell lymphoma in the rituximab era: an analysis of the Surveillance, Epidemiology and End Results database. Am J Hematol. 2014;89(3):310-4.
388. Zamo A, Johnston P, Attygalle AD, Laurent C, Arber DA, Fend F. Aggressive B-cell lymphomas with a primary bone marrow presentation. Histopathology. 2020;77(3):369-79.
389. Ciavarella S, Vegliante MC, Fabbri M, De Summa S, Melle F, Motta G, et al. Dissection of DLBCL microenvironment provides a gene expression-based predictor of survival applicable to formalin-fixed paraffin-embedded tissue. Ann Oncol. 2018;29(12):2363-70.
390. Wong PP, Munoz-Felix JM, Hijazi M, Kim H, Robinson SD, De Luxan-Delgado B, et al. Cancer Burden Is Controlled by Mural Cell-beta3-Integrin Regulated Crosstalk with Tumor Cells. Cell. 2020;181(6):1346-63 e21.

391. Jackson HW, Fischer JR, Zanotelli VRT, Ali HR, Mechera R, Soysal SD, et al. The single-cell pathology landscape of breast cancer. Nature. 2020;578(7796):615-20.
392. Damond N, Engler S, Zanotelli VRT, Schapiro D, Wasserfall CH, Kusmartseva I, et al. A Map of Human Type 1 Diabetes Progression by Imaging Mass Cytometry. Cell Metab. 2019;29(3):755-68 e5.
393. Overgaard NH, Jung JW, Steptoe RJ, Wells JW. CD4+/CD8+ double-positive T cells: more than just a developmental stage? J Leukoc Biol. 2015;97(1):31-8.
394. Hillhouse EE, Delisle JS, Lesage S. Immunoregulatory CD4(-)CD8(-) T cells as a potential therapeutic tool for transplantation, autoimmunity, and cancer. Front Immunol. 2013;4:6.
395. Blanco P, Pitard V, Viallard JF, Taupin JL, Pellegrin JL, Moreau JF. Increase in activated CD8+ T lymphocytes expressing perforin and granzyme B correlates with disease activity in patients with systemic lupus erythematosus. Arthritis Rheum. 2005;52(1):201-11.
396. Schroeder MA, Rettig MP, Lopez S, Christ S, Fiala M, Eades W, et al. Mobilization of allogeneic peripheral blood stem cell donors with intravenous plerixafor mobilizes a unique graft. Blood. 2017;129(19):2680-92.
397. Petrenko O, Li J, Cimica V, Mena-Taboada P, Shin HY, D'Amico S, et al. IL-6 promotes MYC-induced B cell lymphomagenesis independent of STAT3. PloS one. 2021;16(3):e0247394.
398. Roussel M, Lhomme F, Roe CE, Bartkowiak T, Gravelle P, Laurent C, et al. Mass cytometry defines distinct immune profile in germinal center B-cell lymphomas. Cancer Immunol Immunother. 2020;69(3):407-20.
399. Kadic E, Moniz RJ, Huo Y, Chi A, Kariv I. Effect of cryopreservation on delineation of immune cell subpopulations in tumor specimens as determinated by multiparametric single cell mass cytometry analysis. BMC Immunol. 2017;18(1):6.
400. Leelatian N, Doxie DB, Greenplate AR, Mobley BC, Lehman JM, Sinnaeve J, et al. Single Cell Analysis of Human Tissues and Solid Tumors with Mass Cytometry. Cytometry B Clin Cytom. 2017.
401. Bagwell CB, Hunsberger B, Hill B, Herbert D, Bray C, Selvanantham T, et al. Multi-site reproducibility of a human immunophenotyping assay in whole blood and peripheral blood mononuclear cells preparations using CyTOF technology coupled with Maxpar Pathsetter, an automated data analysis system. Cytometry B Clin Cytom. 2020;98(2):146-60.
402. Takahashi K, Sivina M, Hoellenriegel J, Oki Y, Hagemeister FB, Fayad L, et al. CCL3 and CCL4 are biomarkers for B cell receptor pathway activation and prognostic serum markers in diffuse large B cell lymphoma. Br J Haematol. 2015;171(5):726-35.

10. Appendix

10.1 Myeloid antibody panel

Myeloid Panel				
Metal Tag	**Marker**	**Clone**	**Vendor**	**µl per test (100µl staining volume)**
89 Y	CD45	HI30	Fluidigm	0.5
141 Pr				
142 Nd	CD19	HIB19	Fluidigm	0.5
143 Nd	HLA-DR	L243	Fluidigm	0.25
144 Nd	CD38	HIT2	Fluidigm	0.5
145 Nd	PECAM-1 (CD31)	WM59	Fluidigm	0.5
146 Nd	CD64	10.1	Fluidigm	0.5
147 Sm	CD11c	Bu15	Fluidigm	0.5
148 Nd	CD14	M5E2	Fluidigm	0.125
149 Sm	CD56	NCAM16.2	Fluidigm	0.5
150 Nd				
151 Eu	CD123	6H6	Fluidigm	0.5
152Sm				
153 Eu	CCR2 (CD192)	K036C2	Fluidigm	0.5
154 Sm	CD3	UCHT1	Fluidigm	0.25
155 Gd	CD172a	15-414	*Biolegend	2
156 Gd				
158 Gd	CD33	WM53	Fluidigm	0.25
159 Tb	CD274	29E.2A3	Fluidigm	1
160 Gd				
161 Dy				
162 Dy	CD8	RPA-T4	Fluidigm	0.25
163 Dy	CD272	MIH26	Fluidigm	0.5
164 Dy	CD86	IT2.2	*eBiosciences	0.7
165 Ho	CD163	GHI/61	Fluidigm	0.5
166 Er	CD13	WM15	*Biolegend	0.3
167 Er	CD11b	ICRF44	Fluidigm	0.5
168 Er	MMR (CD206)	15-2	Fluidigm	1
169 Tm	CD32	FUN-2	Fluidigm	0.25
170 Er	CD40	HB14	*Miltenyi	0.3
171 Yb				
172 Yb	CX3CR1	2A9-1	Fluidigm	1
173 Yb	CD91	A2MR-α2	*BD biosciences	1
174 Yb				
175 Lu	CXCR4 (CD184)	12G5	Fluidigm	0.5
176 Yb	CD4	RPA-T4	Fluidigm	0.5
209 Bi	CD16	3G8	Fluidigm	0.5

*Indicates custom in-house conjugated antibody

10.2 T cell and lymph node panels

T cell and Lymph node panels				
Metal Tag	**Marker**	**Clone**	**Vendor**	**µl per test (100µl staining volume)**
89 Y	CD45	HI30	Fluidigm	0.5
141 Pr	CD47	B6H12	*eBiosciences	0.9
142 Nd	CD19	HIB19	Fluidigm	0.5
143 Nd	CD197	G043H7	*Biolegend	1.6
144 Nd	CD38	HIT2	Fluidigm	0.5
145 Nd				
146 Nd				
147 Sm	CD20	2H7	Fluidigm	0.5
148 Nd	CD14	M5E2	Fluidigm	0.125
149 Sm	CD56	NCAM16.2	Fluidigm	0.5
150 Nd	CD223 (LAG-3)	11C3C65	Fluidigm	1
151 Eu				
152 Sm				
153 Eu	GATA3	REA174	*Miltenyi	2
154 Sm	CD3	UCHT1	Fluidigm	0.25
155 Gd	T-bet	4B10	*eBiosciences	1.6
156 Gd	CD366 (TIM-3)	F38-2E2	*Biolegend	1.75
158 Gd	CD134 (OX40)	ACT35	Fluidigm	1
159 Tb				
160 Gd	CD28	CD28.2	Fluidigm	0.5
161 Dy	CD25	MA251	*Biolegend	6
162 Dy	CD8	RPA-T4	Fluidigm	0.25
163 Dy				
164 Dy				
165 Ho	CD314 (NKG2D)	BAT221	*Miltenyi	5
166 Er	FoxP3	PCH101	*eBiosciences	1.6
167 Er	CD27	L128	Fluidigm	0.5
168 Er				
169 Tm	CD45RA	HI100	Fluidigm	0.25
170 Er	CD152 (CTLA-4)	14D3	Fluidigm	1
171 Yb	CD226 (DNAM-1)	DX11	Fluidigm	0.5
172 Yb	CD279 (PD-1)	EH12.2H7	*Biolegend	1.2
173 Yb	Granzyme B	GB11	Fluidigm	0.5
174 Yb	CD127	A019D5	*Biolegend	3
175 Lu	Perforin	B-D48	Fluidigm	0.5
176 Yb	CD4	RPA-T4	Fluidigm	0.5
209 Bi	CD16	3G8	Fluidigm	0.5

*Indicates custom in-house conjugated antibody. Grey indicates lymph node panel only.

10.3 Cytokine panel

Cytokine Panel				
Metal Tag	**Marker**	**Clone**	**Vendor**	**µl per test (100µl staining volume)**
89 Y	CD45	HI30	Fluidigm	0.5
141 Pr	IL-10	JES3-9D7	*Biolegend	1
142 Nd	CD19	HIB19	Fluidigm	0.5
143 Nd	HLA-DR	L243	Fluidigm	0.25
144 Nd	CD38	HIT2	Fluidigm	0.5
145 Nd				
146 Nd				
147 Sm	CD20	2H7	Fluidigm	0.5
148 Nd	CD14	M5E2	Fluidigm	0.125
149 Sm	CD56	NCAM16.2	Fluidigm	0.5
150 Nd	IL-1RA	MA5-29353	*Invitrogen	3
151 Eu	CD123	6H6	Fluidigm	0.5
152Sm	TNFα	Mab11	Fluidigm	1
153 Eu				
154 Sm	CD3	UCHT1	Fluidigm	0.25
155 Gd	T-bet	4B10	*eBiosciences	1.6
156 Gd	CCL3 (MIP-1α)	Polyclonal	*R & D systems	0.6
158 Gd	IL-2	MQ1-17H12	*Biolegend	2
159 Tb				
160 Gd	CD28	CD28.2	Fluidigm	0.5
161 Dy	IL-6	MQ2-13A5	*Biolegend	2
162 Dy	CD8	RPA-T4	Fluidigm	0.25
163 Dy	TGFβ	TW4-6H10	Fluidigm	0.5
164 Dy				
165 Ho	IFNɣ	B27	*Biolegend	0.7
166 Er	FoxP3	PCH101	*eBiosciences	1.6
167 Er	CD27	L128	Fluidigm	0.5
168 Er				
169 Tm	CD45RA	HI100	Fluidigm	0.25
170 Er	IFNα	7N4-1	*BD biosciences	5
171 Yb	Ki67	Ki67	*Biolegend	2
172 Yb	CD279 (PD-1)	EH12.2H7	*Biolegend	1.2
173 Yb	Granzyme B	GB11	Fluidigm	0.5
174 Yb				
175 Lu	Perforin	B-D48	Fluidigm	0.5
176 Yb	CD4	RPA-T4	Fluidigm	0.5
209 Bi	CD16	3G8	Fluidigm	0.5

*Indicates custom in-house conjugated antibody.

10.4 Imaging mass cytometry panel

IMC Panel				
Metal Tag	**Marker**	**Clone**	**Vendor**	**Dilution**
89 Y				
141 Pr	alpha SMA	1A4	Fluidigm	1/200
142 Nd	HLA-DR	LN3	*Biolegend	1/50
143 Nd	CD34	ICO115	*Cell Signalling Technology	1/25
144 Nd	CD14	EPR3653	Fluidigm	1/100
145 Nd	T-bet	D6N8B	Fluidigm	1/50
146 Nd	CD16	EPR16784	Fluidigm	1/50
147 Sm	CD163	EDHu-1	Fluidigm	1/100
148 Nd	CD30	E4L4I	*Cell Signalling Technology	1/40
149 Sm				
150 Nd	CD10	Polyclonal	*R & D systems	1/50
151 Eu	CD31	EPR3094	Fluidigm	1/100
152Sm	CD45	CD45-2B11	Fluidigm	1/100
153 Eu	LAG3	D2G40	Fluidigm	1/50
154 Sm	CD11c	D3V1E	*Cell Signalling Technology	1/50
155 Gd	FOXP3	236A/E7	Fluidigm	1/50
156 Gd	CD4	EPR6855	Fluidigm	1/200
158 Gd	MUM1/IRF4	Polyclonal	*R & D systems	1/62.5
159 Tb	CD68	KP1	Fluidigm	1/50
160 Gd				
161 Dy	CD20	H1	Fluidigm	1/400
162 Dy	CD8	C8/144B	Fluidigm	1/100
163 Dy				
164 Dy	TIM-3	D5D5R	*Cell Signalling Technology	1/25
165 Ho	PD-L1	E1L3N	*Cell Signalling Technology	1/50
166 Er	B7H4	H74	Fluidigm	1/50
167 Er	Granzyme B	EPR20129-217	Fluidigm	1/100
168 Er	ki67	B56	Fluidigm	1/50
169 Tm	collagen 1	polyclonal	Fluidigm	1/300
170 Er	CD3	polyclonal	Fluidigm	1/100
171 Yb	CX3CR1	8E10.D9	*Biolegend	1/25
172 Yb	PD-1	EH12.2H7	*Cell Signalling Technology	1/33
173 Yb	CD45RA	HI100	*Biolegend	1/66
174 Yb				
175 Lu	CD206	E2L9N	*Cell Signalling Technology	1/33
176 Yb	Anti Histone H3	D1H2	Fluidigm	1/300
209 Bi				

*Indicates custom in-house conjugated antibody.